Experimental Investigation of the Shear Behaviour of Slender Concrete Beams Reinforced with GFRP

by

Timothy Tedford

A thesis

presented to the University of Waterloo

in fulfillment of the

thesis requirement for the degree of

Master of Applied Science

in

Civil Engineering

Waterloo, Ontario, Canada, 2019

AUTHOR'S DECLARATION

I hereby declare that I am the sole author of this thesis. This is a true copy of the thesis including revisions that has been accepted by my examiners.

I understand this thesis may be made available electronically to the public.

ABSTRACT

Glass fibre-reinforced polymers (GFRP) are being used as longitudinal and shear reinforcement in specialized concrete applications. GFRP products are designed as direct replacements for conventional steel reinforcement and GFRP reinforced concrete (RC) beams exhibit similar flexural behaviour to steel RC beams. The shear behaviour of RC beams reinforced with GFRP shear reinforcement is less studied and is normally modelled using semi-empirical formulations based on existing steel reinforcement guidelines. These models are calibrated based on the existing set of experimental tests on GFRP RC beams which is limited at a maximum tested shear-span-to-depth (a/d) ratio of 4.5.

A parametric study on the effect of slenderness on the shear behaviour of GFRP beams was conducted by Barrage (2017) using ABAQUS, a finite element analysis software, and concluded that the existing models used by CSA and ACI may not be suitable to predict the behaviour of overly slender RC beams with GFRP shear reinforcement.

The purpose of this research was to investigate the behaviour of slender GFRP RC beams and confirm the applicability of existing code models and the analysis by Barrage (2017).

The experimental program being presented tested 10 slender GFRP RC beams. The beams had a/d ratios of 4.5, 6.5, 8.5 and 10.5 and included specimens with and without transverse reinforcement. These specimens failed in shear or flexure capturing the full range of slender shear behaviour. Two additional beams with a/d ratios of 4.5 and 6.5 were tested to examine stirrup spacing requirements. These specimens were tested under monotonic loading in three-point bending.

The results of the experimental program showed strong correlation with existing research on shorter beams. The reduced stiffness of the GFRP longitudinal reinforcement caused a reduction in aggregate interlock and overall decreased shear strength. This effect was more pronounced with increasing slenderness. Additionally, the tests indicated that with increasing slenderness the GFRP stirrups are under-utilized and failure is concrete controlled.

CSA S806 (2012) and ACI 440 (2003) provisions well predicted the failure loads of the test specimens and CSA S806 well predicted the governing mode of failure and deflections at service load levels. Existing stirrup spacing requirements in CSA S806 were found to be overly limiting for GFRP stirrups.

The results indicated that proper detailing can prevent stirrup bend rupture observed in previous tests. None of the tested specimens failed due to stirrup rupture.

The ABAQUS models used by Barrage were found to have reasonably good predictions of beam behaviour. The models were found to generally over-predict the stiffness of specimens and ultimate load capacity. Additionally, the models were unable to capture the failure mechanism that governs in GFRP beams showing a more ductile response that lead to over-predictions of ultimate loads.

Further research investigating the detailing requirements to prevent stirrup rupture are recommended. Additionally, further research isolating the effects of GFRP shear reinforcement by testing specimens with steel longitudinal reinforcement and GFRP shear reinforcement are recommended to further examine the behaviour of GFRP stirrups. Finally, investigation into proper modelling of shear crack failure mechanisms in FEA is required to better predict beam behaviour.

ACKNOWLEDGEMENTS

I would like to extend my thanks first to my supervisor, Professor M.A. Polak, for her guidance and support of this research and patience with the research program.

Additional gratitude needs to be extended to the CEE lab staff, Richard Morrison, Douglas Hirst and Peter Volcic, for their assistance, guidance and expertise in the construction and testing portions of this research. Special thanks to Douglas Hirst for his supervision of my lab work.

I would also like to thank all of the students that assisted with the construction of the test specimens. I could not have done it without you. In particular, thank you to Graeme Milligan, Dan Lahey and Phillip Lochan for their many hours spent tying cages and assembling formwork with me.

Thank you to all of my fellow graduate students who provided much needed advice and aid in the pursuit of this degree. To Graeme Milligan who counseled and let me use him as a sounding board, to Colin Van Niejenhuis for his advice based on years of lab experience, to Ryan Barrage for continually running and adjusting his FEA models, to Piotr Wiciak for putting up with my weird office habits and to Terence Ma for his inspiration and friendship throughout this whole process.

I would also like to thank those who have supported me through my research: my family for always being there to help despite distance and differences, my church community at FBC for providing a home away from home and comfort in the hard times and my friends and fellows at P2C for their continued encouragement and provision of shoulders to lean on.

My deepest gratitude to you all and those others who have helped me. I only made it this far by your aid and support.

DEDICATION

To my God and Saviour. May this work be pleasing in your sight.

TABLE OF CONTENTS

LIST OF FIGURES

LIST OF TABLES

LIST OF SYMBOLS

The following is a list of symbols that are used in this thesis. Each symbol is defined when it first appears, this table is only for reference. Some symbols are similar except for an indicator that they apply to FRP members. These symbols are grouped together.

Symbol	Units	Definition
a	mm	Shear span, distance from support to point of load application
a	mm	Depth of the concrete compression block
A_R	mm^2	Sectional area of longitudinal reinforcement
A_V, A_{fV}	mm^2	Area of shear reinforcement within a single spacing
a/d	-	Ratio of shear span to the depth of longitudinal reinforcement
b, b_w	mm	Width of the concrete compressive zone (equivalent for rectangular sections)
c	mm	Depth from extreme compression fibre to the neutral axis at failure
d	mm	Depth from the extreme compression fibre to the centroid of the tensile longitudinal reinforcement
d_v	mm	Effective shear depth
E_R, E_F	GPa	Axial stiffness of longitudinal reinforcement
f_c'	MPa	Specified concrete compressive strength
f_{fv}	MPa	Ultimate allowable stress in the transverse GFRP reinforcement
f_r	MPa	Stress in longitudinal reinforcement at failure
f_y	MPa	Yield strength of steel
k	-	Ratio of depth of neutral axis to reinforcement depth
k_m	-	Modification factor for moment interaction
k_r	-	Modification factor for the stiffness of longitudinal reinforcement
M_{cr}	kN m	Cracking moment
M_{dc}	kN m	Decompression moment
M_f	kN m	Factored applied moment
M_r	kN m	Flexural resistance of a member
s	mm	Spacing of transverse reinforcement
V_c	kN	Concrete contribution to the overall shear resistance of a beam
V_f	kN	Factored applied shear
V_r	kN	Shear resistance of a beam
V_p	kN	Prestressing contribution to the overall shear resistance of a beam
V_{ss}	kN	Transverse steel reinforcement contribution to the overall shear resistance of a beam
V_{sF}, V_f	kN	Transverse FRP reinforcement contribution to the overall shear resistance of a beam

α_1	-	Ratio of average stress in rectangular compression block to the specified concrete strength
β_1	-	Ratio of depth of rectangular compression block to depth to the neutral axis
ϵ_c	-	Compressive strain of concrete at failure
ε_1	-	Longitudinal strain at mid
λ	-	Factor to account for effect of concrete density of shear resistance
ϕ_c	-	Material resistance factor for concrete, taken as 1 for this research
ϕ_{FRP}	-	Material resistance factor for FRP, taken as 1 for this research
ρ_{Fw}	-	Longitudinal reinforcement ratio
θ	degrees	Angle of inclination of the principal compressive stress to the longitudinal axis of the member

CHAPTER 1 - INTRODUCTION

1.0 Overview

Glass fibre reinforced polymers (GFRP) are used as a replacement material for steel reinforcement in concrete beams. GFRP bars provide higher tensile strengths than steel rebar and do not corrode when exposed to acidic environments. Due to the increased costs associated with GFRP, replacement typically occurs for members that are expected to see intensive corrosion or need to be electromagnetically neutral.

FRP is not a new class of materials and has been adopted into the codes of the most prevalent design agencies (ACI, BS, CSA, FIB, ISIS, JSCE and EU). However, the codes are based on a limited set of experimental specimens. Due to the necessity for empirical calibration of the equations governing the use of GFRP as shear reinforcement, the models may not be valid for members outside of the range of tested specimens.

Building off previous work done by Krall (2014), this study will examine the effects of shear-span to depth (a/d) ratio on the shear and flexural behaviour of glass fibre reinforced polymer (GFRP) reinforced concrete beams and compare the results to models used in North America as well as recently developed Finite Element Analysis (FEA) models by Barrage (2017) and Stoner (2015). This research will ensure the safety and applicability of code models for slender beam applications and develop the understanding of the GFRP-concrete composite.

1.1 Research Motivation

Current codes and theory for the use of GFRP as reinforcement in concrete are still developing. Many design guidelines use a semi-empirical approach to develop codes for design guidelines where existing steel reinforced concrete guidelines are experimentally calibrated to be used for GFRP RC design. These provisions can be overly limiting to the use of GFRP reinforcement, especially GFRP shear reinforcement which shows promise for use in industry.

Additionally, these codes are based on incomplete research. The vast majority of GFRP RC beam tests are performed on relatively short beams, with 95% of existing tests focusing on beams with a/d ratios of 4.5 or less. Significant research has been done (Barrage, 2017; Stoner, 2015) to use FEA models to extend existing beam databases through calibration and parametric studies. These models indicate that GFRP behaves very differently from steel reinforcement as the beam slenderness increases. This behaviour is most pronounced in the shear behaviour of the modelled beams.

Finally, the manufacturers of GFRP reinforcing are continually improving their methods and products. Due to the variability in behaviour of GFRP products with each specific manufacturer, much of the existing research needs to be revisited as the quality and performance of GFRP bars and stirrups is improved. Often, manufacturers specifically address issues raised in previous research when improving upon their products. This includes advances in bond strength, bend strength and stiffness of GFRP reinforcing material.

Therefore, further experimental tests of GFRP RC beams are required to investigate the mechanics of slender GFRP RC beams, extend the specimen database for comparison to code models, validate FEA

analyses to allow for further and more useful parametric studies and to test further innovations in GFRP product development.

1.2 Objectives and Scope

This research has three main goals: to investigate the mechanics of slender GFRP RC beams with a specific focus on shear behaviour, to test the usefulness of existing code models for predicting the behaviour of slender GFRP RC beams and to experimentally validate FEA parametric studies done by Stoner (2015) and Barrage (2017).

The test program is focused around two main parameters. The primary parameter of study was the a/d ratio of the specimens. The a/d ratio is a measure of the shear span to reinforcement depth of a concrete beam and is analogous to the slenderness of a beam. It is the defining parameter in most design standards to determine whether a beam is slender; any beam with an a/d ratio less than 2.5 is considered "short" by the requirements of CSA S806 and requires a deep beam analysis. This investigation is focused on extending the database of slenderness tests up to the shear-flexural transition. That is, the a/d ratio at which a beam with a given cross section would transition from shear controlled failure into flexure controlled failure. Extending the database to this transition allows studying the full range of shear failures with regard to slenderness as beams with greater slenderness will fail in flexure rather than shear. The program is centered on shear dominated beams with only the most slender beams designed to fail in flexure. This focuses the investigation on the shear behaviour of the specimens which is less understood than the flexural behaviour.

Second, the GFRP stirrup spacing varied among the specimens. As GFRP stirrups are a new and developing product, the design standards can be overly limiting. This is especially true in detailing considerations. Therefore, two stirrup spacings were considered. The first follows the CSA S806-R12 (Canadian Standards Association (CSA), 2012) guidelines for RC GFRP beams. The second follows a more conventional spacing that would be used if the stirrups were steel. Using these spacings aids in the investigation of the shear behaviour of transversely reinforced GFRP beams while also allowing direct comparison to existing standards. A control group of beams without transverse reinforcement allowed for isolation of the effects of the GFRP stirrups and direct analysis of the concrete contribution to shear resistance.

The specimens were tested under single-point, static loading with simple supports. The analysis presented is based on failure modes, deflected shape, internal strains, crack patterns and moment-deflection curves.

1.3 Thesis Organization

This thesis is divided in six chapters.

Chapter 1 provides an overview of the research motivations, objectives and scope.

Chapter 2 provides important background to the research as well as a peer review of related research. GFRP as a material is discussed along with current design procedures and their underlying theory. Previous research into the behaviour of GFRP RC beams under shear is discussed with a particular focus on the a/d ratio of the specimens presented. Additionally, a brief overview of the purpose and method of FEA parametric studies is presented along with a review of the studies driving the research.

Chapter 3 describes the experimental test program design, specimen construction and test methodology.

Chapter 4 presents the observed experimental behaviour of each specimen and their associated autopsy results.

Chapter 5 presents the analysis of the experimental results. Specimens are compared to determine the effect of slenderness and stirrup spacing on the shear behaviour of GFRP RC beams. Results are contrasted with current code predictions and any discrepancies are discussed. The FEA analysis results produced by Stoner (2015) and Barrage (2017) are also compared to the experimental behaviour of the specimens.

Chapter 6 presents the conclusions of the research and recommendations for future work.

CHAPTER 2 - BACKGROUND AND LITERATURE REVIEW

2.0 Fibre Reinforced Polymer Reinforcing Materials

The fibre-reinforced polymer (FRP) class of materials encompasses a set of composite materials where long, strong fibres are embedded into a weaker matrix material. The material properties of FRP vary based on the fibre material, matrix material, ratio of fibre to matrix and the orientation of the fibres inside the matrix. This variability allows for a wide range of FRP products with each product being tailor-made to suit a specific application. Generally, FRPs exhibit excellent corrosion resistance, high strengths in the direction of the fibre, linear-elastic stress strain behaviour and varying stiffness.

FRP materials in the civil engineering industry most commonly use glass, carbon, aramid and basalt fibres, with glass and carbon fibre reinforced polymers (GFRP and CFRP respectively) being most commonly used in civil engineering applications.

GFRP is mainly used to produce longitudinal and transverse reinforcement to replace steel in reinforced concrete. The fibres are designed to be very long and run unidirectionally providing strength and stiffness along the length of the bar but little transverse strength. These fibres are typically embedded in a thermoset polyester or vinylester resin matrix. GFRP rebar products are characterized by strengths in the range of 500-1200 MPa and elastic moduli in the range of 30-80 GPa. GFRP is a relatively inexpensive material, with prices that approximate conventional steel for straight bars with large diameters. GFRP prices increase if the bar sizes used are small or if bent bars or stirrups are required.

CFRP are most commonly used in repairs and retrofits, though some research has been done on their use as plain longitudinal reinforcement, transverse reinforcement or as prestressing tendons. CFRP is most commonly seen in the civil engineering industry in mats, plates, and specialized components. Carbon fibres are run bi-diretionally through the mat, or laid randomly in an epoxy matrix to provide consistent material properties in two directions. Much of the research on CFRP products is focused on their use in repairs or strengthening of reinforced concrete elements. CFRP products are often characterized by strengths above 1000 MPa and elastic moduli greater than steel. However, CFRP is expensive and its applications are limited to small-scale projects due to its costs.

Aramid fibres are largely falling out of use, due to the high cost associated with their production and a lack of any advantage over glass or carbon fibres.

Basalt fibres have recently been investigated as a potential substitute for glass fibres; basalt fibres provide similar strengths and potentially higher moduli of elasticity while being environmentally friendly to manufacturer (Tomlinson & Fam, 2015). At present, very few manufacturers have adopted basalt fibre limiting its use.

This thesis will be focusing on the use of GFRP to replace conventional steel reinforcement in reinforced concrete (RC) beams, specifically on the effects of using GFRP as both longitudinal and transverse reinforcement.

2.1 GFRP Use in Civil Engineering Today

GFRP, despite being readily available for twenty years, is used infrequently in civil engineering applications. GFRP is typically used either as a replacement for all steel reinforcement in a particular

member or as a replacement in specific areas where corrosion is expected to be severe. It is used in civil engineering projects in both the building and transportation sectors.

In transportation applications, GFRP is used as an alternative material to stainless steel when designing members in areas of high potential corrosion. GFRP has proven to be more effective than epoxy-coated rebar and other low cost alternatives. Stainless steel rebar is a ready replacement; however, the cost of stainless steel is much higher than conventional rebar and even higher than GFRP reinforcement. As such, standard practice today is to utilize longitudinal GFRP or stainless steel rebar in select portions of members along drainage paths and on exposed surfaces in bridges to mitigate corrosion concerns.

In building applications, GFRP is used commonly in hospital and research facilities that require the construction of rooms with low electro-magnetic interference. Conventional rebar and stainless steel cages can cause sensitive equipment to malfunction. This includes sensitive recording equipment in laboratories and MRI machines in hospitals. GFRP, being electro-magnetically inert, is often used in the reinforcement of walls and slabs for rooms housing such sensitive equipment.

2.2 Reinforced Concrete Beam Mechanics

2.2.1 Flexure

While the flexural behaviour of beams is not the focus of this research, the flexural behaviour of RC beams can have significant impacts on the shear behaviour. Therefore, flexural behaviour will be described briefly to highlight areas that will impact the shear behaviour.

Concrete beams are reinforced with steel or GFRP primarily to improve their flexural behaviour. Concrete is a material that is relatively strong in compression but extremely weak in tension. As flexure is applied to the beam the concrete below the neutral axis quickly exceeds its tensile capacity and cracks. Without reinforcement, the crack quickly propagates through the section and causes a sudden, catastrophic failure. Reinforcement is added to provide tensile resistance to the cracked portion of the beam while the uncracked concrete provides the primary compressive resistance. This allows for the formation of a moment-couple that resists flexure.

This composite action is only possible if the reinforcement is fully bonded to the concrete allowing the transfer of stress between the two materials. Therefore, the beam can fail in flexure in three ways: by exceeding the compressive capacity of the uncracked section, by exceeding the tensile capacity of the reinforcement or by exceeding the bond strength of the tensile reinforcement to the cracked concrete. With proper detailing, GFRP longitudinal reinforcement has been shown to provide sufficient bond strength (Okelo & Yuan, 2005; Hao, Wang, Zhang, & Ou, 2007) to ignore the potential bond failure and as such will not be discussed further.

The compressive capacity of the uncracked section is derived from concrete stress behaviour and the composite behaviour of the beam under flexure. Concrete has a non-linear stress strain relationship in compression. The concrete stress-strain behaviour is dependent on the exact composition of the concrete, however many codes recommend the use of the Hognestad parabola to model concrete compressive behaviour. This derivation is dependent only on the concrete strength and is applicable for use in most cases of normal strength concrete.

Due to the differing stiffness and area of the reinforcing material and the concrete compressive zone, the neutral axis of a RC beam is often higher than the midspan of the beam at failure. The exact location of the neutral axis can be determined through a strain compatibility analysis of a section of the concrete.

Using the assumptions of plane strain behaviour (applicable for slender concrete beams), by replacing the concrete compressive zone with an equivalent rectangular stress block, ignoring the tensile resistance of cracked concrete and by assuming a failure mode (concrete controlled or reinforcement controlled) the depth of the neutral axis can be determined with strain compatibility. Beams reinforced with steel are often designed to allow for the steel to yield prior to concrete crushing. This allows for significant ductility in the beam. However, due to the brittle nature of FRP reinforcing materials, FRP reinforced beams are designed for a concrete crushing failure. As such, the depth of the concrete compression block can be determined in accordance with Equation 2.1.

$$a = \frac{\left[\left(A_R E_R \epsilon_c + \sqrt{A_R E_R \epsilon_c}\right)^2 + 4[\alpha_1 \beta_1 f_c' b] A_R E_R d \epsilon_c\right]}{2\alpha_1 \beta_1 f_c' b} \tag{2.1}$$

where A_R and E_R are the area and stiffness of the longitudinal reinforcement, ϵ_c is the compressive strain of concrete at failure, α_1 and β_1 are parameters of the concrete stress block, f_c' is the concrete compressive stress, b is the width of the concrete compressive section, and d is the depth to the centroid of the tensile reinforcement.

The depth of the neutral axis is determined according to Equation 2.2.

$$c = \frac{a}{\beta_1} \tag{2.2}$$

The stress in the longitudinal reinforcement can be calculated according to Equation 2.3.

$$f_r = E_r \epsilon_c \left(\frac{\mathrm{d}}{\mathrm{c}} - 1\right)$$

The final flexural strength can be determined from a moment analysis and calculation of the couple moment according to Equation 2.4.

$$M_r = A_r f_r \left(d - \frac{a}{2}\right) \tag{2.4}$$

The depth of the neutral axis and the overall strength of the beam are proportional to an increase in longitudinal reinforcement stiffness. It is also apparent from the behaviour of composite materials that a decrease in longitudinal reinforcement stiffness causes a decrease in overall beam stiffness. Both of these properties of the flexural behaviour of RC beams impact shear behaviour.

The deflected shape of beams under flexure can be found using integration methods. The stiffness of the beam depends on the depth of flexural cracking and the stiffness of the concrete and longitudinal reinforcement. The moment of inertia of the section varies non-linearly after cracking due to tension stiffening. Methods to account for the changing moment of inertia will be discussed for each design standard.

2.2.2 Shear

The shear behaviour of GFRP RC beams is less understood than the flexural behaviour. Due to the non-yielding nature of GFRP, common models such as the truss model and Modified Compression Field Theory (MCFT) need to be recalibrated. Extensive research has been done on beams with and without stirrups and current models for predicting the shear behaviour of steel reinforced beams accurately predict behaviour of normal size beams with a/d ratios less than 6.5 (Razaqpur & Spadea, 2015). This section will summarize the theory behind the shear behaviour of GFRP RC beams and the research that has been completed thus far.

By taking a section along a shear crack, Figure 2.1 four different mechanisms can be seen contributing to the overall shear resistance of a slender RC beam: the contribution from stirrups, the contribution from the uncracked concrete portion, the contribution from the aggregate interlock along the cracks and the contribution from the dowel action of the reinforcement (Macgregor, 2000).

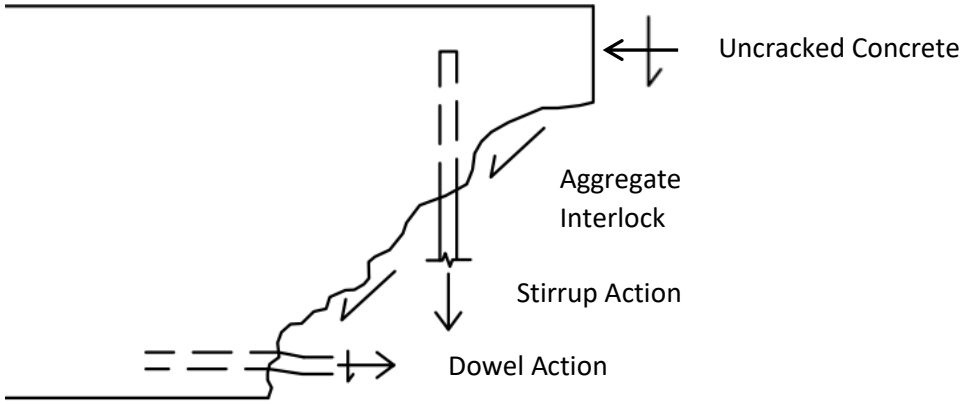

Figure 2.1 – Concrete shear mechanisms

The contribution from stirrups is the resistance to crack opening provided by the transverse reinforcement in the beam. Since crack surfaces are not smooth, and aggregate interlock is present, a crack must widen sufficiently for differential movement along the crack surface. The addition of transverse reinforcement restricts this crack opening. As such, the contribution from stirrups is related to the stiffness, strength and amount of transverse reinforcement used. Additionally, the stirrup contribution tends to increase as the stirrup crosses the crack closer to perpendicular. The stirrup contribution for GFRP transverse reinforcement behaves similarly to the steel contribution. The GFRP reinforcement resists crack opening and develops tensile stresses as a result. Further examination of the behaviour of GFRP transverse reinforcement is discussed in Section 2.4.

The uncracked concrete contribution is the shear carrying capacity of the concrete compressive zone. This concrete can carry significant shear stress as the flexural compression stress keeps the principal tensile stress below the tensile capacity of the concrete. The uncracked concrete contribution is impacted by the depth of the neutral axis and the concrete stress-strain behaviour. In beams with GFRP longitudinal reinforcement, the lower stiffness of the reinforcement causes a reduced uncracked compression zone and reduces its ability to resist shear (Razaqpur & Spadea, 2015).

Aggregate interlock is the resistance to crack differential translation caused by the non-smooth crack surface of the concrete. Due to the heterogeneous nature of concrete and the relative strength of the aggregate compared to the cement matrix for low and mid strength concrete, shear cracks propagate largely around aggregate. This causes resistance to crack sliding and a tendency for increased shear forces to widen the cracks. Aggregate interlock is a complex mechanism that is affected by the concrete mix design, concrete compressive strength and the flexural stiffness of the beam. Beams reinforced with longitudinal GFRP exhibit lower aggregate interlock due to increased crack widths (Yost, Gross, & Dinehart, 2001).

Dowel action is the result of induced tensile forces in the longitudinal reinforcement due to the crack opening and the shear resistance of the longitudinal reinforcement itself. The addition of tensile stress to longitudinal reinforcement necessitates extra care in detailing the longitudinal reinforcement. This is especially true in areas that have lower flexural loads combined with high shear loads. It has been theorized that dowel action in GFRP RC beams will be less than in steel RC beams due to the lower transverse stiffness and strength of GFRP deformed bars (Yost, Gross, & Dinehart, 2001). The exact impact of using GFRP reinforcement on dowel action has not been investigated.

Generally, models for concrete behaviour group the uncracked concrete contribution, aggregate interlock and dowel action into one concrete contribution. This is largely due to the difficulty in separating the effects of the three mechanisms.

Two additional factors have been identified that can impact the shear resistance of concrete reinforced beams. They are the residual tensile stresses across cracks and arch action. The residual tensile stresses occur due to the retention of small portions of concrete crossing small cracks. This causes some of the tensile strength to remain until the crack widens (American Conrete Institiute (ACI), 2000). This effect is noticeable in very shallow beams and is not considered relevant to this research.

Of particular interest to this research is the effect of arch action in concrete beams. Arch action is the ability of concrete to directly transmit loads applied at midspan to the supports through compression. This occurs most noticeably in deep beams and walls where the load can be transmitted with low resultant tensile stresses developing.

RC beams also exhibit arch action. Beams with sufficiently short shear spans will evidence uncracked sections running to the support separated from the rest of the beam by a shear crack. This portion of the concrete acts as a tied arch due to the tensile reinforcement present in RC beams. Research has shown that for a/d ratios less than 2.5, arch action is the dominant method of load transfer. Both CSA and ACI mandate the use of strut-and-tie modelling to design these short beams. For beams with a/d ratios greater than 2.5, CSA and ACI use sectional methods to determine shear strength. Largely, these models only consider arch action implicitly. However, research has shown that arch action contributes up to 20% of the shear resistance in beams with a/d ratios up to 4 (Kim & Jeong, 2011).

2.2.3 Modified Compression Field Theory (MCFT)

MCFT is a method for predicting the shear behaviour of reinforced concrete elements developed by Vecchio and Collins (1988). This theory uses constitutive relationships and material properties to predict the angle of principle compressive stress in a concrete beam and the resultant stresses. In MCFT, failure can occur due to crushing of the compressive struts, by exceeding the sustainable value of the average

tensile stress perpendicular to the cracks in the web and by exceeding the stress at which the crack slips (Macgregor, 2000).

MCFT provides a rational method for calculating the shear capacity of RC beams. As MCFT is the basis for the CSA S806 code provisions for shear design, further details on the use and limitations of MCFT is presented in Section 2.5.1.

2.3 GFRP as Longitudinal Reinforcement

GFRP can be used to produce long bars geometrically similar to conventional steel reinforcement. These bars are manufactured by pultrusion, where spools of glass fibre are pulled through a resin bath and shaped by a die. After pultrusion, a bond mechanism is produced by cutting ribs into the bar, coating with a rough sand finish or some other method to produce a mechanical bond.

By directing the fibres uniaxially, GFRP longitudinal reinforcement is able to use all the benefits of the fibre-resin composite. The overall stiffness of the composite is maximized along with strength. Since the reinforcement is required largely to resist tension loading, GFRP bars are able to satisfy flexural strength requirements for RC concrete. However, due to their significantly reduced stiffness in comparison to conventional steel, concrete members reinforced by GFRP are often governed by deflection constraints. Additionally, GFRP is not very useful as compression reinforcement as the composite does not properly utilize the fibres in compression.

RC members reinforced with GFRP are designed to fail in a concrete-compression controlled failure. GFRP bars are extremely brittle and dissipate very little energy in failure. As such, RC members are designed to keep the GFRP bars from rupture. This approach has two effects. First, it allows for some provision of ductility in the member. Second, the GFRP behaves very similarly to conventional steel over-reinforced members as the steel does not yield in that class of RC member. Therefore, theory and code provisions that govern the design of RC members need only be modified to account for differing material strengths, elastic moduli, and stochastic properties.

Along with the direct effects on flexural design, the use of GFRP as longitudinal reinforcement has significant effects on the shear behaviour of the beam. Studies done by Gross et al (2003) and Yost, Gross and Dinehart (2001) demonstrated a significant reduction in aggregate interlock due to a general increase in deflections. Studies by Gross et al (2003) and Krall (2014) showed some impact of longitudinal reinforcement ratio on the shear capacity of RC beams. This impact was found to be marginal by Gross et al (2003) and only applicable to non-transversely reinforced beams by Krall (2014).

Additionally, the reduced stiffness of GFRP raises the neutral axis of the RC beam at failure. This causes a lengthening in the shear cracks which allows for easier widening as well as reducing the concrete compressive zone that carries shear directly.

Bentz, Massam and Collins (2010) and Acciai et al (2016) demonstrated the flexural behaviour of GFRP beams is well-predicted by current models and therefore the focus of this thesis will be on the shear behaviour of GFRP reinforced beams.

2.4 GFRP as Shear Reinforcement

Due to the thermoplastic nature of the matrix of the GFRP composite, GFRP bars are not bendable post-curing and shear reinforcement must be produced in its final shape. This is in stark contrast to steel

reinforcement that can be bent into shape as needed after production of the straight bars. To create the bent shape of a stirrup, the fibres are often wound through a mold, or around a jig before being bathed in resin. The exact procedure to produce GFRP stirrups varies by manufacturer and is often proprietary.

Straight GFRP bars are loaded unidirectionally in the concrete composite. This allows for the full use of the mechanical properties of the fibres. However, GFRP stirrups suffer a reduction in strength due to the bends in the bar. To transfer forces around the bend, the stirrup must resist transverse loading perpendicular to the fibres. In this direction, GFRP is significantly weaker and relies solely on the properties of the resin material.

Additionally, fibres have been observed to kink or break when bent in a stirrup. This disrupts the flow of stresses around the bend and further reduces the strength of the GFRP stirrup. Typically, the bend strength of GFRP is 40-60% of the straight bar strength, though manufacturers are producing bars that can achieve 70% bend strength.

The significant reduction in strength in GFRP bends has been well documented in research and rupture of stirrup bends is often observed in experimental tests of transversely GFRP reinforced concrete beams (Nagasaka, Fukuyama, & Tanigaki, 1993; Shehata, Morphy, & Rizkalla, 2000; Mahmoud & El-Salakawy, 2012).

Furthermore, the lower stiffness of GFRP stirrups provides less resistance to crack opening. This effect has not been well-studied, as no test specimens with steel longitudinal reinforcement and GFRP stirrups were found in the literature review. Therefore, even though greater crack opening has been observed in beams with GFRP longitudinal and transverse reinforcement the effect was not isolated for GFRP stirrups.

Critically, GFRP stirrups do not behave similar to steel stirrups when used as transverse reinforcement. In standard concrete mechanical theory, steel stirrups are often assumed to be at yield when the shear capacity of a beam is reached. This assumption is critical to solving truss models and it is an underlying assumption of the Modified Compression Field Theory presented by Vecchio and Collins (1988) that is the basis for the CSA shear provisions. However, GFRP bars do not yield and remain elastic until failure. Therefore, the use of GFRP stirrups should exhibit behaviour that differs significantly from that of steel stirrups and require the modification of models. Currently, design codes often treat steel and GFRP reinforcing materials as analogous and introduce various safety factors or conservative estimates to ensure safety. The details of these codes adjustments will be limited to CSA S806-R12 (Canadian Standards Assocation (CSA), 2012) and ACI 440.1R-15 (2006) for the purpose of this thesis.

In the case of design standards based on MCFT, Bentz, Massam and Collins (2010) demonstrated the effectiveness of MCFT predictions of concrete compressive strut angle to beams reinforced with GFRP. With this proven, the majority of design standards adopt a reasonable limit on FRP stirrup strain and use this to analogize FRP shear design to that of conventional steel. The specifics of these code provisions will be discussed in the following sections.

2.5 GFRP Code Provisions

There are many codes that are in use for the design of GFRP RC structures. These include standards produced by CSA, ACI, JSCE and ISO, among others. This thesis will focus on the provisions in CSA S806 “Design and construction of building structures with fibre-reinforced polymers” (Canadian Standards

Assocation (CSA), 2012) and ACI 440.1R-15 “Guide for the design and construction of structural concrete reinforced with fiber-reinforced polymer (FRP) bars” (2006) . These two standards are the governing standards in Canada and the United States for the structural use of FRP reinforcement in concrete with the exception of special cases such as bridges.

The flexural design of FRP reinforced concrete is fairly consistent across different standards. Using the assumptions of plane strain and perfect bond, the standard analysis procedures for steel reinforced concrete apply to FRP reinforced concrete. The principle differences lie in the requirement to avoid FRP longitudinal bar rupture as this explosively releases energy and is an extremely brittle failure. CSA S806 and ACI 440 both limit FRP flexural design to the over-reinforced case. This thesis will focus on the code provisions relating to the shear design of FRP reinforced concrete beams.

2.5.1 CSA S806 Shear Design of FRP Reinforced Concrete Beams

CSA S806 follows similar provisions for the design of FRP reinforced concrete as for steel reinforced concrete. The basis of the provisions is the simplified MCFT developed by Bentz and Collins (2006). MCFT was developed to predict shear behaviour of steel reinforced concrete beams and has the assumptions of plane strain, perfect bond and linear-elastic plastic behaviour of reinforcement. The simplified MCFT has the additional assumption of longitudinal reinforcement yielding.

The factored shear resistance (V_r) of a transversely FRP reinforced concrete beam is defined as the sum of two components as shown in Equation 2.5.

$$V_r = V_c + V_{sF} \tag{2.5}$$

where V_c is the concrete contribution to the shear strength of the beams and V_{sF} is the FRP stirrup contribution to the shear strength of the beam.

This is limited by a maximum value that represents the concrete strut crushing strength defined in Equation 2.6.

$$V_{r,max} = 0.22\phi_c f_c' b_w d_v + 0.5V_p + \left[\frac{M_{dc}V_f}{M_f}\right] \tag{2.6}$$

where ϕ_c is the material resistance factor for concrete, f_c' is the concrete compressive strength, b_w is the concrete web width, d_v is the effective shear depth, V_p is the component in the direction of the applied shear of the effective prestressing force, M_{dc} is the decompression moment, V_f is the factored applied shear and M_f is the factored applied moment.

The concrete contribution, for normal sized members, is determined in accordance with Equation 2.7.

$$V_C = 0.05\lambda\phi_c k_m k_r (f_c')^{\frac{1}{3}} b_w d_v \tag{2.7}$$

where λ is the modification factor for the density of concrete, k_m is the modification for moment interaction defined by Equation 2.8, k_r is the modification factor for the stiffness of longitudinal reinforcement defined by Equation 2.9.

$$k_m = \sqrt{\frac{V_f d}{M_f}} \leq 1.0 \tag{2.8}$$

$$k_r = 1 + (E_F \rho_{Fw})^{\frac{1}{3}} \tag{2.9}$$

This calculation for the concrete contribution to shear is an empirical modification of the provision in CSA A23.3 for steel reinforced concrete members, which for members containing the minimum transverse reinforcement is defined by Equation 2.10.

$$V_c = 0.18\phi_c \lambda \sqrt{f_c'} b_w d_v \tag{2.10}$$

The modifications to the steel reinforced concrete contribution calibrate the equation in line with existing beam tests. This accounts for the reduced aggregate interlock and reduced compressive zone resistance from using a lower stiffness FRP reinforcement material.

The stirrup contribution is unchanged from CSA A23.3 if using steel stirrups and follows Equation 2.11.

$$V_{ss} = \frac{\phi_s A_v f_y d_v}{s} cot\theta \tag{2.11}$$

where ϕ_s is the steel resistance factor, A_v is the area of transverse steel reinforcement, f_y is the steel yield strength, s is the spacing of transverse reinforcement and θ is the angel of the principle compressive stress at the midheight of the section.

If FRP stirrups are used the stirrup contribution is determined according to Equation 2.12.

$$V_{sF} = \frac{0.4\phi_F A_{Fv} f_{Fu} d_v}{s} \cot\theta \tag{2.12}$$

where ϕ_F is the resistance factor for the FRP material being used, A_{Fv} is the area of FRP transverse reinforcement, $f_{Fu}$is the ultimate strength of the FRP transverse reinforcement and is limited to $0.005E_f$, s is the FRP stirrup spacing and θ is the angle of the principle concrete compressive stress at the midheight of the section.

Comparing these two formulations, the FRP stirrup contribution is an empirically modified version of the steel stirrup contribution derived from the MCFT. The formulation varies in two areas: first, the FRP stirrup contribution is reduced to 40% of the equivalent steel contribution; second, the FRP stirrup stress is limited based on the stirrup stiffness. These two adjustments account for the non-yielding nature of FRP reinforcement. Unlike in steel stirrup models, FRP stirrups cannot all be assumed to be carrying the same stress. Therefore, this formulation can be thought of as approximating the average stress in an FRP stirrup at time of shear failure.

CSA S806 contains provisions for the detailing of FRP reinforcement as well. Of particular interest to this research is the maximum FRP stirrup spacing defined by Equation 2.13.

$$s_{max} = 0.6 d_v \cot\theta \leq 400mm \tag{2.13}$$

where d_v is defined as the effective shear depth and θ is defined as the angle of the concrete compressive stress and is defined by the following equation:

$$30° \leq 30° + 7000\varepsilon_1 \leq 60° \tag{2.14}$$

where ε_1 is the longitudinal strain at mid-depth of the section and is calculated as:

$$\varepsilon_1 = \frac{\frac{M_f}{d_v} + (V_f - V_p) + 0.5N_f - A_p f_{po}}{2(E_F A_F + E_p A_p)} \quad (2.15)$$

where N_f is the axial load and V_p, E_f, A_p and f_{po} are parameters related to prestressing.

This is in comparison to the following equation from CSA A23.3-04 for steel stirrups:

$$s_{max} = 0.7 d_v \leq 600mm \quad (2.16)$$

where d_v is defined as the effective shear depth, and θ is defined as the angle of the concrete compressive stress.

No commentary has been provided to justify the spacing of FRP stirrups; however, some reasonable assumptions can be made. $d_v \cot\theta$ is the longitudinal distance that any given shear crack can be expected to span if it runs through the section at the angle θ. Therefore, the provision ensures that a stirrup is crossing every shear crack that would be developed. This determination of crack run is based on the simplified MCFT proposed by Bentz, Vecchio and Collins. (2006). The addition of the $\cot\theta$ factor is unusual. The $0.7d_v$ provision for steel ensures that a stirrup will cross every crack, and the FRP provision includes a lowered requirement of $0.6d_v$ to ensure that the change of material is accounted for.

The effect of this provision is to reduce the stirrup spacing up to:

$$s_{max} = 0.6 d_v \cot 60° = 0.346 d_v \quad (2.17)$$

which is a reduction of approximately 50% from the steel stirrup spacing. This reduction only occurs for beams with low stiffness (i.e. high θ values), though many slender concrete beams reinforced with GFRP have $\theta > 45°$ which results in a reduction of some magnitude. For very stiff beams the spacing is increased to $1.039 d_v$, which exceeds the spacing provided for steel stirrups. It is unclear how much effect this provision has in practice and the literature review did not reveal a significant body of research justifying the change in spacing. As such, it appears that the intention of the provision is to force designers to cross every crack with two stirrups, though no specific rational is given.

The minimum area of FRP shear reinforcement follows closely to the minimum area of steel reinforcement with adjustments for the linear nature of FRP transverse reinforcement. The other provisions governing the use of FRP are similar to steel provisions which allows ease of design by practicing engineers as the calculations are familiar and resemble already known steel design methods.

2.5.2 ACI 440

ACI 440 provides strength provisions for FRP reinforced beams in shear that are similar to steel RC beams with adjustments made for the reduced stiffness of FRP and the differing behaviour of FRP stirrups. The strength provisions use a similar structure to CSA S806, with the total nominal shear resistance V_n equal to the sum of the concrete contribution, V_c, and the FRP stirrup contribution, V_f where V_c and V_f are calculated according to Equations 2.18 and 2.19 respectively.

$$V_c = \frac{2}{5}\sqrt{f_c'} b_w (kd) \quad (2.18)$$

where V_c is the shear resistance contribution from the concrete, f_c' is the concrete compressive strength, b_w is the width of the concrete web, k is the ratio of depth of neutral axis to reinforcement depth and d is the depth to the centroid of the tensile reinforcement.

$$V_F = \frac{A_{fv} f_{fv} d}{s} \tag{2.19}$$

where V_F is the shear resistance contribution from the FRP stirrups, A_{fv} is the area of transverse FRP reinforcement, f_{fv} is the ultimate stress level in the transverse reinforcement and is limited to $0.004E_{fb}$ d is the depth to the centroid of the tensile reinforcement and s is the spacing of the shear reinforcement.

The ACI 440 model for shear strength is largely based on the ACI 318 truss model and has been empirically calibrated for FRP reinforced beams.

ACI 440 provides a maximum stirrup spacing of d/2 or 600 mm, whichever is less, to ensure each crack is intercepted by a stirrup. This matches exactly the provision for steel stirrups.

2.6 Experimentation Validation of Code Models

Much work has been undertaken to experimentally validate the models for GFRP reinforced beam behaviour in both shear and flexure. The experiments vary significantly in purpose, material and setup. This section presents an overview of the existing work done on developing and evaluating the current code models.

2.6.1 Flexure

Studies done by Ascione et al (Ascione, Mancusi, & Spadea, 2010), Alsayed (Alsayed, 1998) and Krall (Krall, 2014) have demonstrated that the GFRP-concrete composite performs as expected under flexural loading. This follows from the simplicity of the concrete model for flexure. The only assumptions that need to be made are plane-strain and low deformations. As such, for the majority of beams, GFRP reinforcement behaves similarly to steel reinforcing before yield.

Due to the high level of confidence in the current GFRP flexural models, as well as the serviceability issues that arise from using GFRP in more slender beams, the flexural behaviour of GFRP beams is not the focus of this research.

2.6.2 Shear

The shear behaviour of beams reinforced with FRP reinforcement is not understood as thoroughly as the flexural behaviour. This is due partly to the relatively recent advent of FRP as internal reinforcement as well as the complexity of the mechanisms behind shear action in RC beams.

In general, experimental verification of the shear models for FRP reinforced beams is limited in size and scope. Very few tests have been conducted when compared with test on steel reinforced specimens, and the majority of theory has been adapted from existing steel theory. Additionally, a large portion of the beams were quarter-scale or smaller, and very few had a/d ratios greater than 4.

By compiling a list of shear tests of FRP beams, 178 specimens were found to be tested. Of these, only 78 had some form of transverse FRP reinforcement. These specimens varied in size, type of GFRP and

purpose for research. Additionally, the vast majority of the beams tested had a/d ratios less than 4.5 and the beams with great a/d ratios either did not use GFRP shear reinforcement or had cross sections smaller than 150x200 mm.

Razaqpur and Spadea (2015) also compiled a list of FRP test specimens and found 391 specimens, 117 with transverse FRP reinforcement. These test specimens had a maximum a/d ratio of 6.5 for the non-transversely reinforced specimens and 4.12 for those with transverse GFRP reinforcement.

In the majority of studies investigated, a significant portion of the tested specimens failed due to rupture of the FRP stirrup at the bend. These stirrups were intercepted by shear cracks at the location of the bend. These failures were often catastrophic and reduced the overall shear capacity of the beams. However, most of the failures occurred within the acceptable range of variation for shear tests and did not appear to limit the models developed from the results.

Strength predictions have been largely validated by numerous studies, however the exact accuracy of the models varies. Studies in the last 10 years have concluded that the existing models are accurate (Bentz, Massam, & Collins, 2010), overly conservative (Al-Khrdaji, Wideman, Belarbi, & Nanni, 2001) (El-Sayed, El-Salakawy, & Benmokrane, 2006) or non-conservative (Ascione, Mancusi, & Spadea, 2010). This is largely to be expected as the stochastic nature of concrete combined with the variability of FRP between manufacturers creates a spread in results. This is largely accounted for in FRP codes and standards with low resistance factors. The aggregate analysis by Razaqpur and Spadea (2015) demonstrates that the existing models provide good estimates of strength.

Bentz, Massam and Collins (2010) proved the applicability of the MCFT model for predicting the angle of the concrete compressive strut in GFRP RC beams. This analysis was based on the existing database of GFRP beams, but in all cases examined the MCFT predictions were reasonably accurate. This allows the application of the simplified MCFT to shear design using GFRP transverse reinforcement.

In general, the existing FRP RC shear models have been proven to apply for normal sized sections that are relatively short. Additionally, relatively few tests have been conducted on beams with FRP stirrups and many of those tests suffered from stirrup ruptures that may be avoidable with advances in technology or detailing. Indeed, Bentz, Massam and Collins (2010) posited that by detailing the stirrup bends to lie below the depth of the longitudinal reinforcement stirrup bend rupture can be avoided.

Additionally, the effects of arch action have largely been ignored by researchers studying the shear behaviour of slender beams. When examining the database of experimentally tested beams, less than 10 beams have been tested with a/d ratios over 4.5, and these beams are all quarter-scale. Therefore, if arch action in FRP reinforced beams is similar to that in steel reinforced beams, the influence of arch action will be implicitly included in the empirically calibrated strength models. The major focus of this research is to investigate the suitability of sectional design methods for beams with a/d ratios over 4.5 where arch action is essentially negligible.

2.7 FEA Modelling of GFRP Reinforced Beams

A large part of the difficulty with determining appropriate formulations and theories for the shear behaviour of FRP reinforced concrete beams is the lack of available research and specimens. FRP use in civil engineering is relatively new, and the products being used have rapidly improved in the last decade. This can most easily be seen in the change from bend strengths of GFRP stirrups of 45% (Nagasaka,

Fukuyama, & Tanigaki, 1993) of straight portion strength to approximately 70% of straight portion strengths (Mohamed & Benmokrane, 2016), though those changes vary on the size of the stirrup.

The studies that have been conducted to investigate the effects of replacing a linear-elastic-plastic material with a strictly linear-elastic material are generally limited in size and scope, with peer reviews revealing less than 200 total specimens with transverse shear reinforcement being tested and published. As such, researchers have attempted to expand upon the limited database by conducting parametric studies using FEA (Stoner, 2015) (Barrage, 2017).

FEA analysis of beams is not based on the same beam level mechanical theories that provide the basis for code designs. Instead, it uses material properties along with constitutive relationships to numerically estimate the behaviour of a GFRP reinforced concrete beam. Models are developed for a given beam or set of beams and calibrated using existing beam databases. These models are then used to simulate testing of hundreds of beams, enabling the performance of parametric studies that would be considered financially infeasible or impractical.

Stoner (Stoner, 2015) developed a FEA model of GFRP reinforced beams for use in parametric studies. This model uses the Concrete Damaged Plasticity Model in ABAQUS to form the constitutive relationships for concrete along with a smeared membrane model for the GFRP stirrups. This model was calibrated using the tests done by Krall (2014).

Barrage (2017) conducted a parametric study using a version of this model which indicated that GFRP shear reinforced beams vary significantly from steel shear reinforced beams with increasing a/d ratio. The results showed that beams with transverse GFRP reinforcement experienced shear controlled failures up to an a/d ratio of 9.5, higher than the expected shear-to-flexure transition of 7.5 predicted by CSA S806. Additionally, the strength provisions of CSA S806 were found to underestimate the shear capacity of slender beams. Barrage (2017) theorized that this was due to additional confinement provided by GFRP stirrups that is not accounted for in the CSA S806 model.

Based on the results of these parametric studies, Barrage recommended experimental tests to validate the modelling and investigate the effect of slenderness of the behaviour of FRP reinforced beams.

The FEA models used by Stoner and Barrage have potential limitations. The models were able to accurately predict behaviour of beams similar to those used for model calibration. These beams had similar sizes and slenderness. It is unknown whether modelling high-slenderness beams will produce similar results as no specimens were able to be used as measures. Additionally, FEA models in general have a tendency to overestimate the stiffness of the reinforced concrete load-displacement response even for the beams with similar parameters to the calibration set. Finally, the models used by Stoner and Barrage use a smeared membrane method for modelling FRP stirrups. This method is unable to take into account the failure of stirrups at bends, a failure method commonly observed in experimental programs.

CHAPTER 3 - RESEARCH METHODOLOGY

3.0 Governing Design Principles

Three overall principles govern the design of the research program: the extension of previous work performed by at the University of Waterloo, the verification of current GFRP RC mechanical theory for beams outside the set of existing test specimens and the verification of the FEA models and parametric studies performed by Stoner (2015) and Barrage (2017).

3.0.1 Extension of Previous Work

First, many of the research design decisions are made to ensure that this research functions as a continuation of work done by Krall (2014), Stoner (2015) and Barrage (2017). As such, the beam cross-sectional design matches one set of beams tested by Krall. This ensures that the results will be easily comparable to the studies conducted by Stoner and Barrage. Additionally, the test program will investigate the shear-flexure transition ratio of 9.5 proposed by Barrage.

3.0.2 Verification of GFRP Reinforced Concrete Mechanical Theory

Second, the program specimens were selected to allow insight into whether current GFRP-concrete composite mechanics assumptions are valid. This largely includes ensuring that the test specimens lie outside the range of already tested specimens. The majority of specimens that have been tested have an a/d ratio of less than 4.5. Therefore, this research program will focus on beams with a/d ratios larger than 4.5. Additionally, the parametric study done by Barrage (2017) indicates that the shear-flexural transition zone is identified incorrectly in existing models. Using the section chosen from Krall and a stirrup spacing of 150 mm, CSA S806 predicts a transition from shear controlled failure to flexure controlled failure at an a/d ratio of 8. Therefore, the specimen set is designed to capture this region to investigate whether the code prediction is correct.

3.0.3 Verification of FEA Analysis

Finally, the program aims to verify the results of work done by Stoner and Barrage to use FEA analysis to extend existing specimen databases. The specimens tested will be compared to the existing FEA models produced for the parametric studies performed by Barrage. As such, to reduce the likelihood of influence from factors that were unconsidered in the construction of those models, the test specimens vary primarily by the parameters that were studied by Barrage. This includes the spacing of GFRP stirrups and the slenderness of the beams.

3.1 Specimen Variables

3.1.1 a/d Ratio

The primary variable of study is the effect of a/d ratio on the flexural behaviour of GFRP beams. The range of a/d ratio is chosen to continue the tests done by Krall (2014), investigate the shear-flexural transition zone and test the results of the parametric studies done by Barrage (2017).

For the cross-section used in this research, this region corresponds to an a/d ratio of 8. Previous work by Krall focused on beams with an a/d ratio of 3.5. The larger body of research tested beams with a/d ratios up to 4.5 for transversely reinforced beams. FEA analysis performed by Barrage indicates that the

beams should be experiencing a primarily shear-controlled failure up to an a/d ratio of 9.5. To allow for integration with existing GFRP beam datasets as well as investigating the anticipated shear-flexural transition zone, beams varied in a/d ratio from 4.5 to 10.5. This corresponds to an overall beam span from 2430 mm to 5670 mm.

3.1.2 Presence of GFRP Stirrups

To examine the effects of GFRP stirrups on flexural behaviour while controlling for the effects of GFRP longitudinal reinforcement, non-shear reinforced beams are used as control specimens. This also allows the expansion of the GFRP beam database to aid in FEA tuning and the isolation of the concrete contribution for slender beams.

3.1.3 Stirrup Spacing

Stirrup spacing is selected based on the provisions in CSA S806 (Equation 2.12). Using these provisions, for the given design depth of 270 mm, the stirrups are limited to a spacing of 89 mm at an a/d ratio of 10.5. For an a/d ratio of 4.5, the required spacing is 123 mm. A further analysis of the code provisions can be found in Section 2.5.

This is a tight spacing and is limiting to the use of GFRP stirrups. Additionally, there are potential constructability issues posed by the use of 89 mm spacing, as concrete flow and consolidation around the stirrups can be impeded if the aggregate size is large or if the workability of the concrete is low.

As a second test variable, specimens differ on stirrup spacing. Specimens with stirrup spacing of 89 (90) mm are constructed for a/d ratios of 4.5 and 6.5. This corresponds to the maximum spacing allowed for the most slender of the specimens. These were not continued for a/d ratios of 8.5 and 10.5 for practical purposes as the number of stirrups required to provide that spacing made construction of the specimens difficult.

3.1.4 Concrete Design

To match existing test data and FEA parametric studies, the concrete strength is to be as close to 52 MPa as possible. This allows direct comparison of the results of previous studies. Additionally, 50 MPa is within the range of common concrete strengths used in RC construction.

Since the smallest stirrup spacing is 90 mm, a small aggregate size of 10 mm is desired to ensure proper consolidation around the stirrups. This also matches with previous work done by Krall (2014).

3.2 Materials

3.2.1 Longitudinal Reinforcement

The longitudinal reinforcement (Figure 3.1) was provided by Schoek Combar. The longitudinal GFRP had a nominal diameter of 16 mm with a guaranteed tensile strength of 1000 MPa with an elastic modulus of 64 GPa. The bars are produced through pultrusion using E-CR glass fibre and a vinylester resin matrix. Ribs are cut into the bars to provide mechanical bond.

3.2.2 Transverse Reinforcement

The transverse reinforcement was supplied by B&B FRP. The stirrups are produced using E-CR glass and a vinylester resin. The stirrups are manufactured by filling a High Density Polypropylene sheath with the fibres and resin. This sheath is then wound around a jig to provide the desired shape. Individual stirrups are cut from the continuous wound bar. The ribs are produced by the pressure from the sheath. An example stirrup with the sheathing removed at one portion to show the underlying bar can be seen in Figure 3.1.

Figure 3.1 – GFRP stirrup with bend protector removed

A test regimen was carried out by Mohamed and Benmokrane (2016) that found a straight portion strength and stiffness to be 800 MPa and 45 GPa respectively. Additionally, the bent portion strength was approximately 70% of the straight portion strength.

3.3 Specimen Design

3.3.1 Section Design

The specimen cross section followed the BM 16 series of beams tested by Krall (2014). Six longitudinal bars were used in two rows of reinforcement with a design depth of 270 mm (Figure 3.2).

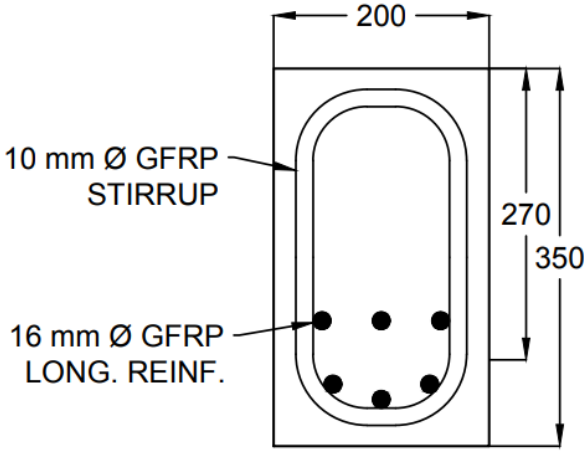

Figure 3.2 – Design cross-section

This design provides a nominal flexural capacity of approximately 130 kN·m according to CSA S806. The flexural failure mode is compressive crushing of the concrete in the flexural compression region.

Stirrup spacing was varied with specimens designed with no stirrups, stirrups spaced at 90 mm and stirrups spaced at 150 mm.

3.3.2 Slenderness and Specimen Details

The research program consisted of the construction and testing of 10 specimens. The specimens varied in transverse reinforcement and a/d ratio.

The full selection of specimens can be seen in Table 3.1. Capacity and failure modes are predicted using CSA S806.

Table 3.1 – Specimen details

Specimen	a/d	Stirrup Spacing (mm)	Peak Load - CSA S806 (kN)	Failure Mode - CSA S806
BM 4.5-N	4.5	N/A	109.0	Shear
BM 4.5-90		90	170.5	Shear
BM 4.5-150		150	149.7	Shear
BM 6.5-N	6.5	N/A	90.7	Shear
BM 6.5-90		90	144.5	Shear
BM 6.5-150		150	127.0	Shear
BM 8.5-N	8.5	N/A	80.3	Shear
BM 8.5-150		150	110.4	Flexure
BM 10.5-N	10.5	N/A	80.3	Shear
BM 10.5-150		150	86.0	Flexure

3.4 Specimen Construction

3.4.1 Formwork

A single gang-form was constructed for the specimen casting. This form can be seen in Figure 3.3**.** Forms were constructed to an out of straightness tolerance of 1/500. Forms were constructed from 3/4" one-sided formply, with all walls being double sheathed to allow lap splicing and provide strength. A floor and subbase was constructed from standard 4’x8’ plywood sheets covered with formply. 2x4 kickers were provided at one foot intervals around the exterior of the form to brace against movement and form-buckling. Every specimen was formed with an additional one meter overhanging portion on either side of the support to ensure full anchorage of the longitudinal reinforcement.

Figure 3.3 – Gang form for specimen casting

3.4.2 Cages

The reinforcement cages used plastic ties to conform to procedures followed by Krall (2014) and general industry best practices for GFRP cages (Figure 3.4). Black-nylon zip ties were utilized. These ties largely performed as expected, though occasional breakages occurred due to the brittle nature of black nylon. These observations are in line with those recorded by Krall.

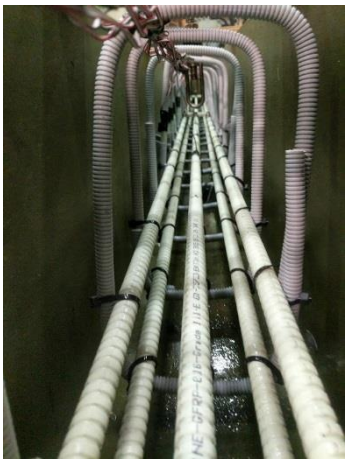

Figure 3.4 – GFRP cage in formwork with instrumentation

Cages with stirrups were tied without the use of compression reinforcement. While this is not the standard construction practice, the two layers of tension reinforcement allowed for cage rigidity and the lack of compression reinforcement allowed for easy specimen post-mortem investigation.

Cages without stirrups used short, evenly spaced transverse pieces of GFRP bar to tie each row of longitudinal reinforcement. These bars were added after a significant lack of rigidity was observed with the longer cages. Due to the remedial nature of these additions, the bars were tied with standard steel tie wire. Neither of these changes from the original design program are expected to have significant impact on the results of the experiments.

3.4.3 Concrete Cast

Beams were cast from longest to shortest, with the order of cast for each series being BM XX-150, BM XX-90 BM XX-N.

The concrete was placed using a crane and hopper to move mix from the supplied ready mix truck into the forms in the lab. Due to the geometric constraints of the lab and the formwork, this pour took place from 13:00 to 15:15 on March 7, 2019. Surface finishing was completed by 4:15. Due to the length of the pour, additional super plasticizer was added to the concrete approximately halfway through the cast, after beams BM 10.5-150, BM 10.5-N and BM 8.5-150 were already poured.

Concrete slump was measured at the beginning of the pour as 135 mm (5 3/8”). Air entrainment was not measured on site, as it was not of primary importance to the research.

3.4.4 Cylinders

Sixty concrete cylinders were prepared per CSA A23.2. All of the cylinders were prepared from the initial batch of concrete, before the addition of the extra super plasticizer. Cylinders were prepared to have five cylinders available for 7-day, 28-day and test day compressive strength tests. The results of the cylinder tests for compressive strength can be seen in Table 3.2.

Table 3.2 – Concrete compressive strengths

Days Elapsed	Specimen Tested	Concrete Strength (MPa)
7	N/A	39.3
28	N/A	50.2
40	BM 4.5-N	50.6
41	BM 4.5-90	50.3
48	BM 4.5-150	50.7
53	BM 6.5-N	50.7
60	BM 6.5-90	50.6
62	BM 6.5-150	51.0
64	BM 8.5-N	54.3
68	BM 8.5-150	53.5
70	BM 10.5-N	54.2
75	BM 10.5-150	51.1
Average Strength of Tested Specimens		51.7

3.4.5 Construction Issues

During construction of the formwork, geometric irregularities emerged. These included longitudinal out-of-straightness, warping of the formply and gaps in the form joints. The majority of these issues resulted from a combination of the length of forms being constructed and the relative inexperience of the constructor. However, the longitudinal out-of-straightness and formply warping were found to be within

reasonable limits and did not affect the final behaviour of the beams during testing. Additionally, the form joints were sealed with a silicone based caulking to prevent the accidental joining of specimens and the loss of concrete or water through leaks. The lasting effect of these irregularities is that the specimen height was approximately 5-10 mm greater than designed, as seen in the image of BM 10.5-90 below. This change in specimen geometry (and associated change in depth) was taken into account in the analysis of the beams and the expected capacities were recalculated.

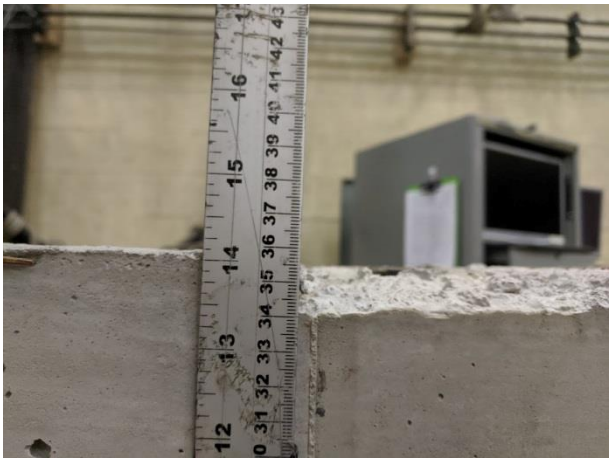

Figure 3.5 – Increase in specimen size

Additional issues were encountered during the tying of the GFRP cages. First, the stirrups that were used were not of strictly uniform shape or dimensions as result of the production process. As such, the cages were very time-consuming to construct, and the exact depth of the reinforcement varied slightly along the length of the beam. Additionally, the stirrups were unable to be oriented completely vertically. This was due mainly to the out-of-straightness of the stirrups themselves. These issues were more pronounced in the cages with 90 mm stirrup spacing. Specimen post-mortems were conducted to examine the effect of the stirrup out-of-straightness and no differential movement or failure of these stirrups was observed.

Also, due to the length of the pour, the concrete was significantly less viscous by the end of the pour. As such, two primary issues occurred. The first was improper concrete consolidation. This was due to concrete stiffening as well as misapplication of concrete vibration. This was observed on the end cantilevers of BM 4.5-N (Figure 3.6). However, as these portions of these beams lie outside the critical shear span area, the effect of the cavities can be ignored.

Figure 3.6 – Areas of localized cavities due to lack of consolidation in BM 4.5-N

The second, more critical, issue observed was the reduction in concrete area around anchor points and strapping. During finishing, concrete strapping was not removed due to concerns about form wall buckling. This led to trapped air pockets beneath the strapping resulting in a reduction of concrete on the compression surface of the beams. This issue could have been avoided with proper vibration and the removal of strapping as the concrete set. For the majority of the beams, these problem areas lie outside the shear span. However, for BM 4.5-N patch repairs were required (Figure 3.7). The affected area was first ground down to the matrix, all dust and material was removed, and a non-shrink grout patch was set in place of the missing concrete.

Figure 3.7 – Missing compressive concrete in BM 4.5-N

Patches were only required for BM 4.5-N. The patch was not observed to have failed during testing.

Finally, the finishing on the top surface of the beams was poor. This was due to the inexperience of the finishers as well as the presence of strapping and anchors. Where it was needed, sharp edges and large areas of concrete extrusion were ground off to provide a more uniform surface and avoid stress concentrations.

3.4.6 Instrumentation

Internal instrumentation was prepared and applied during the construction of the specimens. Instrumentation included longitudinal strain gauges on the top middle bar of the longitudinal reinforcement at one-quarter, one-half and three-quarters shear span length on all beams. Additionally, beams with transverse reinforcement had strain gauges on the first stirrup on either side of the one-quarter, one-half and three-quarters shear span points. In total, there were three internal strain gauges on beams with no shear reinforcement, and nine internal gauges on beams with shear reinforcement (Figure 3.8).

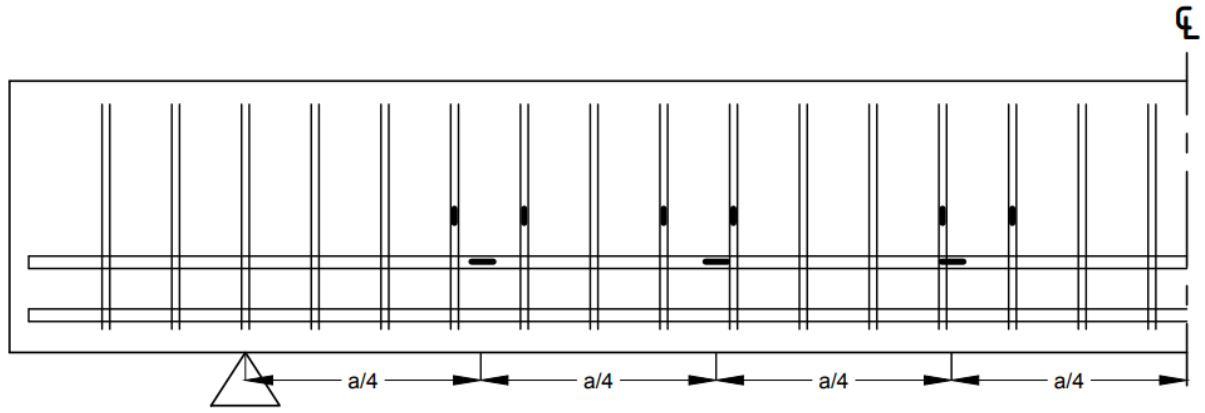

Figure 3.8 – Location of internal strain gauges

Strain gauges were applied using the prescribed supplier methods before tying the reinforcement cages. This was done as access to the reinforcement is heavily limited after the cages are tied due to the small size and tight spacing of the cages. Any gauges damaged during tying or cage placement were replaced before casting.

Gauge leads were run out of the top of beams without shear reinforcement, and longitudinally through the compression zone of beams with shear reinforcement. After seven days of curing, gauges were tested to determine if they were damaged or rendered inoperable during the pour. Of the 66 internal strain-gauges, two gauges were determined to be completely inoperable after casting. Further damage to gauges and leads was discovered during testing and is discussed in the observations sections for each beam.

Additionally, eight external displacement measures were used during testing. Displacements were measured vertically at quarter-span and half-span locations, with two string pots measuring displacement on either side of the beam, for a total of six vertical displacement measurements. Also, two externally mounted string pots were attached at the quarter-span locations to provide a measure of concrete shear displacement. These pots were moved to the eighth span location on BM 10.5-N and BM 10.5-150 as the critical shear region was located closer to the midspan on those specimens.

3.5 Testing

Testing was done in opposite order of casting. Testing began with BM 4.5-N, proceeded to BM 4.5-90 and so forth util BM 10.5-150.

3.5.1 Test Setup

Beams were tested under single point loading at the centre span of each beam. This was done to match the previous tests by Krall and to ensure that a/d spans of 10.5 were geometrically feasible to test. Support conditions were roller-pin. The beam setup, including support condition and instrumentation location, can be seen in Figure 3.9.

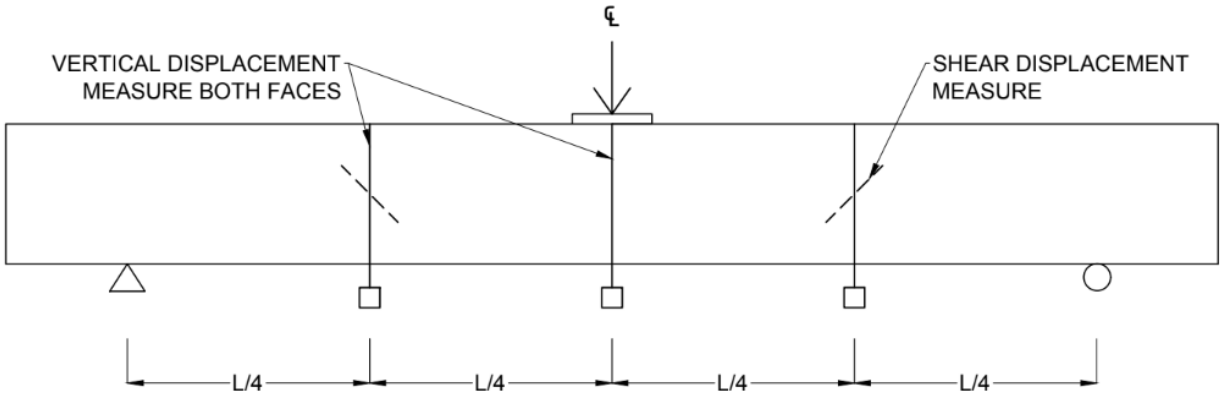

Figure 3.9 – Location of internal strain gauges

String pots were used to measure deflection at quarter and half-span locations along the beam. Pots were attached to aluminum bars mounted directly to the top surface of the concrete, with an overhanging distance to allow for protection of the string pots and the measurement of displacement on both sides of the beam. A total of six string pots were used to measure displacement on the beam.

Additionally, string pots were attached to the exterior lateral surface of the beam to measure concrete shear strain. These pots were rotated at 45° to the horizontal in order to capture overall concrete shear stresses for FEA model validation. These pots were only attached on the West side of beams so as to not interfere with the crack tracking on the East face of the beams.

A load plate (200mm x 400 mm) was attached to the top face of the beam at midspan to facilitate testing. This plate was attached with HydroStone, a quick setting cementitious product produced by USG, and preloaded with 1 kN of force to ensure proper levelling and set. The load plate also doubled as the attachment location for the midspan displacement pots.

3.5.2 Test Equipment

The tests were performed using a Uniroyal Test Frame, with a maximum load capacity of 250 kN and a maximum deflection capacity of approximately 350 mm. Strain gauge, string pot and frame output data were recorded using a single DAQ connected to a Windows 7 workstation.

3.5.3 Beam Handling

Due to the length and a/d ratio of the test specimens, extra care was taken during handling to ensure that the beams were not damaged or significantly cracked prior to testing. Lift anchors were placed at third-points along each beam to prevent cracking due to lifting. Additionally, at no time prior to testing were beams unsupported over a distance longer than the test span length.

3.5.4 Data Collection

Three streams of information were collected, two of which were combined in a single output program. First, the input load and displacement was measured directly from the test frame on a separate workstation that controlled the frame. This allowed redundancy of load-displacement data in case of loss of results. This data was sampled at 1 Hz. Frame load and displacement measured directly from sensors on the frame, along with string pot displacements and internal strains, were measured together through the DAQ. This data was sampled at 100 Hz.

Crack tracking was performed on all beams tested, with cracks being tracked at three load intervals before failure. The load intervals were arbitrarily selected to allow for examination of crack propagation, with the last load interval being 70% of the expected failure load to allow for safe loading conditions. Cracks were drawn and measured by hand as well as photographed for redundancy in measurement.

Select beam tests were recorded in full using a GoPro camera. This was done to allow for better examination of failure modes due the brittle failures of GFRP reinforced beams.

CHAPTER 4 - EXPERIMENTAL RESULTS

4.0 Test Procedure

All beams were tested in a three-point bending, uni-directional static test with variable load rate, following the test procedure laid out in Krall. All specimens were tested using displacement controlled loading rates. The load rates were matched with those used by Krall, with rates being adjusted for increased a/d ratio using the following formula.

$$NewRate = OldRate * \left(\frac{NewLength}{OldLength}\right)^2 \quad (4.1)$$

where $NewRate$ is the load rate used in the testing program, $OldRate$ is the load rate used by Krall, and the lengths are corresponding lengths of specimens tested.

Since the load rate is specified in mm of vertical deflection per minute, and the flexural stiffness of a beam is inversely proportional to the square of its length, the rates are adjusted by the square ratio of the respective beam lengths. This ensures a similar rate of stress application to the concrete as that used by Krall. The load rates for a given length of beam can be seen in Table 4.1.

Table 4.1 – Specimen testing loads and load rates

Specimen	Safe Testing Load (kN)	Load Rate 1 (mm/min)	Load Rate 2 (mm/min)	Load Rate 3 (mm/min)
BM 4.5-N	78.2	0.54	0.72	2.88
BM 4.5-90	148.0			
BM 4.5-150	126.2			
BM 6.5-N	64.8	0.78	1.04	4.16
BM 6.5-90	106.8			
BM 6.5-150	106.8			
BM 8.5-N	57.4	1.02	1.36	5.44
BM 8.5-150	81.6			
BM 10.5-N	57.1	1.26	1.68	6.72
BM 10.5-150	66.1			

In general, the load rate is slow up to a nominal load to allow for identification of any unexpected behaviour and observation of the uncracked and cracked behaviour of the beam. The load rate is then increased to allow testing in a reasonable time frame while remaining slow enough to see low relaxation when the testing is halted for crack tracking. This load rate is kept until 70% of the expected ultimate strength of the beam at which point safety measures are implemented to keep clear of the beam until failure. These measures are necessary due to the possibility for sudden explosive failure due a GFRP bar rupture and the slenderness of the specimens. After 70% of the ultimate load is reached, the load rate is increased a final time to test until failure.

Beams were tested up to failure, with failure being defined as the sudden and brittle loss of strength associated with the concrete-controlled failure of GFRP reinforced beams. In case of more ductile

behaviour, testing was continued until a post-peak reduction of at least 20% was reached or a noticeable second peak behaviour was observed. Select beams were tested to catastrophic failure to provide sample data to compare with post-peak FEA results, however due to concerns about damage to testing equipment this procedure was limited to beams BM 6.5-150, BM 8.5-150, and BM 10-150. BM 10.5-N also failed catastrophically due to a sudden shear collapse.

4.1 Measured Parameters

4.1.1 Peak Load

Peak load was measured in two data streams. The controller for the testing machine measured the inputted load and displacement at rate of 10 Hz. The testing machine also outputted from the load cell load and displacement data at 1000 Hz. These two streams of data largely correlated with each other, with a difference of under 5% in all cases. In the cases of BM 8.5-N, the data outputted through the DAQ (load-displacement, strain gauges and external displacements) were lost during testing. As such, the peak load was determined based on the data from the controller.

4.1.2 Angle of Principle Compressive Stress

After testing, the principal shear crack was identified on beams that exhibited shear controlled failure and the inclination at mid-depth was measured from records post testing. This angle is an approximation of the angle of principle compressive stress used in MCFT.

4.2 General Observations

4.2.1 Cracking

Every specimen exhibited severe cracking prior to failure. Cracking began at midspan with flexural cracking, but all specimens showed a combination of flexural and shear cracking at failure. Crack tracking sheets up to the beam safe load along with beam failure crack patterns can be found in Appendix A.

4.2.2 Longitudinal Strains

Internal strain gauges captured the longitudinal strains. After sufficient cracking, longitudinal strains followed expected trends with the strains varying exponentially with distance from load application.

During loading, especially of beams without shear reinforcement, noises occurred indicating slipping and resettling of reinforcement. This behaviour was captured by certain strain gauges and is discussed in the observations for each beam.

4.2.3 Stirrup Strains

In general, stirrups closer to the critical shear region adjacent to the load application experienced higher strains. There is a significant degree of variability in the observed stirrup strains, though there is a clear pattern that the strains increase significantly with proximity to the critical shear region.

4.2.4 Shear Displacement

The exterior string pots used to capture concrete shear displacements did not provide meaningful data. Little data was captured unless the measurement crossed a crack which only occurred in select beams. In those cases, the shear displacement increased with increased flexural displacement but the data trends varied significantly by beam and crack location. As such, the shear displacement data will not be discussed in detail but can be found in Appendix C.

4.2.5 Failure Mode

Beams generally followed expected trends for failure modes with a transition from shear-controlled to flexure-controlled failure being observable. No longitudinal or transverse reinforcement was observed to fail. After testing, all beams that contained transverse reinforcement and that failed in a brittle manner were dissected to determine if the transverse reinforcement was intact. In all cases, transverse reinforcement as found intact with no evidence of slippage or fracture. A typical section from BM 6.5-150 at the critical region is shown in Figure 4.1. The sections were made by cutting through the beams with a handheld concrete saw and the stirrup was removed from this section. Before removal, the stirrup showed no evidence of rupture or of bond breaking. Additional, examination of the concrete around the stirrup location showed no evidence of crushing, cracking or deformation indicative of localized bond failure.

Figure 4.1 – Typical post-failure section at critical shear region

Due to the usage of single point load application to increase beam slenderness, flexural crushing failures and shear strut crushing failures occurred at the same location. Therefore, crack patterns at failure and post-peak behaviour are used to determine which mechanism controlled failure.

4.2.6 Post-Peak Behaviour

All beams reinforced with transverse reinforcement demonstrated some post-peak strength. In beams with increased slenderness, this behaviour can be described as two-peak behaviour where after an initial sudden loss of strength the beam resists increasing load until a second peak is reached.

In all cases, the initial peak load remained the highest load resisted by the beam. Most specimens were not tested to catastrophic failure as that was not the purpose of this research and to protect lab equipment. Testing was halted for most specimens after a clear second peak or ongoing trend of losing strength was reached.

4.2.7 Naming Conventions

Gauges and displacement measurements are labelled based on their distance from the nearest support. Therefore, a longitudinal gauge located at the one-quarter shear span location is labelled a/4. Additionally, for stirrups which have two gauges located one either side of each longitudinal location, the stirrups are labelled N and F for there proximity to the load application. Therefore, the stirrup farthest from midspan is labelled a/4-F, while the closest stirrup is labelled 3a/3-N,

4.3 BM 4.5 - N

4.3.1 Load Displacement and Failure

BM 4.5-N had a shear span of approximately 1.22m and had no transverse reinforcement. The specimen failed in a classic shear-controlled crack pattern with symmetrical cracking appearing on both sides of the load application which can be seen in Figure 4.2. The specimen cracking allowed a continuous strut to run to the support from point of load application. This behaviour is indicative of the influence of arch action on the beam. The angle of inclination of the critical shear crack corresponding to the angle of the principal compressive stress was measured at 45°.

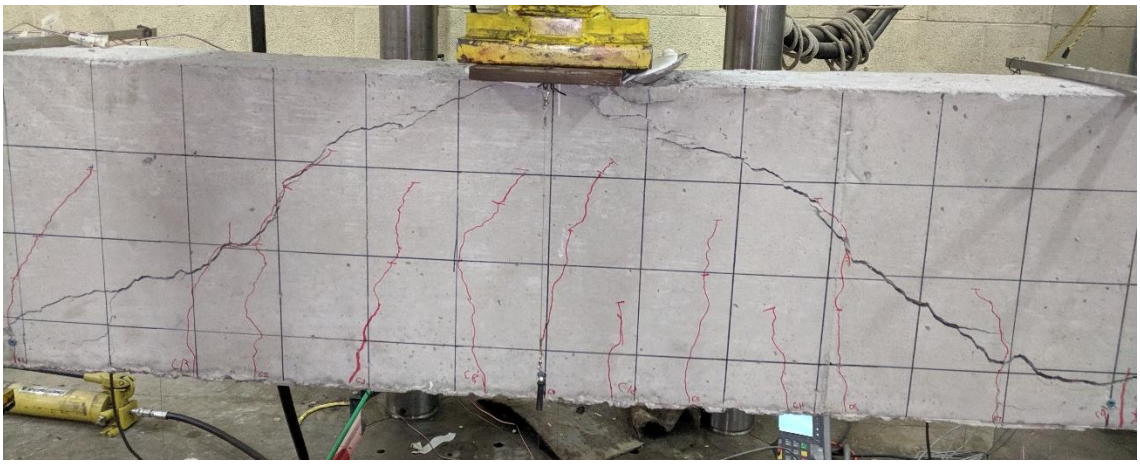

Figure 4.2 – BM 4.5-N: Crack patterns at failure

BM 4.5-N reached a peak load of 107.96 KN. This peak load corresponded to a displacement of 12.59 mm.

The specimen exhibited an approximately bilinear bending behaviour as shown in Figure 4.3. The cracking load can be estimated from the load displacement curve as around 25 KN. As cracking intensified, the beam displayed significant sudden load relaxation associated with bond slip of longitudinal reinforcement.

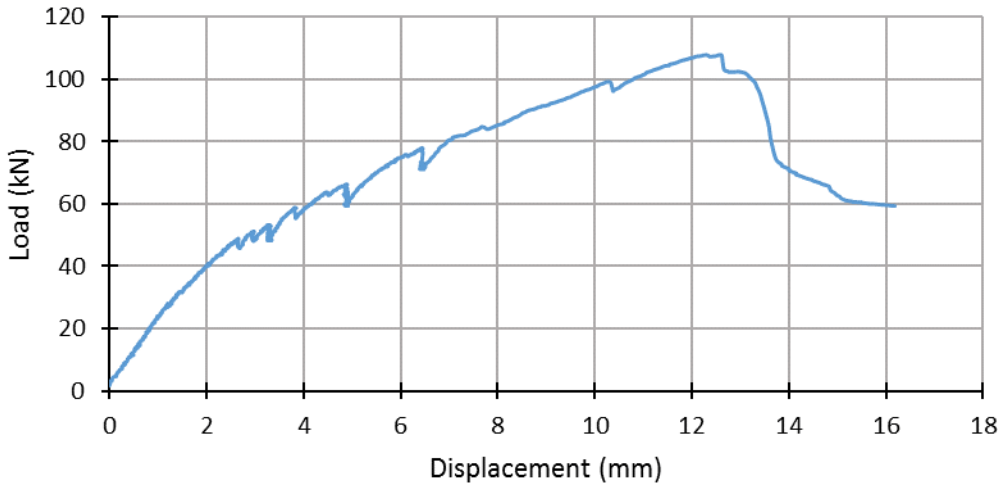

Figure 4.3 – BM 4.5-N: Load vs Displacement

Testing was halted at 52.9 KN, 66 KN and 78 KN for crack tracking. During these halts, the specimen released approximately 4.5 KN, 6.8 KN, and 7.8 KN respectively. The maximum recorded crack width was 0.2 mm.

The strength of the specimen declined drastically post peak. The critical shear cracks widened significantly, and the beam appeared to be supported almost entirely by the longitudinal reinforcement. Upon release of the testing load, the beam returned elastically to a displacement of approximately 7mm.

4.3.2 Longitudinal Reinforcement Behaviour

BM 4.5-N had a shear span of 1.22m with gauges located at 915 mm, 610 mm and 305 mm from the point of load application respectively. The maximum strain in the longitudinal reinforcement was 3950 microstrain corresponding elastically to 253 MPa or 25.3% of the expected tensile strength (Figure 4.4).

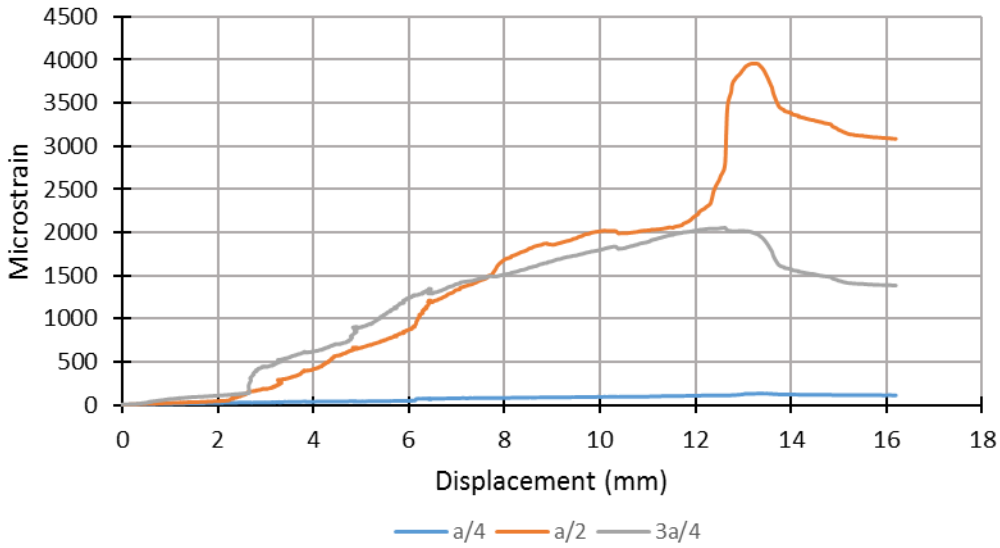

Figure 4.4 – BM 4.5-N: Longitudinal bar strains vs displacement

Specimen BM 4.5-N displayed increased stresses at half-shear span than at three-quarters shear span. This is likely due to increased stress from dowel action across the critical shear crack.

4.3.3 Displacement Behaviour

Figure 4.5 shows the measured average displacements at quarter and half span locations versus the measured displacement from the testing machine. BM 4.5-N displayed symmetric behaviour during testing.

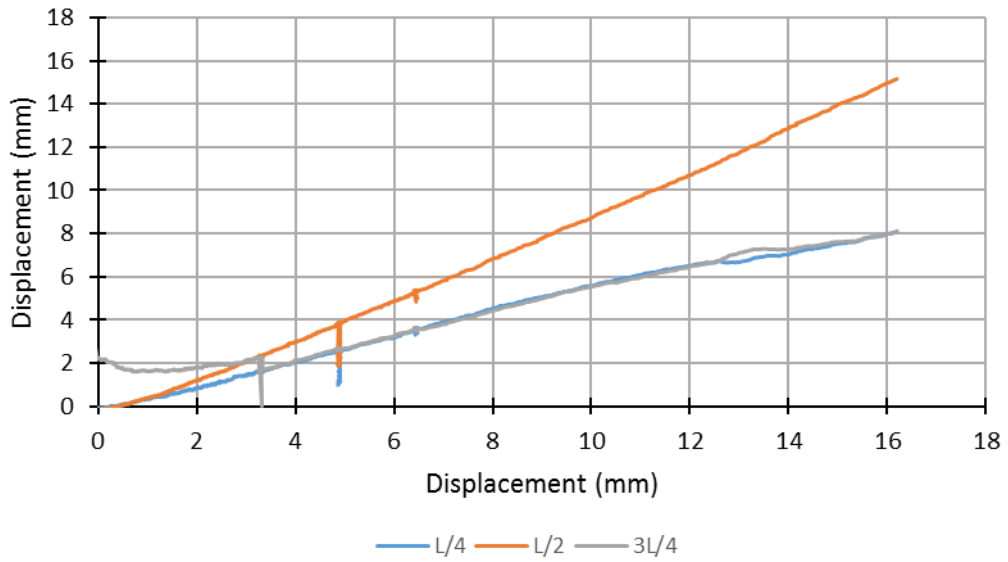

Figure 4.5 – BM 4.5-N: Displacement at measured locations vs displacement at load application

4.4 BM 4.5-90

4.4.1 Load Displacement and Failure

BM 4.5-90 had a shear span of approximately 1.22m and a 10M GFRP stirrups spaced at 90 mm. The specimen failed due to concrete crushing and shear crack propogation next to the load application. BM 4.5-90 failed in a combined shear-flexural mode as evidenced by the crack pattern in Figure 4.6. The sudden loss of strength in the load-displacement curve at failure indicates that the failure was initiated by shear mechanisms. The angle of inclination of the critical shear crack corresponding to the angle of the principal compressive stress was measured at 45°.

Figure 4.6 – BM 4.5-90: Crack patterns at failure

BM 4.5-90 reached a peak load of 222.5 kN with a corresponding displacement of 27.0 mm.

The specimen displayed bilinear bending stiffness with a cracking load of approximately 25 kN. During testing no longitudinal bar slip was observed. No effects of bar slip were observed in the load-displacement response of the beam (Figure 4.7).

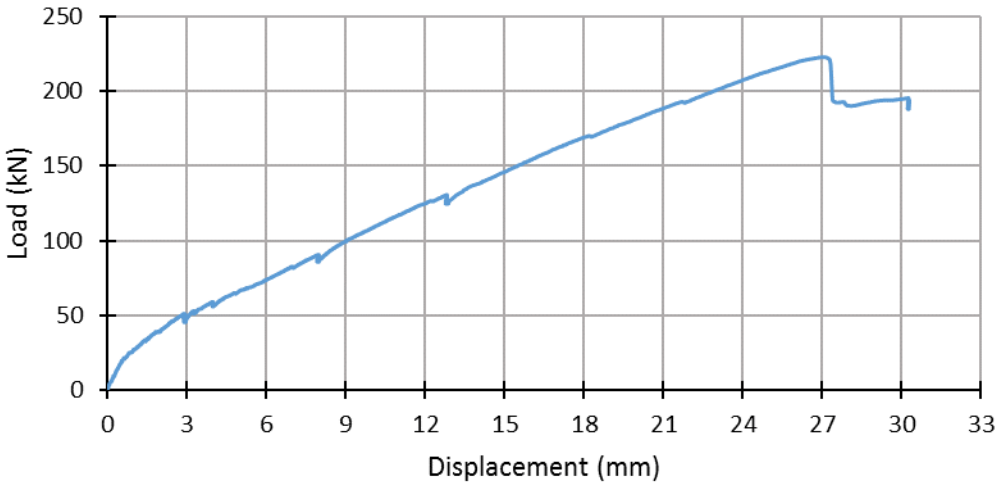

Figure 4.7 – BM 4.5-90: Load vs displacement

Testing was halted at 50 KN, 90 KN and 130 KN for crack tracking. During these halts, the specimen released approximately 5 KN, 5 KN, and 5.6 KN respectively. The maximum observed crack width was 0.5 mm.

The specimen retained approximately 86% of its strength post-peak. The specimen retained this strength until the cracking caused by the concrete crushing propagated fully into the critical shear region at which point sudden loss of strength was observed. Upon release of the testing load, the beam returned elastically to a displacement of approximately 4.7 mm.

4.4.2 Longitudinal Reinforcement Behaviour

BM 4.5-90 had a shear span of 1.22m with gauges located at 915 mm, 610 mm and 305 mm from the point of load application. The maximum strain in the longitudinal reinforcement was 6640 microstrain corresponding elastically to 425 MPa or 42.5% of the expected tensile strength (Figure 4.8).

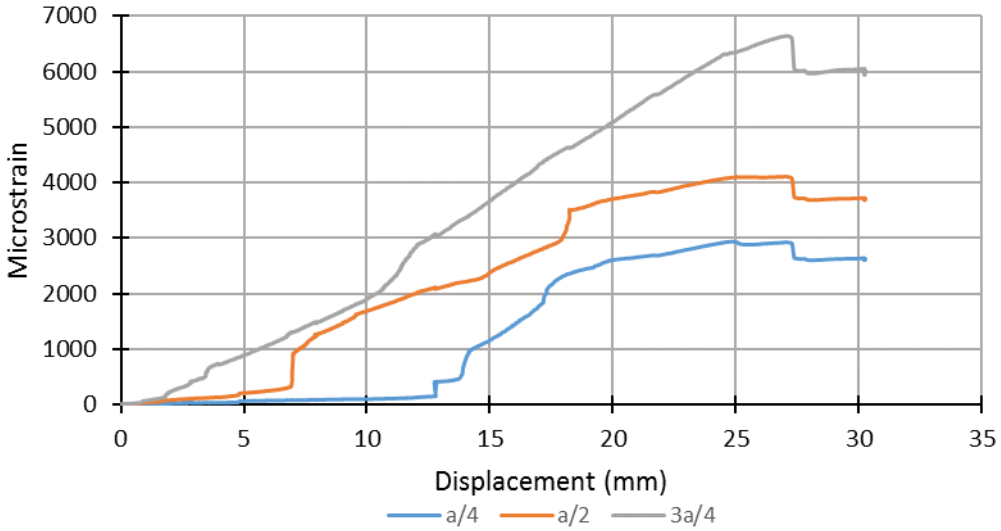

Figure 4.8 – BM 4.5-90: Longitudinal bar strains vs displacement

The stress in the longitudinal reinforcement largely followed expected trends. With increasing proximity to the midspan, the stress in the reinforcement increased. The longitudinal reinforcement displayed a roughly linear relationship to the displacement at 3a/4. The reinforcement close to the support had a non-linear relationship with the displacement indicating a mixed shear-flexural response in those regions.

4.4.3 Transverse Reinforcement Behaviour

Strain gauges were placed on stirrups adjacent on either side to the location of the longitudinal strain gauges. The maximum observed stirrup strain was 4260 microstrain corresponding elastically to a stress of 192 MPa or approximately 24% of the maximum straight bar strength of the stirrups (Figure 4.9).

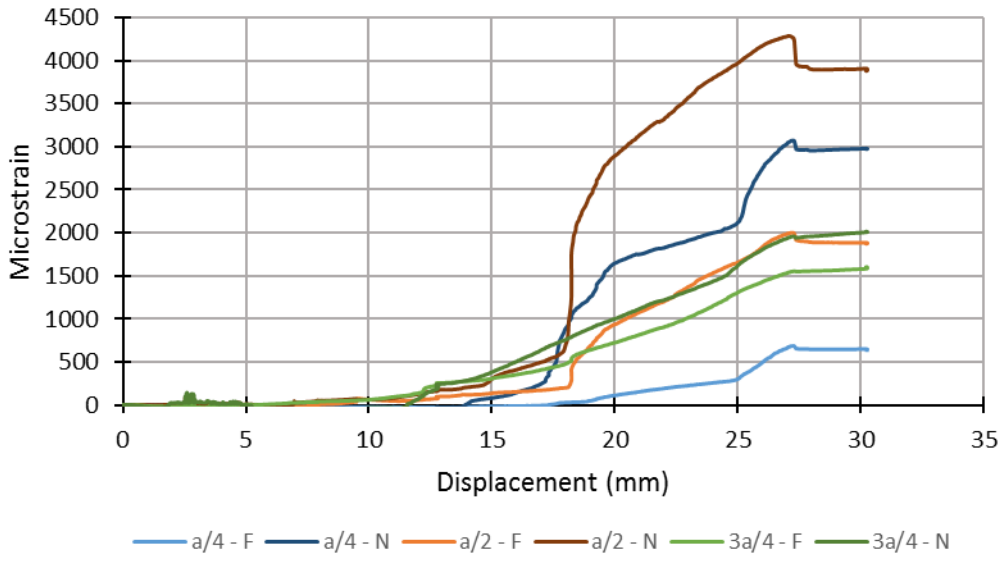

Figure 4.9 – BM 4.5-90: Strain in stirrups vs displacement

Stirrups engaged with the propagation of cracking as expected. No stirrup failures were observed.

The strain in the stirrups varied greatly with location. The maximum strain was observed at the quarter span location on the side closest to the load. Stirrups located next to each other displayed significant variations in measured stress. The average strain across stirrups at failure corresponded to a stress of 102 MPa which is lower than the average stress of 194 MPa predicted by CSA S806.

4.4.4 Displacement Behaviour

Figure 4.10 shows the measured average displacements at quarter and half span locations versus the measured displacement from the testing machine. BM 4.5-90 displayed symmetric behaviour during testing.

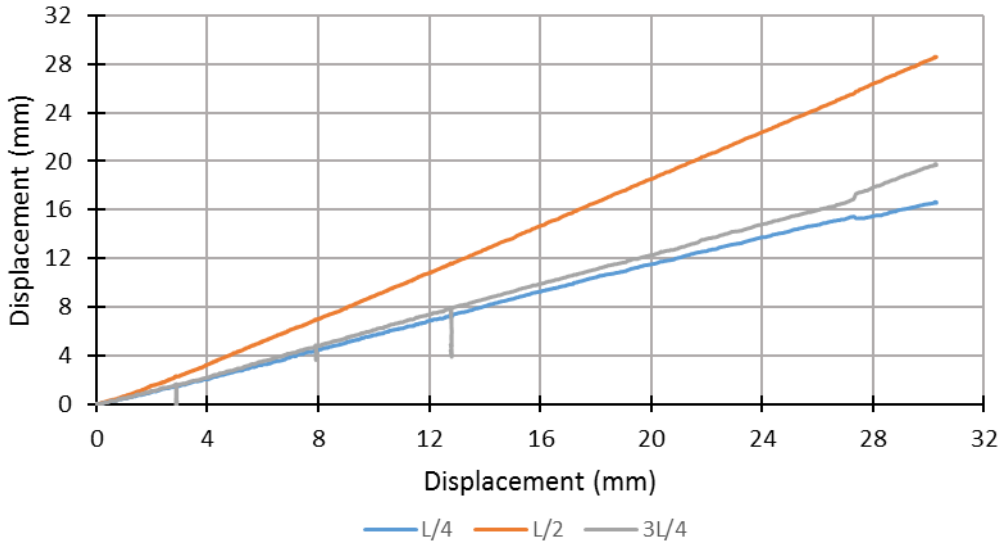

Figure 4.10 – BM 4.5-90: Displacement at measured locations vs displacement at load application

4.5 BM 4.5-150

4.5.1 Load Displacement and Failure

BM 4.5-150 had a shear span of approximately 1.22m and a 10M GFRP stirrups spaced at 150 mm. The specimen failed due to the widening of the critical shear crack and concrete crushing next to the load application. BM 4.5-150 failed in a shear dominated mode as evidenced by the crack pattern in Figure 4.11. The angle of inclination of the critical shear crack corresponding to the angle of the principal compressive stress was measured at 41°.

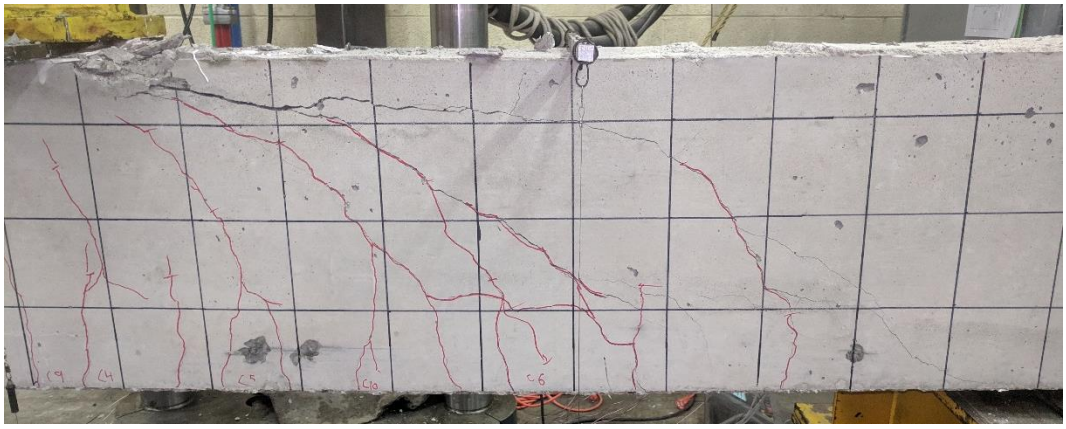

Figure 4.11 – BM 4.5-150: Crack patterns at failure

BM 4.5-150 reached a peak load of 171.2 kN with a corresponding displacement of 20.4 mm. The specimen displayed bilinear bending stiffness with a cracking load of approximately 25 kN (Figure 4.12). During testing, sounds indicated that some longitudinal bar slip occurred though there was no evidence of extensive bar slip.

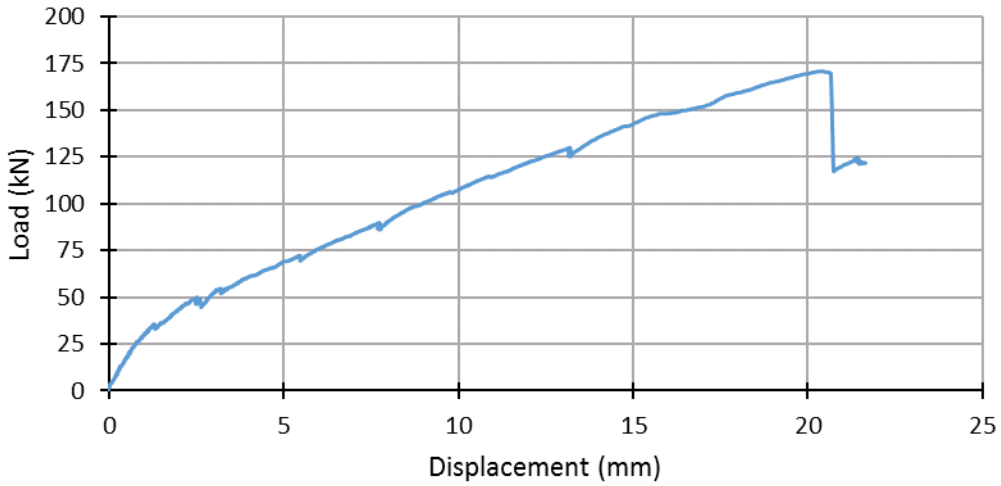

Figure 4.12 – BM 4.5-150: Load vs displacement

Testing was halted at 50 KN, 90 KN and 130 KN for crack tracking. During these halts, the specimen released approximately 4.5 KN, 4.6 KN, and 5.0 KN respectively. The maximum observed crack width was 0.25 mm.

The specimen retained approximately 69% of its strength post-peak. The specimen held this strength until the cracking caused by the concrete crushing propagated into the shear region. Upon release of the testing load, the beam returned elastically to a displacement of approximately 5.4 mm.

4.5.2 Longitudinal Reinforcement Behaviour

BM 4.5-N had a shear span of 1.22m with gauges located at 915 mm, 610 mm and 305 mm from the point of load application respectively. The maximum strain in the longitudinal reinforcement was 4530 microstrain corresponding elastically to 290 MPa or 29.0% of the expected tensile strength (Figure 4.13).

The longitudinal strain gauges were placed 915 mm, 610 mm and 305 mm from the midspan. The maximum observed stress in the longitudinal reinforcement was observed to be 290 MPa representing 29.0% of the expected tensile strength.

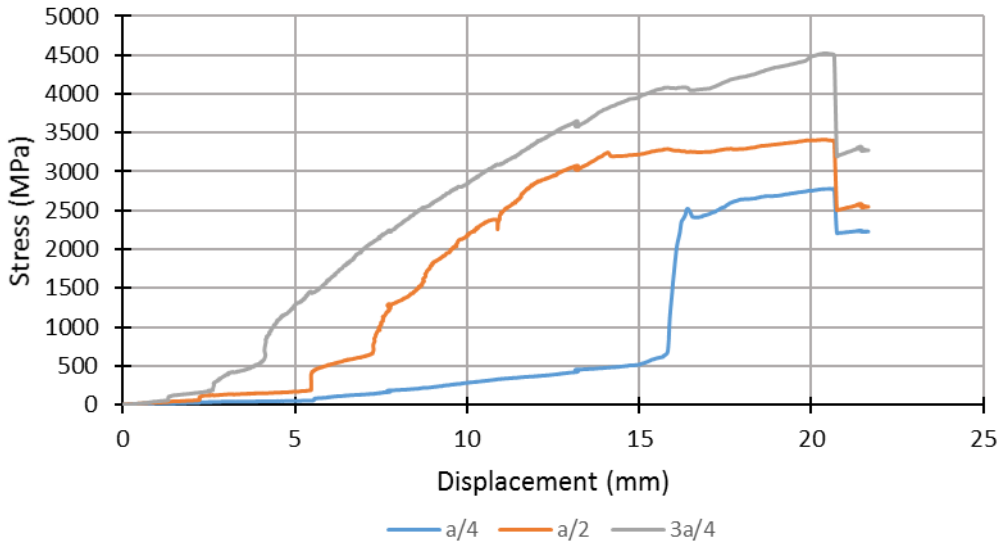

Figure 4.13 – BM 4.5-150: Longitudinal bar strains vs displacement

The stress in the longitudinal reinforcement largely followed expected trends. With increasing proximity to the midspan, the stress in the reinforcement increased. The longitudinal reinforcement displayed a roughly linear relationship to the displacement at 3a/4 and a/2. The reinforcement closest to the support had low strain until a sudden spike at approximately 75% of the max displacement. This spike was likely caused by a crack forming near the gauge.

4.5.3 Transverse Reinforcement Behaviour

Strain gauges were placed on stirrups adjacent on either side to the location of the longitudinal strain gauges. The maximum observed stirrup strain was 8130 microstrain corresponding elastically to a stress of 366 MPa, approximately 45% of the maximum straight bar strength of the stirrups (Figure 4.14).

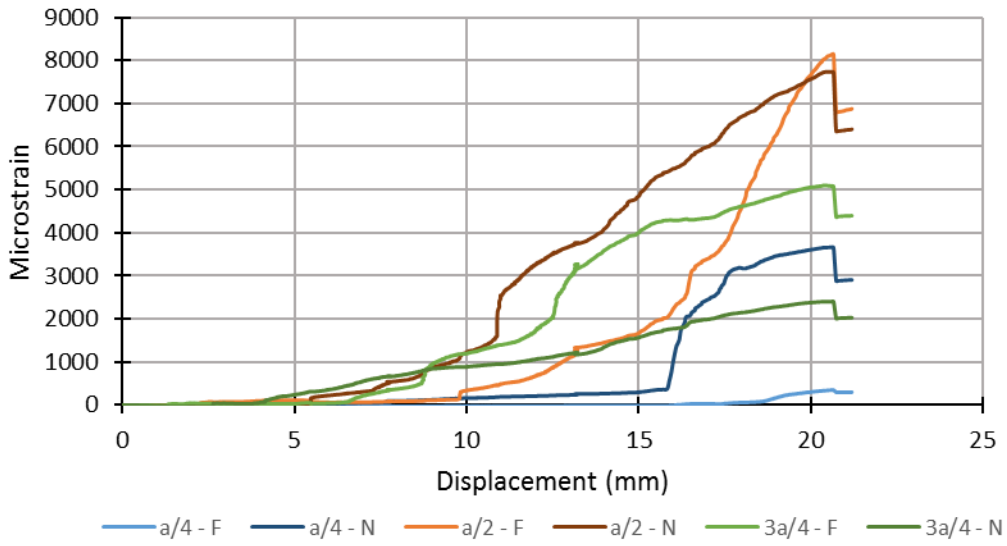

Figure 4.14 – BM 4.5-150: Strain in stirrups vs displacement

Stirrups engaged with the propagation of cracking as expected. No stirrup failures were observed.

The strain in the stirrups varied greatly with location. The maximum observed strains were at a/2. Stirrups close together displayed similar strains, though a/4-N displayed a sudden increase in strain at 75% of the max displacement of the beam. This is likely due to the formation or widening of a significant shear crack and it corresponds to a jump in the strain carried by a/2-F. The average strain across stirrups at the peak load corresponded to a stress of 205 MPa which is significantly higher than the average stress of 128 MPa predicted by CSA S806.

4.5.4 Displacement Behaviour

Figure 4.15 shows the measured average displacements at quarter and half span locations versus the measured displacement from the testing machine. BM 4.5-90 displayed symmetric behaviour during testing.

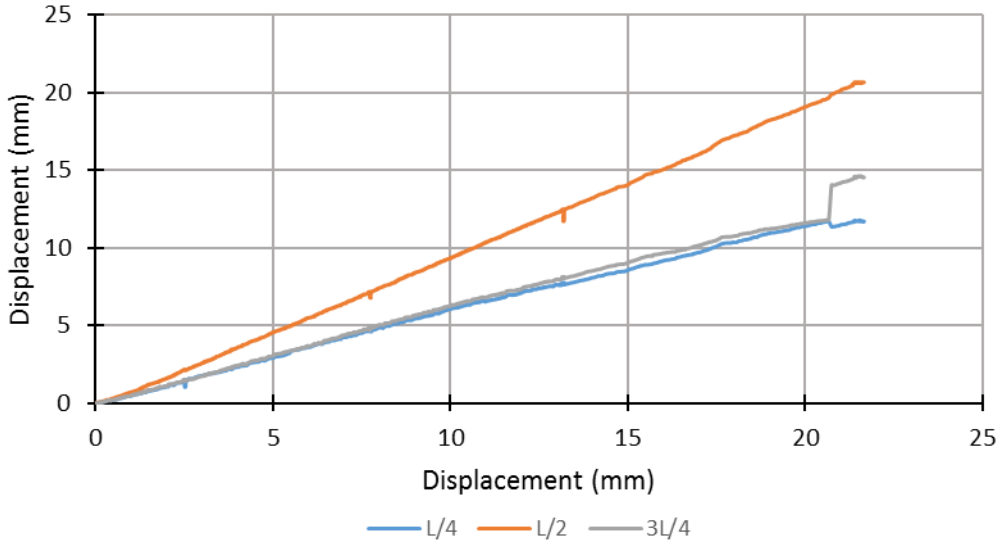

Figure 4.15 – BM 4.5-150: Displacement at measured locations vs displacement at load application

4.6 BM 6.5-N

4.6.1 Load Displacement and Failure

BM 6.5-N had a shear span of approximately 1.78m and no transverse reinforcement. The specimen displayed a very brittle failure due to the opening of the critical shear crack as seen in Figure 4.16. The angle of inclination of the critical shear crack corresponding to the angle of the principal compressive stress was measured at 37°.

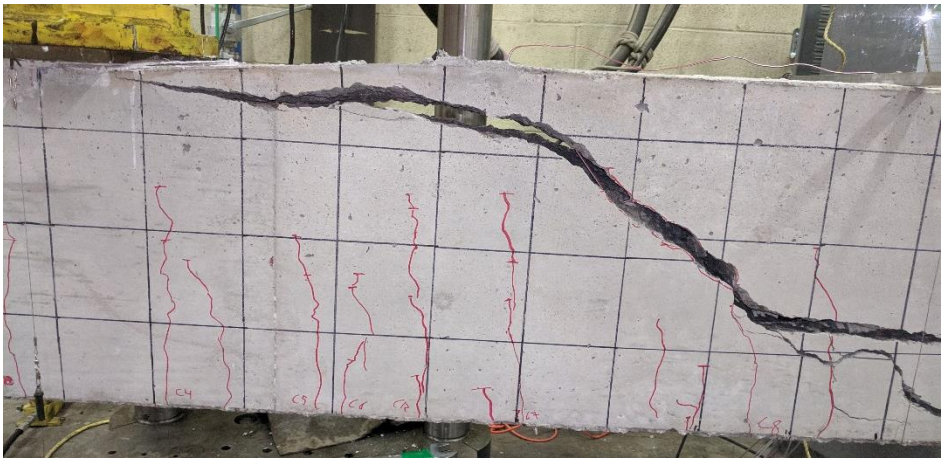

Figure 4.16 – BM 6.5-N: Crack patterns at failure

BM 6.5-N reached a peak load of 79.3 kN with a maximum displacement of 14.8 mm.

The specimen displayed bilinear bending stiffness with a cracking load of approximately 15 kN. During testing significant longitudinal bar slip was indicated by loud popping noises. The load-displacement response of the beam also indicates significant bar slip (Figure 4.17)

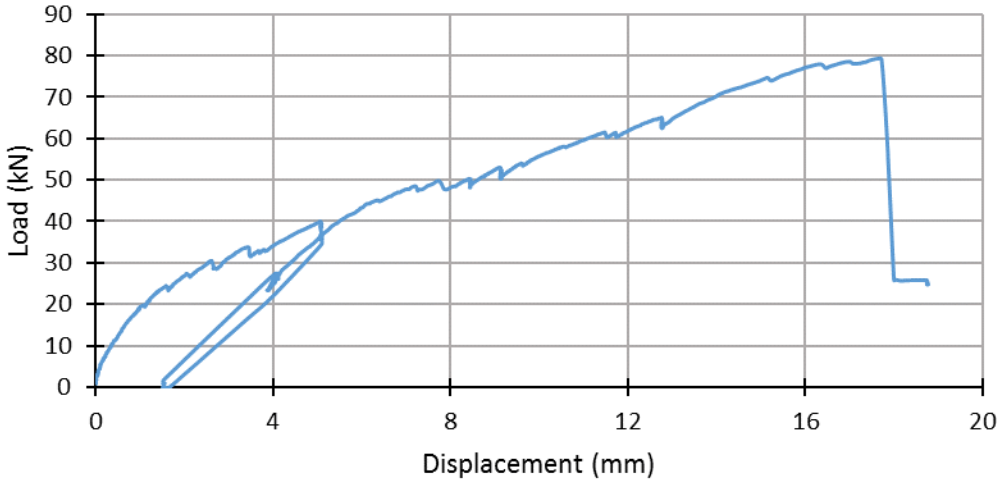

Figure 4.17 – BM 6.5-N: Load vs displacement

Testing was halted at 40 KN, 53 KN and 65 KN for crack tracking. Due to an equipment failure, the load was completely released during the first halt. Additionally, the specimen released approximately 2.7 KN and 2.5 kN during the other halts. The beam displayed a permanent deformation and decreased

stiffness when reloading as expected. The specimen appeared to match the original loading trend once reaching a load of approximately 50 kN. The maximum observed crack width was 0.25 mm.

This failure was very brittle, with the specimen retaining only 32% of its strength post-peak. This strength was largely provided by the longitudinal reinforcement as the critical shear crack quickly widened. Upon release of the testing load, the beam returned to a displacement of approximately 9.6 mm.

4.6.2 Longitudinal Reinforcement Behaviour

BM 6.5-N had a shear span of 1.78 m with gauges located at 1335 mm, 890 mm and 445 mm from the point of load application. The maximum strain in the longitudinal reinforcement was 2580 microstrain corresponding elastically to 165 MPa or 16.5% of the expected tensile strength of the bar (Figure 4.18). Immediately after peak load, the longitudinal reinforcement displayed an increase in strain and stress up to 863 MPa, 86.3% of the bar's tensile capacity. This increase is due to the longitudinal reinforcement providing continuity with the widening of the critical shear crack and brittle failure of the beam.

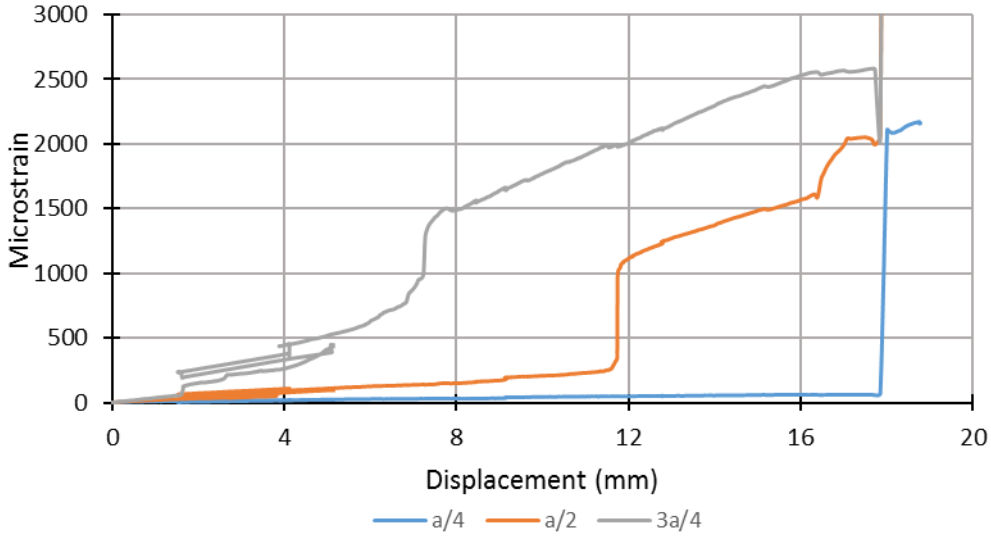

Figure 4.18 – BM 6.5-N: Longitudinal bar strains vs displacement

The longitudinal reinforcement saw very low strain, especially at a/4. This indicates that the behaviour of the beam was largely shear controlled, and that the flexural cracking did not extend to the support. Additionally, the strain behaviour is largely non-linear with respect to displacement except close to the midspan.

4.6.3 Displacement Behaviour

Figure 4.19 shows the measured average displacements at quarter and half span locations versus the measured displacement from the testing machine. BM 6.5-N displayed symmetric behaviour during testing.

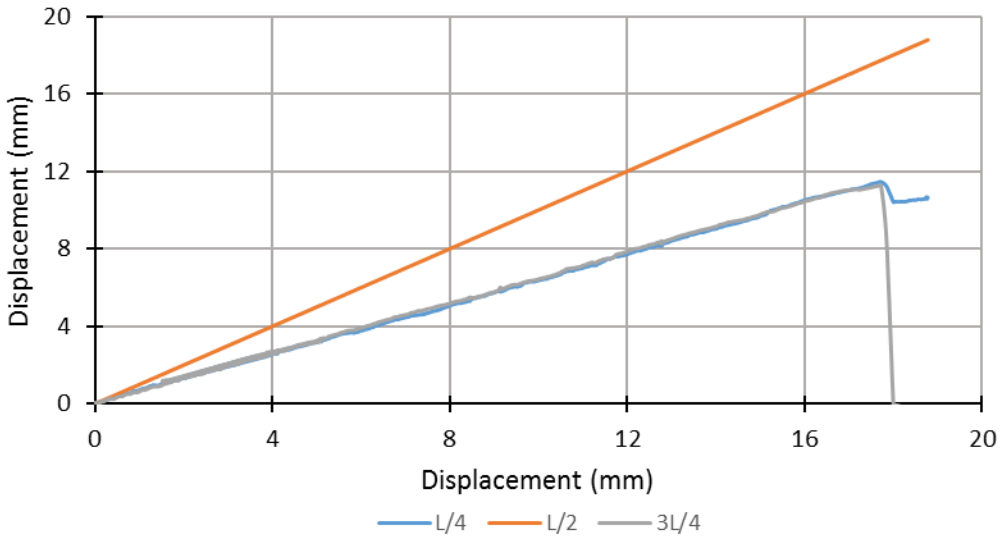

Figure 4.19 – BM 4.5-N: Displacement at measured locations vs displacement at load application

4.7 BM 6.5-90

4.7.1 Load Displacement and Failure

BM 6.5-90 had a shear span of approximately 1.78m and 10M GFRP stirrups spaced at 90 mm. The specimen failed due to concrete crushing next to the load application. BM 6.5-90 failed in a flexure dominated manner. There was evidence of shear cracking and the beginning of the formation of a critical shear crack, however this was not yet extensive (Figure 4.20).

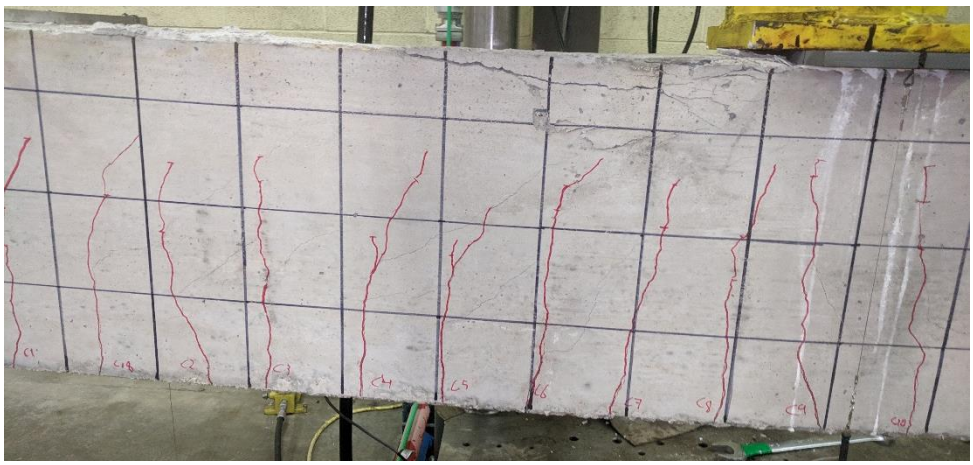

Figure 4.20 – BM 6.5-90: Crack patterns at failure

BM 6.5-90 reached a peak load of 145.6 kN with a corresponding displacement of 45.3 mm.

The specimen displayed bilinear bending stiffness with a cracking load of approximately 15 kN as seen in Figure 4.21. There was no evidence of longitudinal bar slip.

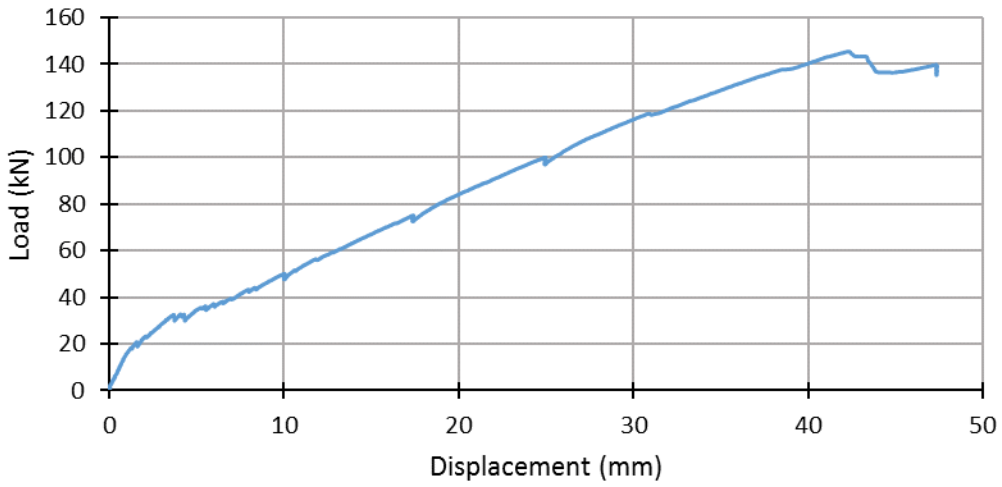

Figure 4.21 – BM 6.5-90: Load vs displacement

Testing was halted at 50 KN, 75 KN and 100 KN for crack tracking. During these halts, the specimen released approximately 2.4 KN, 2.4 KN, and 3.0 KN respectively. The maximum observed crack width was 0.25 mm.

The specimen exhibited a ductile behaviour post-peak, retaining approximately 93% of its strength post-peak. This is indicative of an over-reinforced flexural-controlled failure. The specimen held this strength until a critical shear crack developed. Upon release of the testing load, the beam returned elastically to a displacement of approximately 7.7 mm.

4.7.2 Longitudinal Reinforcement Behaviour

BM 6.5-90 had a shear span of 1.78 m with gauges located at 1335 mm, 890 mm and 445 mm from the point of load application. The maximum strain in the longitudinal reinforcement was 4800 microstrain corresponding elastically to 307 MPa or 30.7% of the expected tensile strength (Figure 4.22).

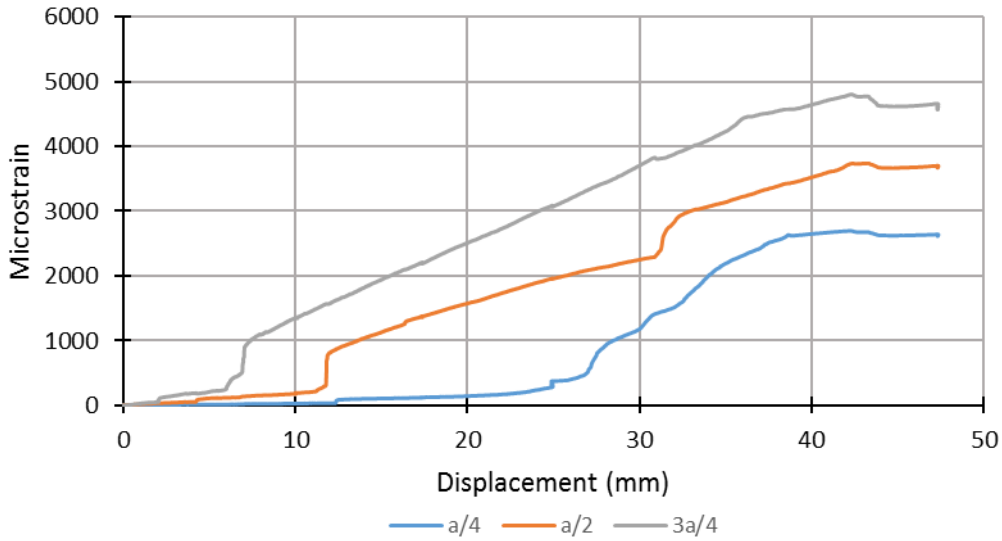

Figure 4.22 – BM 6.5-90: Longitudinal bar strains vs displacement

The stress in the longitudinal reinforcement largely followed expected trends for a flexure-controlled beam. With increasing proximity to the midspan, the stress in the reinforcement increased. The longitudinal reinforcement displayed a roughly linear relationship to the displacement at 3a/4 and a/2 after the bar was engaged at that location. At failure, the measured strains indicate full engagement of the bar at all locations. This indicates greater flexural development of the beam.

4.7.3 Transverse Reinforcement Behaviour

Strain gauges were placed on stirrups adjacent on either side to the location of the longitudinal strain gauges. The maximum observed stirrup strain was 2510 microstrain corresponding elastically to a stress of 113 MPa or approximately 14% of the maximum straight bar strength of the stirrups (Figure 4.23).

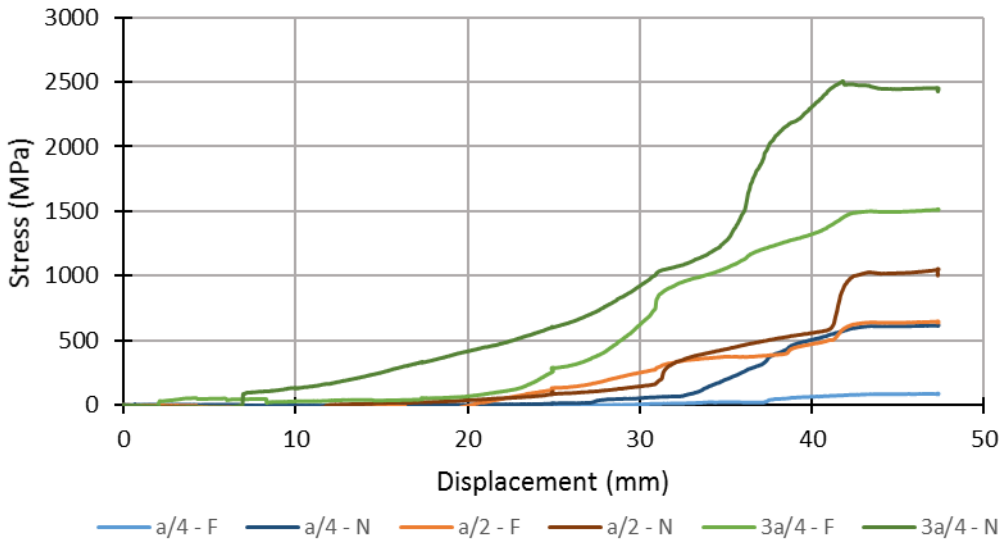

Figure 4.23 – BM 6.5-90: Strain in stirrups vs displacement

The observed strains indicate higher engagement of the stirrups closer to the load application. It is likely that the stirrups located closer to the midspan that were not gauged experienced even higher strains. This behaviour is expected of a slender beam. Stirrups close to one another varied significantly in measured strain, though the pattern of higher strains closer to the midspan holds true.

The average strain across stirrups at the peak load corresponded to a stress of 48 MPa, significantly lower than the 170 MPa predicted by CSA S806. The observed stress is likely lower due to the location of the strain gauges as the critical shear crack appeared to be forming within a/4 from the load.

4.7.4 Displacement Behaviour

Figure 4.24 shows the measured average displacements at quarter and half span locations versus the measured displacement from the testing machine. BM 6.5-90 displayed symmetric behaviour during testing.

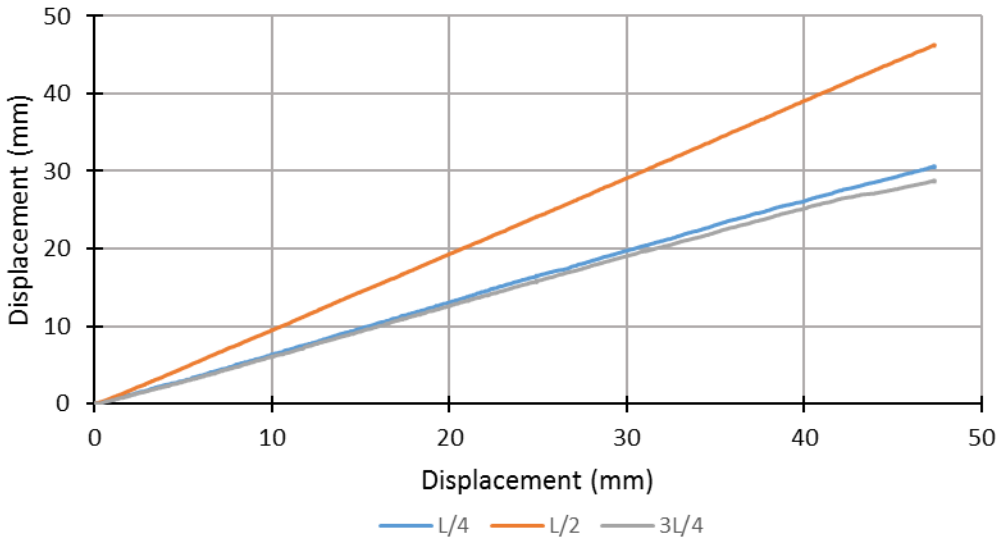

Figure 4.24 – BM 6.5-90: Displacement at measured locations vs displacement at load application

4.8 BM 6.5-150

4.8.1 Load Displacement and Failure

BM 6.5-150 had a shear span of approximately 1.78 m and 10M GFRP stirrups spaced at 150 mm. The specimen failed due to concrete crushing next to the load application. BM 6.5-150 failed in a combined flexure-shear mode. Extensive shear cracking was observed at failure indicated significant shear action along with the crushing and crack patterns associated with a flexural failure (Figure 4.25). Due to the sudden loss of strength exhibited immediately after peak load and video recording, the failure was initiated by shear crack propagation into the flexural region. The angle of inclination of the critical shear crack corresponding to the angle of the principal compressive stress was measured at 54°.

Figure 4.25 – BM 6.5-150: Crack patterns at failure

BM 6.5-150 reached a peak load of 141.0 kN with a corresponding displacement of 38.7 mm.

The specimen displayed bilinear bending stiffness with a cracking load of approximately 15 kN. During testing no longitudinal bar slip was observed. No effects of bar slip were observed in the load-displacement response of the beam (Figure 4.26).

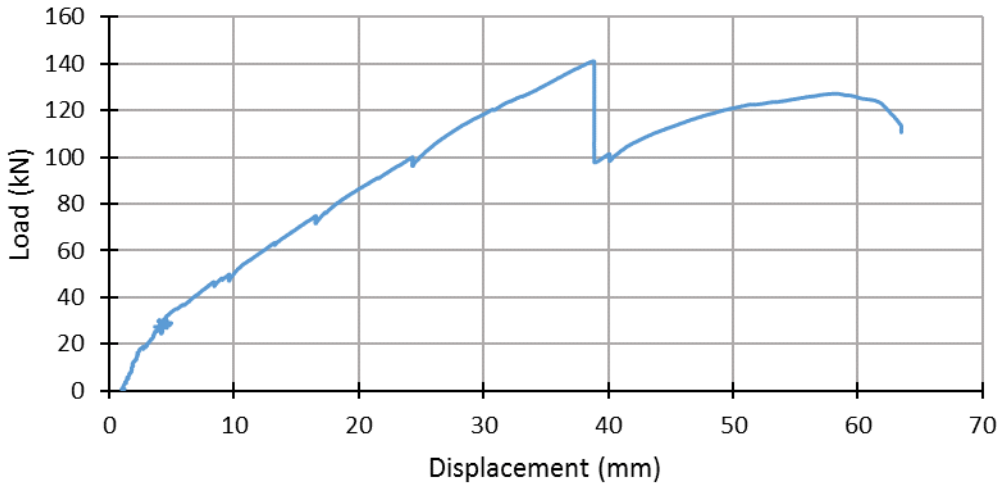

Figure 4.26 – BM 6.5-150: Load vs displacement

Testing was halted at 50 KN, 75 KN and 100 KN for crack tracking. During these halts, the specimen released approximately 2.7 KN, 3.2 KN, and 3.7 KN respectively. The maximum observed crack width was 0.4 mm.

The specimen exhibited a brittle behaviour post-peak, retaining approximately 69% of its strength post-peak. This is indicative of a shear-controlled failure despite the crack pattern indicating a combined flexural-tension failure. After this sudden loss of strength, the beam was able to support up to 127.2 kN after before significant flexural crushing crippled the load carrying capacity. This behaviour, coupled with video evidence, suggests that the failure was initiated by shear crack propagation into the flexural region before flexural crushing occurred. Upon release of the testing load, the beam returned elastically to a displacement of approximately 7.7 mm.

4.8.2 Longitudinal Reinforcement Behaviour

BM 4.5-90 had a shear span of 1.78 m with gauges located at 1335 mm, 890 mm and 445 mm from the point of load application. The maximum strain in the longitudinal reinforcement was 4450 microstrain corresponding elastically to 289 MPa or 28.9% of the expected tensile strength (Figure 4.27).

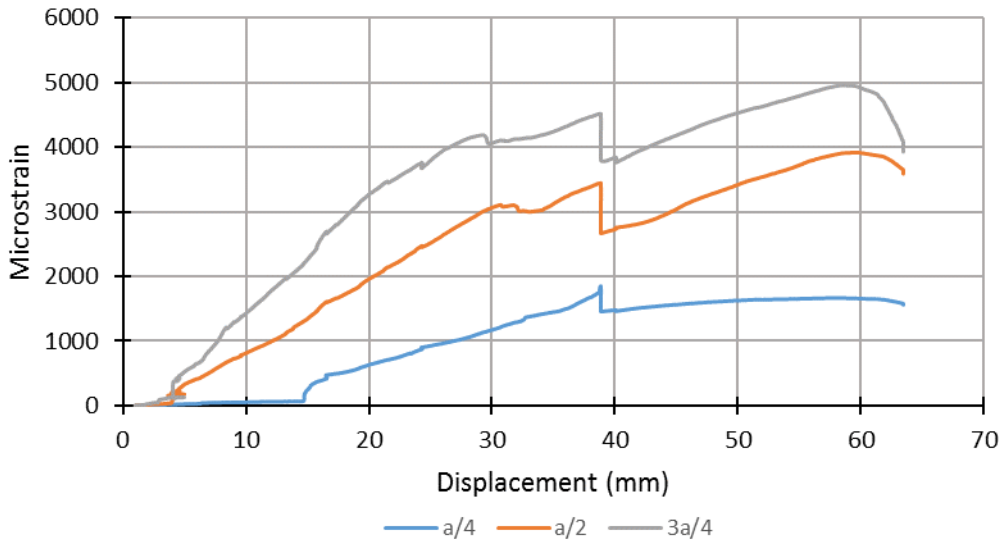

Figure 4.27 – BM 6.5-150: Longitudinal bar strains vs displacement

The stress in the longitudinal reinforcement followed expected trends except around peak load. At 85% of the peak load, the reinforcement closer to the midspan (gauges a/2 and 3a/4) experienced a reduction in strain that does not correspond to any variation on the load-displacement curve. This is likely due to load redistribution within the beam as the stirrups displayed an increase in stress at the same load.

Aside from the behaviour at 85% of peak load, the longitudinal reinforcement followed expected patterns. Post peak, the reinforcement developed greater strains than before peak load indicating an initial shear controlled failure followed by the flexure controlled loss of final strength. The ultimate stress experienced in the reinforcement was 31.7% of the tensile capacity.

4.8.3 Transverse Reinforcement Behaviour

Strain gauges were placed on stirrups adjacent on either side of the longitudinal strain gauges. The maximum observed stirrup strain was 4280 microstrain corresponding elastically to a stress of 193 MPa or approximately 24% of the maximum straight bar strength of the stirrups (Figure 4.28). After peak load, the stirrup closest to the midspan experienced strains up to 5240 microstrain. Gauges 3a/4-N and 3a/4-F ultimately stopped functioning. This could be due destruction of the lead wires from increased displacements or a crack forming at or near to the gauge itself.

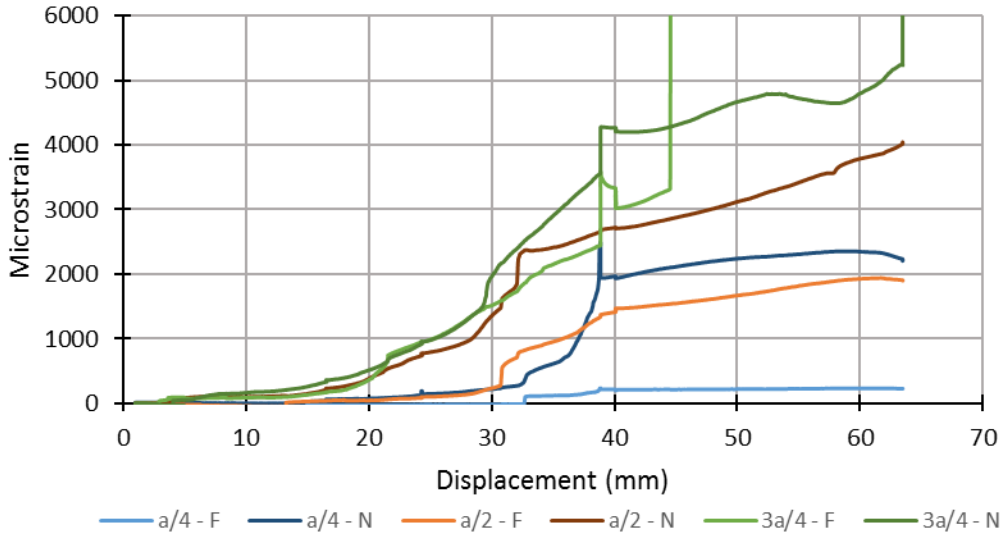

Figure 4.28 – BM 6.5-150: Strain in stirrups vs displacement

The observed strains indicate higher engagement of the stirrups closer to the load application. It is likely that the stirrups located closer to the midspan that were not gauged experienced even higher strains. This behaviour is expected of a slender beam. Stirrups close to one another varied significantly in measured strain, and the specific stirrup strains appear to be heavily influenced by crack location.

The average strain across stirrups at the peak load corresponded to a stress of 111 MPa, very close to the 114 MPa predicted by CSA S806. This observed average stress is likely lower than the real average stress due to the overall trend of increasing stress with proximity to the midspan.

4.8.4 Displacement Behaviour

Figure 4.29 shows the measured average displacements at quarter and half span locations versus the measured displacement from the testing machine. BM 6.5-150 displayed symmetric behaviour during testing.

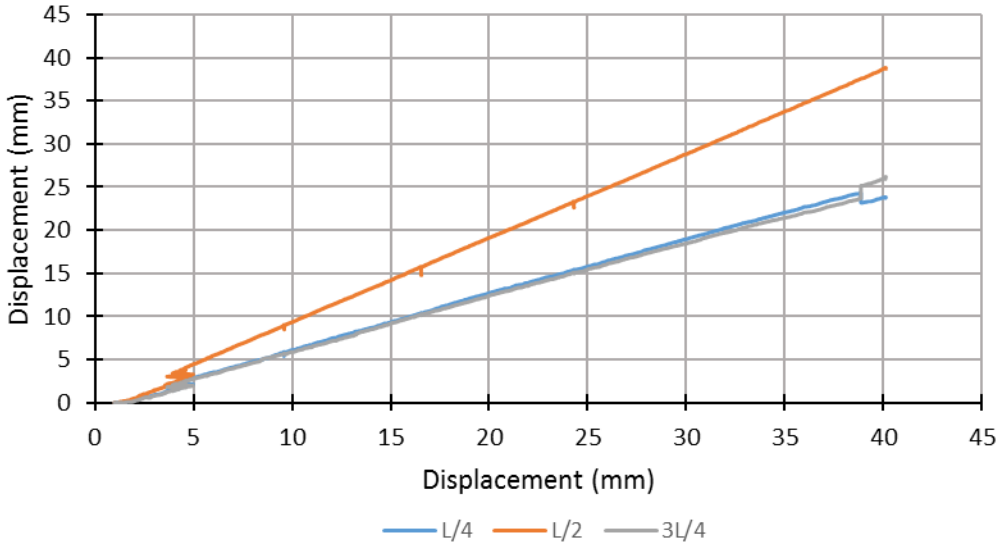

Figure 4.29 – BM 6.5-150: Displacement at measured locations vs displacement at load application

4.9 BM 8.5-N

4.9.1 Load Displacement and Failure

BM 8.5-N had a shear span of approximately 2.30 m and no transverse reinforcement. The specimen failed due to the propagation of a shear crack into the flexural region followed by crushing of the concrete next to the load application (Figure 4.30). This sequence is indicative of a shear dominated failure. The angle of inclination of the critical shear crack corresponding to the angle of the principal compressive stress was measured at 60°.

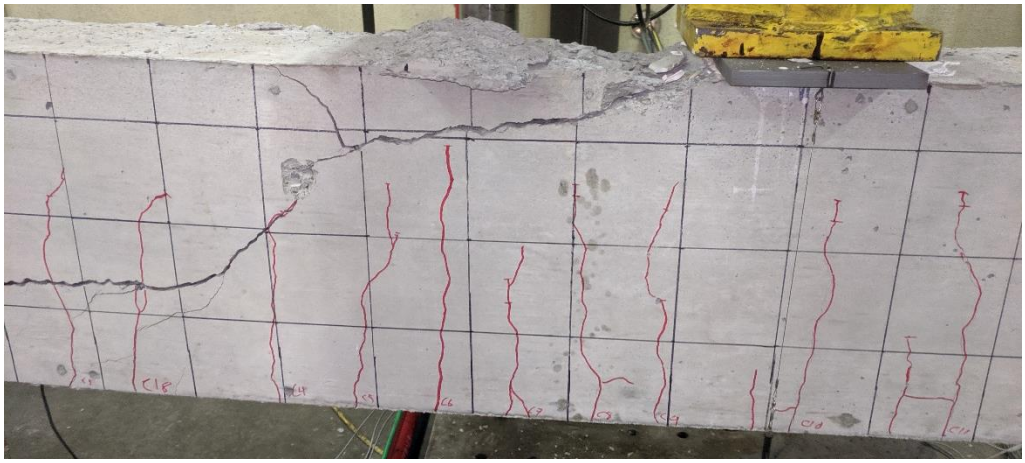

Figure 4.30 – BM 8.5-N: Crack patterns at failure

BM 8.5-N reached a peak load of 89.5 kN with a corresponding displacement of 51.1 mm.

The specimen displayed bilinear bending stiffness with a cracking load of approximately 5 kN. There was significant noise during testing indicating longitudinal bar slip. The load-displacement behaviour also displayed evidence of longitudinal bar slip (Figure 4.31)

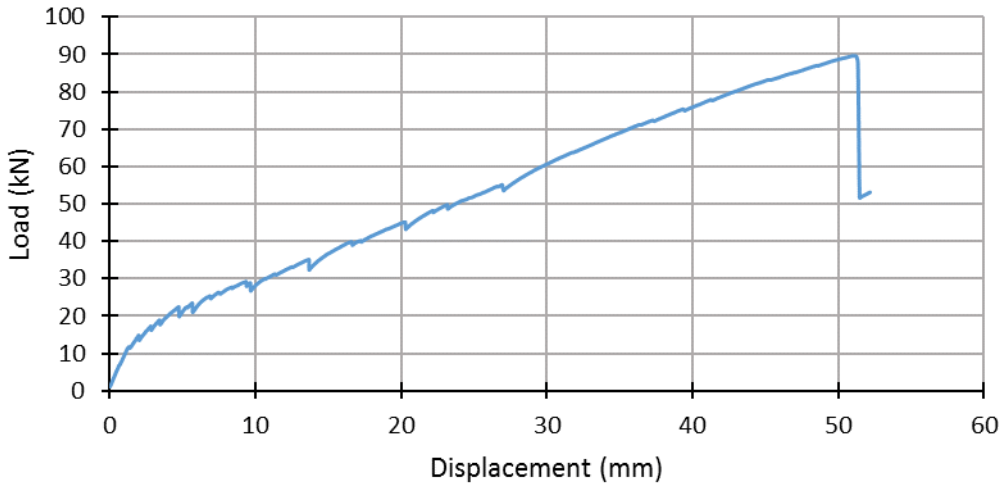

Figure 4.31 – BM 8.5-N: Load vs displacement

Testing was halted at 35 KN, 45 KN and 55 KN for crack tracking. During these halts, the specimen released approximately 2.9 KN, 2 KN, and 1.6 KN respectively. The maximum observed crack width was 0.45 mm.

The specimen exhibited a brittle behaviour post-peak, retaining approximately 59% of its strength post-peak. This is indicative of a shear-controlled failure. Testing was ceased after this sudden loss of strength to protect test equipment.

Due to an error during data collection, only load-displacement and crack pattern data is available for BM 8.5-N. Data that was processed through the DAQ was lost at the conclusion of testing.

4.10 BM 8.5-150

4.10.1 Load Displacement and Failure

BM 8.5-150 had a shear span of approximately 2.30 m and 10M GFRP stirrups at 150 mm. The specimen failed due to concrete crushing next to the load application. BM 8.5-N failed in combined shear-flexure mode. The failure was initiated with the delamination of the concrete compressive zone with the almost simultaneous propagation of a shear crack into the flexural compression zone (Figure 4.32). The failure was not immediately noticed due to a lack of noise and large retention of strength. This specimen was tested significantly past peak load as the initial peak was difficult to detect. The flexural crushing and subsequent delamination propagated down through the section until a final loss of strength (Figure 4.33). The angle of principle compressive stress was measured as 52°.

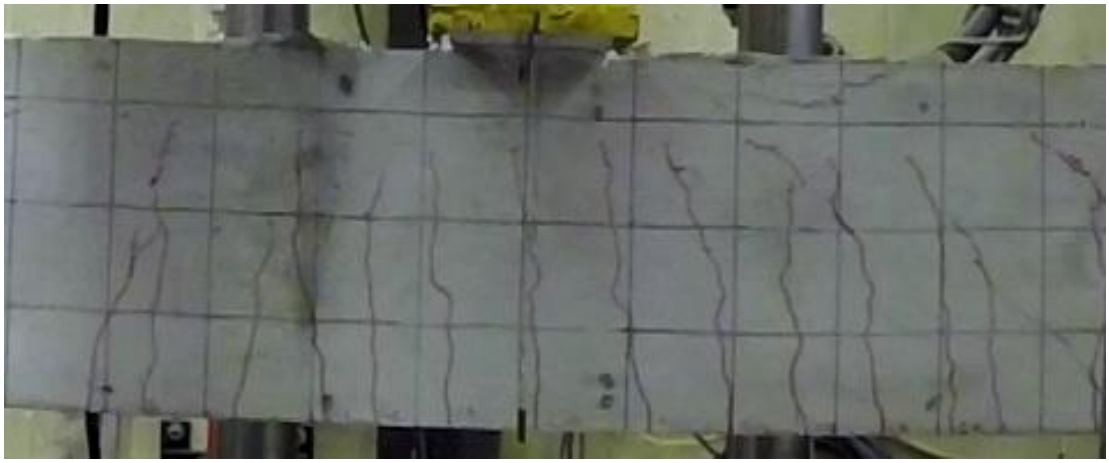

Figure 4.32 – BM 8.5-150: Crack patterns at failure

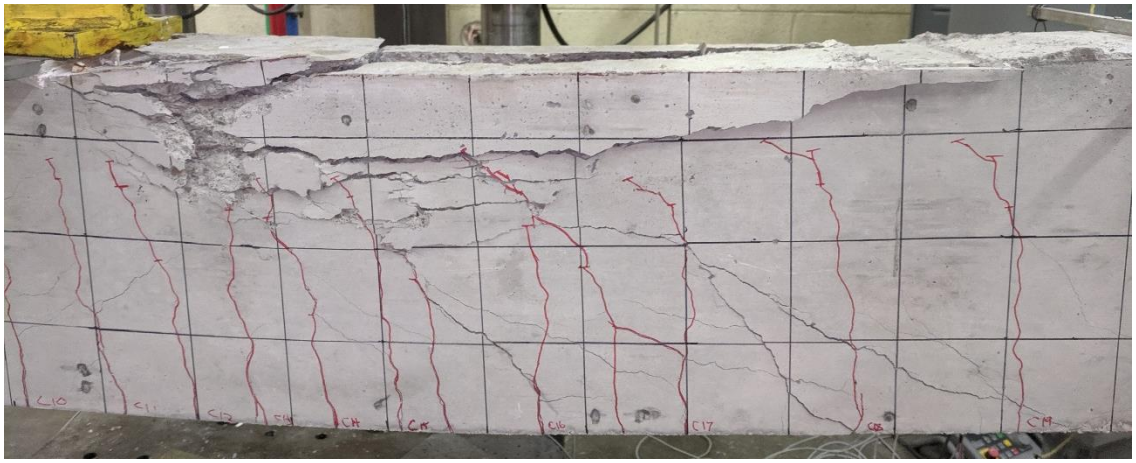

Figure 4.33 – BM 8.5-150: Propagation of flexural crushing and delamination post-peak

BM 8.5-150 reached a peak load of 113.5 kN with a corresponding displacement of 71.0 mm.

The specimen displayed bilinear bending stiffness with a cracking load of approximately 5 kN. There was no evidence of significant bar slip during testing. There was no evidence of bar slip on in load-displacement response of the beam (Figure 4.34).

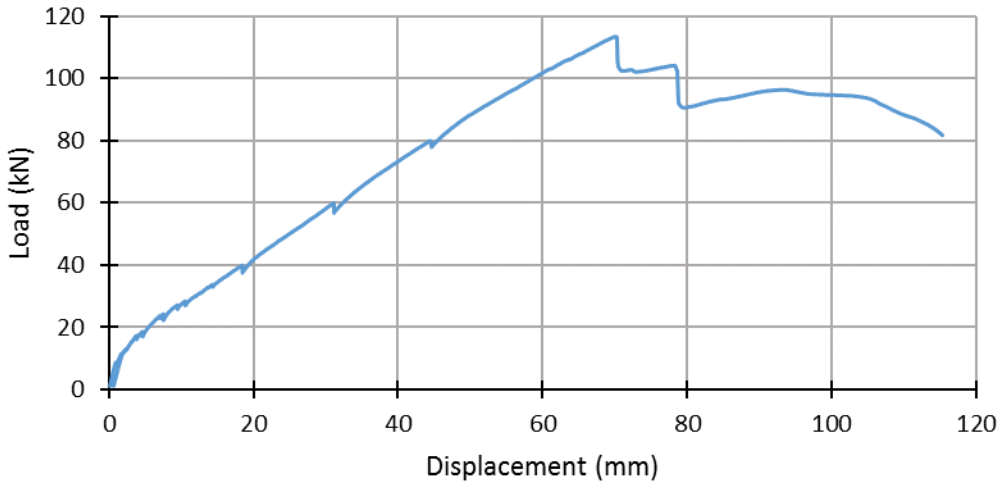

Figure 4.34 – BM 8.5-150: Load vs displacement

Testing was halted at 40 KN, 60 KN and 80 KN for crack tracking. During these halts, the specimen released approximately 2.4 KN, 3.2 KN, and 2.2 KN respectively. The maximum recorded crack width was 0.6 mm.

The specimen exhibited a multi-stage failure. The first stage was the flexural crushing and delamination of the concrete compression zone accompanied by the sudden propagation of a shear crack into the compression zone. After further loading, the delamination developed significantly while the crushing and shear cracking propagated extensively. Finally, the shear cracking and flexural crushing developed sufficiently to destroy the load carrying capacity of the beam. Overall, this was a very ductile failure for a FRP reinforced beam with post-peak loads remaining over 80% of the peak load.

4.10.2 Longitudinal Reinforcement Behaviour

BM 4.5-N had a shear span of 2.30 m with gauges located at 1725 mm, 1150 mm and 575 mm from the midspan. The maximum strain in the longitudinal reinforcement at the peak load was 5360 microstrain corresponding elastically to 343 MPa or 34.3% of the tensile capacity of the bar (Figure 4.35).

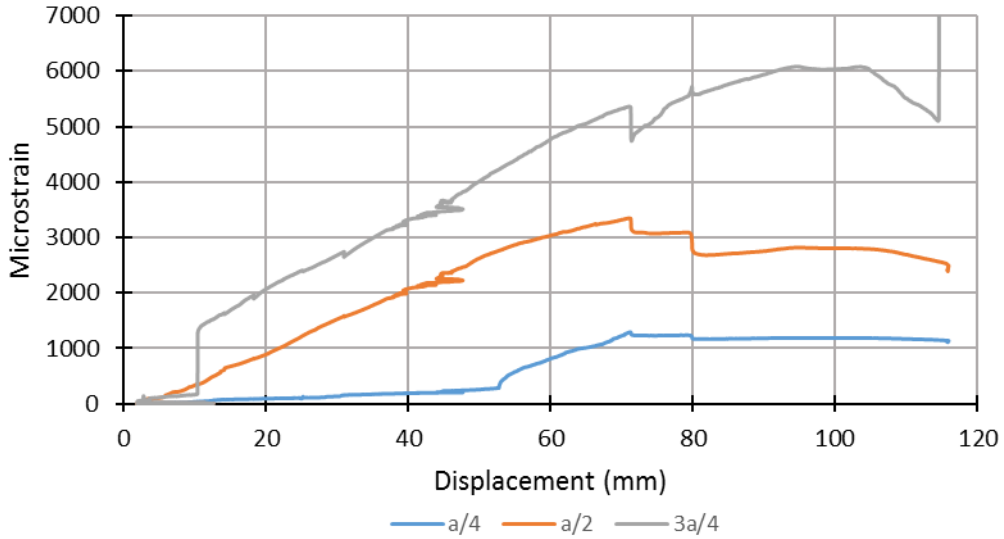

Figure 4.35 – BM 8.5-150: Longitudinal bar strains vs displacement

The stress in the longitudinal reinforcement largely followed expected trends with roughly linear behaviour with respect to displacement once the bar was engaged. After the peak load, the load distributed in an unusual pattern with the strain greatly increasing close to the midspan and decreasing elsewhere. This could be indicative of a stress redistribution into the shear reinforcement.

The ultimate strain corresponded to a stress of 767 MPa and occurred after significant shear cracking had developed. The longitudinal reinforcement provided continuity for the beam after the load-carrying capacity was destroyed.

4.10.3 Transverse Reinforcement Behaviour

Strain gauges were placed on stirrups adjacent on either side of the longitudinal strain gauges. The maximum observed stirrup strain at peak load was 2450 microstrain correlated to a stress of approximately 110 MPa or 13.8% of the maximum straight bar strength of the stirrups. After peak load, the stirrup closest to the midspan experienced strains corresponding to stresses up to 375 MPa. Gauges a/4-N and 3a/4-F experienced some technical issues, with a/4-N only properly recording significantly past peak deflection.

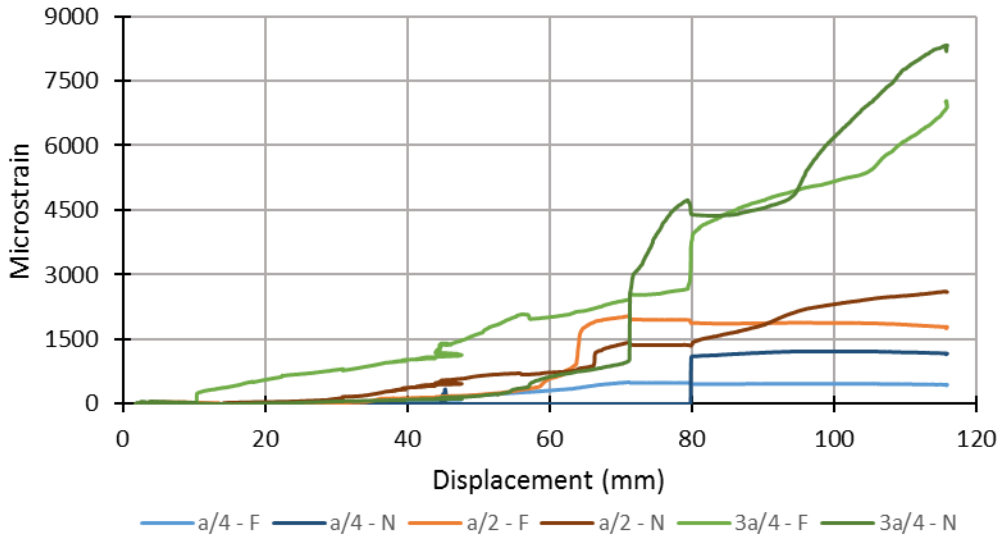

Figure 4.36 – BM 8.5-150: Strain in stirrups vs displacement

Stirrups engaged with the propagation of cracking as expected. No stirrup failures were observed.

The observed strains indicate generally higher engagement of the stirrups closer to the load application. It is likely that the stirrups closer to midspan experienced even higher strains but were not measured. This behaviour is consistent with beam theory and observations from other tests. Stirrups close to one another varied significantly in measured strain, and the specific stirrup strains appear to be heavily influenced by crack location.

The average strain across stirrups at failure corresponded to a stress of 67 MPa, significantly lower than the 103 MPa predicted by CSA S806. This observed average stress may be lower than the real average stress due to the overall trend of increasing stress with proximity to the midspan.

4.10.4 Displacement Behaviour

Figure 4.37 shows the measured average displacements at quarter and half span locations versus the measured displacement from the testing machine. The displacement of the specimen was largely symmetrical until after peak load when the side that experienced failure first also experienced increased deflections.

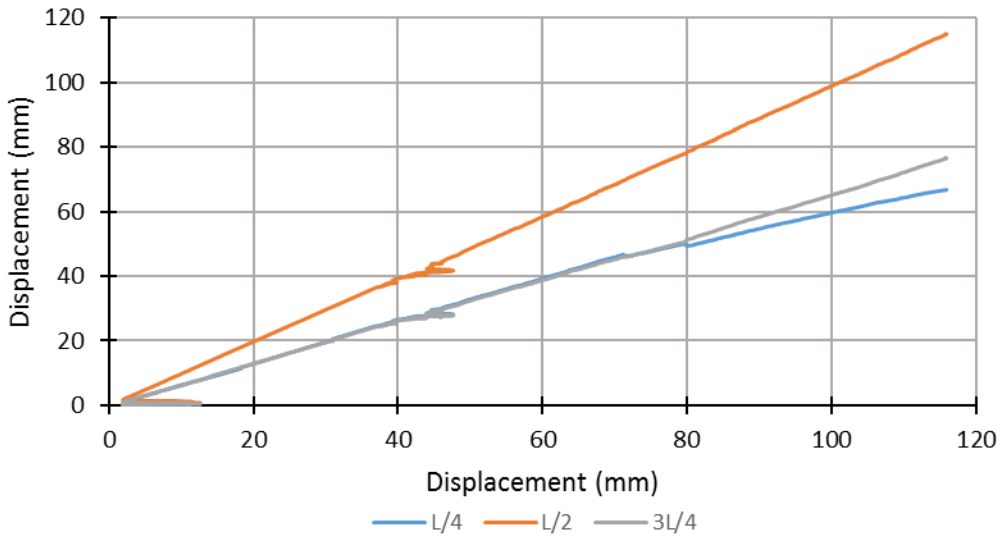

Figure 4.37 – BM 8.5-150: Displacement at measured locations vs displacement at load application

4.11 BM 10.5-N

4.11.1 Load Displacement and Failure

BM 10.5-N had a shear span of approximately 2.84 m and no transverse reinforcement. The specimen failed due to the sudden formation and widening of a shear crack. This crack ran from the compression zone down through the section and then above and parallel to the longitudinal reinforcement (Figure 4.38). This shear crack caused a sudden and catastrophic failure. The angle of inclination of the critical shear crack corresponding to the angle of the principal compressive stress was measured as 69°.

Figure 4.38 – BM 10.5-N: Catastrophic shear failure

BM 10.5-N reached a peak load of 93.0 kN with a corresponding displacement of 97.1 mm.

The specimen displayed linear bending stiffness with initial cracking likely to have occurred during test setup and beam handling. There was some auditory indication that the longitudinal reinforcement was slipping during testing as well as evidence of slip in the load-displacement response (Figure 4.39).

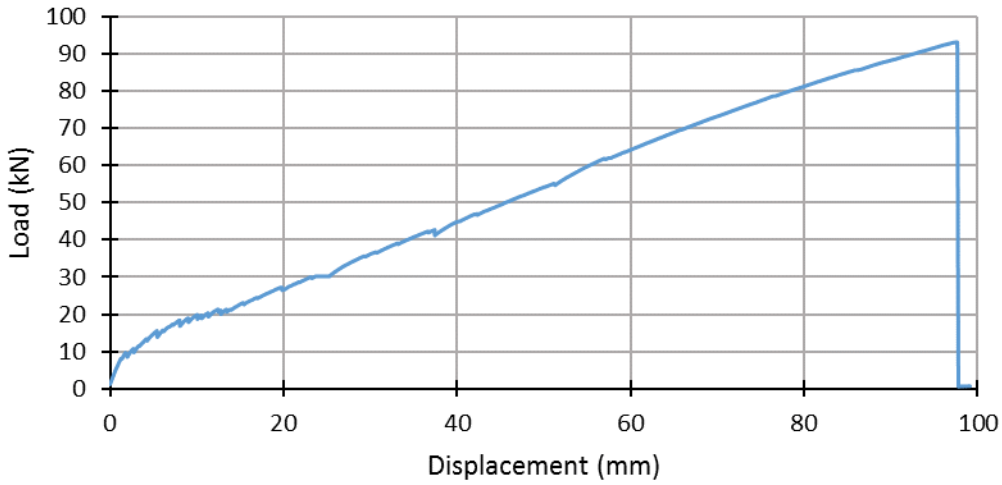

Figure 4.39 – BM 10.5-N: Load vs displacement

Testing was halted at 30 KN, 42.5 KN and 55 KN for crack tracking. During these halts, the specimen released approximately 0.5 KN, 1.5 KN, and 2.7 KN respectively. The maximum recorded crack width was 0.4 mm.

The specimen exhibited a brittle, catastrophic failure with no load-carrying capacity post peak. The longitudinal reinforcement ruptured during failure due to massively increased stress from providing continuity after the shear crack propagated through the section.

4.11.2 Longitudinal Reinforcement Behaviour

BM 10.5-N had a shear span of 2.84 m with gauges located at 2160 mm, 1420 mm and 710 mm from the midspan. The gauges at 1420 mm and 710 mm failed prior to testing. The strain in the longitudinal reinforcement at peak load was 1590 microstrain corresponding elastically to a stress of 102 MPa or 10.2% of the tensile capacity of the bar (Figure 4.40). This stress is likely much lower than the maximum that would be present at midspan or closer to the shear critical crack.

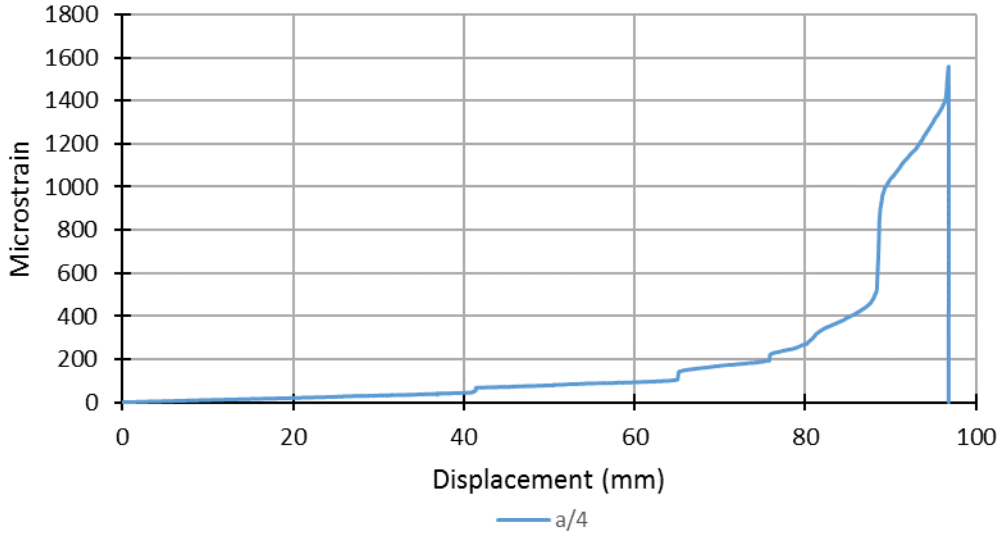

Figure 4.40 – BM 4.5-N: Longitudinal bar strains vs displacement

Due to the failure of the strain gauges, limited patterns can be drawn regarding the behaviour of the longitudinal reinforcement. However, BM 10.5-N is the only beam to see significant development of the reinforcement at a/4. This is likely due to the formation of the critical shear crack at approximately a/2, far outside of the expected critical shear region. The crack may have formed here due to voids caused by the casting of lift anchors into the compression surface.

4.11.3 Displacement Behaviour

Figure 4.41 shows the measured average displacements at quarter and half span locations versus the measured displacement at half span. The displacement measurements from the testing machine did not match measured displacements or observed behaviour. BM 10.5-N displayed symmetric behaviour during testing.

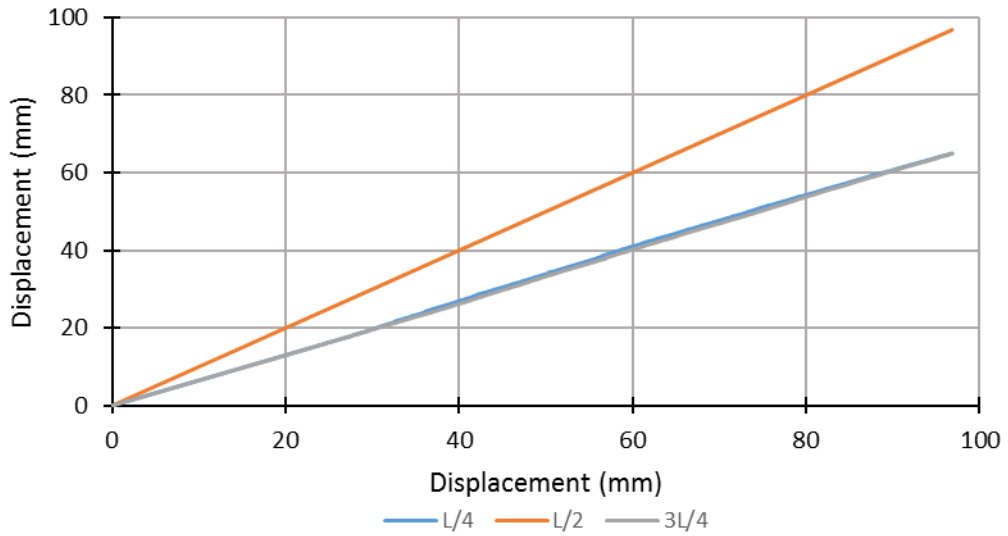

Figure 4.41 – BM 10.5-N: Displacement at measured locations vs displacement at midspan

4.12 BM 10.5-150

4.12.1 Load Displacement and Failure

BM 10.5-N had a shear span of approximately 2.84 m and 10M GFRP stirrups spaced at 150 mm. The beam failed in a flexural controlled manner with failure beginning with the crushing of concrete next to the load application and the delamination of concrete in the compression zone (Figure 4.42). The propagation of a shear crack into the compression region was also observed but the failure began before the shear crack fully formed.

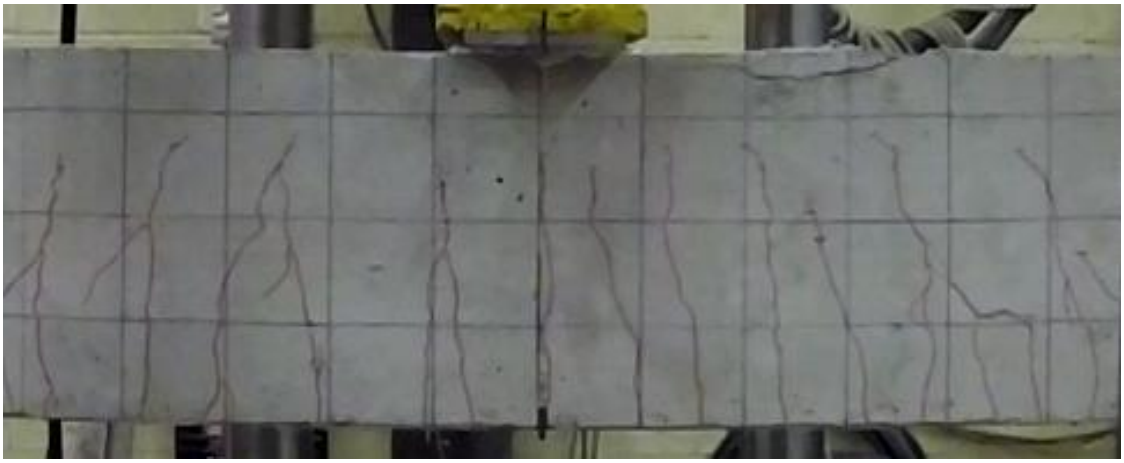

Figure 4.42 – BM 10.5-150: Crack patterns at failure

BM 10.5-150 reached a peak load of 81.71 kN with a corresponding displacement of 78.0 mm.

The specimen displayed bilinear bending stiffness with cracking occurring at a load less than 5 kN. During testing no longitudinal bar slip was observed. No effects of bar slip were observed in the load-displacement response of the beam (Figure 4.43).

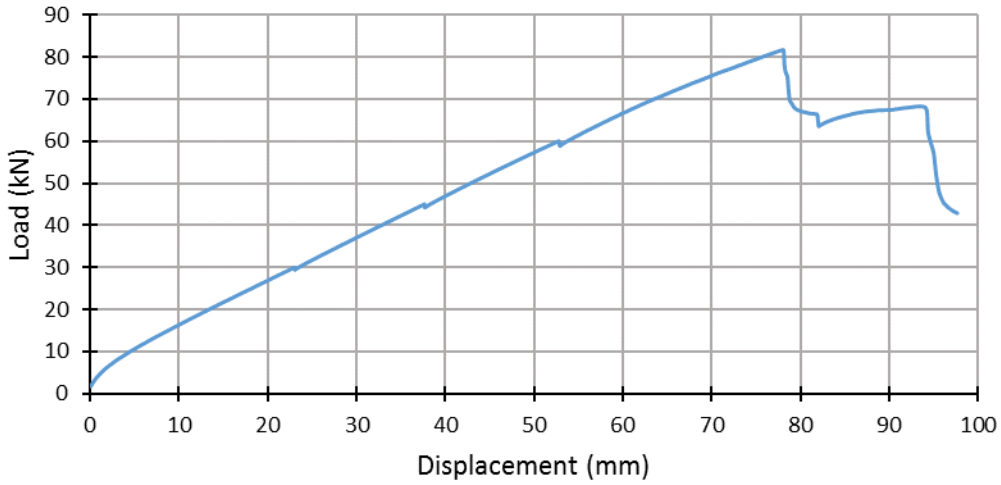

Figure 4.43 – BM 10.5-150: Load vs displacement

Testing was halted at 30 KN, 45 KN and 60 KN for crack tracking. During these halts, the specimen released approximately 0.6 KN, 0.8 KN, and 1.1 KN respectively. The maximum observed crack width was 0.5 mm.

The specimen exhibited a multi-stage failure. The first stage was the crushing of concrete beside the load application accompanied by delamination of the concrete compressive zone. Immediately after the flexural failure a shear crack developed and propagated up to the top surface of the beam. With further loading, the cracking extended parallel to the top surface of the beam and ran above the top of the stirrups. This continued until a large portion of the concrete compression zone was delaminated causing a drastic reduction in strength.

After the peak load the beam retained 78% of its strength which indicates that the concrete within the stirrups was largely undamaged and still functioning to provide flexural capacity.

4.12.2 Longitudinal Reinforcement Behaviour

BM 10.5-150 had a shear span of 2.84 m with gauges located 1725 mm, 1150 mm and 575 mm from the midspan. The strain in the longitudinal reinforcement at peak load was 3340 microstrain corresponding elastically to a stress of 214 MPa or 21.4% of the tensile capacity of the bar (Figure 4.44). Post-peak, the strain in the longitudinal reinforcement increased up to a maximum of 5050 microstrain corresponding to 328 MPa.

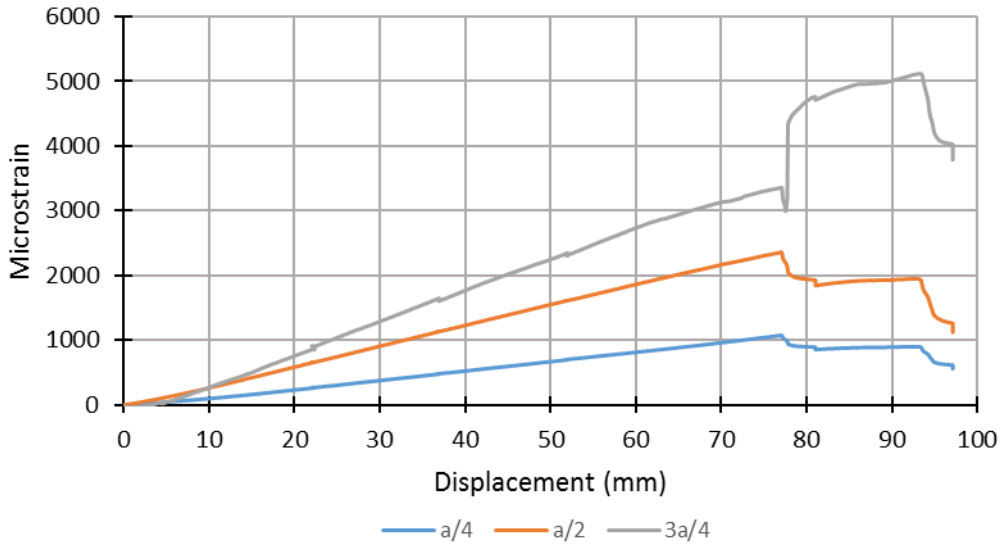

Figure 4.44 – BM 10.5-150: Longitudinal bar strains vs displacement

The stress in the longitudinal reinforcement followed expected trends with linear behaviour with respect to displacement up to peak load. After the peak load, stresses decreased as expected with the decease in applied load at a/4 and a/2. At 3a/4, the stress increased greatly. This could be due to a reduced moment arm from the loss of compression concrete or to increased stresses from dowel action. Due to the location of the gauge relative to the midspan, it is more likely that the increased stress was caused by dowel action.

4.12.3 Transverse Reinforcement Behaviour

Strain gauges were placed on stirrups adjacent on either side of the longitudinal strain gauges. The maximum observed stirrup strain at peak load was 670 microstrain corresponding elastically to a stress of approximately 30 MPa, 3.8% of the maximum straight bar strength of the stirrups (Figure 4.45). After peak load, the stirrup closest to the midspan experienced strains up to 3300 microstrain. Gauges a/4-N and 3a/4-N were inoperable during testing.

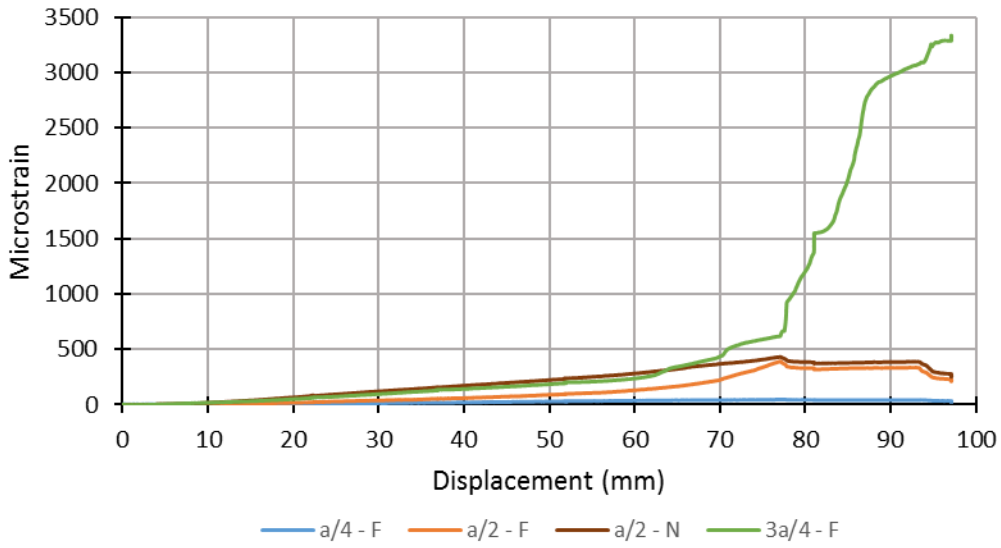

Figure 4.45 – BM 10.5-150: Strain in stirrups vs displacement

The observed strains were much lower than anticipated. At peak load, the average stress in the stirrups at peak load was calculated as 17 MPa. This could be due to the flexure governed failure, however the beam failed at 80% of its maximum shear capacity so further stirrup development would be expected. The gauges were located far from the midspan and likely see reduced strains due to their distance from the load application.

The sharp increase in stress in stirrup 3a/4-F is likely due to the shear cracking developed after the peak load was reached. This crack extended back from the point of load application and ran through the location of stirrup 3a/4-F.

4.12.4 Displacement Behaviour

Figure 4.46 shows the measured average displacements at quarter and half span locations versus the measured displacement at half span. The displacement measurements from the testing machine did not match measured displacements or observed behaviour. BM 10.5-150 displayed symmetric behaviour during testing.

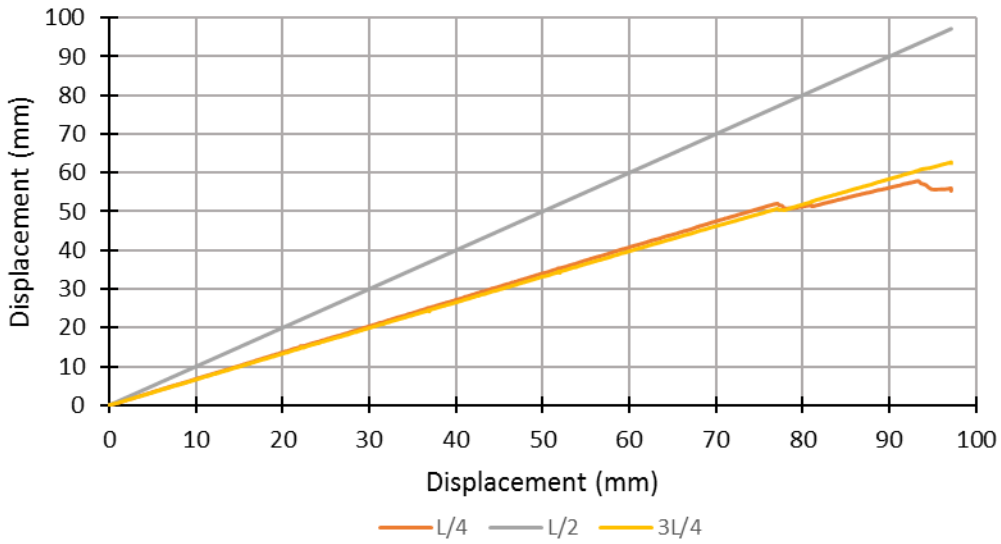

Figure 4.46 – BM 10.150-N: Displacement at measured locations vs displacement at midspan

4.13 Autopsy

In order to investigate the behaviour of the GFRP reinforcement, beams BM 4.5-150, BM 6.5-150, BM 8.5-N, BM 8.5-150 and BM 10.5-150 were dissected using a concrete saw. Cuts were made at every stirrup that crossed the failure zone for beams with stirrups. BM 8.5-N was cut longitudinally to reveal the bottom row of reinforcement (Figure 4.47).

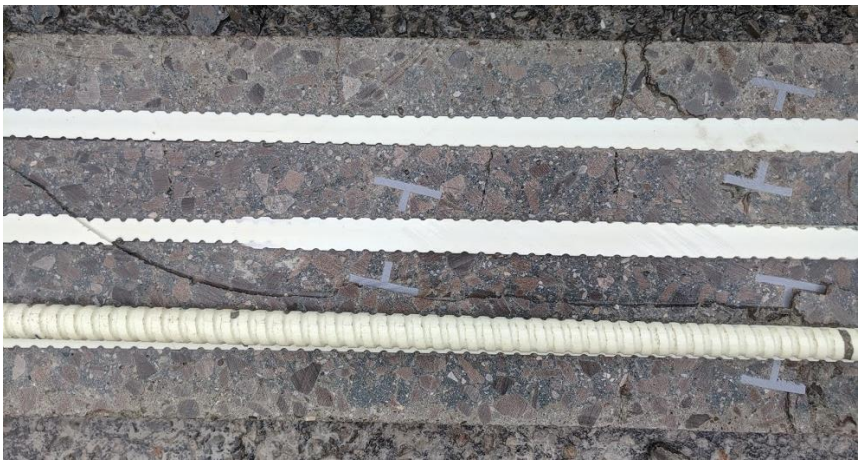

Figure 4.47 – Longitudinal cut through BM 8.5-150

The purpose of the autopsy was to determine if the brittle failure of any of the beams was due to stirrup rupture and to determine where the bond between the GFRP reinforcement (longitudinal and transverse) was maintained throughout testing.

The autopsies revealed no stirrup ruptures, and no evidence of stirrup bond slip.

Additionally, the longitudinal section taken from BM 8.5-N was hampered by extensive cracking. The majority of the bar appeared to have maintained strong bond throughout testing. As evidenced by

longitudinal crack patterns observed during testing (Figure 4.48), the bar did experience bond slip, but the autopsy was unable to determine exact locations.

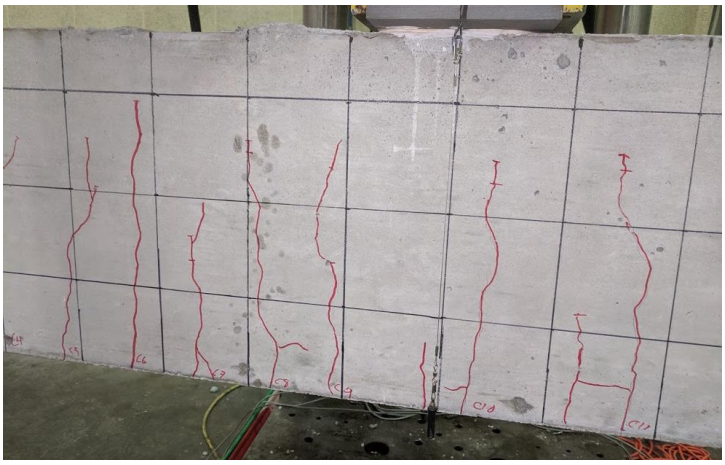

Figure 4.48 – Longitudinal cracks at level of reinforcement on BM 8.5-N

CHAPTER 5 - DISCUSSION OF RESULTS

5.0 General

A summary of the specimens and their peak loads, peak stresses, peak deflection and observed failure modes can be seen in Table 5.1. Beams exhibited a range of failure modes which was expected as the slenderness approached the shear-flexure transition range.

Table 5.1 – Specimen peak loads, displacements and failure modes

Specimen	a/d	Stirrup Spacing (mm)	P_{peak} (kN)	δ_{peak} (mm)	Failure Mode
BM 4.5-N	4.5	N/A	108.0	12.6	Shear Cracking
BM 4.5-90		90	222.5	27.0	Shear Cracking/Strut Crushing
BM 4.5-150		150	171.2	20.4	Shear Cracking/Strut Crushing
BM 6.5-N	6.5	N/A	79.3	14.8	Shear Cracking
BM 6.5-90		90	145.6	45.3	Flexural Crushing
BM 6.5-150		150	141.0	38.7	Shear Cracking
BM 8.5-N	8.5	N/A	89.5	51.1	Shear Cracking
BM 8.5-150		150	113.5	71.0	Flexural Crushing/Shear Cracking
BM 10.5-N	10.5	N/A	93.0	97.1	Shear Cracking
BM 10.5-150		150	81.7	78.0	Flexural Crushing

This section will discuss the effects of slenderness of failure mode, peak load and reinforcement behaviour. Additionally, the suitability of current codes to predict slender GFRP RC beam behaviour will be investigated and the predictions of beam behaviour using FEA by Barrage and Stoner will be compared to observed behaviour. Finally, various detailing measures for GFRP reinforced beams will be presented.

5.1 Failure Mode

The failure mode of each beam was determined by examining crack patterns at failure (Appendix B) and video recordings of failure. In general, the beams failed according to anticipated failure modes. BM 10.5-150 is the exception, as it failed due to early flexural crushing.

All beams without transverse reinforcement failed due to sliding along a critical shear crack. These beams behave functionally similar to steel RC beams with no transverse reinforcement, and exhibited extremely brittle behaviour.

The failure modes of the beams with transverse reinforcement differed from predicted behaviour. It would be expected from the lower stiffness of GFRP stirrups that the shear cracks would be sufficiently wide to cause a loss of aggregate interlock and differential movement across the crack interface. This would result in a sudden catastrophic failure. However, this was not observed during testing. Instead, the shear failures followed a pattern similar to the one observed by Johnson and Sheik (2016). At peak

load, there was crushing of the concrete next to the load application and the critical shear crack extended up into the compression region. It is generally difficult to distinguish whether the crushing occurred before the crack propagated. The failures were identified as shear or flexure dominated by whether the initial cracking after peak load caused delamination of the top concrete cover (observed to be indicative of a flexural failure by Johnson and Sheik) or if the cracking immediately connected with existing shear cracks. BM 8.5-10 showed a clear combination of the two failures, but due to the relatively low extension of the shear crack prior to failure it is identified as primarily flexure controlled.

This behaviour indicates that the stirrups provided a significant amount of strength through confinement. The failures always showed concrete spalling outside of the stirrups and post-peak testing of BM 6.5-150 and BM 8.5-150 showed that the concrete within the stirrups retained its load carrying capacity. The initial drop of strength observed in the transversely reinforced GFRP beams is due to a reduction in section depth rather than the material effects of concrete crushing. In both these beams, after the initial crushing and crack propagation, the beam regained up to 90% of the peak strength as the concrete within the stirrups developed its compressive strength.

BM 6.5-90 and 10.5-150 displayed clear flexural crushing behaviour before the formation of critical shear cracks BM 10.5-150 was predicted to fail in flexure, while BM 6.5-90 was not. In the case of BM 6.5-90, it exceeded the expected shear capacity before failing in flexure. The flexural nature of the failure can be seen from the failure crack patterns (there is clear delamination of the concrete cover before extensive shear crack development) and the specimen also displayed the most ductile behaviour post-peak as the flexural crushing progressed normally until the development of a critical shear crack. This beam was close to the shear-flexure transition and it is likely that the flexural failure was caused by the stochastic nature of concrete.

BM 10.5-150 displayed clear flexural failure at the peak load. It failed earlier than expected as it failed at a load lower than BM 10.5-N, though BM 10.5-N exceeded the expected flexural strength. While clearly a flexural failure, BM 10.5-150 did not display the relatively ductile behaviour associated with concrete crushing and instead followed the behaviour observed by Johnson and Sheik (2016). The initial crushing caused the concrete cover to delaminate. This is likely due to a flaw in the construction or another unknown factor that caused a sudden brittle failure in the compression zone.

For the beams reinforced with stirrups at 150 mm spacing, the failure modes transitioned from shear dominated to flexure dominated around a/d of 8.5. This is in line with the expected behaviour based on the simplified MCFT and plane strain beam theory. The beams without transverse reinforcement did not experience flexural crushing as expected due to the low shear capacity of slender beams.

No bar or stirrup rupture was observed except in the case of the catastrophic shear failure of BM 8.5-N where the longitudinal reinforcement ruptured after the critical shear crack formed. This was unexpected, as every test program of RC beams with GFRP transverse reinforcement observed failures due to stirrup rupture at the bends. Upon further examination, the failures oberseved in studies performed by Bentz, Massam and Collins (2010), Krall (2014) and Mahmoud and El-Salakawy (2012) show that the stirrup bends ruptured due to shear cracks crossing near to or over the bend of the stirrup. In this program, the stirrup bend ended below the top layer of longitudinal reinforcement. Since the critical shear cracks propagated longitudinally above the level of the longitudinal reinforcement, the cracks never crossed a stirrup bend. Additionally, upon autopsy of the tested specimens, there is no

evidence that the stirrup bond slipped or was inadequate to transfer the stresses to the concrete. Therefore, it is likely that the bends did not experience a significant level of stress.

The test specimens constructed for this program used stirrups with a bend radius of approximately 30 mm, or 3 $\emptyset_b$. This is the smallest allowable radius in the CSA S806 provisions and is unusual due to concerns about bend strength of GFRP stirrups among designers and producers. Additionally, testing performed by Mohamed and Benmokrane (2016) indicated that these stirrups have a bend strength that is 70% of the straight bar strength. Most researchers recommend using 45% of the straight bar strength as an assumption for the strength of GFRP bends. No stirrup was observed to exceed 50% of the straight bar strength.

Due to the combination of these factors, no bend ruptures occurred during testing. If the lack of bend ruptures is due to the distance from the bend to the shear crack then special detailing could provide adequate protection from possible brittle and sudden failures due to stirrup. This hypothesis is in line with the proposal by Bentz, Massam and Collins (2010) who observed similar behaviour in a large beams with multiple layers of reinforcement.

5.1.1 Shear Crack Development

Table 5.2 shows the run, angle and number of stirrups crossed for the critical shear crack for each specimen. In every case except BM 10.5-N, the shear crack crossed from directly adjacent to the applied load to the level of the longitudinal reinforcement.

Table 5.2 – Critical shear crack measurements

Specimen	Run (mm)	θ_{exp} (°)	θ_{MCFT} (°)	Stirrups Crossed	Depth (mm)
BM 4.5-N	850	45	44	0	300
BM 4.5-90	750	45	53	9	300
BM 4.5-150	600	41	50	7	280
BM 6.5-N	1100	37	47	0	260
BM 6.5-150	650	45	53	8	260
BM 8.5-N	1100	47	49	0	300
BM 10.5-N	1450	46	53	0	250

During the post testing autopsy of beams BM 4.5-150, BM 6.5-150, BM 8.5-150 and BM 10.5-150, the shear cracking was confirmed to only pass through the bend region of stirrups at the extremities of the cracks. This is likely the reason that no stirrup failures were observed, as the bend regions were not stressed significantly as the majority of the stirrup action was done by stirrups located nearer to the crack center. Crack tracking done during testing supports this hypothesis. At up to 70% of the peak load of all specimens, shear cracking was observed to extend only above the top level of reinforcement. The cracking reached the bottom side of the beam by joining with flexural cracking.

The angle of principle compressive stress was well predicted for beams without transverse reinforcement. However, MCFT was found to over predict the angle for beams with shear reinforcement. This result is largely outside the scope of this research, however further investigation

may be warranted on the applicable of MCFT to accurately predict beam behaviour of slender GFRP RC beams with stirrups.

5.2 Peak Load

The effect of slenderness on peak load depends on the mode of failure. In general, the more slender the beam the lower the peak load. This holds true for all the specimens with stirrups as can be seen in Figure 5.1. This follows the MCFT theory extended to FRP by Bentz, Massam and Collins (2010) where the stirrup contribution to the overall shear resistance is a function of the longitudinal strain at midsection. The increased concrete strain corresponds to higher crack widths and reduced aggregated interlock and reduced effectiveness of stirrups.

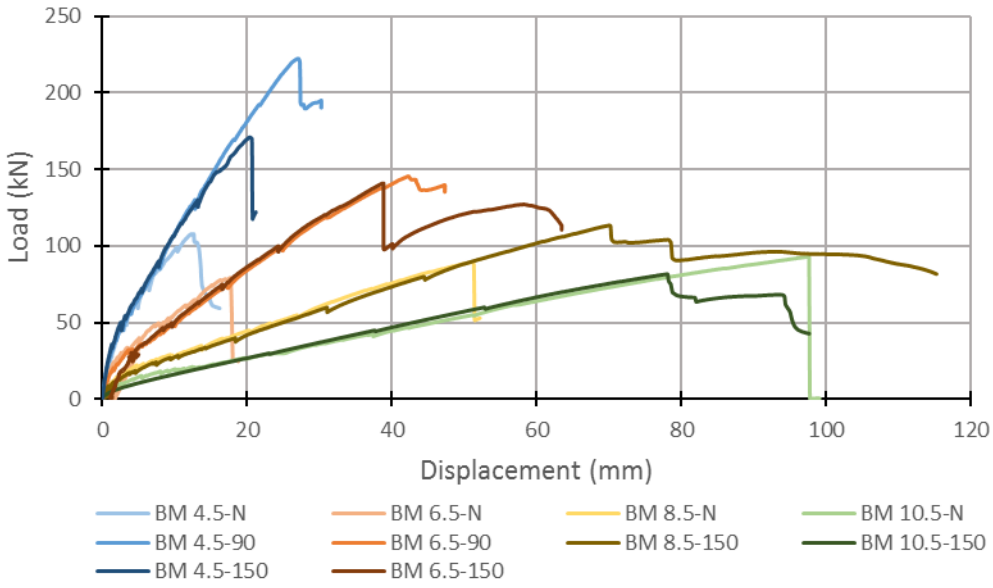

Figure 5.1 – Load vs displacement of all specimens

This behaviour does not extend to the beams without transverse reinforcement. While BM 4.5-N has a significantly higher shear capacity, the other beams have similar peak loads despite increasing slenderness. This indicates that the beams are behaving in a functionally sectional manner, with the maximum shear load being a function of section properties rather than beam slenderness. BM 4.5-N likely has an increased capacity due to the remaining influence of arch action. This is consistent with the research done on arch action in beams with lower slenderness (Kim & Jeong, 2011). Additionally, the more slender beams had much higher deflections at peak load. Despite the increased deflections, the more slender beams had similar crack widths and angles of principle compressive stress indicating that the concrete was behaving similar in shear. These results imply that the concrete contribution for GFRP reinforced beams is unaffected by the flexural stiffness of the beam.

While there is a clear reduction in peak load with increasing slenderness, the effect of the increased moment arm with increased slenderness contributes to the difference in peak loads. When comparing resultant midspan moments with displacement (Figure 5.2) it can be seen that the trend is dependent on transverse reinforcing. The highly reinforced beams, BM X.X-90, all failed close to the expected moment capacity of the section. This indicates that the decrease in peak loads was largely due to the moment arm increase. For beams with no transverse reinforcement or low transverse reinforcement,

the applied moment increased with slenderness indicating that shear mechanisms were more dominant in failure. This trend only applied up to a slenderness of 8.5 when the beams transitioned to fully flexure dominated failures. Therefore, increased slenderness corresponded to decreased shear capacity for beams in the BM X.X-150 series.

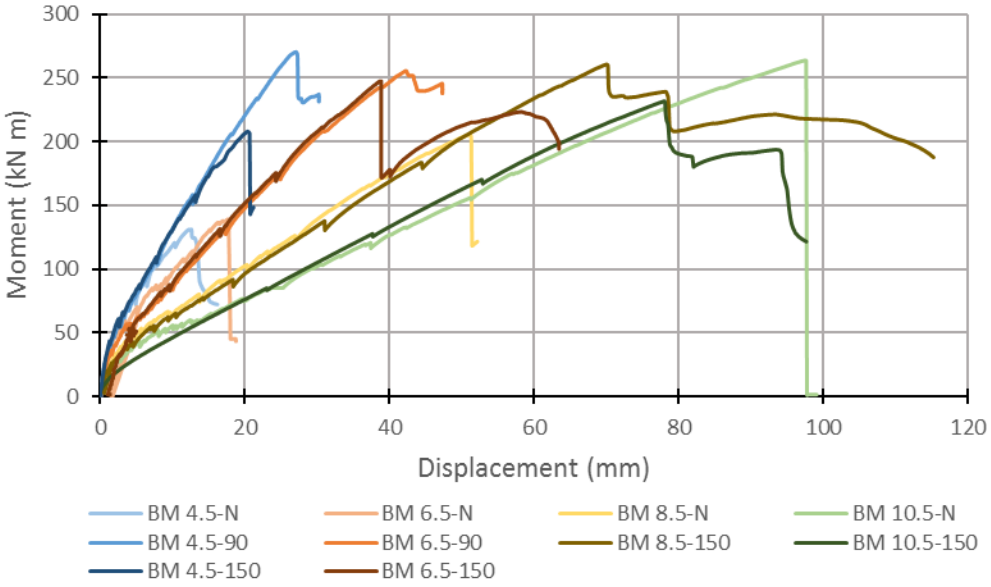

Figure 5.2 – Moment vs displacement of all specimens

Based on established theory, the peak load in shear is a combination of a concrete contribution and a stirrup contribution. The stirrup contribution can be calculated by using the average measured stress in the stirrups at peak load. The concrete contribution can be found by subtracting the stirrup contribution from the total resistance (Table 5.3).

Table 5.3 – Calculated stirrup and concrete contributions to shear resistance averaging all stirrups

Specimen	Average Stirrup Stress (MPa)	V_{max} (kN)	V_s (kN)	V_c (kN)
BM 4.5-N	N/A	53.98	0.00	53.98
BM 4.5-90	102	111.25	16.02	95.23
BM 4.5-150	205	85.60	32.20	53.40
BM 6.5-N	N/A	39.65	0.00	39.65
BM 6.5-150	95	70.50	14.98	55.52
BM 8.5-N	N/A	44.75	0.00	44.75
BM 10.5-N	N/A	46.50	0.00	46.50

A more appropriate approximation of the stirrup contribution may be obtained by using the average stress of the stirrups crossing the shear crack. BM 4.5-90 and BM 4.5-150 had critical shear cracks that engaged all of the gauged stirrups. BM 6.5-150 engaged stirrups a/4-F, a/2-N, a/2-F, 3a/4-N and 3a/4-F.

BM 8.5-150 engaged stirrups a/2-N, 3a/4-N and 3a/4-F. Using the adjusted averages, the stirrup and concrete contributions can be recalculated (Table 5.4).

Table 5.4 – Calculated stirrup and concrete contributions to shear resistance by averaging shear critical stirrups

Specimen	Average Stirrup Stress (MPa)	V_{max} (kN)	V_s (kN)	V_c (kN)
BM 4.5-N	N/A	53.98	0.00	53.98
BM 4.5-90	102	111.25	16.02	95.23
BM 4.5-150	205	85.60	32.20	53.40
BM 6.5-N	N/A	39.65	0.00	39.65
BM 6.5-150	112	70.50	17.64	52.86
BM 8.5-N	N/A	44.75	0.00	44.75
BM 8.5-150	131	56.75	20.65	36.10
BM 10.5-N	N/A	46.50	0.00	46.50

There is no clear pattern to the relationship between the two contributions. The addition of GFRP stirrups increases the concrete contribution for BM 4.5-90, but does not change it for BM 4.5-150. The addition of stirrups for BM 8.5-150 decreases the concrete contribution from the unreinforced case. This lack of pattern can be attributed to a lack of strain information for all stirrups crossing the critical shear crack and the difficulty of measuring the maximums strains in a given stirrup.

With crack longitudinal runs of up to 1 m, there are potentially 10 stirrups crossing the critical shear crack. Only six stirrups were gauged per beam, and these stirrups are distributed along the length of the shear span. A better estimate of the stirrup contribution could be obtained if every stirrup was gauged along the shear span to capture the full engagement of the stirrups along the critical shear crack.

Additionally, the stirrups were only gauged at the midheight of the stirrup. While the stirrups are expected to have developed stress at midheight, the maximum stress would occur where the stirrup intercepts the crack.

Therefore, to properly determine a stirrup contribution in a RC beam, every stirrup would need to be gauged along the height of the stirrup expected to experience significant stress. This level of gauging was outside the scope of this research, and therefore the division of concrete and stirrup contributions to shear cannot be examined closely for this research program.

5.3 Longitudinal Reinforcement Behaviour

There is no clear trend in the behaviour of the longitudinal reinforcement in this study. Most of the failures were shear controlled, and the GFRP reinforcing bars did not develop to their full flexural capacity because a shear failure occurred first. Since the gauge closest to midspan are located at 3a/4 and not at midspan, and the upper layer of reinforcement was gauged rather than the lower, the maximum longitudinal strains would be expected to be higher than the recorded values. Using the strain at peak load for BM 10.5-150 and adjusted based on the relationship of longitudinal stress to bending moment and distance from neutral axis, the strain in the bottom row of reinforcement is estimated at

366 MPa. This is much lower than the expected 480 MPa to cause an over reinforced flexural failure. Therefore, the longitudinal reinforcement either experience lower strains than expected or the measurements failed to capture the longitudinal reinforcement behaviour in flexure. Due to the lack of additional information and the body of research supporting the flexural behaviour of GFRP RC beams, it is likely that the reinforcement behaved as expected at the midspan.

It would be expected that the observed longitudinal reinforcement strains would decrease at a slenderness 6.5 due to the loss of tied arch action and increase as slenderness increases above 6.5 due to the shift to flexural controlled behaviour. The observed strains generally match this behaviour (Figure 5.3), however more tests are recommended if this behaviour is to be verified.

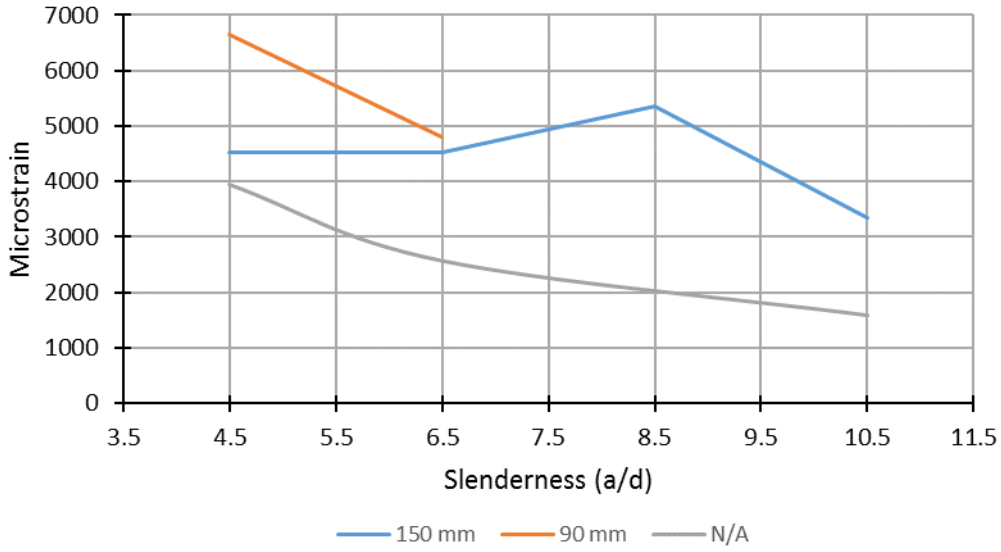

Figure 5.3 – Maximum longitudinal strain vs beam slenderness

5.4 Transverse Reinforcement Behaviour

With increasing slenderness, the transverse reinforcement experienced lower maximum and average strains (Figure 5.4). With increasing slenderness, the stirrups are developing less and using less of their maximum strength. This behaviour can largely be attributed to the effects of decreased longitudinal stiffness from the use of GFRP longitudinal reinforcement. With a lower stiffness, the longitudinal strain in the concrete increases. This reduces the concrete compressive strength while also allowing for larger crack development as the longitudinal strain is perpendicular to the stirrup orientation. Therefore, shear crack failure will occur lower stirrup strains.

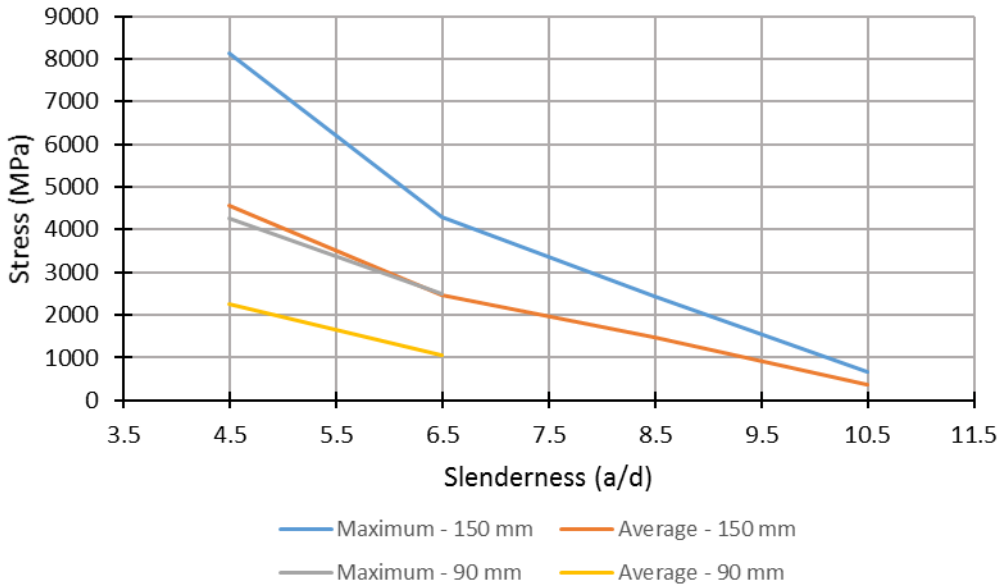

Figure 5.4 – Stirrup strains by spacing vs beam slenderness

At an a/d ratio of 4.5, there is also the residual affect of arch action. The concrete is confined by this action and the overall displacements are lowered. This allows for significantly more development of the stirrups than more slender beams.

5.5 Comparison to Current Code Provisions

CSA S806 and ACI 440 code provisions are compared against the experimental results on the basis of peak load, displacement at 70% of the experimental peak load and the governing failure mode.

5.5.1 CSA

CSA predictions for peak strength and deflection at 70% of peak load were in line with experimental results (Table 5.5 & 5.6).

Table 5.5 – Comparison of experimental load and failure behaviour to CSA S806 predictions

Specimen	P_{exp} (kN)	P_{CSA} (kN)	$\frac{P_{exp}}{P_{CSA}}$	Failure Mode	CSA Governing Failure Mode
BM 4.5-N	108.0	109.0	99%	Shear Cracking	Shear
BM 4.5-90	222.5	170.5	131%	Shear Cracking/Strut Crushing	Shear
BM 4.5-150	171.2	149.7	114%	Shear Cracking/Strut Crushing	Shear
BM 6.5-N	79.3	90.7	87%	Shear Cracking	Shear
BM 6.5-90	145.6	144.5	101%	Flexural Crushing	Shear
BM 6.5-150	141.0	127.0	111%	Shear Cracking	Shear
BM 8.5-N	89.5	80.3	111%	Shear Cracking	Shear
BM 8.5-150	113.5	110.4	103%	Flexural Crushing/Shear Cracking	Flexure
BM 10.5-N	93.0	80.3	116%	Shear Cracking	Shear
BM 10.5-150	81.7	86.0	95%	Flexural Crushing	Flexure

Table 5.6 – Comparison of experimental deflection behaviour to CSA S806 predictions

Specimen	δ_{exp} (mm)	$\delta_{CSA\ S806}$ (mm)	$\delta_{CSA\ A23.3}$ (mm)	$\frac{\delta_{exp}}{\delta_{CSA\ S806}}$	$\frac{\delta_{exp}}{\delta_{CSA\ A23.3}}$
BM 4.5-N	5.5	5.7	6.9	96%	126%
BM 4.5-90	14.8	11.8	14.7	125%	99%
BM 4.5-150	11.0	9.1	11.3	121%	103%
BM 6.5-N	9.9	12.6	15.4	79%	155%
BM 6.5-90	25.0	23.3	29.0	107%	116%
BM 6.5-150	22.9	22.6	28.1	102%	123%
BM 8.5-N	31.2	32.0	39.7	97%	127%
BM 8.5-150	43.4	40.6	50.6	107%	117%
BM 10.5-N	60.5	62.7	78.1	96%	129%
BM 10.5-150	49.9	55.1	68.5	91%	137%
			Average	102%	123%

The majority of specimens fell within reasonable variations of the CSA strength predictions. BM 4.5-90 had the largest variation from the CSA predicted capacity. CSA S806 implicitly considers the effects of arch action, and BM 4.5-N did not greatly exceed the expected capacity, so it is unlikely that the effect of arch action alone caused the increase in capacity. The specimen did exhibit much higher stirrup strains than expected, so it is likely that the arch action and the confinement provided by the tighter stirrup spacing combined to provide significant additional resistance to crack opening while increasing the stress in the stirrups. BM 4.5-150 also had increased capacity and it is possible that the stirrups perform better while arch action is still active. Further tests would be required to confirm the combination effects of arch action and confinement.

CSA S806 provides good estimates of deflection at 70% of peak load. At loads higher than 70% and lower than 20% of the peak load the CSA estimates varied from the actual testing. Predictions for BM 45-90 and BM 4.5-150 where significantly non-conservative. CSA S806 uses stiffness approximation of the bending behaviour modified by the extent of flexural cracking of the beam where tension stiffening is neglected. This formulation provides a good estimate of behaviour of flexure governed beams where flexural cracking has developed enough to eliminate tension stiffening. This reinforces the conclusions of Kharal and Sheikh (2017) that tension stiffening is reduced in beams with GFRP longitudinal reinforcement. However, this formulation has significantly non-conservative estimates of deflection for the beams with an a/d ratio of 4.5. CSA A23.3 presents another method (Equation 5.1) for calculating deflections based on empirical calibrations for steel beams.

$$\Delta = K\left(\frac{5}{48}\right)\frac{Ml^2}{E_c I_e} \tag{5.1}$$

where K is 1.0 for simply supported beams, M is the applied moment, l is the span length, E_c is the concrete stiffness and I_e is the effective moment of inertia which varies based on the applied moment in

relation to the cracking moment. CSA A23.3 provides better estimates of displacement for both BM 4.5-90 (Figure 5.5) and BM 4.5-150 (Figure 5.6).

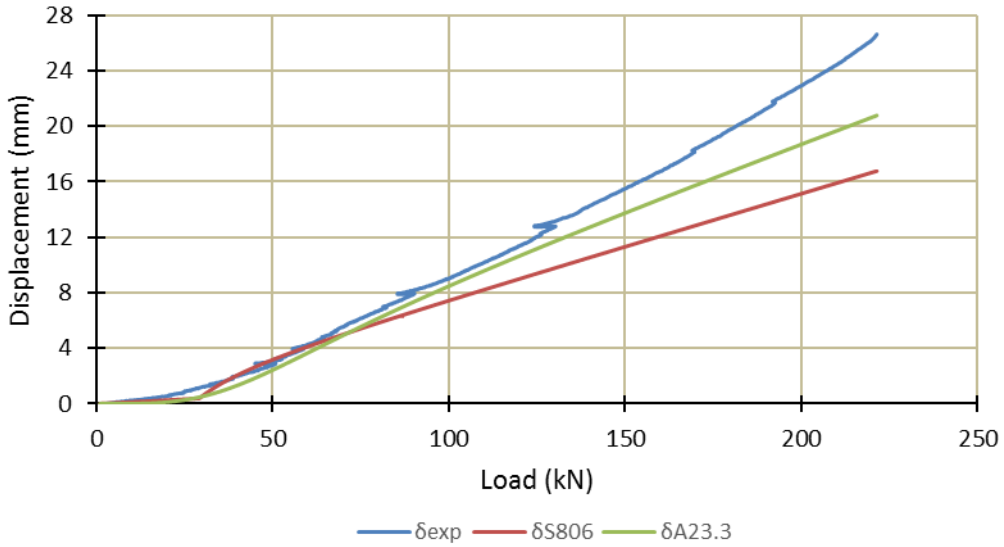

Figure 5.5 – Comparison of CSA deflection estimates for BM 4.5-90

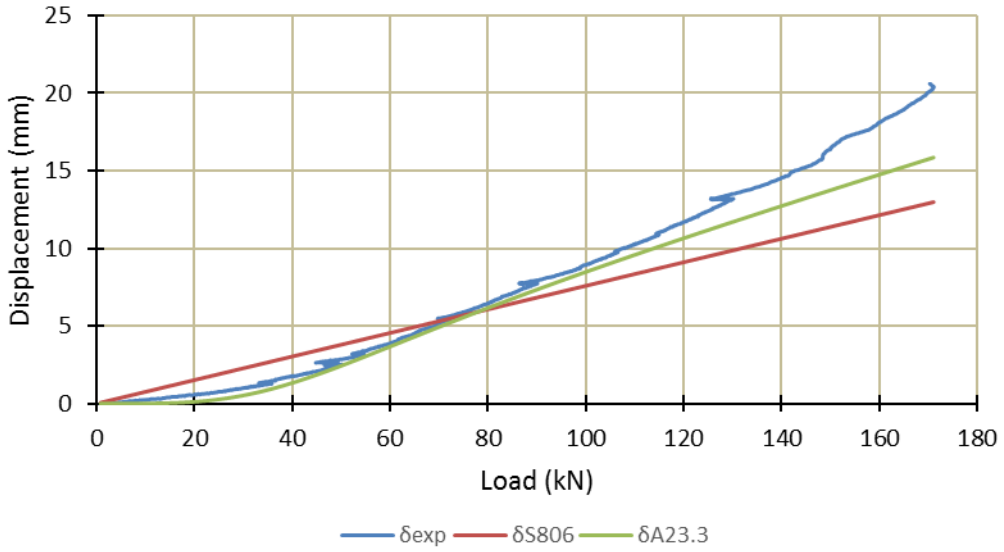

Figure 5.6 – Comparison of CSA deflection estimates for BM 4.5-150

CSA A23.3 is able to predict the deflections to within 20% at up to 80% of the peak load. Since deflection is a service state the loads being checked are typically 40%-70% of the beam capacity. CSA A23.3 displays better predictions for both BM 4.5-90 and BM 4.5-150 but when it is used to predict the behaviour of more slender beams it becomes increasingly non-conservative (due to the reduction in tension stiffening) (Table 5.6). Overall, CSA S806 provides better deflection estimates for long beams where tension stiffening has been reduced by more extensive cracking.

No justification for the reduced stirrup spacing in CSA S806 was observed in the results. The beams with stirrup spacing of 150 mm behaved as expected. No cracks formed between stirrups and there was no

bend ruptures. Additionally, the peak loads and deflections of beams with 150 mm stirrup spacing were in line with CSA predictions. Also, their failure patterns were comparable to the more heavily reinforced specimens. The major effect of the tighter stirrup spacing appears to be an increase in ductility. BM 4.5-90 and BM 6.5-90 showed more ductile failures than their counterparts with 150 mm spacing. However, the failures are shear dominated and neither set of specimens displayed any significant degree of ductility when compared with flexural failures. The requirement of reduced stirrup spacing for beams transversely reinforced with FRP is overly conservative.

5.5.2 ACI

The ACI 440-12R provisions provided acceptable predictions for the peak loads of the specimens, varying predictions for the deflections and incorrect predictions of governing failure modes (Table 5.7).

Table 5.7 – Comparison of specimen load and failure behaviour to ACI 440 predictions

Specimen	$\mathbf{P_{exp}}$ (kN)	$\mathbf{P_{ACI}}$ (kN)	$\frac{\mathbf{P_{exp}}}{\mathbf{P_{ACI}}}$	Failure Mode	ACI Governing Failure Mode
BM 4.5-N	108.0	79.8	135%	Shear Cracking	Shear
BM 4.5-90	222.5	225.1	99%	Shear Cracking/Strut Crushing	Flexure
BM 4.5-150	171.2	183.5	93%	Shear Cracking/Strut Crushing	Shear
BM 6.5-N	79.3	79.8	99%	Shear Cracking	Shear
BM 6.5-90	145.6	155.8	93%	Flexural Crushing	Flexure
BM 6.5-150	141.0	155.8	90%	Shear Cracking	Flexure
BM 8.5-N	89.5	80.3	111%	Shear Cracking	Shear
BM 8.5-150	119.2	110.4	108%	Flexural Crushing/Shear Cracking	Flexure
BM 10.5-N	93.0	80.3	116%	Shear Cracking	Shear
BM 10.5-150	81.7	86.0	95%	Flexural Crushing	Flexure

Table 5.8 – Comparison of specimen deflection behaviour to ACI 440 predictions

Specimen	$\boldsymbol{\delta_{exp}}$ (mm)	$\boldsymbol{\delta_{ACI}}$ (mm)	$\frac{\boldsymbol{\delta_{exp}}}{\boldsymbol{\delta_{ACI}}}$
BM 4.5-N	5.5	8.47	65%
BM 4.5-90	14.8	17.61	84%
BM 4.5-150	11.0	13.53	81%
BM 6.5-N	9.9	18.78	53%
BM 6.5-90	25.0	34.71	72%
BM 6.5-150	22.9	33.61	68%
BM 8.5-N	79.8	89.95	89%
BM 8.5-150	43.4	119.86	36%
BM 10.5-N	60.5	93.48	65%
BM 10.5-150	49.9	82.08	61%
		Average	67%

The peak loads were found to be in acceptable accordance with ACI 440 with the exception of BM 4.5-N. This is likely due to the specimens being near to the shear-flexure transition as ACI 440 predicted flexural failures for specimens that experienced shear failures. ACI 440 does not include a reduction in the concrete contribution to account for increased displacements and lowered aggregate interlock. As a result, the shear resistance does not reduce with beam slenderness. Due to the nature of this research focusing on the shear-flexure transition, the difference in predicting failure modes does not significantly impact peak load predictions. However, this is potentially dangerous for designers as flexural failures in GFRP RC beams are much more ductile than shear failures.

The peak load of BM 4.5-N, BM 8.5-N and BM 10.5-N were under predicted. This indicates that ACI 440 does not correctly predict the concrete contribution to shear resistance. BM 6.5-N does not follow the trend for unreinforced specimens and appears to have failed earlier than would be expected (Figure 5.7). All other specimens had increased strength relative to the ACI 440 predictions. As the transversely reinforced specimens had generally lower peak loads than the ACI 440 predictions, it is likely that ACI 440 over predicts the contribution from stirrups in shear as the concrete contribution has been shown to be under predicted.

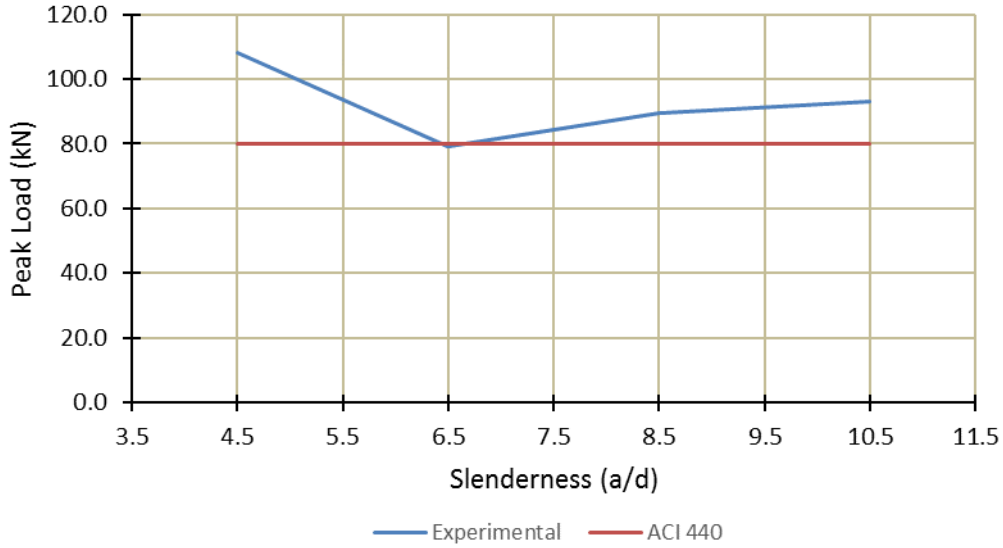

Figure 5.7 – Comparison of peak loads of non-transversely reinforced specimens with ACI 440

The ACI 440 predictions of deflection at 70% of peak load were quite accurate. The largest differentials were with BM 6.5-N which displayed unusual load-displacement behaviour and BM 10.5-150 which was at the limits of practically useful a/d ratios.

In addition, the ACI 440 provision on stirrup spacing was justified by the results of the test program. Beams with a stirrup spacing of 150 mm behaved as expected and no failures at bends or due to cracks without stirrups occurred.

5.6 Comparison of Beam Behaviour to FEA Models by Barrage (2017)

The experimental program showed some agreement with the FEA models developed by Barrage (2017). The load displacement responses predicted in the FEA modelling followed the trends of the tests, but a

overall stiffer response was predicted. Additionally, the models were unable to predict brittle failure modes. This caused an increase in apparent ductility in the models and an overprediction of strength for beams with stirrups spaced at 150 mm. A comparison of the peak loads and displacements with the experimental data can be seen in Table 5.8. Load-displacement curves comparing the experimental results to the FEA models can be found in Appendix D.

5.6.1 Peak Loads and Displacements

Table 5.9 - Comparison of specimen behaviour to predictions by Barrage (2017)

Specimen	Exp. Peak Load	FEA Peak Load	Difference	Exp. Peak Deflection	FEA Peak Deflection	Difference
BM 4.5-N	108.0	130.6	21.0%	12.6	22.3	77.4%
BM 4.5-90	222.5	227.9	2.4%	27.0	26.4	-2.2%
BM 4.5-150	171.2	226.0	32.0%	20.4	26.3	29.1%
BM 6.5-N	79.3	93.2	17.6%	14.8	27.8	87.8%
BM 6.5-90	145.6	179.6	23.3%	42.3	54.0	27.6%
BM 6.5-150	141.0	155.5	10.3%	38.7	44.8	15.6%
BM 8.5-N	89.5	78.7	-12.1%	51.1	47.3	-7.3%
BM 8.5-150	113.5	128.4	13.1%	71.0	75.9	6.9%
BM 10.5-N	93.0	98.7	6.1%	97.0	77.6	-20.0%
BM 10.5-150	81.7	107.9	32.0%	78.0	117.5	50.6%

For the majority of specimens, the FEA models predicted strength to within ±25%. The exceptions were BM 4.5-150 and BM 10.5-150. BM 4.5-150 failed due to the widening of a critical shear crack. This failure was accompanied by a sudden drop in load carrying capacity. This behaviour was not captured on the FEA models due the CDPM (Concrete Damaged Plasticity Model) used in the FEA analysis. CPDM is unable to accurately model the sudden brittle nature of shear crack widening and propagation. BM 4.5-90 failed in a more conventional manner with no sudden drop of load carrying capacity and as such is much better predicted by the FEA model. BM 10.5-150 failed in flexure at the expected load. The FEA models predicted a much higher capacity. This model does not follow the general trend of decreasing capacity with increasing slenderness and the prediction is likely caused by an error in that specific model.

Peak deflections are overestimated for the beams where the peak load is overestimated. These peak deflections correspond to the peak load from the FEA model rather than the experimental peak load. The modelled beams displayed greater ductility when entering failure and often carried higher loads with decreasing stiffness at failure. This behaviour was not observed in the experimental tests where the beams had a bilinear stiffness behaviour with a sudden brittle failure.

5.6.2 Stiffness

The FEA models overpredicted beam stiffness and underpredicted deflections. This was observed by Barrage (2017) in his study. These predictions were up to 30% off for BM 4.5-150 (Figure 5.8), though in

the majority of specimens the deflections are estimated within 15% for a given load. The models display a more parabolic load-displacement curve similar to steel RC beams. Testing found that the real load-displacement curves are more bilinear due to the concrete delamination at peak load and the lack of pronounced crushing behaviour.

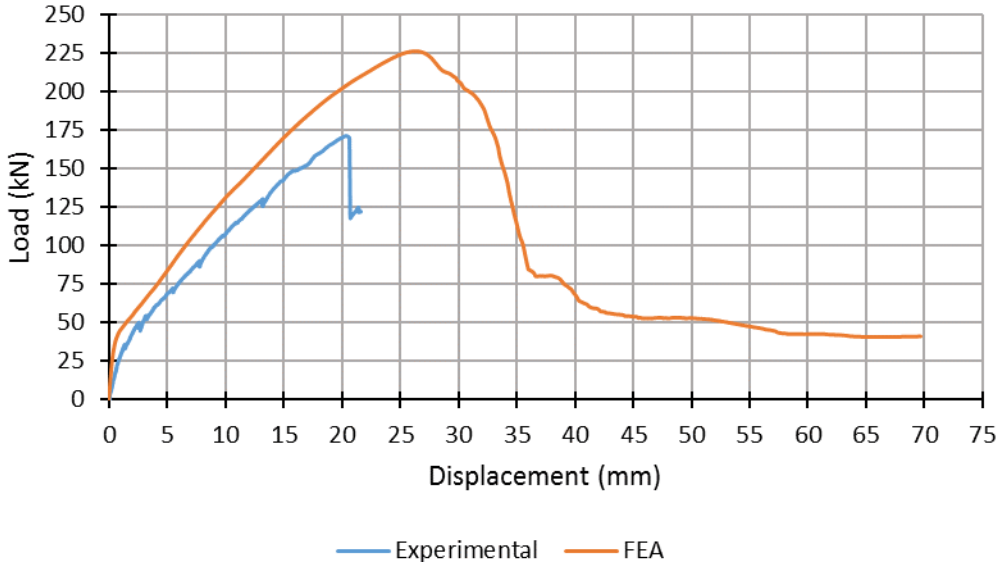

Figure 5.8 – Comparison of experimental and FEA modelled load-displacement for BM 4.5-150

5.6.1 Stirrup Strains

The stirrup strains in BM 4.5-150 versus those in the FEA model can be seen in Figure 5.9. Strains in the FEA model are taken at midheight on the stirrup (the location of the gauges in the experimental specimens) and at the location of maximum strain. This specimen is representative for all specimnes of the general trend of comparison between the FEA predictions and experimentally observed stirrup strains. The rest of the specimens will not be compared in detail.

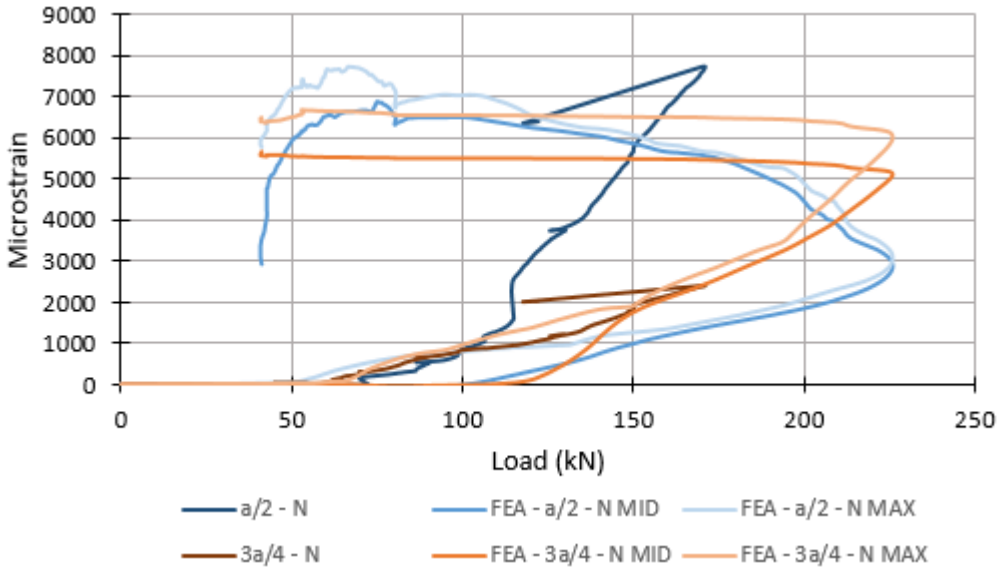

Figure 5.9 – Comparison of experimental and FEA modelled stirrup strains for BM 4.5-150

The stirrups in the FEA models experience much lower strain at similar loads at the half-shear span location and good estimates for the three-quarters shear span location. Both the peak strain in the stirrups is relatively well-predicted by the FEA, however the location of the peak strain is changed. The stirrups in the FEA model do not show the same trends in strain based on proximity to the load application observed in the test specimens. In general, the FEA models show a much more distributed load among the stirrups in contrast to the highly concentrated results from the test program.

There are two sources for this discrepancy. The first that the FEA models used a smeared stirrup model to approximate stirrup behaviour. This model approximates the behaviour of the stirrup over the whole depth and width of the section and may not be suitable to investigate localized effects. The FEA strains are averages over the width of the smeared element while the gauges are measuring strain at a single location on a bar. These averages may not be suitable to approximate behaviour as straight portion strains may be distributed across the depth and width of the membrane approximation.

The second source of error lies in the mechanism behind the development of stress in the stirrups. In the real specimens, the stirrups are stressed by the formation of cracks. The stirrups resist the opening of the cracks and stirrup stresses are highest at the crack interfaces. The FEA models developed by Stoner (2015) and used by Barrage (2017) used a concrete damaged plasticity model which models cracks through changing material properties rather than through discrete fractures. This has the overall effect of smoothing the FEA stirrup stresses whereas the measured stresses have significant spikes immediately after intercepting cracks.

5.6.2 Crack Patterns

The crack patterns from the FEA models (Figure 5.10) on the critical shear span are not very representative of the actual observed behaviour (Figure 5.11). The crack angle, extent of cracking and cracks causing failure are not captured in the FEA models. This is a result of using the CPDM model and is part of the reason that some failure loads are over predicted.

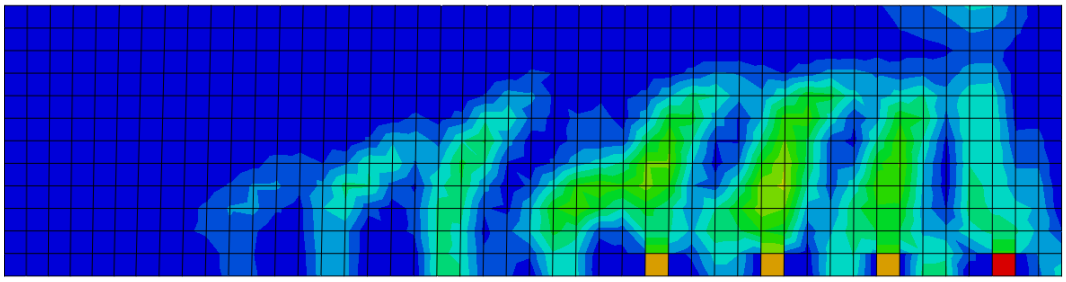

Figure 5.10 – FEA modelled crack patterns for BM 4.5-150

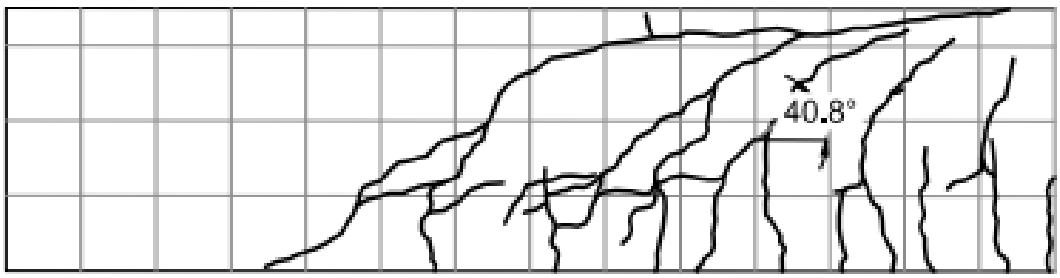

Figure 5.11 – Experimentally observed crack patterns on shear critical span for BM 4.5-150 - mirrored

CHAPTER 6 - CONCLUSIONS & RECOMMENDATIONS

6.0 Conclusions

The purpose of this research program was to investigate the shear behaviour of slender GFRP reinforced concrete beams and compare to predictions by existing models and FEA analysis. The current body of shear research on GFRP reinforced beams is focused on relatively short members and has not been confirmed to accurately model slender specimens.

The test program consisted of single point bending tests on 10 specimens with longitudinal GFRP reinforcement. 6 of these specimens had transverse GFRP reinforcement while the other 4 had no transverse reinforcement.

Based on the analysis of the results of the test program, the following conclusions may be drawn:

1. **Increasing the slenderness of transversely reinforced GFRP RC beams decreases the shear capacity of the beam. This is caused by the lessening of aggregate interlock due to increased deflections and wider crack widths. Additionally, the increased slenderness decreases the development of stirrups and longitudinal bars further decreasing capacity. This effect is prominent only in beams that are further from the shear-flexure transition ratio.**

2. **Increasing the slenderness of GFRP RC beams has no significant effect on the moment capacity of the beam.**
    a. **The moment capacity is reached in BM 8.5-150 and BM 10.5-150 at expected levels.**
    b. **The flexural capacity in terms of kN of applied load decreases solely by the impact of beam span on moment calculations.**

3. **Slender GFRP RC beams behave similar to shorter beams.**
    a. **Deflections and crack widths are increased due to reduced longitudinal stiffness.**
    b. **Shear capacities are reduced compared to steel RC beams by lower concrete confinement, less aggregate interlock and lower development of the stirrups**

4. **GFRP stirrup rupture can be avoided in slender beams with sufficient detailing. The stirrup ruptures are associated with cracks crossing in the bend region of the stirrup. Detailing stirrup bends to lie below the depth of the longitudinal reinforcement can reduce stresses in the bend to negligible levels in relation to straight portion stresses.**

5. **CSA S806-12R provides good predictions of beam capacity and failure mode up to a/d ratios of 10.5.**

6. **CSA S806-12R provides conservative predictions of beam deflection.**

7. **Provision 8.4.6.1 of CSA S806-12R is overly conservative and beams with larger stirrup spacing show similar accuracy for strength and deflection predictions.**

8. **ACI 440 provides good predictions of beam strength and deflection for slender beams.**

9. **ACI 440 does not accurately predict failure mode of slender beams.**
    a. **Failure modes are generally incorrect for beams with transverse reinforcement.**

10. **ACI 440 under predicts the concrete contribution to shear resistance and over predicts the stirrup contribution.**

11. **The FEA modelling done by Barrage (2017) provide reasonable approximations of experimental behaviour**
    a. **The peak strengths predicted by the models are accurate to within 25% for most specimens.**
    b. **The models fail to properly predict the stiffness and ductility of shear failures of the slender beams with transverse GFRP reinforcement.**

6.1 Recommendations for Future Research

Further research is recommended to better investigate the applicability of design codes to slender GFRP RC beams in shear and to better model the behaviour of these beams in FEA. The recommendations are as follows:

1. Additional specimen testing of beams with greater depth and differing cross-sections is recommended to confirm that CSA S806-12 Cl 8.4.6.1 is overly limiting of stirrup spacing.

2. Due to the potential benefits of using GFRP stirrups due to their corrosion resistance, there is the potential that beams with steel longitudinal reinforcement and GFRP stirrups could prove useful. Testing of these specimens is recommended. This would also allow the isolation of the effects of using GFRP stirrups in place of conventional steel further contributing to the understanding of the shear mechanics of GFRP RC beams.

3. FEA modelling performed by Barrage (2017) showed overall higher stiffness and an inability to properly account for the failure mechanisms of the beams. The tested specimens displayed a sudden loss of strength immediately after peak load due to the formation of a critical shear crack, the spalling of top concrete cover or a combination of the two modes. The FEA models on the whole were unable to capture this behaviour. Further research is recommended to properly model these phenomena to improve the accuracy and reliability of FEA models for predicting behaviour of GFPR RC beams.

REFERENCES

Acciai, A., D'Ambrisi, A., De Stefano, M., Feo, L., Focacci, F., & Nudo, R. (2016). Experimental response of FRP reinforced members without transverse reinforcement: Failure modes and design issues. Composites Part B: Engineering, 89, 397-407.

Al-Khrdaji, T., Wideman, M., Belarbi, A., & Nanni, A. (2001). Shear strength of GFRP RC beams and slabs. *Proceedings of the International Conference on Composites in Construction - CCC 2001*(1), 409-414.

Alsayed, S. (1998). Flexural Behaviour of Concrete Beams Reinforced with GFRP Bars. *Cement and Concrete Composites, 20*, 1-11.

American Concrete Institure (ACI). (2006). *Guide for the Design and Construction of Concrete Reinforced with FRP Bars Reported by ACI Committee 440.* Farmington Hills, Michigan: American Conrete Institute.

American Conrete Institiute (ACI). (2000). *Recent Approaches to Shear Design of Structural Concrete (ACI 445R-99).* Farmington Hills, Michigan: American Concrete Institute.

Ascione, L., Mancusi, G., & Spadea, S. (2010). Flexural Behaviour of Concrete Beams Reinforced With GFRP Bars. *Strain*, 460-469.

Barrage, R. (2017). *Finite Element Modelling of FRP Reinforced Concrete Beams and Comparative Analysis of Current Strength Prediction Methods.* University of Waterloo.

Bentz, E. C., & Collins, M. P. (2006). Development of the 2004 Canadian Standards Association (CSA) A23.3 shear provisions for reinforced concrete. *Canadian Journal of Civil Engineering, 33*(5), 521-534.

Bentz, E., Massam, L., & Collins, M. (2010). Shear Strength of Large Concrete Members with FRP Reinforcement. *Journal of Composites for Construction, 14*(6), 637-646.

Bentz, E., Vecchio, F., & Collins, M. (2006). Simplified Modified Compression Field Theory for Calculating Shear Strength of Reinforced Concrete Elements. *ACI Structural Journal, 103*(4), 614-624.

Canadian Standards Assocation (CSA). (2012). *Design and construction of building structures with fibre-reinforced polymers (S806).* Mississauga, Ontario: Canadian Standards Assocation.

El-Sayed, A., El-Salakawy, E., & Benmokrane, B. (2006). Shear Strength of Reinforced Concrete Beams without Transverse Reinforcement. *ACI Structural Journal, 103*(2), 235-243.

Gross, S., Yost, J., Dinehart, D., Svensen, E., & Liu, N. (2003). Shear Strength of Normal and High Strength Concrete Beams Reinforced with GFRP Bars. *International Conference on High Performance Materials in Bridges* (pp. 426-437). Reston, Virginia: American Society of Civil Engineers. doi:10.1061/40691(2003)38

Hao, Q., Wang, Y., Zhang, Z., & J, O. (2007). Bond strength improvement of GFRP rebars with different rib geometries. *Journal of Jhejiang University SCIENCE A, 8*(9), 1356-1365.

Johnson, D., & Sheikh, S. (2016). Experimental investigation of glass fiber-reinforced polymer-reinforced normal-strength concrete beams. *ACI Structural Journal, 113*(6), 1165-1174.

Kharal, Z., & Sheikh, S. (2017). Tension stiffening and cracking behavior of glass fiber-reinforced polymer-reinforced concrete. *ACI Materials Journal, 114*(2), 299-310.

Kim, W., & Jeong, J. (2011). Decoupling of Arch Action in Shear-Critical Reinforced Concrete Beams. *ACI Structural Journal, 108*(4), 395-428.

Krall, M. (2014). *Tests on Concrete Beams with GFRP Flexural and Shear Reinforcements & Analysis Method for Indeterminate Strut-and-Tie Models with Brittle Reinforcements.* Waterloo, Ontario: Univeristy of Waterloo.

Mahmoud, K., & El-Salakawy, E. (2012). Effect of Transverse Reinforcement Ratio on the Shear Strength of GFRP-RC Continuous Beams. *Journal of Composites for Construction, 16*(6), 615-625.

Mohamed, K., & Benmokrane, B. (2016). *Bend Strength of MST-BAR GFRP Bent Bars.* University of Sherbrooke. Sherbrooke, QC: University of Sherbrooke.

Nagasaka, T., Fukuyama, H., & Tanigaki, M. (1993). Shear Performance of Concrete Beams Reinforced with FRP Stirrups. *Special Publication of the ACI, 138*(47), 789-812.

Nakamura, H., & Higai, T. (1995, December). Evaluation of Shear Strength of Concrete Beams Reinforced with FRP. *(English Translation) Concrete Library International of Japanese Society of Civil Engineers, 26*, 111-123.

Okelo, R., & Yuan, R. L. (2005). Bond Strength of Fiber Reinforced Polymer Rebars in Normal Strength Concrete. *Journal of Composites for Construction, 9*(3), 203-213.

Razaqpur, A., & Isgor, B. (2004). Concrete Contribution to the Shear Resistance of Reinforced Polymer Reinforced Concrete Members. *Journal of Composites for Construction, 8*(5), 452-460.

Razaqpur, A., & Spadea, S. (2015). Shear Strength of FRP Reinforced Concrete Members with Stirrups. *Journal of Composites for Construction, 19*(1), 4014025.

Shehata, E., Morphy, R., & Rizkalla, S. (2000). Fibre reinforced polymer shear reinforcement for concrete members : behaviour and design guidelines. *Canadian Journal of Civil Engineering, 27*, 859-872.

Stoner, J. (2015). *Finite Element Modelling of GFRP Reinforced Concrete Beams.* Waterloo, Ontario: University of Waterloo.

Vecchio, F., & Collins, M. (1988). Predicting the Response of Reinforced Concrete Beams Subjected to Shear Using Modified Compression Field Theory. *ACI Structural Journal*(85).

Yost, J., Gross, S., & Dinehart, D. (2001). Shear Strength of Normal Strength Concrete Beams Reinforced with Deformed GFRP Bars. *Journal of Composites for Construction, 5*(4), 268-275.

APPENDIX A - CRACK TRACKING AND CRACK WIDTHS DURING TESTING

A.0 Series BM 4.5 – N

Date: April 16 **Beam:** 4.5-N **Load Level:** 52.9 kN

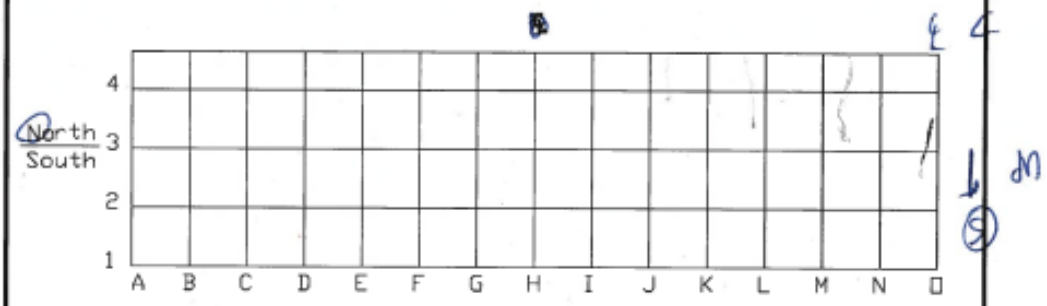

General Comments:

Crack	Location			
	Label	X (mm)	Y (mm)	Width (mm)
C4				0.1
C5				0.1
C6				0.1
C7				0.05
C3				0.1
C2				0.05
C1				0.05

Figure A.1 - Crack tracking of north side of BM 4.5-N at 52.9 kN

Date: April 16 Beam: 4.5-N Load Level: 52.9 kN

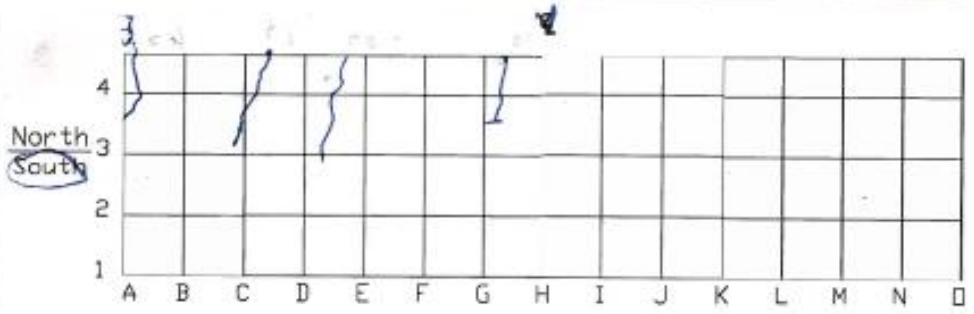

General Comments:

Crack	Location			
	Label	X (mm)	Y (mm)	Width (mm)
C1				
C2				
C3				
C4				

Figure A.2 - Crack tracking of south side of BM 4.5-N at 52.9 kN

Date: Apr. 16. 19 Beam: 4.5N Load Level: 66 kN

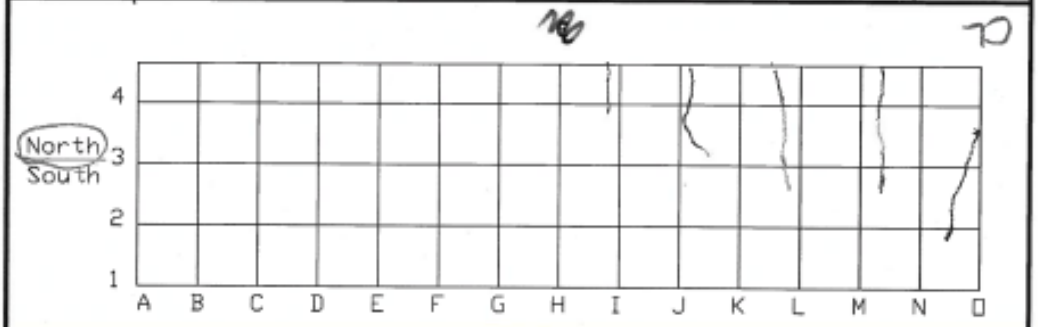

General Comments:

Crack	Location			
	Label	X (mm)	Y (mm)	Width (mm)
C9				0.05
C7				0.05
C6				0.1
C5				0.1
C4				0.25
C8				0.1
C3				0.1
C2				0.15
C1				0.1

Figure A.3 - Crack tracking of north side of BM 4.5-N at 66 kN

Date: April 16 Beam: BM 4.5-N Load Level: 66 kN

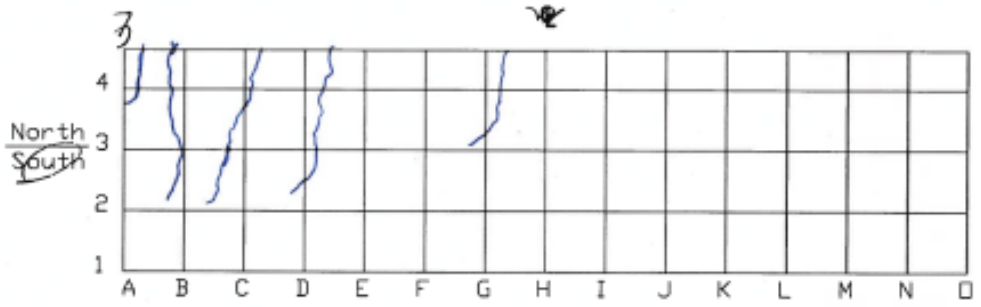

General Comments:

Crack	Location			
	Label	X (mm)	Y (mm)	Width (mm)

Figure A.4 - Crack tracking of south side of BM 4.5-N at 66 kN

Date: Apr.16.19 Beam: 4.5N Load Level: 78kN

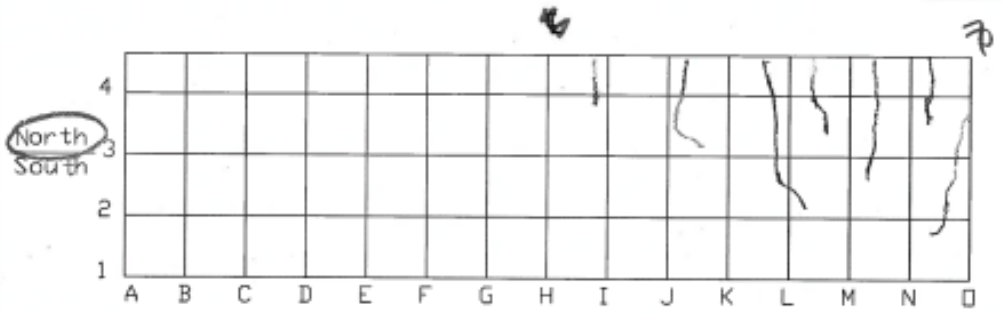

General Comments:

Crack	Location			
	Label	X (mm)	Y (mm)	Width (mm)
C10				0.1
C12				0.1
C13				0.1
C12				0.2
C3				0.15
C8				0.15
C4				0.2
C1				0.05
C5				0.1
C11				0.1
C6				0.15
C7				0.1
C9				0.05

Figure A.5 - Crack tracking of north side of BM 4.5-N at 78 kN

Date: Apr. 16, 19 Beam: 4.5 N Load Level: 78 kN

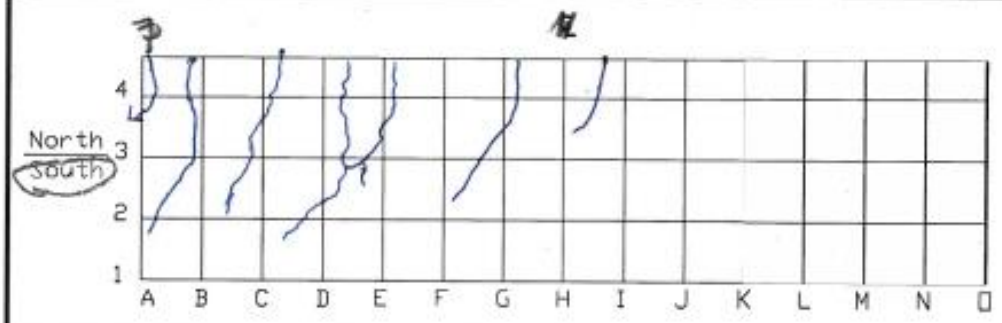

General Comments:

Crack	Location			
	Label	X (mm)	Y (mm)	Width (mm)

Figure A.6 - Crack tracking of south side of BM 4.5-N at 78 kN

A.1 Series BM 4.5 – 90

Date: Apr. 17 **Beam:** 4.5 90 **Load Level:** 50 kN

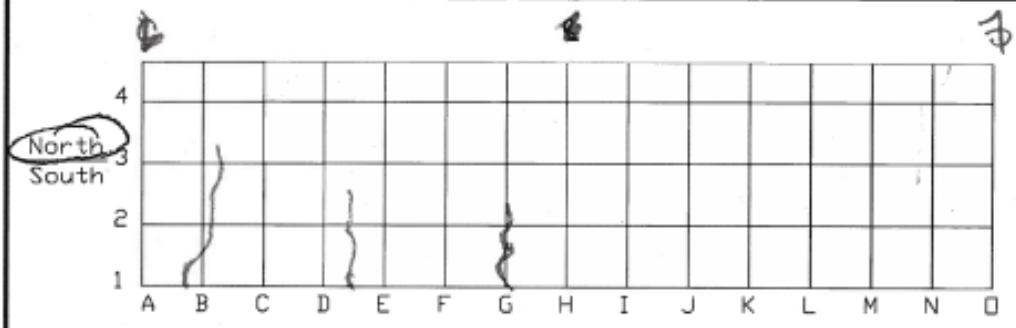

General Comments:

Crack	Location			
	Label	X (mm)	Y (mm)	Width (mm)
C5				
C6				
C7				

Figure A.7 - Crack tracking of north side of BM 4.5-90 at 50 kN

Date: April 17 Beam: BM 4.5-90 Load Level: 50 kN

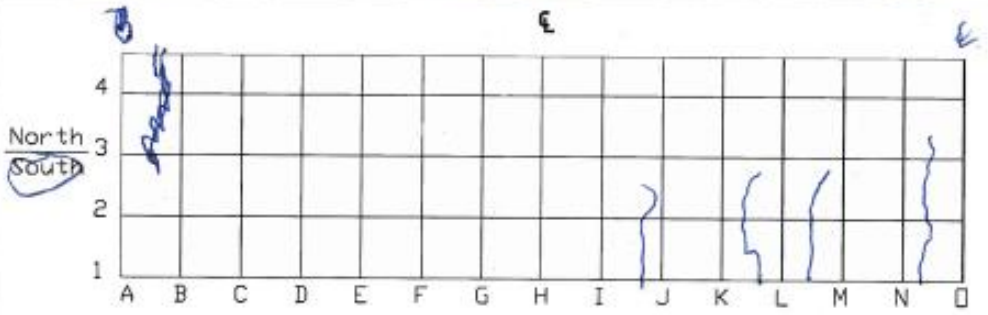

General Comments:

Crack	Location			
	Label	X (mm)	Y (mm)	Width (mm)
C1				0.05
C2				0.05
C3				0.1
C4				0.1
C5				0.15
C6				0.1
C7				0.05
C8				

Figure A.8 - Crack tracking of south side of BM 4.5-90 at 50 kN

Date: Apr 17 Beam: 4.5-90 Load Level: 90

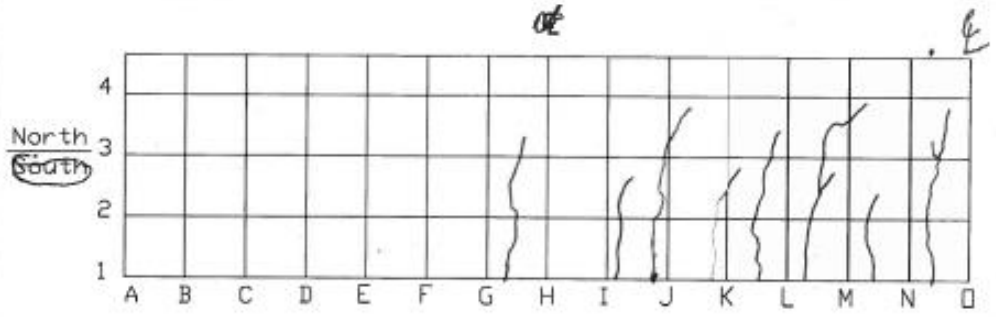

General Comments:

Crack	Location			
	Label	X (mm)	Y (mm)	Width (mm)
C1				0.2
C2				0.2
C3				0.2
C4				0.3
C5				0.2
C6				0.3
C7				0.15
C8				0.2
C9				0.1
C10				0.2

Figure A.9 - Crack tracking of north side of BM 4.5-90 at 90 kN

Date: Apr. 17 Beam: 4.5 90 Load Level: 90 kN

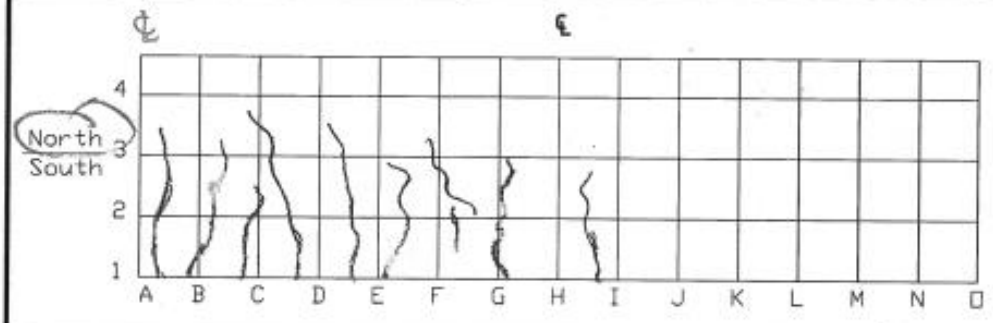

General Comments:

Crack	Location			
	Label	X (mm)	Y (mm)	Width (mm)

Figure A.10 - Crack tracking of south side of BM 4.5-90 at 90 kN

Date: Apr 17 Beam: 4.5 40 Load Level: 130 kN

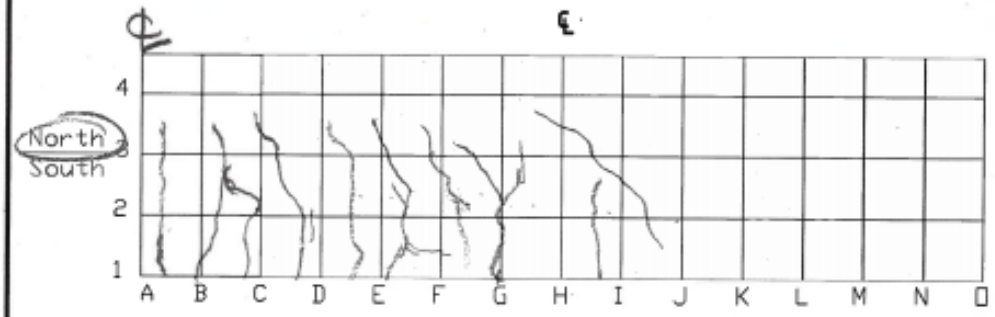

General Comments:

Crack	Location			
	Label	X (mm)	Y (mm)	Width (mm)
C1				0.35
C2				0.45
C3				0.45
C4				0.5
C5				0.3
C6				0.5
C7				0.35
C8				0.3
C9				0.2
C10				0.5

Figure A.11 - Crack tracking of north side of BM 4.5-90 at 130 kN

Date: April 17 Beam: BM 4.5-90 Load Level: 130 kN

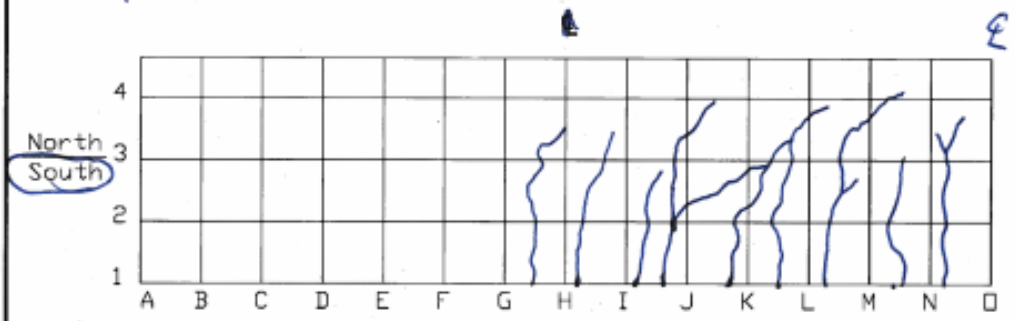

General Comments:

Crack	Location			
	Label	X (mm)	Y (mm)	Width (mm)

Figure A.12 - Crack tracking of south side of BM 4.5-90 at 130 kN

A.2 Series BM 4.5 - 150

Date: Apr 22 **Beam:** 4.5-150 **Load Level:** 50 kN

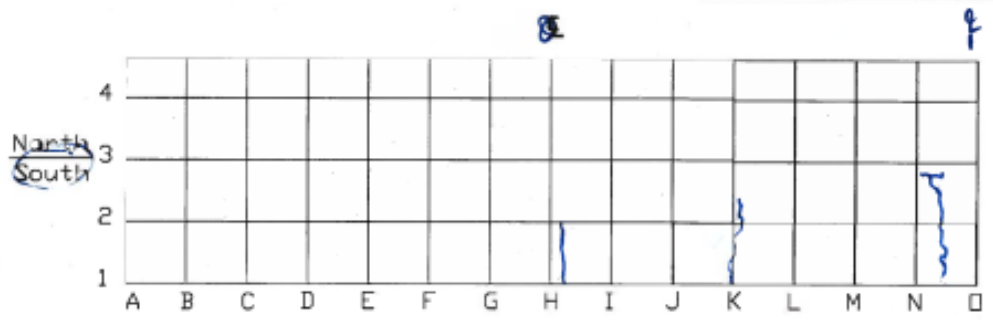

General Comments:

Crack	Location			
	Label	X (mm)	Y (mm)	Width (mm)
C1				0.05
C2				0.05
C3				0.1
C4				0.2
C5				0.15
C6				0.1

Figure A.13 - Crack tracking of south side of BM 4.5-150 at 50 kN

Date: Apr 22 Beam: 4.5-150 Load Level: 50 kN

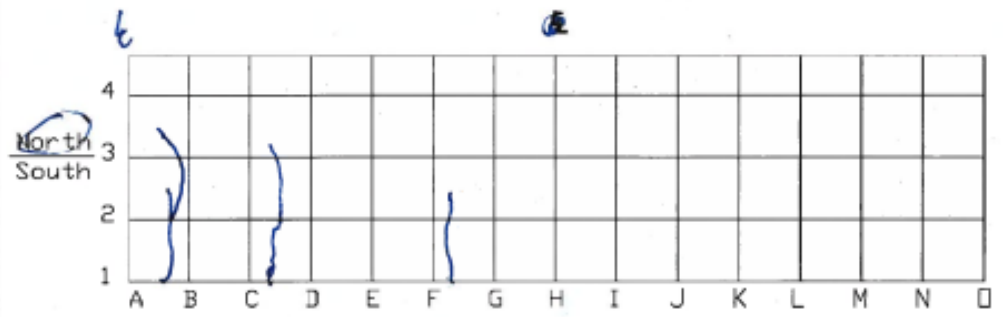

General Comments:

Crack	Location			
	Label	X (mm)	Y (mm)	Width (mm)

Figure A.14 - Crack tracking of north side of BM 4.5-150 at 50 kN

Date: Apr 22 Beam: 4.5-150 Load Level: 90 kN

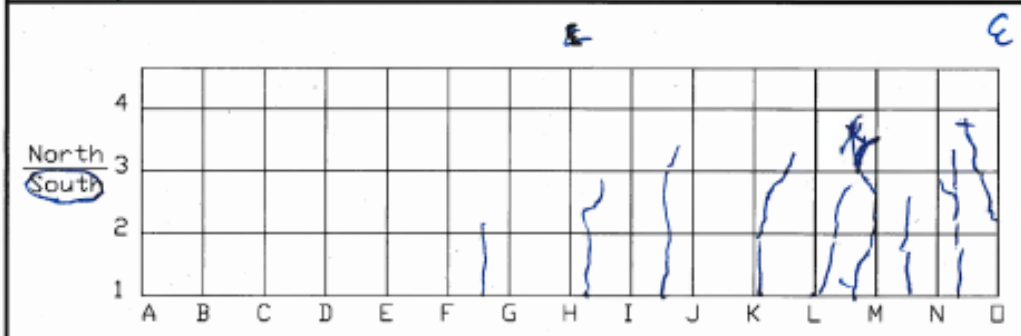

General Comments:

Crack	Location			
	Label	X (mm)	Y (mm)	Width (mm)
C1				0.05
C2				0.1
C3				0.1
C4				0.2
C5				0.15
C6				0.2
C7				0.1
C8				0.1
C9				0.1
C10				0.1

Figure A.15 - Crack tracking of south side of BM 4.5-150 at 90 kN

Date: Apr 22 Beam: 4.5-150 Load Level: 90 kN

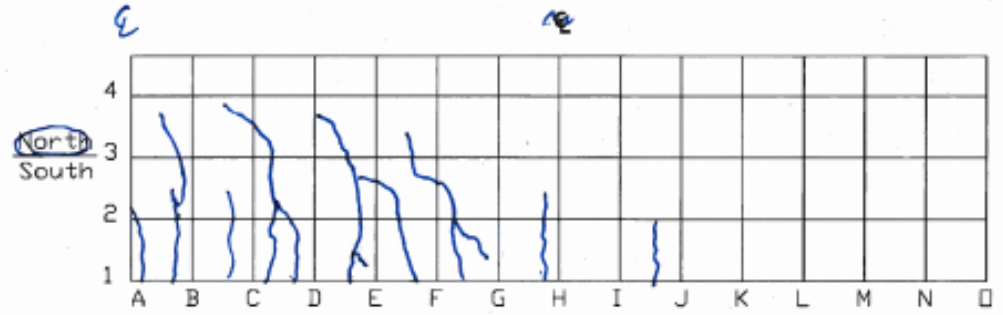

General Comments:

Crack	Location			
	Label	X (mm)	Y (mm)	Width (mm)

Figure A.16 - Crack tracking of north side of BM 4.5-150 at 90 kN

Date: Apr 27 Beam: 4.5 – 150 Load Level: 130 kN

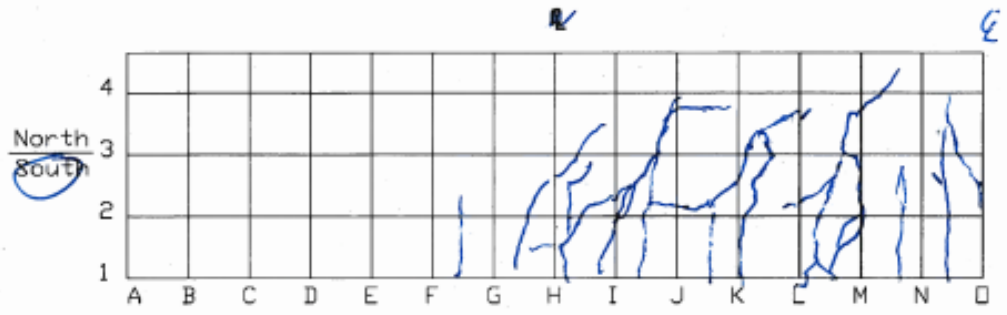

General Comments:

Crack	Location			
	Label	X (mm)	Y (mm)	Width (mm)
C1				0.1
C2				0.25
C3				0.15
C4				0.2
C5				0.15
C6				0.3
C7				0.15
C8				0.25
C9				0.15
C10				0.25

Figure A.17 - Crack tracking of south side of BM 4.5-150 at 130 kN

Date: Apr 22 Beam: 4.5-150 Load Level: 130 kN

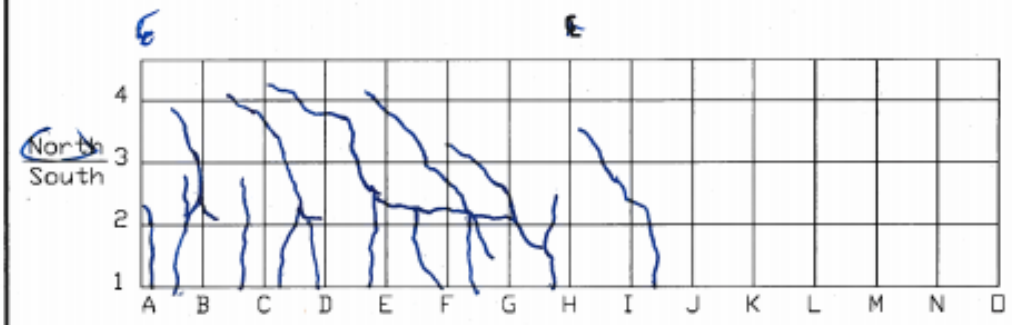

General Comments:

Crack	Location			
	Label	X (mm)	Y (mm)	Width (mm)

Figure A.18 - Crack tracking of north side of BM 4.5-150 at 130 kN

A.3 Series BM 6.5 – N

Date: April 29 **Beam:** 6.5-N **Load Level:** 40 kN

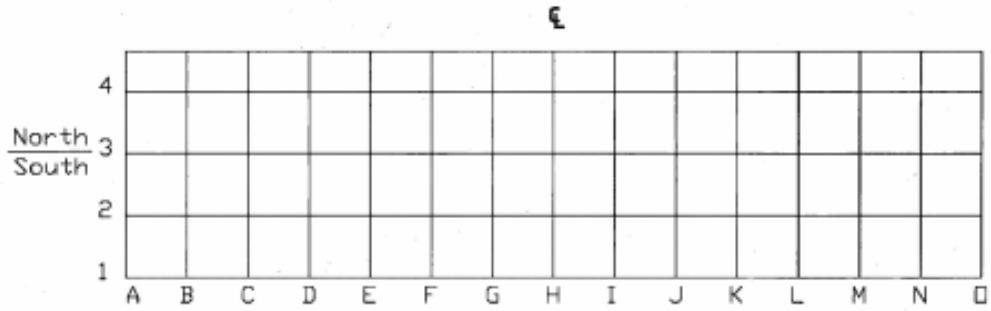

General Comments:

Crack	Location			
	Label	X (mm)	Y (mm)	Width (mm)
C1				0.1mm
C2				0.05
C3				0.1
C4				0.1
C5				0.05
C6				0.1
C7				0.1
C8				0.05
C9				0.1
C10				0.1

Figure A.19 - Crack widths of BM 6.5-N at 40 kN

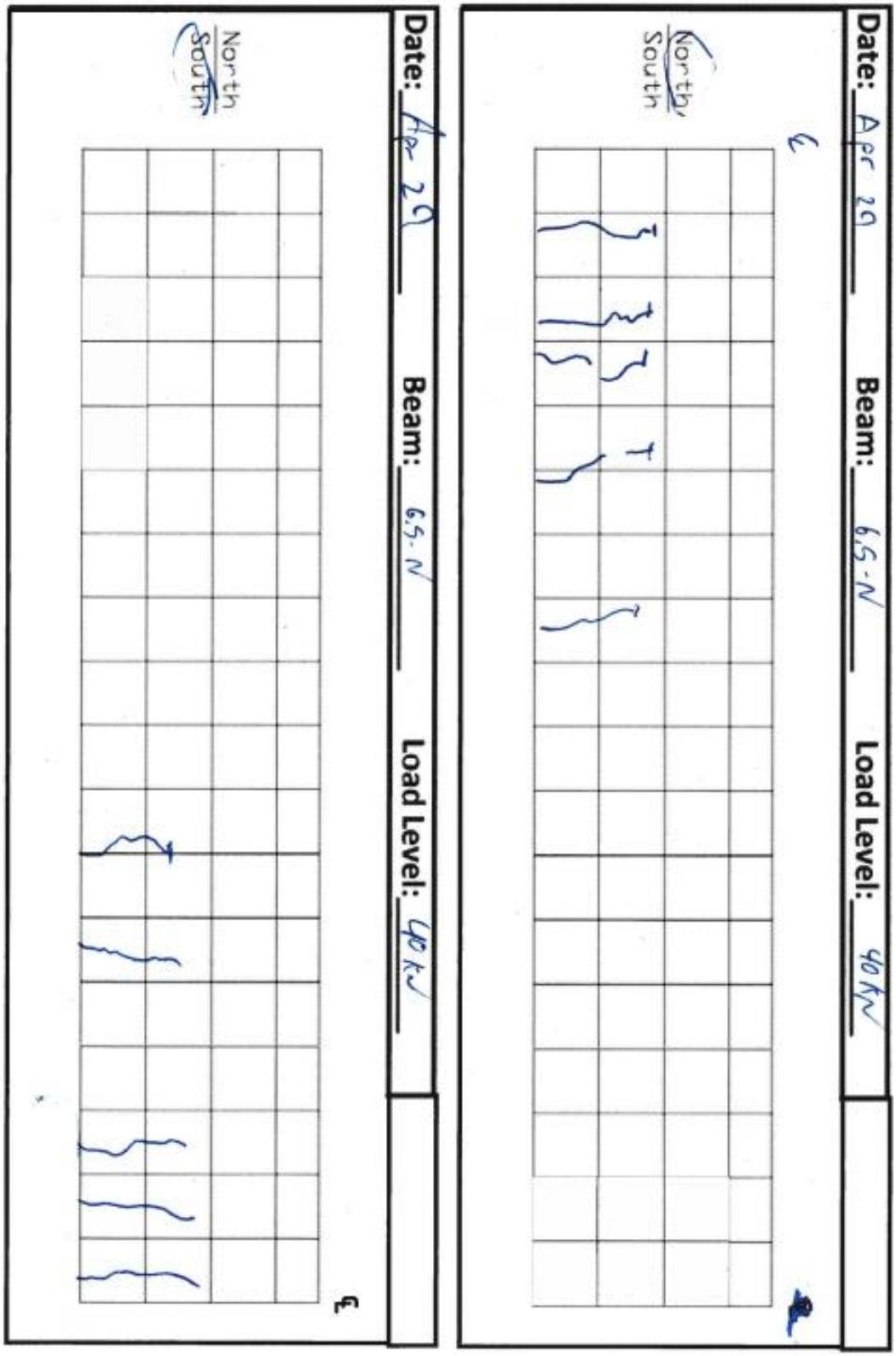

Figure A.20 - Crack tracking of BM 6.5-N at 40 kN

Date: Apr 29 Beam: 6.5-N Load Level: 53 kN

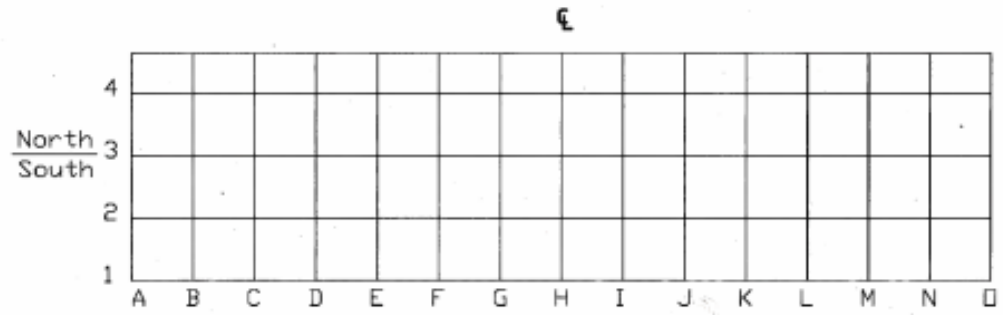

General Comments:

Crack	Location			
	Label	X (mm)	Y (mm)	Width (mm)
C9				0.1
C1				0.1
C11				0.05
C2				0.15
C3				0.1
C10				0.2
C4				0.15
C5				0.1
C6				0.1
C7				0.1
C8				0.1
C12				0.05

Figure A.21 - Crack widths of BM 6.5-N at 53 kN

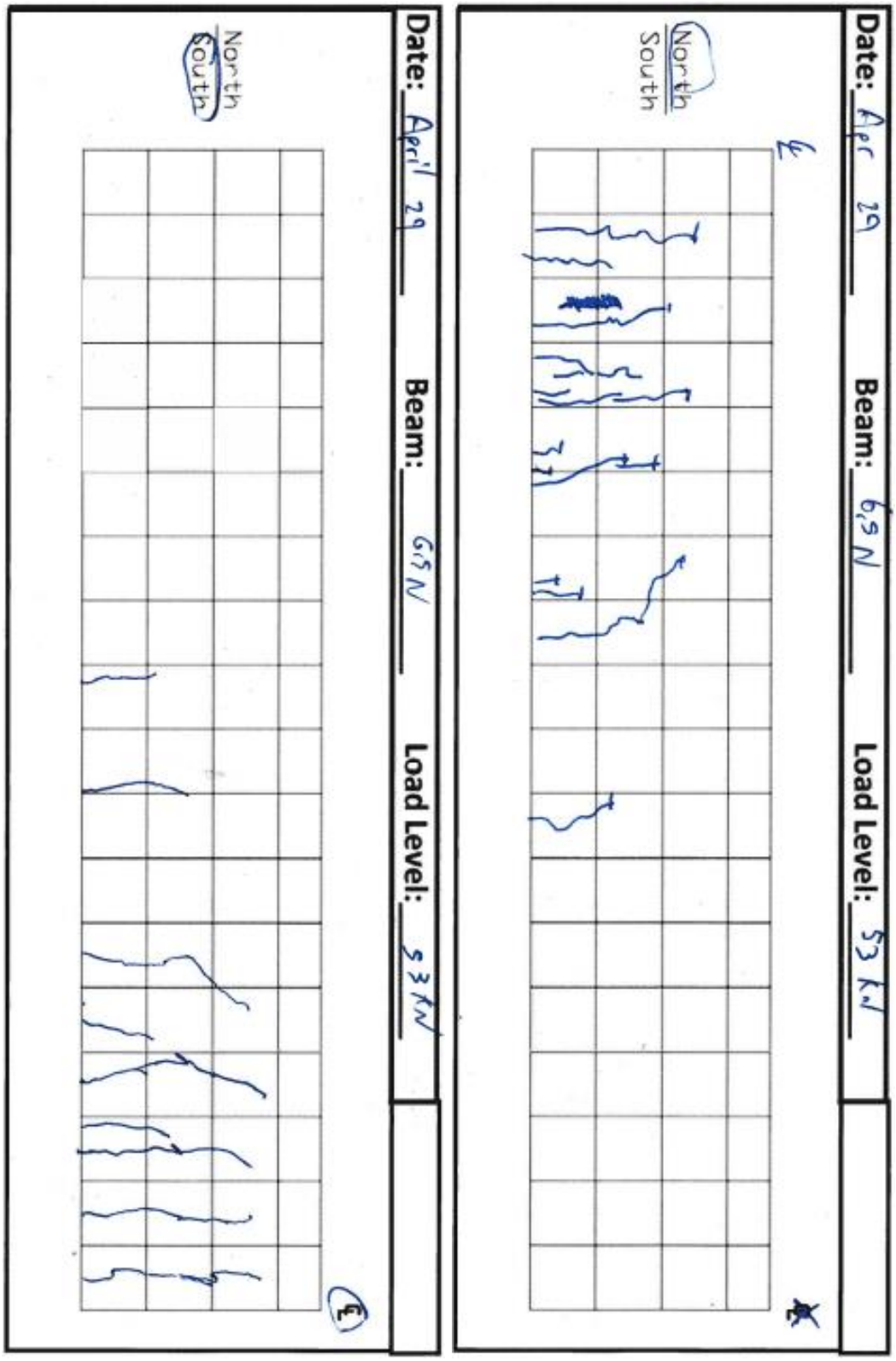

Figure A.22 - Crack tracking of BM 6.5-N at 53 kN

Date: Apr 29 Beam: 6.5-N Load Level: 65 kN

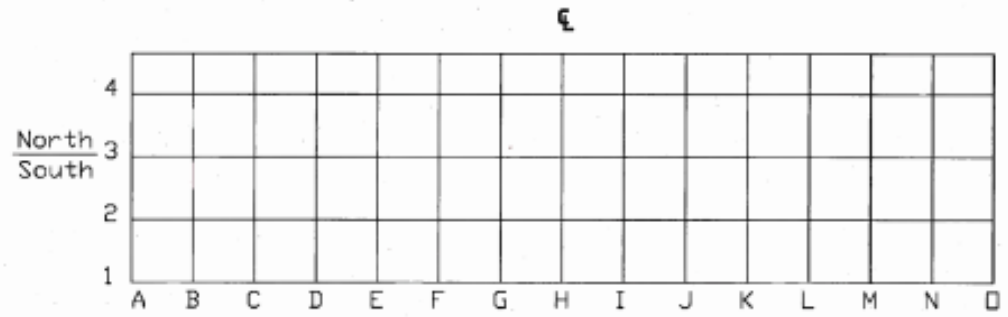

General Comments:

Crack	Location			
	Label	X (mm)	Y (mm)	Width (mm)
C1				0.25
C2				0.2
C3				0.2
C4				0.15
C5				0.1
C6				0.1
C7				0.15
C8				0.1
C9				0.1
C10				0.25
C11				0.1
C12				0.1
C13				0.1

Figure A.23 - Crack widths of BM 6.5-N at 65 kN

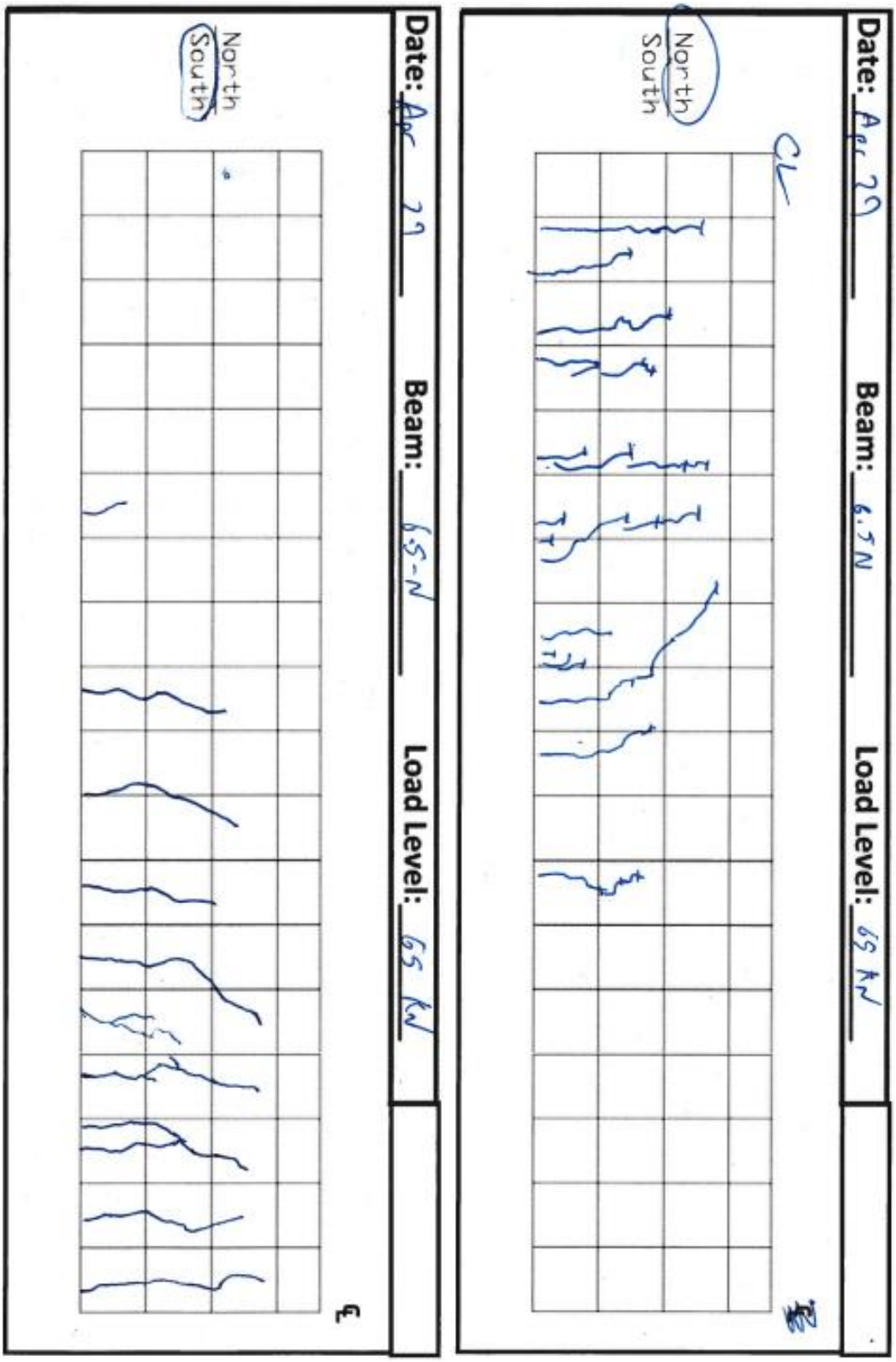

Figure A.24 - Crack tracking of BM 6.5-N at 65 kN

A.4 Series BM 6.5 – 90

Date: May 6, 2019 Beam: Bm 6.5-90 Load Level: 50

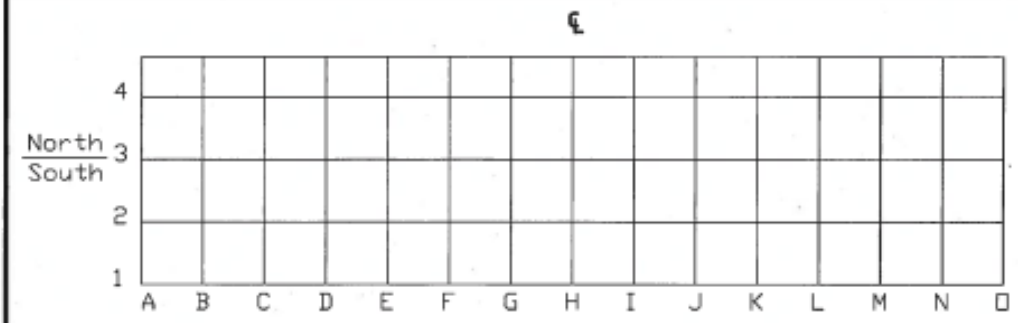

General Comments:

Crack	Location			
	Label	X (mm)	Y (mm)	Width (mm)
C1				0,1
C2				0,1
C3				0,05
C4				0,1
C5				0,1
C6				0,1
C7				0,05
C8				0,05
C9				0,15
C10				0,1
C11				0,1
C12				0,15
C13				0,1
C14				0,1
C15				0,1
C16				0,05
C17				0,05

Figure A.25 - Crack widths of BM 6.5-90 at 50 kN

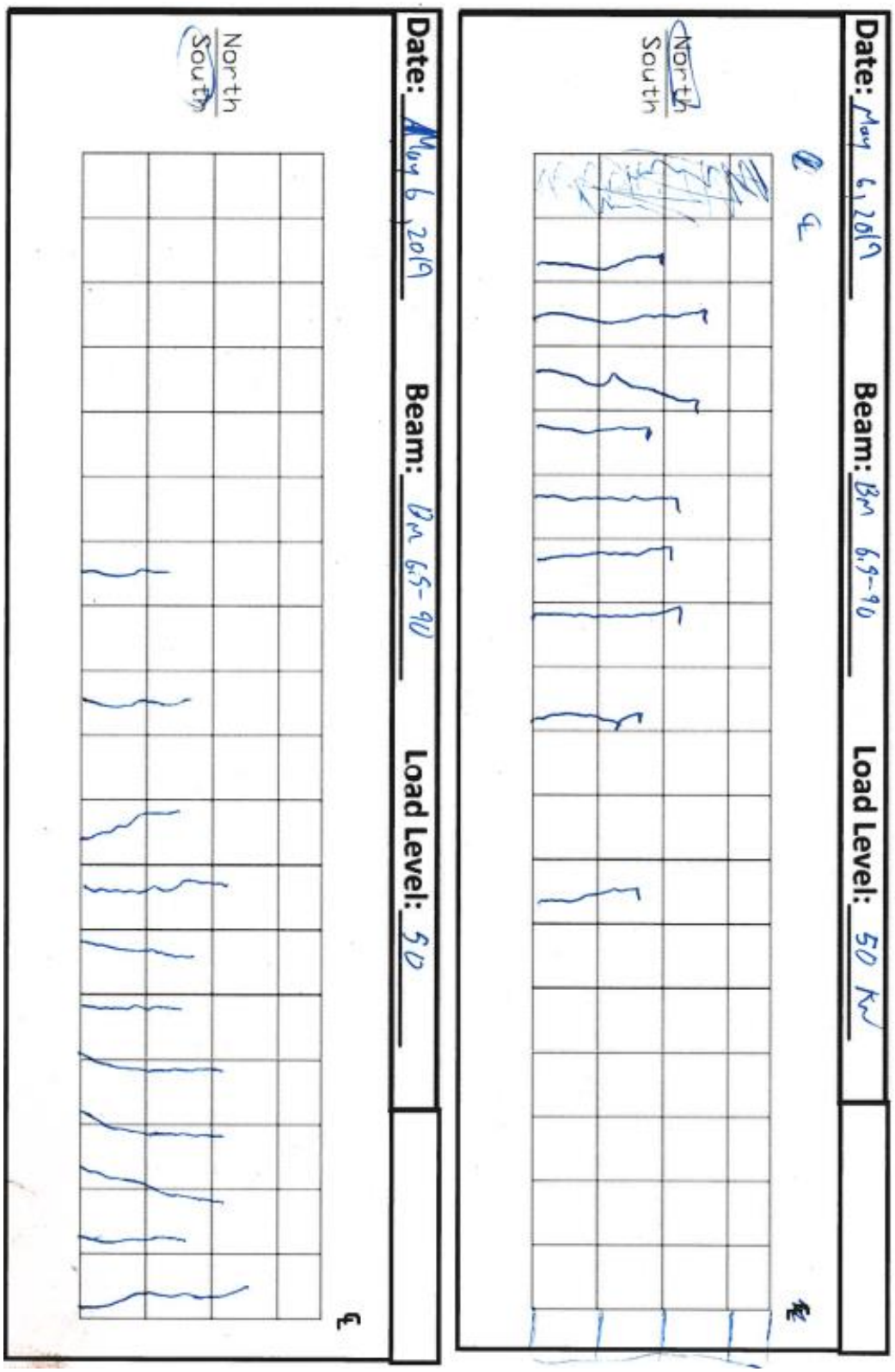

Figure A.26 - Crack tracking of BM 6.5-90 at 50 kN

Date: May 6, 2019 Beam: BM 6.5-90 Load Level: 75

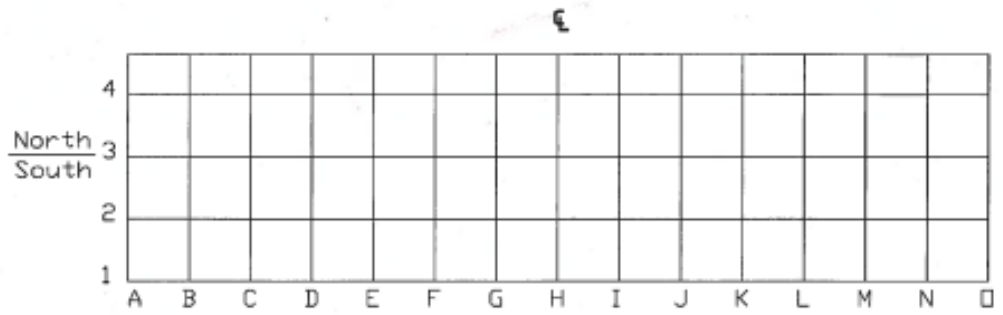

General Comments:

Crack	Location			
	Label	X (mm)	Y (mm)	Width (mm)
C1				0.1
C2				0.1
C3				0.1
C4				0.2
C5				0.15
C6				0.2
C7				0.15
C8				0.15
C9				0.2
C10				0.15
C11				0.1
C12				0.15
C13				0.1
C14				0.15
C15				0.15
C16				0.1
C17				0.05
C18				0.05
C19				0.05
C20				0.05

Figure A.27 - Crack widths of BM 6.5-90 at 75 kN

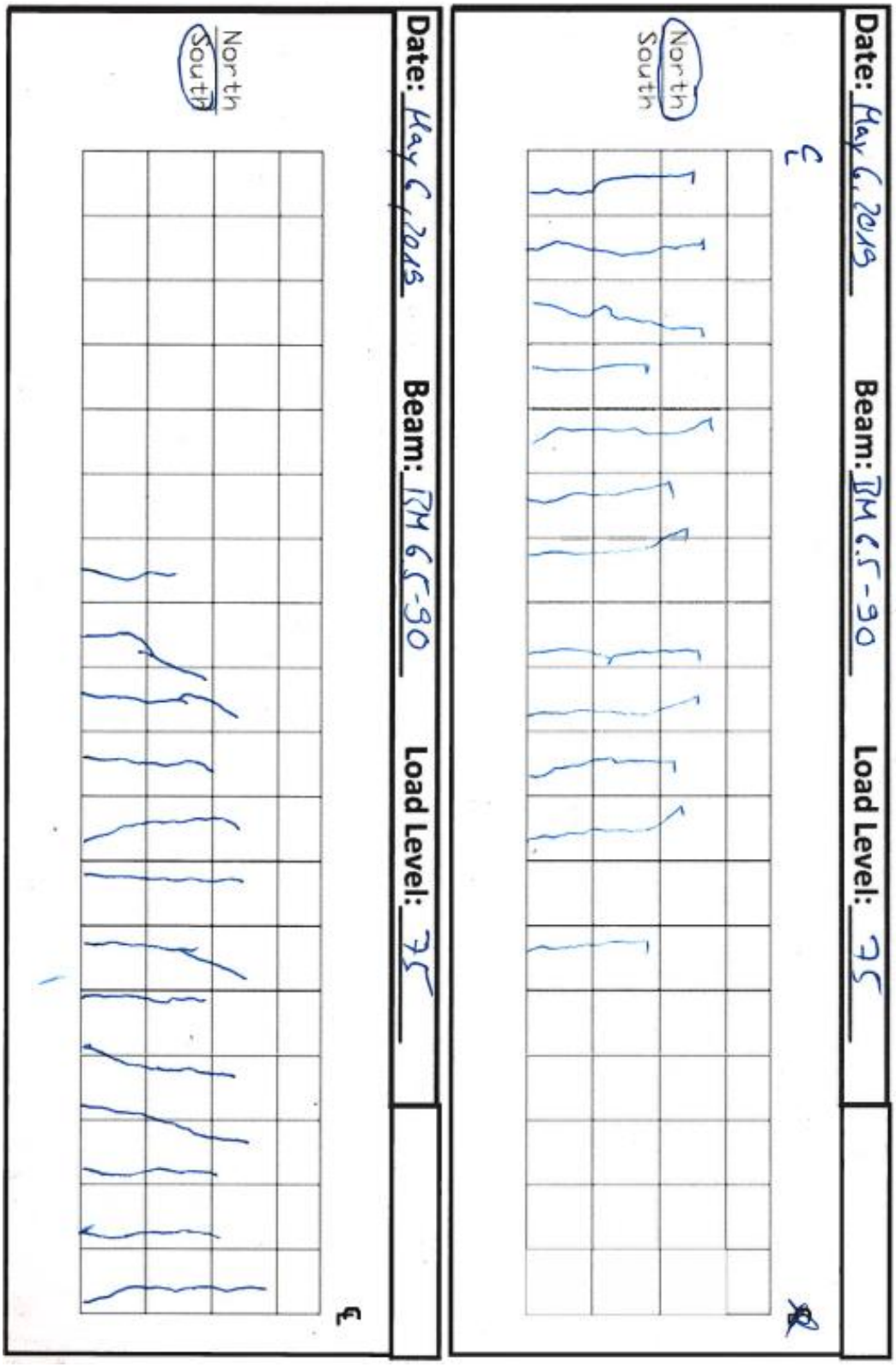

Figure A.28 - Crack tracking of BM 6.5-90 at 75 kN

Date: May 6, 2019 Beam: BM6.5-90 Load Level: 100

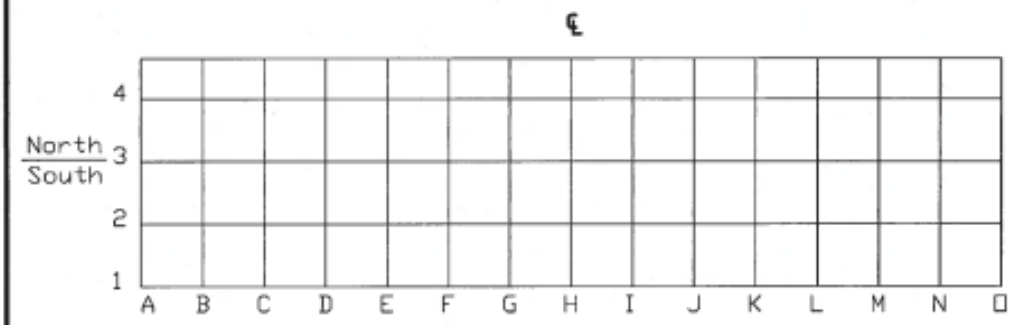

General Comments:

Crack	Location			
	Label	X (mm)	Y (mm)	Width (mm)
C1				0.1
C2				0.15
C3				0.15
C4				0.25
C5				0.2
C6				0.3
C7				0.2
C8				0.25
C9				0.35
C10				0.2
C11				0.1
C12				0.25
C13				0.15
C14				0.15
C15				0.2
C16				0.15
C17				0.1
C18				0.1
C19				0.1
C20				0.05

Figure A.29 - Crack widths of BM 6.5-90 at 100 kN

Figure A.30 - Crack tracking of BM 6.5-90 at 100 kN

A.5 Series BM 6.5 – 150

Date: May 6 **Beam:** BM 6.5-150 **Load Level:** 50

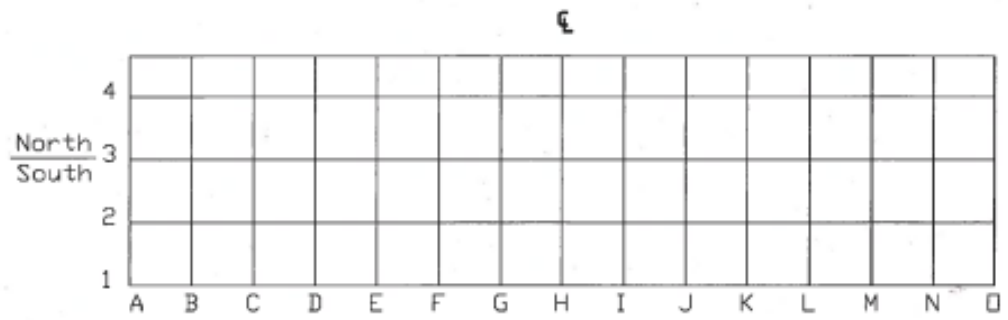

General Comments:

Crack	Location			
	Label	X (mm)	Y (mm)	Width (mm)
C1				0.05
C2				0.05
C3				0.1
C4				0.1
C5				0.1
C6				0.1
C7				0.1
C8				0.05
C9				0.1
C10				0.1
C11				0.15
C12				0.15
C13				0.1
C14				0.05

Figure A.31 - Crack widths of BM 6.5-150 at 50 kN

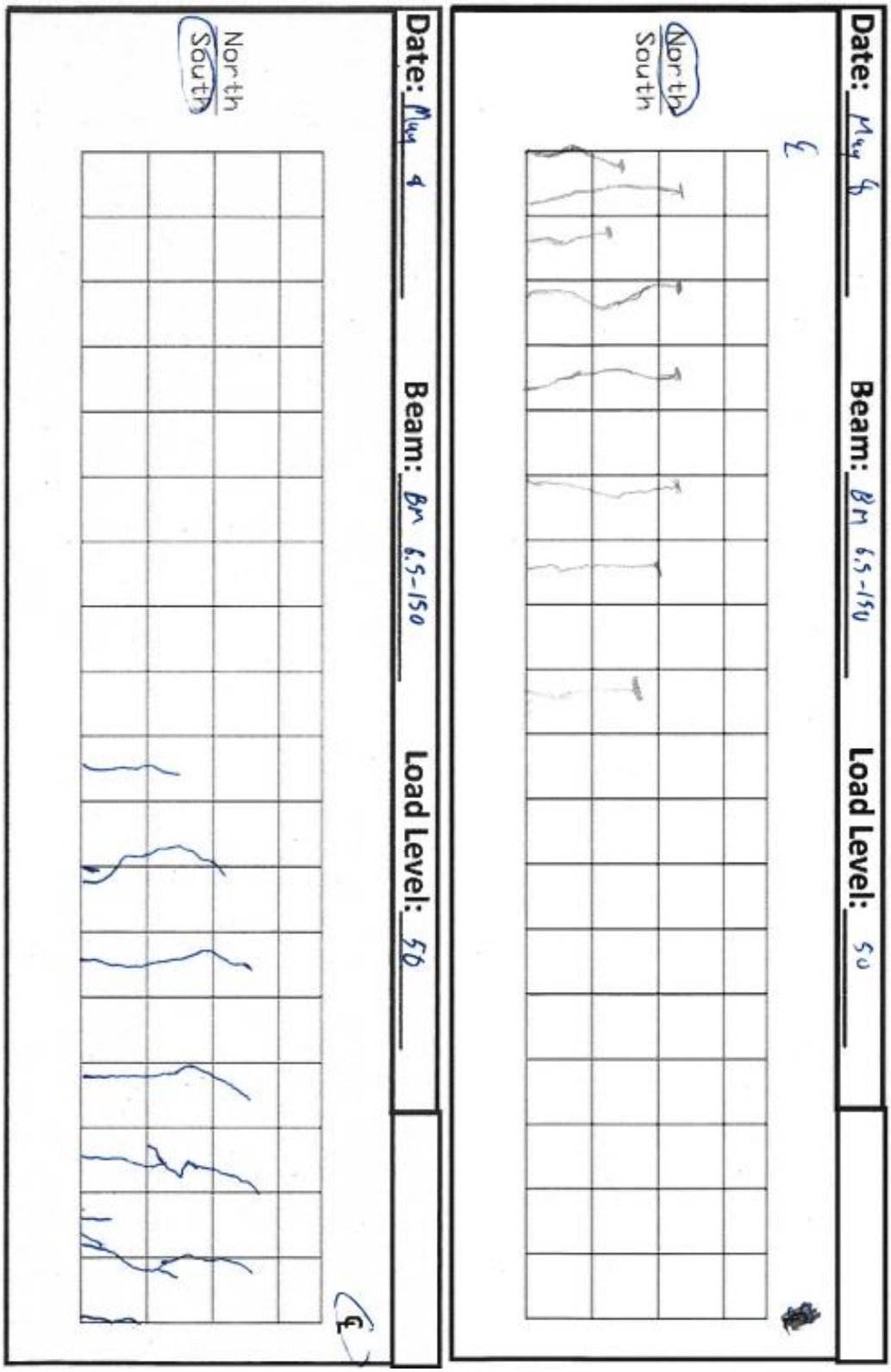

Figure A.32 - Crack tracking of BM 6.5-150 at 50 kN

Date: May 9 Beam: BM 6.5-150 Load Level: 75

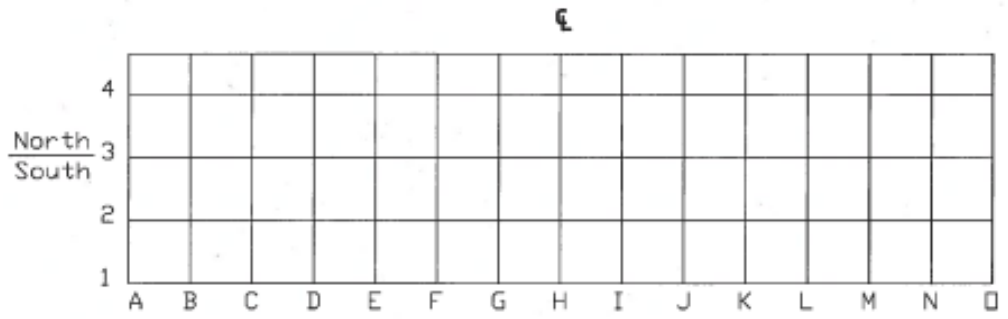

General Comments:

Crack	Location			
	Label	X (mm)	Y (mm)	Width (mm)
C1				0.1
C2				0.1
C3				0.15
C4				0.15
C5				0.2
C6				0.3
C7				0.2
C8				0.25
C9				0.2
C10				0.2
C11				0.25
C12				0.25
C13				0.2
C14				0.15
C15				0.05
C16				0.1

Figure A.33 - Crack widths of BM 6.5-150 at 75 kN

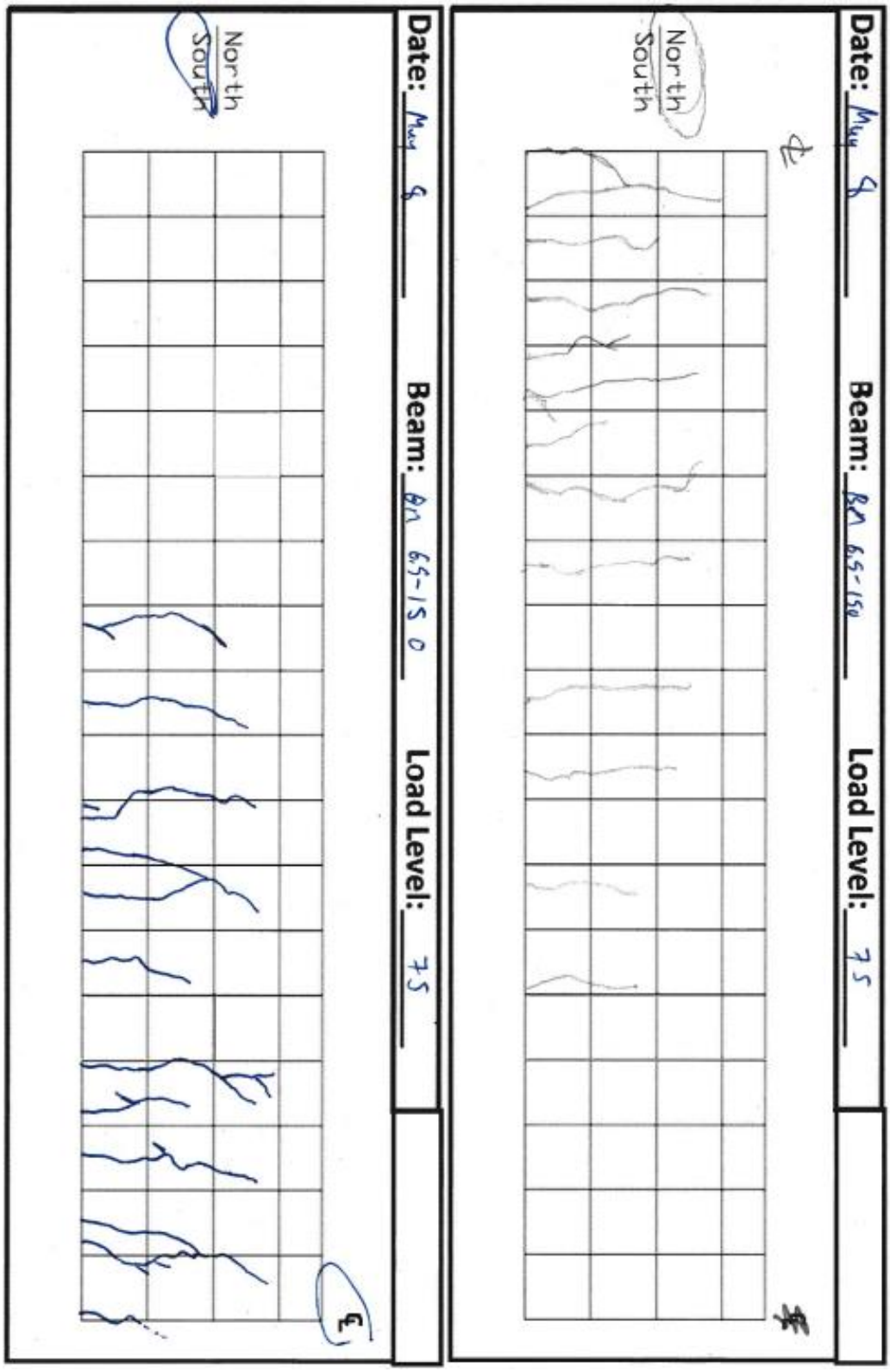

Figure A.34 - Crack tracking of BM 6.5-150 at 75 kN

Date: May 8, 2019 Beam: 6.5 -150 Load Level: 100kN

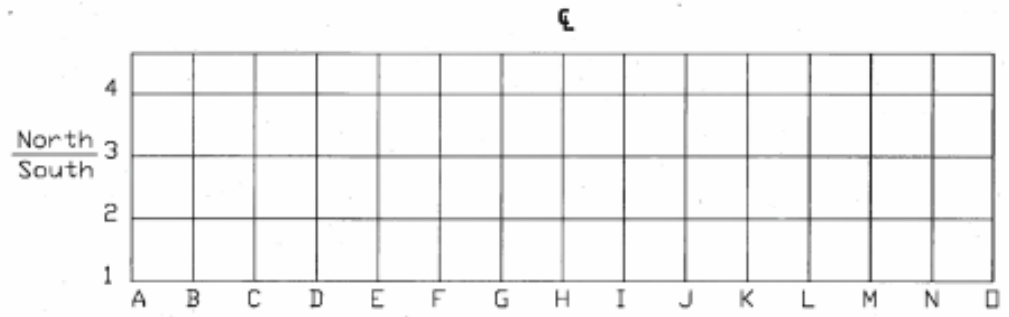

General Comments:

Crack	Location			
	Label	X (mm)	Y (mm)	Width (mm)
C1				0.15
C2				0.15
C3				0.2
C4				0.2
C5				0.15
C6				0.3
C7				0.2
C8				0.2
C9				0.25
C10				0.25
C11				0.4
C12				0.3
C13				0.25
C14				0.2
C15				0.05
C16				0.15

Figure A.35 - Crack widths of BM 6.5-150 at 100 kN

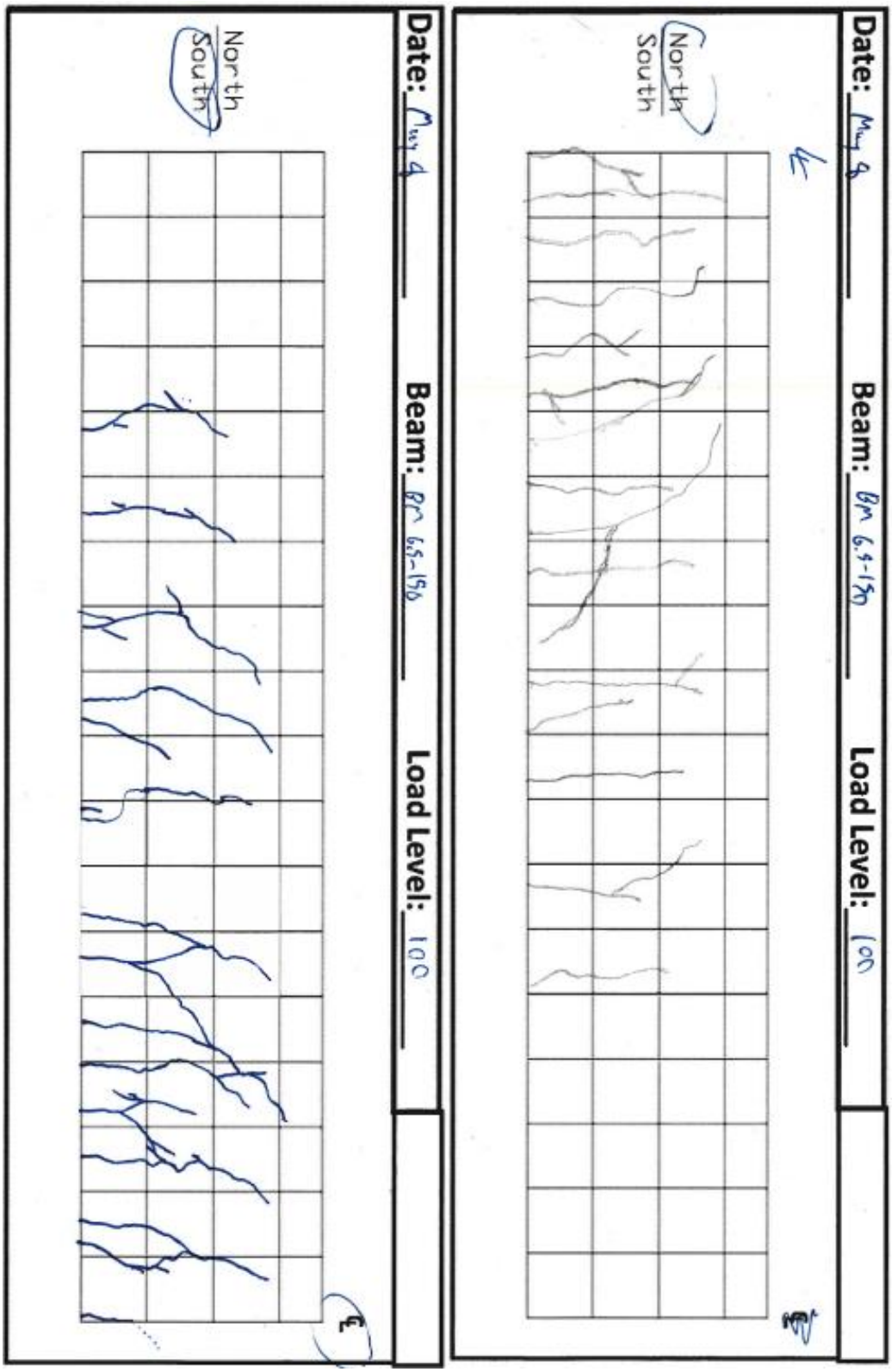

Figure A.36 - Crack tracking of BM 6.5-150 at 100 kN

A.6 Series BM 8.5 – N

Date: May 10 **Beam:** BM 8.5-N **Load Level:** 35

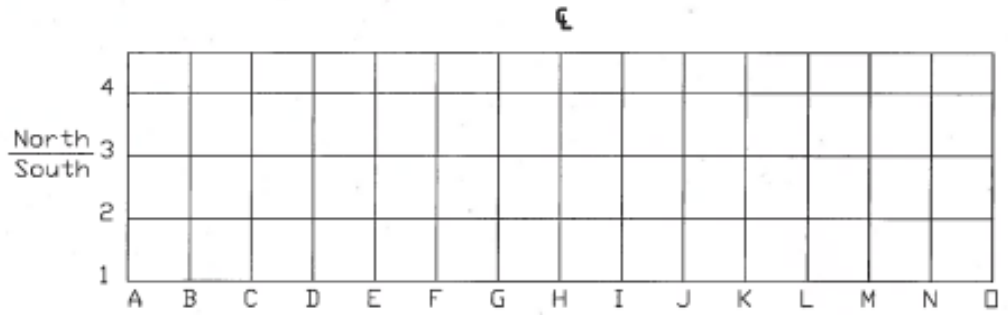

General Comments:

Crack	Location			
	Label	X (mm)	Y (mm)	Width (mm)
C1				0.05
C2				0.1
C3				0.1
C4				0.15
C5				0.1
C6				0.15
C7				0.05
C8				0.2
C9				0.05
C10				0.15
C11				0.2
C12				0.2
C13				0.15
C14				0.1
C15				0.05
C16				0.05
C17				0.05

Figure A.37 - Crack widths of BM 8.5-N at 35 kN

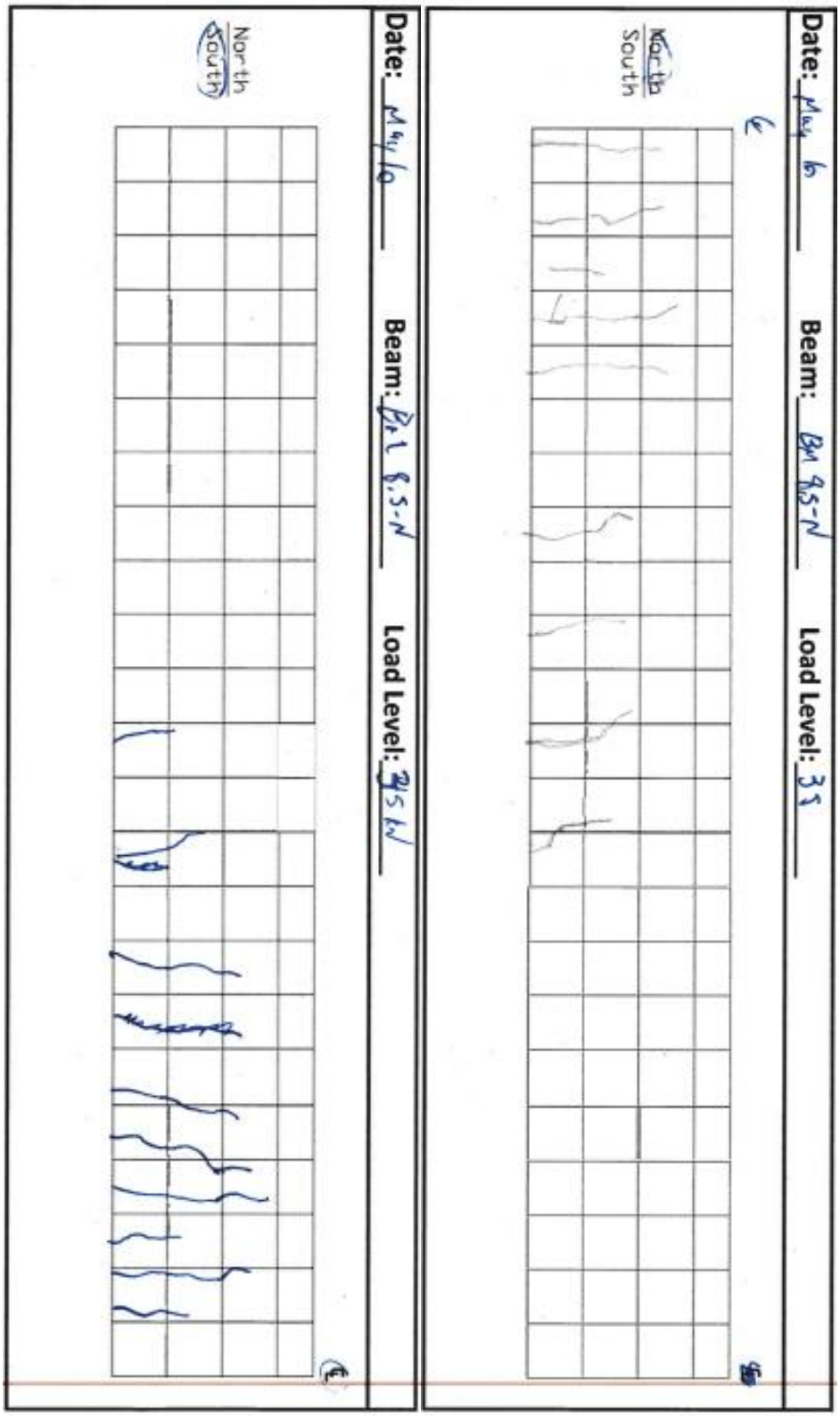

Figure A.38 - Crack tracking of BM 8.5-N at 35 kN

Date: May 10 Beam: BM 8.5-N Load Level: 45

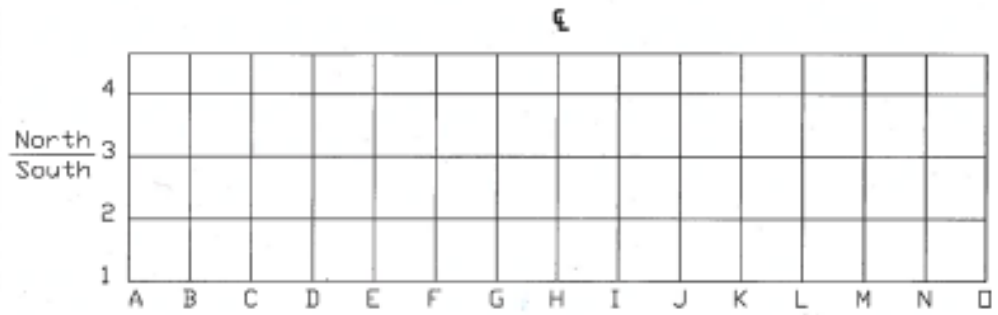

General Comments:

Crack	Location			
	Label	X (mm)	Y (mm)	Width (mm)
C1				0.05
C2				0.15
C3				0.1
C4				0.15
C5				0.2
C6				0.2
C7				0.1
C8				0.4
C9				0.05
C10				0.25
C11				0.3
C12				0.3
C13				0.25
C14				0.1
C15				0.1
C16				0.1
C17				0.05
C18				0.1

Figure A.39 - Crack widths of BM 8.5-N at 45 kN

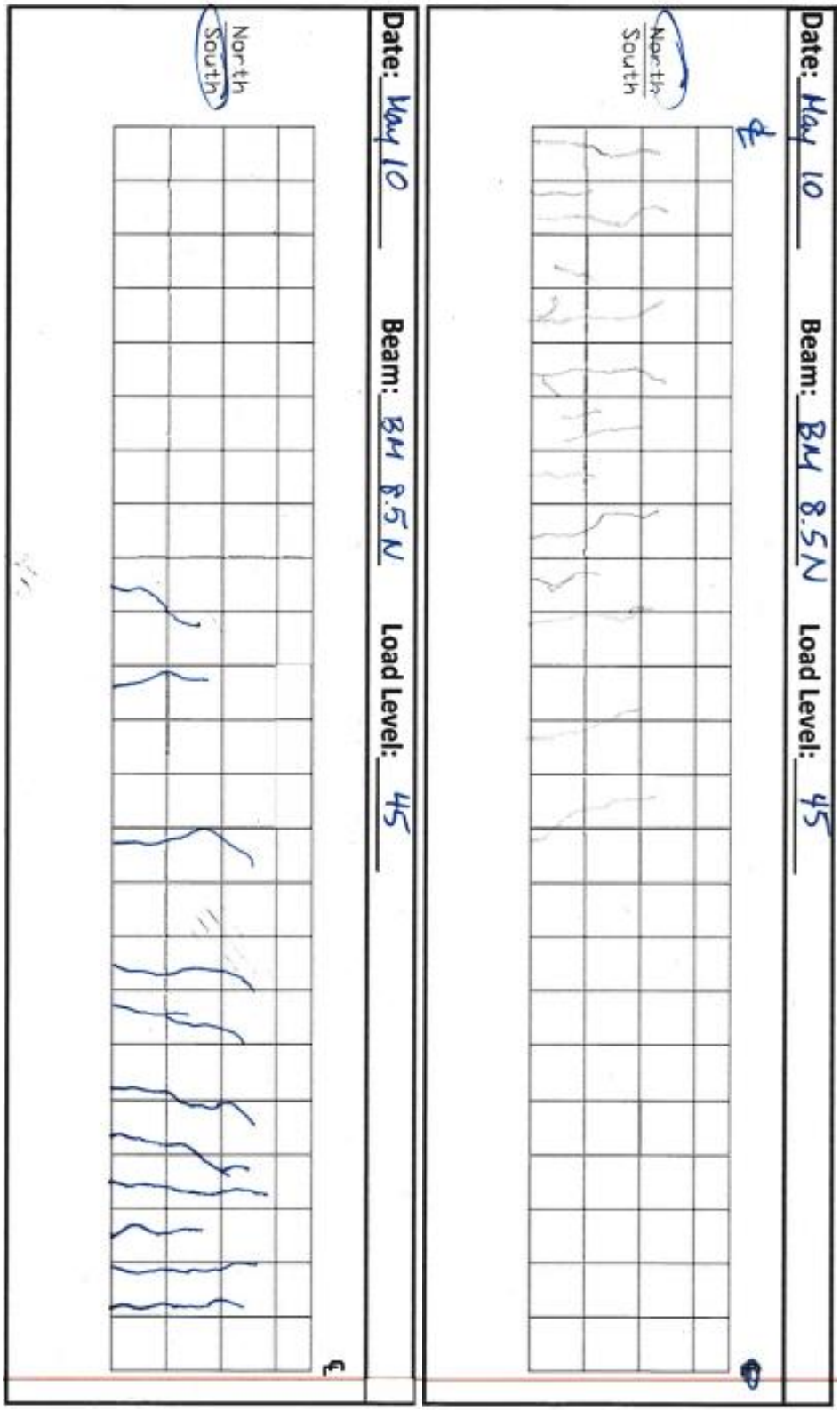

Figure A.40 - Crack tracking of BM 8.5-N at 45 kN

Date: May 10 Beam: Br1 8.5-N Load Level: 55

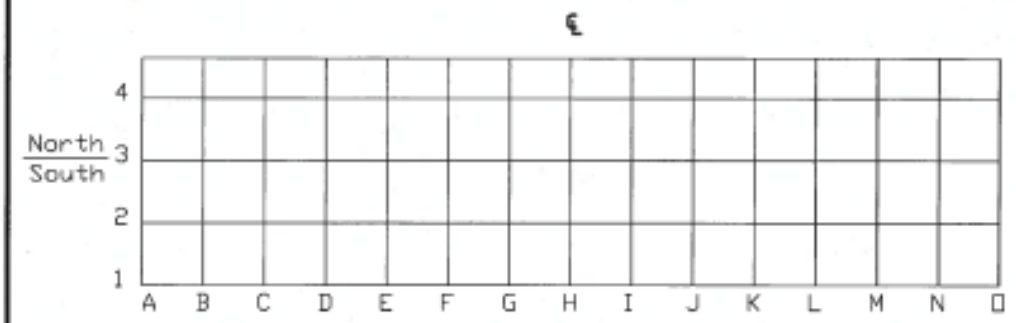

General Comments:

Crack	Location			
	Label	X (mm)	Y (mm)	Width (mm)
C1				0.15
C2				0.15
C3				0.25
C4				0.25
C5				0.2
C6				0.25
C7				0.15
C8				0.5
C9				0.1
C10				0.45
C11				0.35
C12				0.4
C13				0.3
C14				0.1
C15				0.15
C16				0.1
C17				0.15
C18				0.2
C19				0.1

Figure A.41 - Crack widths of BM 8.5-N at 55 kN

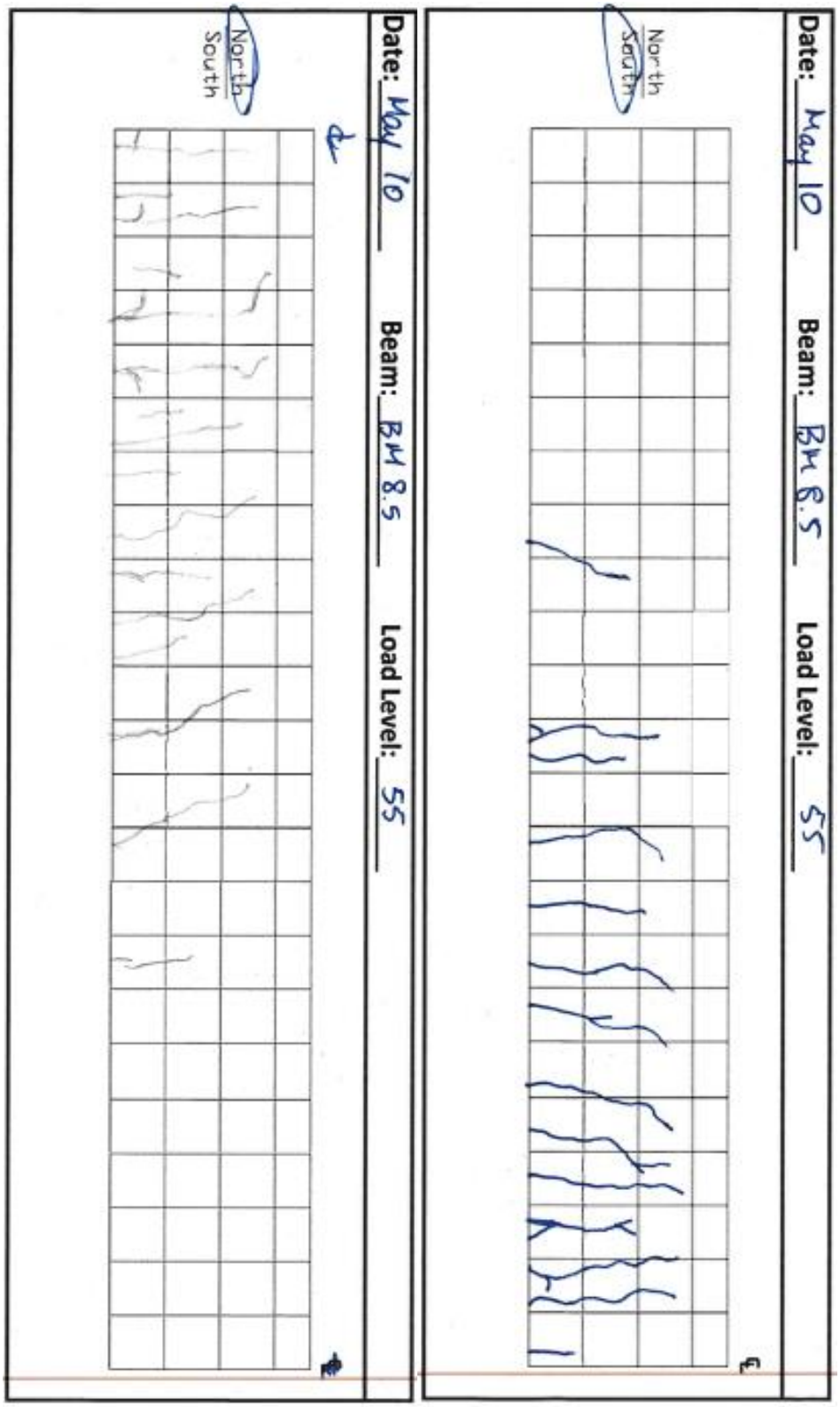

Figure A.42 - Crack tracking of BM 8.5-N at 55 kN

A.7 Series BM 8.5 – 150

Date: May 14, 2019 Beam: BM8.5-150 Load Level: 40

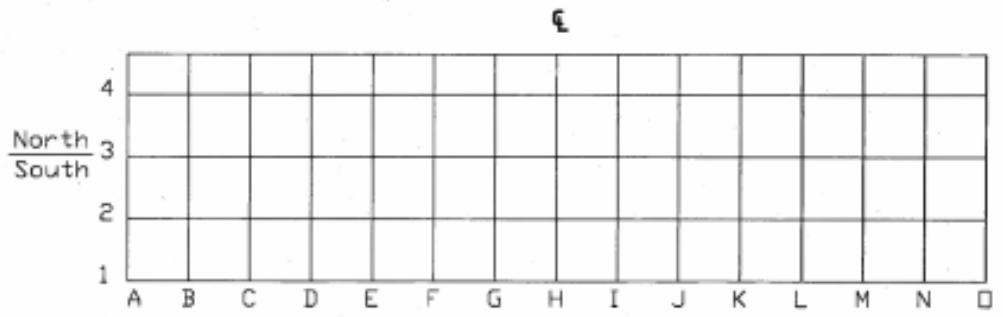

General Comments:

Crack	Location			
	Label	X (mm)	Y (mm)	Width (mm)
C1				0.05
C2				0.1
C3				0.05
C4				0.15
C5				0.1
C6				0.15
C7				0.15
C8				0.05
C9				0.15
C10				0.05
C11				0.1
C12				0.05
C13				0.1
C14				0.05
C15				0.2
C16				0.15
C17				0.1
C18				0.15
C19				0.1
C20				0.05
C21				0.05

Figure A.43 - Crack widths of BM 8.5-150 at 40 kN

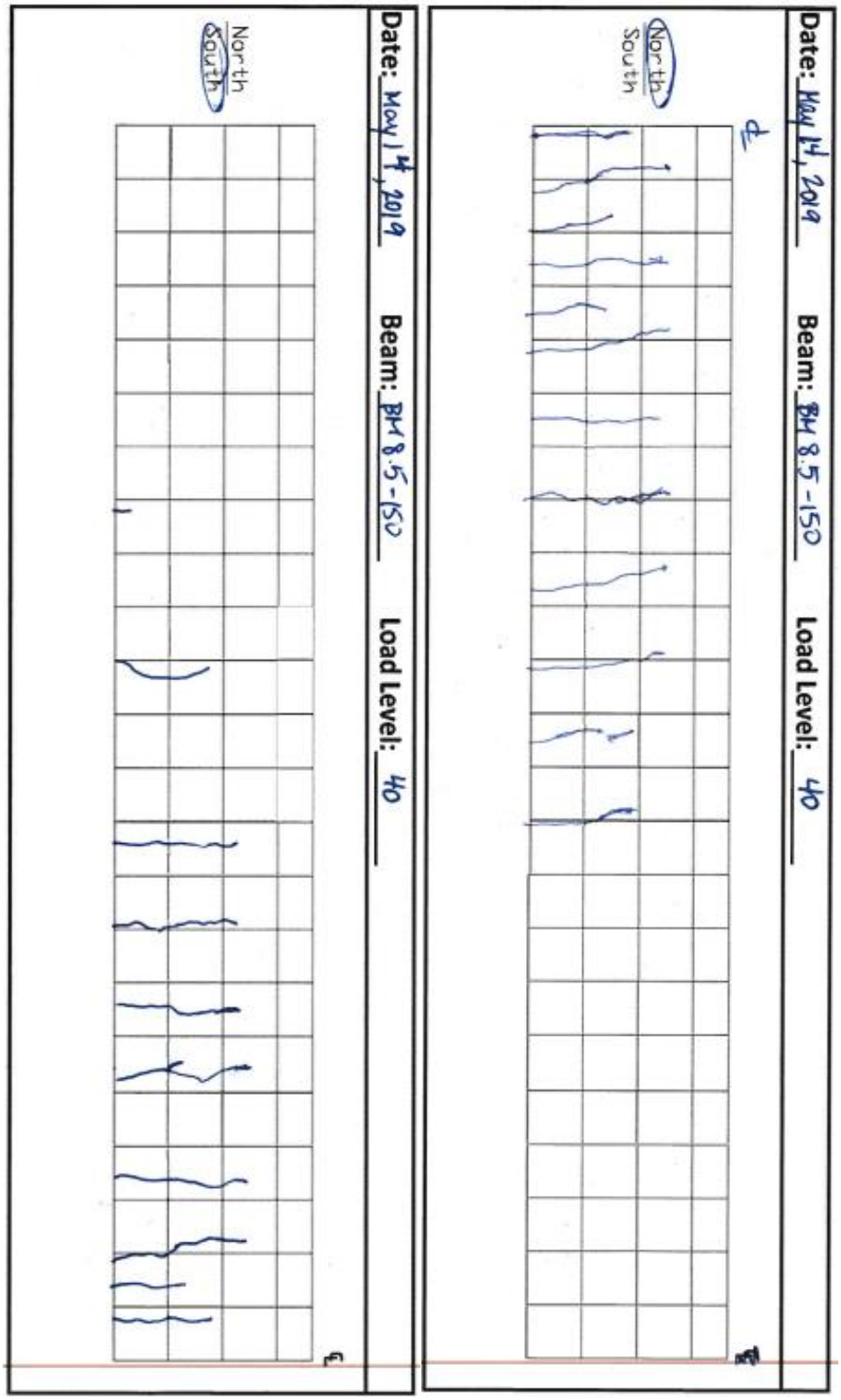

Figure A.44 - Crack tracking of BM 8.5-150 at 40 kN

Date: May 14, 2019 Beam: BM 8.5-150 Load Level: 60

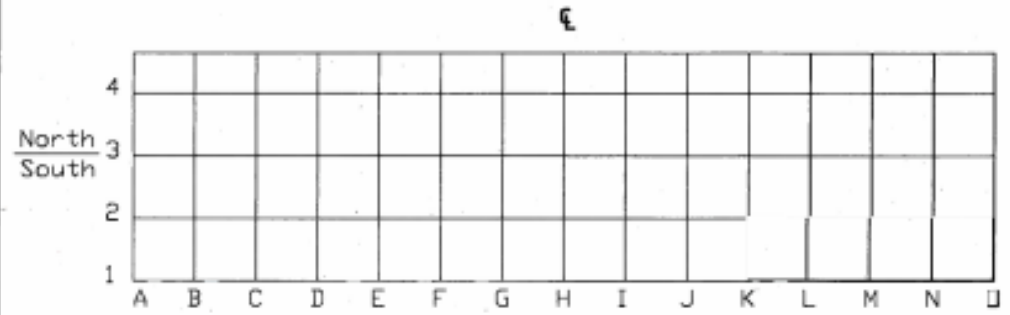

General Comments:

Crack	Location			
	Label	X (mm)	Y (mm)	Width (mm)
C1				0.1
C2				0.2
C3				0.2
C4				0.25
C5				0.35
C6				0.4
C7				0.5
C8				0.1
C9				0.4
C10				0.3
C11				0.4
C12				0.1
C13				0.2
C14				0.1
C15				0.25
C16				0.25
C17				0.2
C18				0.3
C19				0.25
C20				0.2
C21				0.15
C22				0.

Figure A.45 - Crack widths of BM 8.5-150 at 60 kN

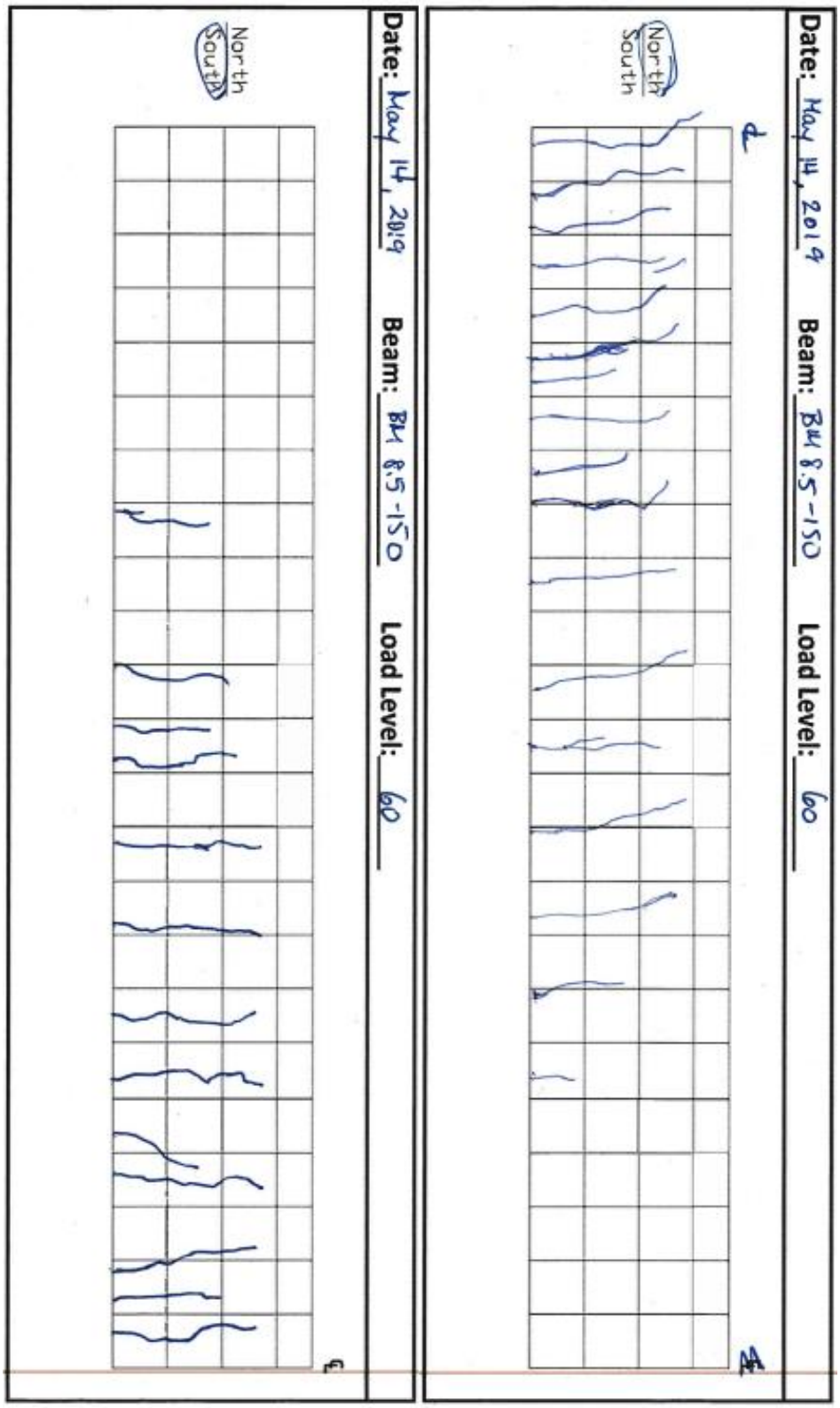

Figure A.46 - Crack tracking of BM 8.5-150 at 60 kN

Date: May 14, 2019 Beam: BM 8.5-150 Load Level: 80

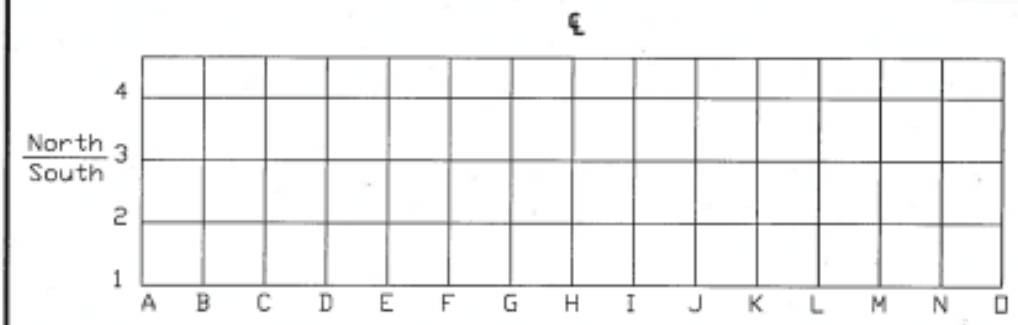

General Comments:

Crack	Location			
	Label	X (mm)	Y (mm)	Width (mm)
C1				0.15
C2				0.3
C3				0.6
C4				0.5
C5				0.5
C6				0.4
C7				0.5
C8				0.2
C9				0.5
C10				0.5
C11				0.6
C12				0.2
C13				0.25
C14				0.25
C15				0.4
C16				0.3
C17				0.4
C18				0.4
C19				0.45
C20				0.25
C21				0.3

Figure A.47 - Crack widths of BM 8.5-150 at 80 kN

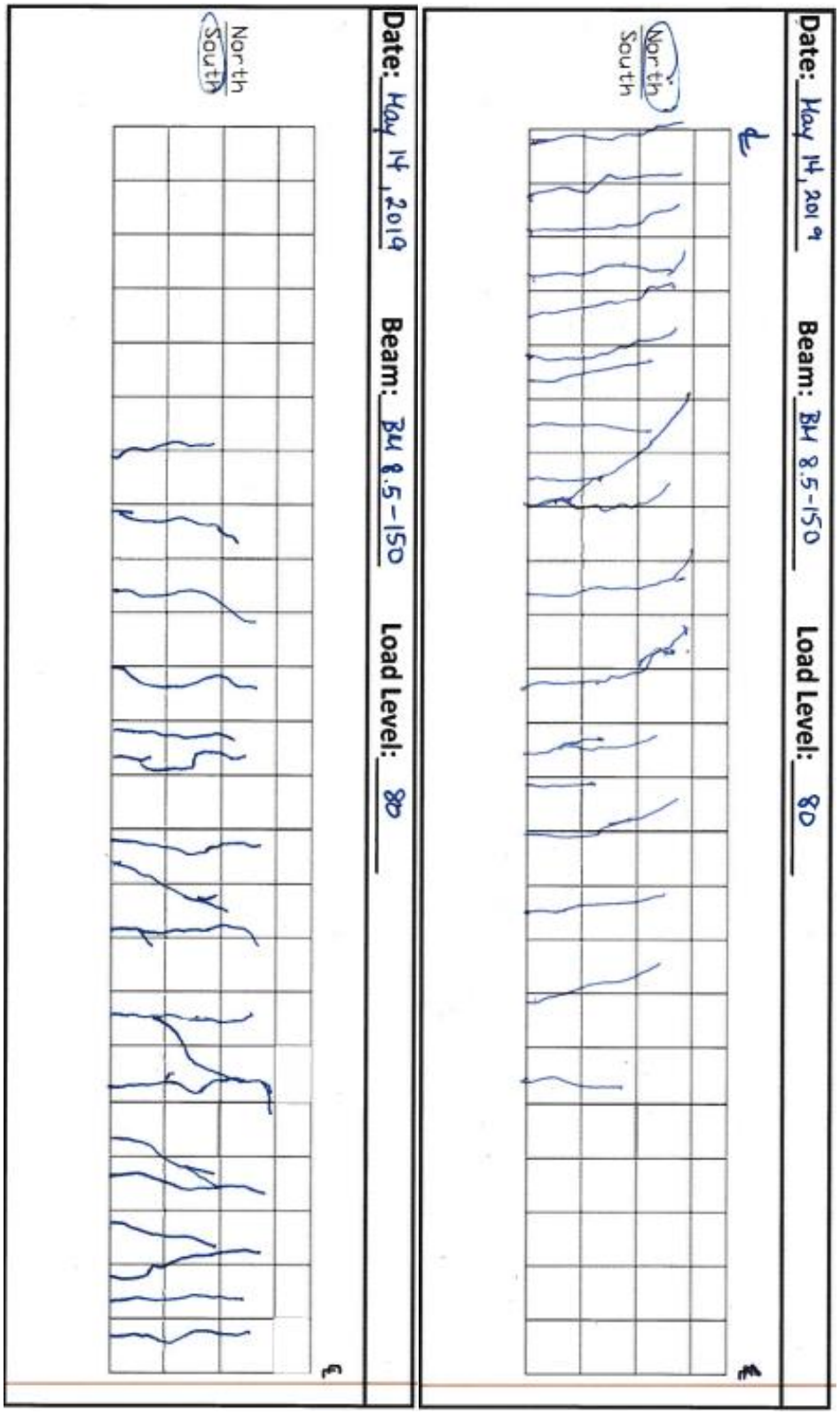

Figure A.48 - Crack tracking of BM 8.5-150 at 80 kN

A.8 Series BM 10.5 – N

Date: May 11 Beam: Bm 10.5-N Load Level: 30 kN

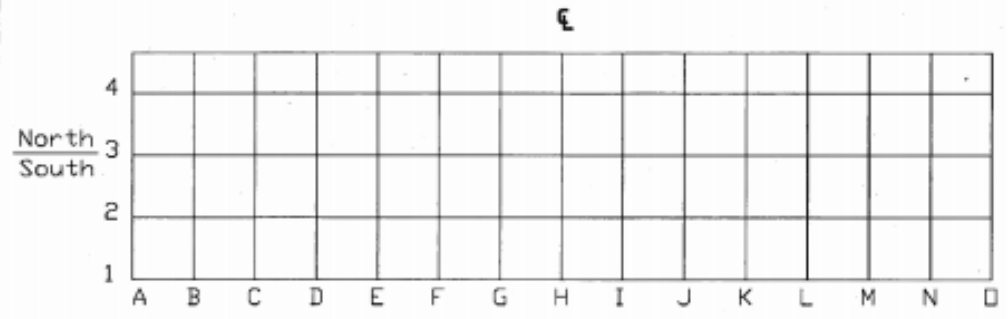

General Comments:

Crack	Location			
	Label	X (mm)	Y (mm)	Width (mm)
C1				0.15
C2				0.1
C3				0.05
C4				0.10
C5				0.20
C6				0.10
C7				0.20
C8				0.05
C9				0.20
C10				0.15
C11				0.15
C12				0.20
C13				0.10
C14				0.20
C15				0.15
C16				0.20
C17				0.10
C18				0.10
C19				0.05
C20				0.05
C21				0.15
C22				0.15
C23				0.15
C24				0.10

Figure A.49 - Crack widths of BM 10.5-N at 30 kN

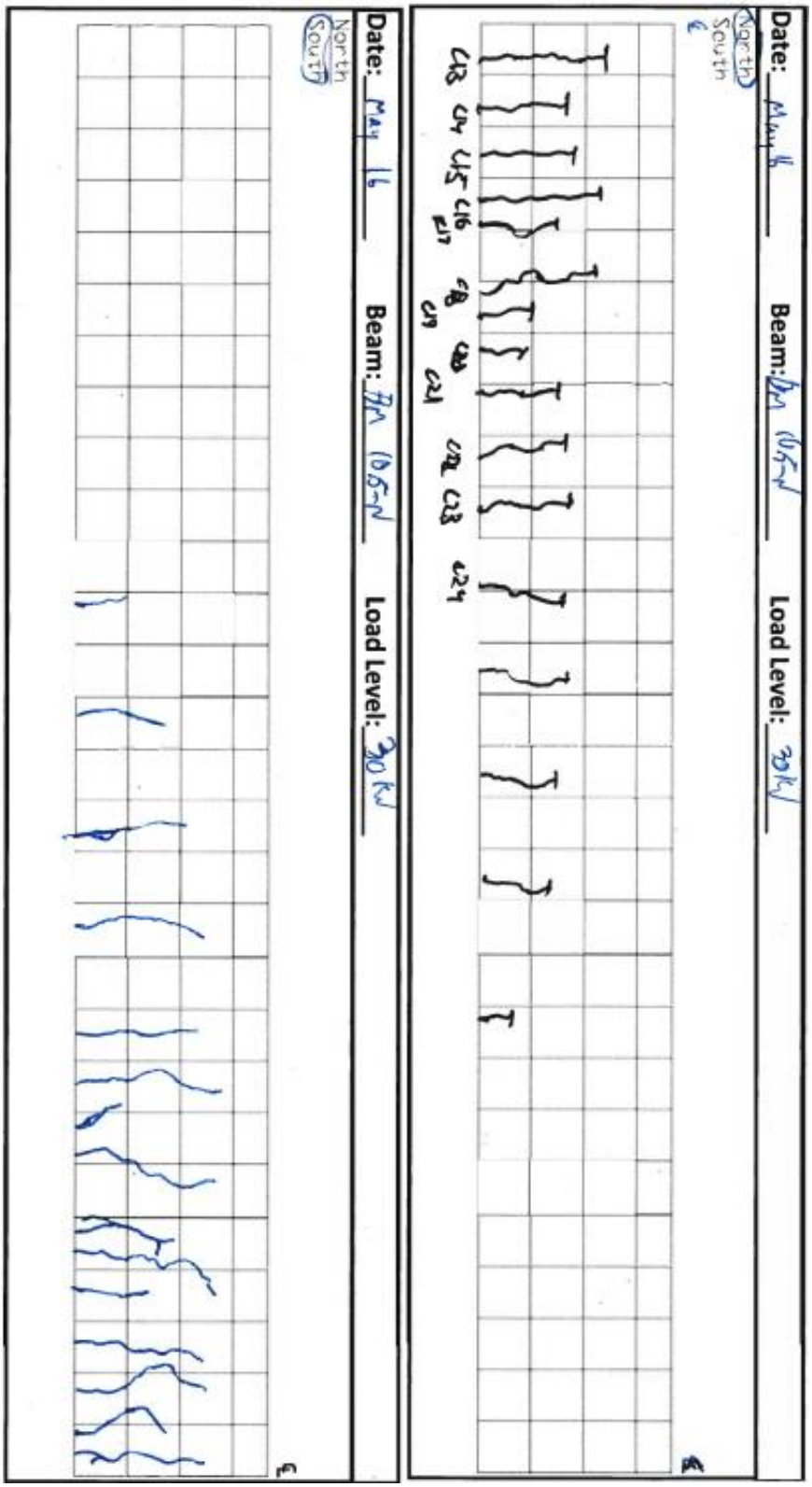

Figure A.50 - Crack tracking of BM 10.5-N at 30 kN

Date: May 16 Beam: BM 10.5-N Load Level: 42.5

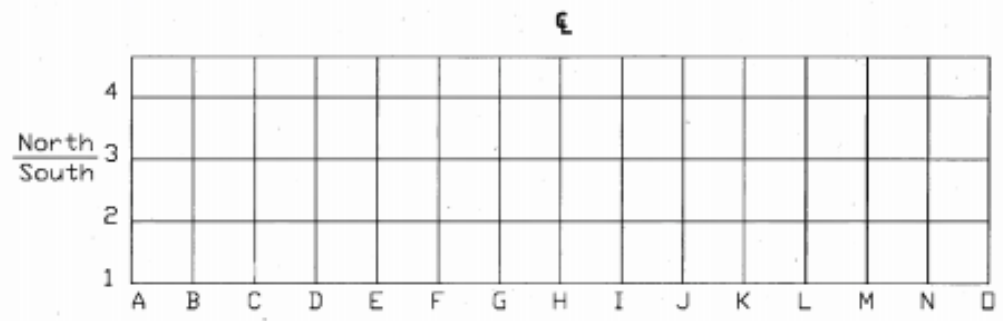

General Comments:

Crack	Location			
	Label	X (mm)	Y (mm)	Width (mm)
C1				0.20
C2				0.10
C3				0.10
C4				0.10
C5				0.25
C6				0.15
C7				0.15
C8				0.10
C9				0.20
C10				0.10
C11				0.20
C12				0.25
C13				0.15
C14				0.30
C15				0.15
C16				0.20
C17				0.15
C18				0.15
C19				0.05
C20				0.10
C21				0.15
C22				0.15
C23				0.10
C24				0.15

Figure A.51 - Crack widths of BM 10.5-N at 42.5 kN

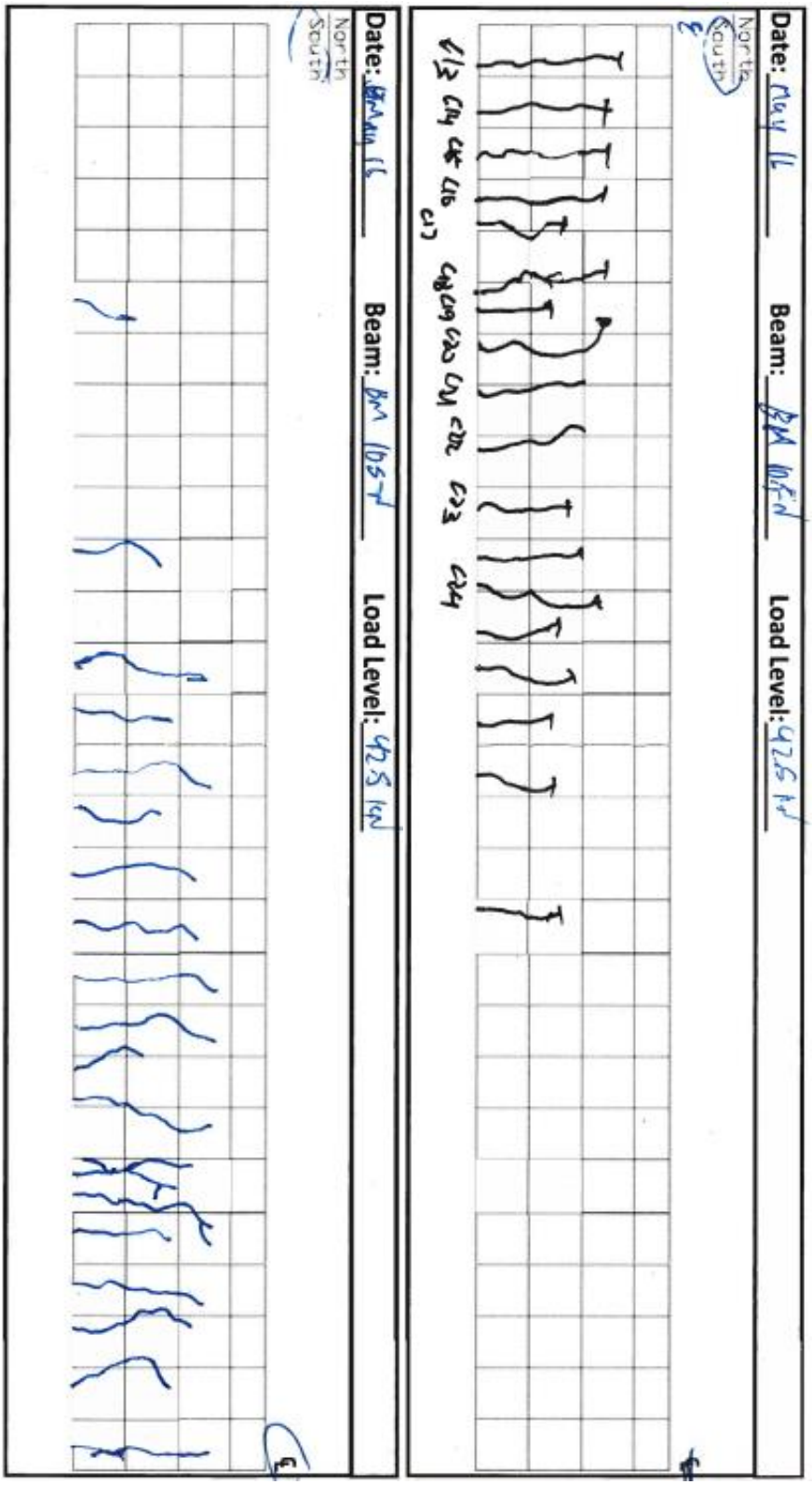

Figure A.52 - Crack tracking of BM 10.5-N at 30 kN

Date: May 16 Beam: BM 10.5-N Load Level: 55 KN

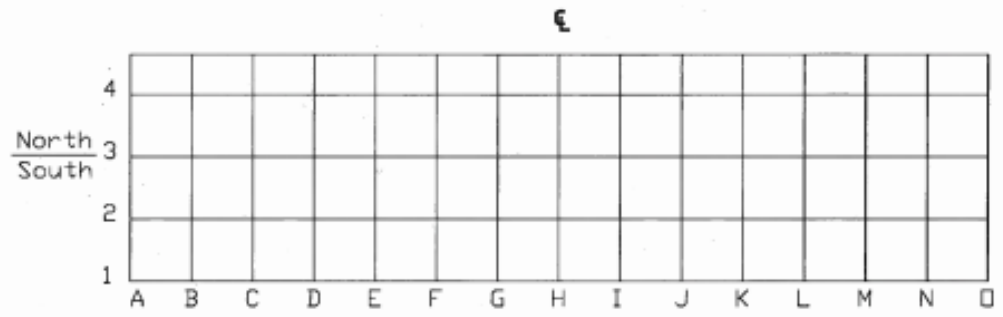

General Comments:

Crack	Location			
	Label	X (mm)	Y (mm)	Width (mm)
C1				0.15
C2				0.20
C3				0.25
C4				0.15
C5				0.20
C6				0.25
C7				0.15
C8				0.20
C9				0.40
C10				0.20
C11				0.35
C12				0.25
C13				0.25
C14				0.40
C15				0.30
C16				0.40
C17				0.30
C18				0.15
C19				0.10
C20				0.10
C21				0.25
C22				0.75
C23				0.10
C24				0.20

Figure A.53 - Crack widths of BM 10.5-N at 55 kN

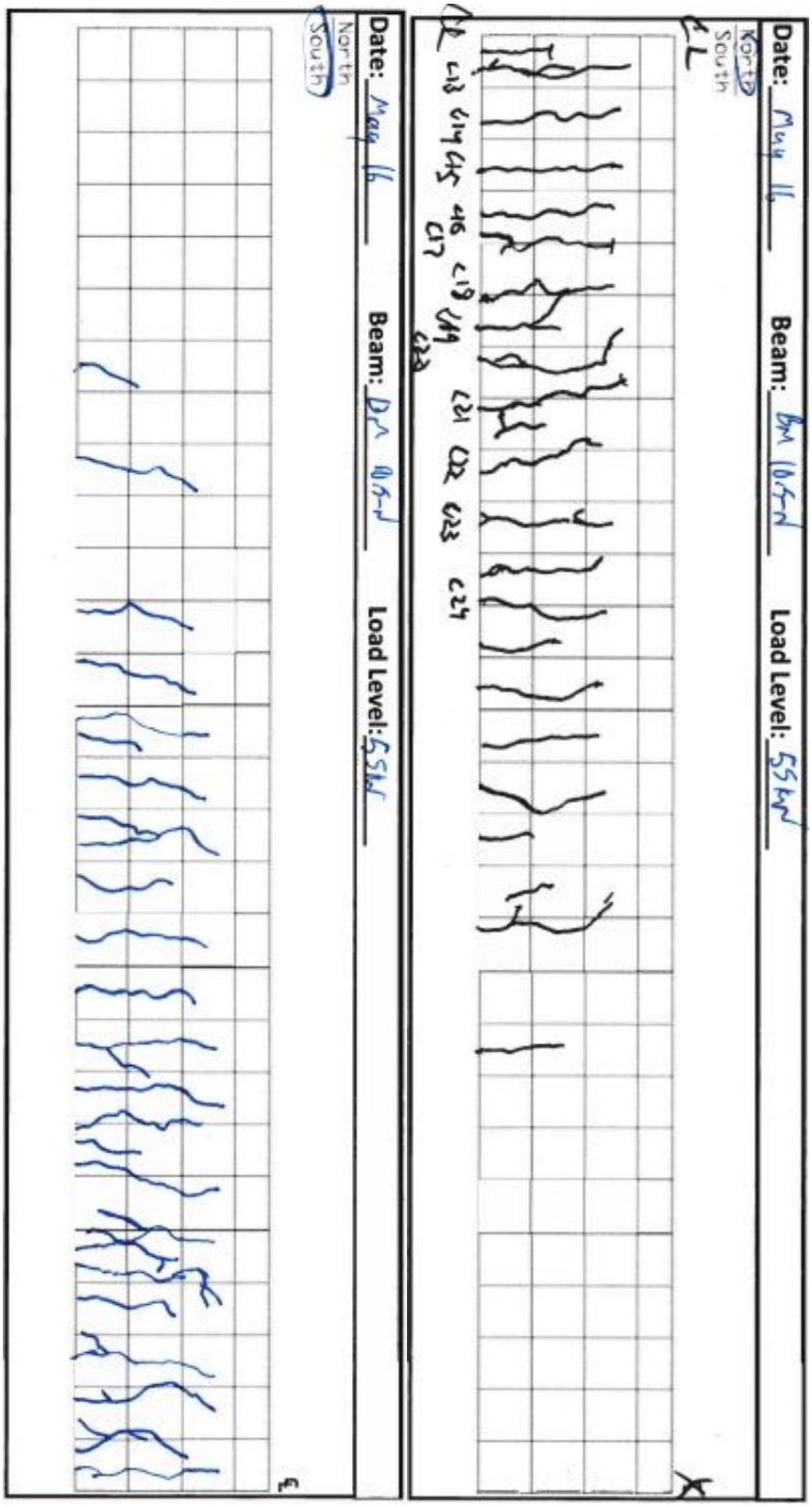

Figure A.54 - Crack tracking of BM 10.5-N at 55 kN

A.9 Series BM 10.5 – 150

Date: May 21 **Beam:** Bm 10.5-150 **Load Level:** 30

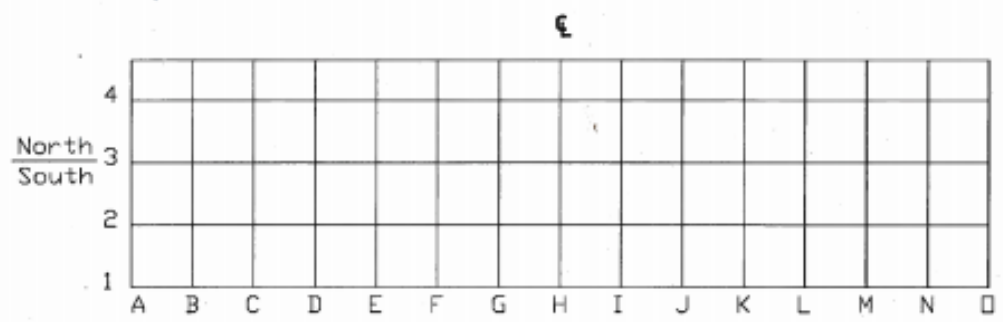

General Comments:

Crack	Location			
	Label	X (mm)	Y (mm)	Width (mm)
C1				0.1
C2				0.15
C3				0.2
C4				0.1
C5				0.15
C6				0.2
C7				0.05
C8				0.25
C9				0.2
C10				0.2
C11				0.15
C12				0.15
C13				0.3
C14				0.4
C15				0.25
C16				0.25
C17				0.2
C18				0.3
C19				0.1

Figure A.55 - Crack widths of BM 10.5-150 at 30 kN

Date: May 21 Beam: BM 10.5-150 Load Level: 30

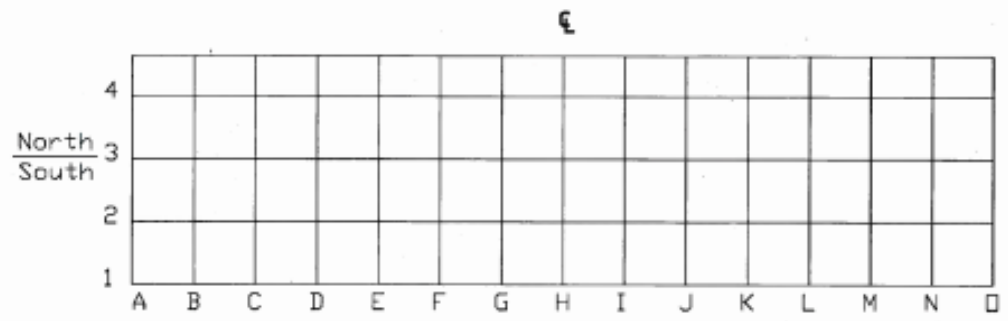

General Comments:

Crack	Location			
	Label	X (mm)	Y (mm)	Width (mm)
C20				0.3
C21				0.25
C22				0.25
C23				0.2
C24				0.05
C25				0.15
C26				0.1
C27				0.15
C28				0.1
C29				0.25
C30				0.05
C31				0.1
C32				0.05
C33				0.05

Figure A.56 - Crack widths of BM 10.5-150 at 30 kN

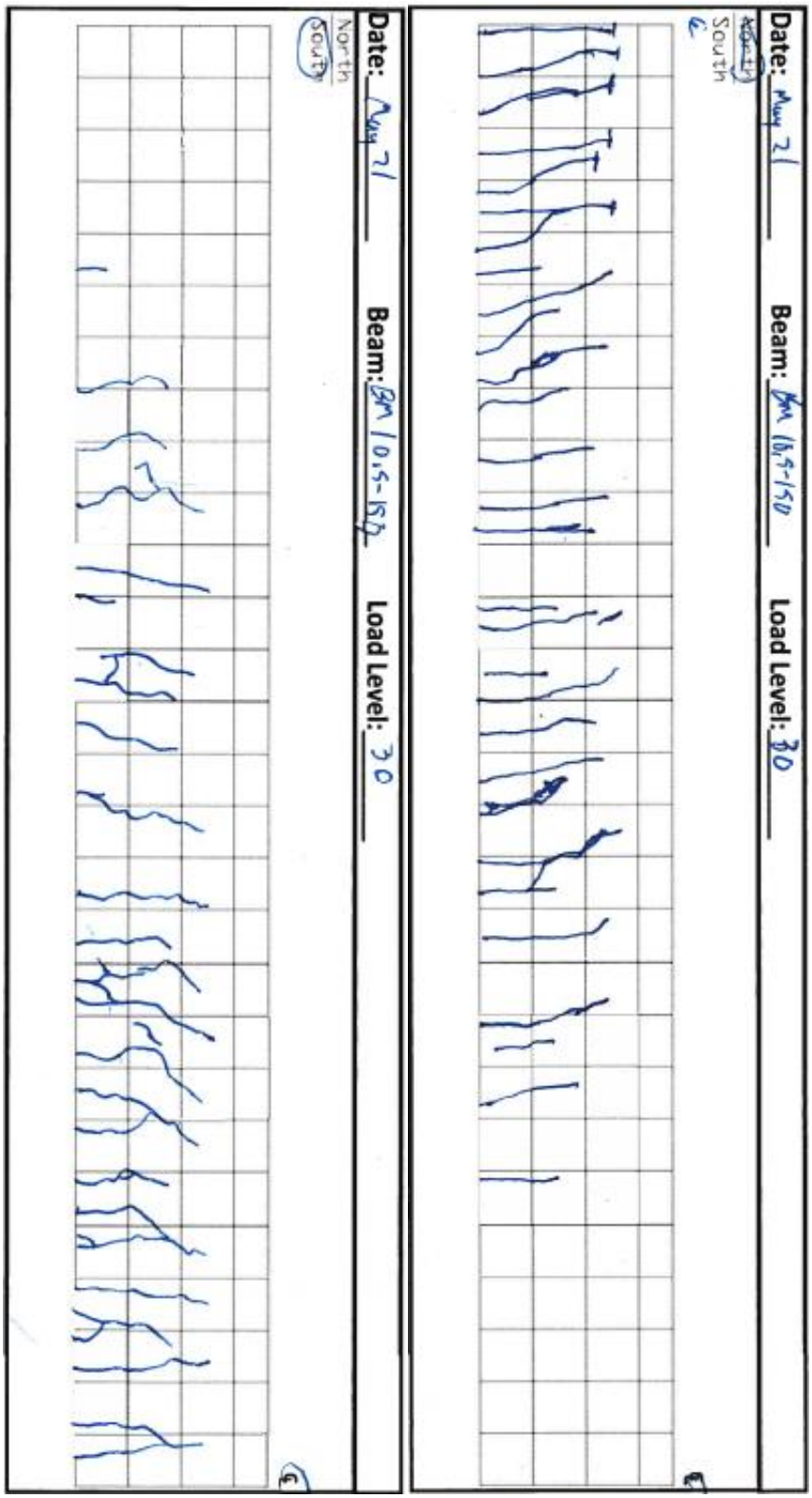

Figure A.57 - Crack tracking of BM 10.5-150 at 30 kN

Date: May 7 | Beam: BM 10.5-150 | Load Level: 45

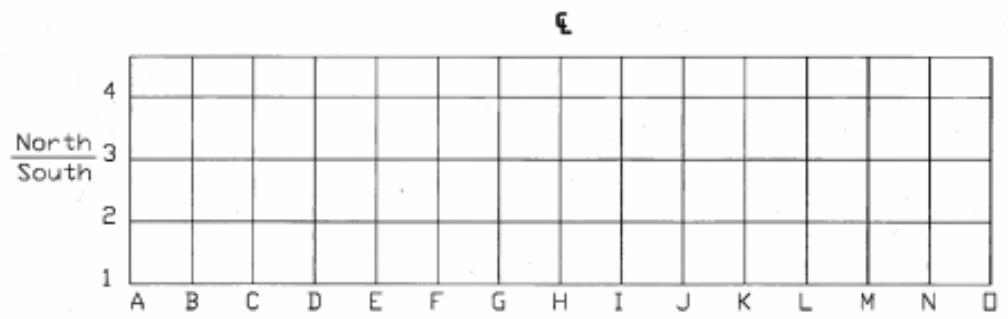

General Comments:

Crack	Location			
	Label	X (mm)	Y (mm)	Width (mm)
C1				0.15
C2				0.2
C3				0.3
C4				0.1
C5				0.25
C6				0.25
C7				0.05
C8				0.3
C9				0.3
C10				0.25
C11				0.3
C12				0.25
C13				0.4
C14				0.3
C15				0.3
C16				0.25
C17				0.3
C18				0.25
C19				0.1

Figure A.58 - Crack widths of BM 10.5-150 at 45 kN

Date: May 21 Beam: BM 10.5-150 Load Level: 45

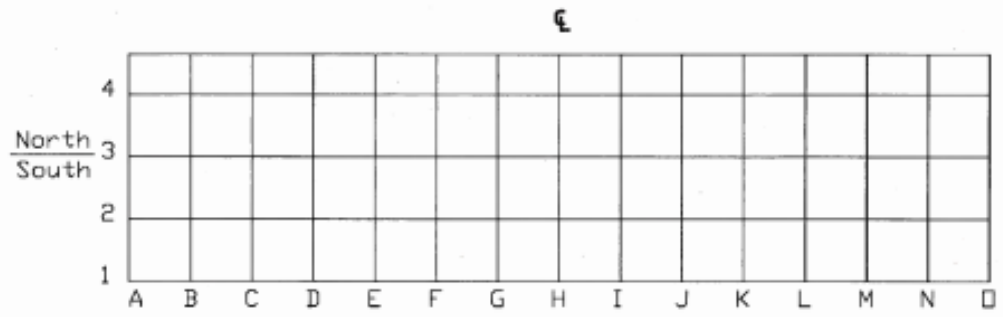

General Comments:

Crack	Location			
	Label	X (mm)	Y (mm)	Width (mm)
C20				0.45
C21				0.4
C22				0.35
C23				0.3
C24				0.1
C25				0.15
C26				0.15
~~C27~~				0.15
C28				0.1
C29				0.1
C30				0.05
C31				0.05
C32				0.05
C33				0.1

Figure A.59 - Crack widths of BM 10.5-150 at 45 kN

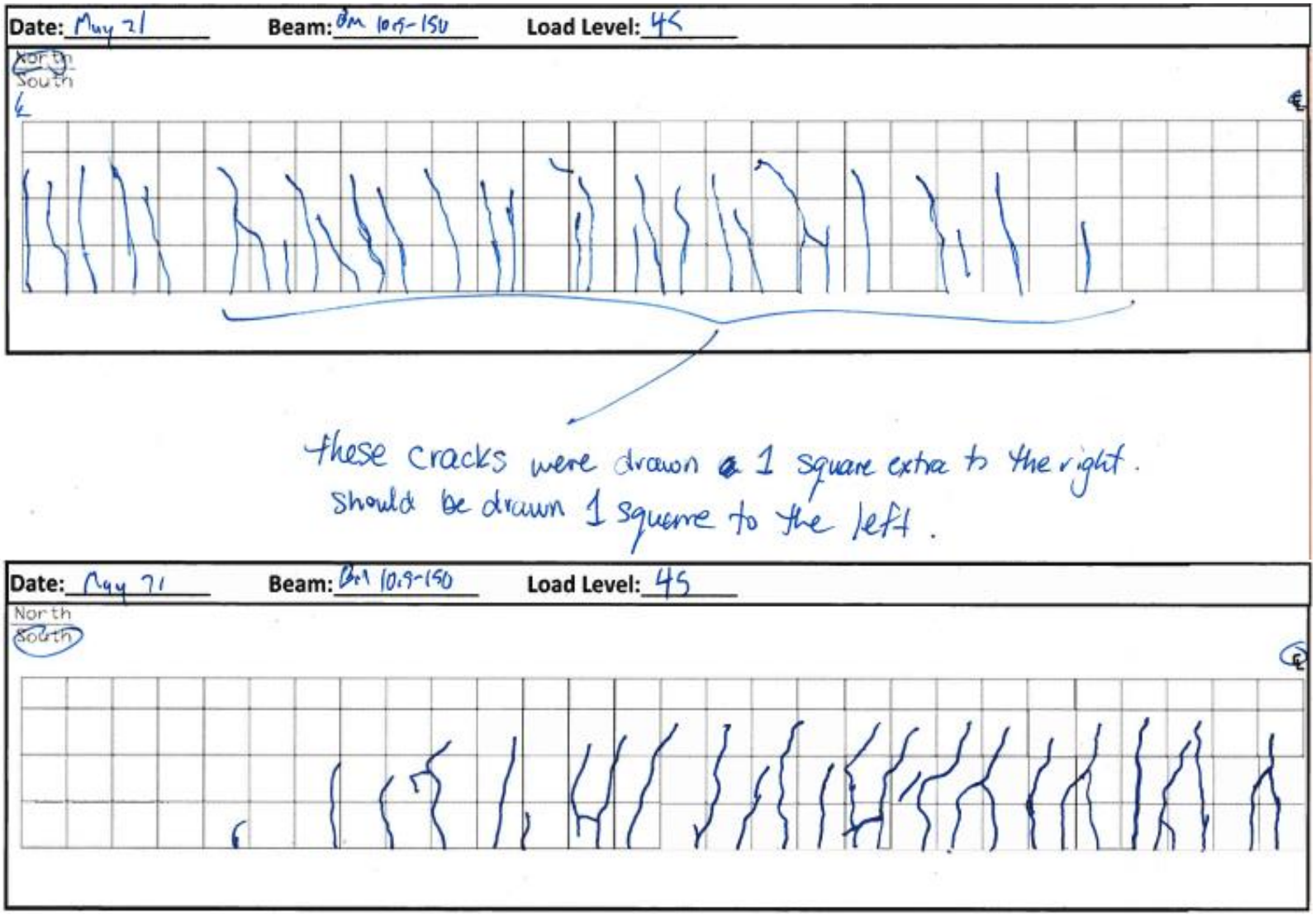

Figure A.60 - Crack tracking of BM 10.5-150 at 45 kN

Date: May 21 Beam: BM 10.5-150 Load Level: 60

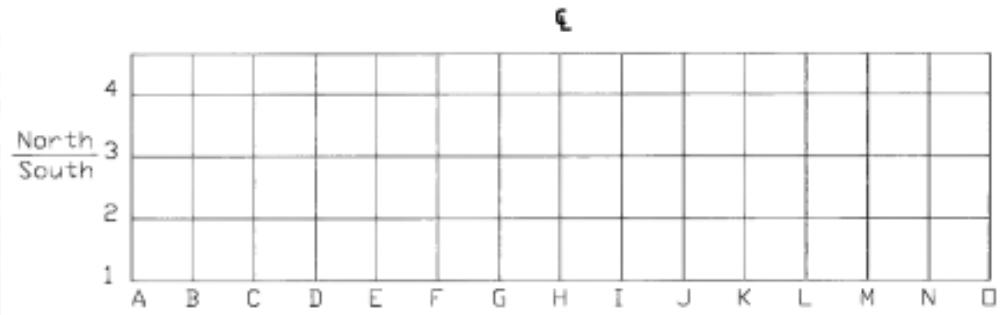

General Comments:

Crack	Location			
	Label	X (mm)	Y (mm)	Width (mm)
C1				0.15
C2				0.2
C3				0.35
C4				0.15
C5				0.4
C6				0.45
C7				0.05
C8				0.4
C9				0.3
C10				0.3
C11				0.4
C12				0.4
C13				0.5
C14				0.4
C15				0.4
C16				0.4
C17				0.4
C18				0.45
C19				0.15

Figure A.61 - Crack widths of BM 10.5-150 at 60 kN

Date: May 21 Beam: BM 10.5-150 Load Level: 60

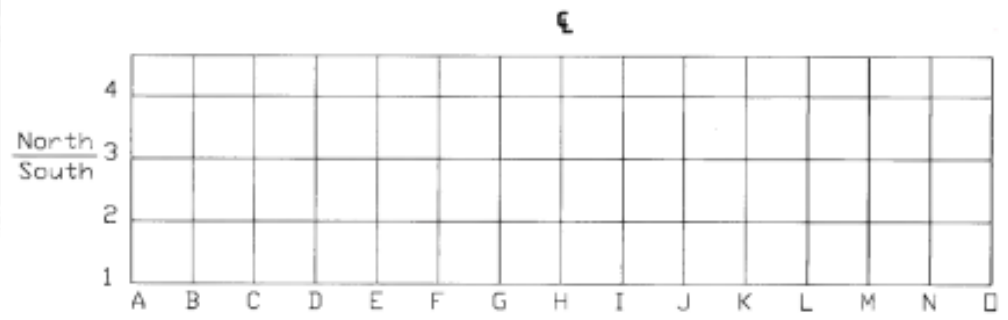

General Comments:

Crack	Location			
	Label	X (mm)	Y (mm)	Width (mm)
C20				0.5
C21				0.4
C22				0.35
C23				0.35
C24				0.1
C25				0.15
C26				0.25
C27				0.2
C28				0.1
C29				0.1
C30				0.1
C31				0.15
C32				0.1
C33				0.1

Figure A.62 - Crack widths of BM 10.5-150 at 60 kN

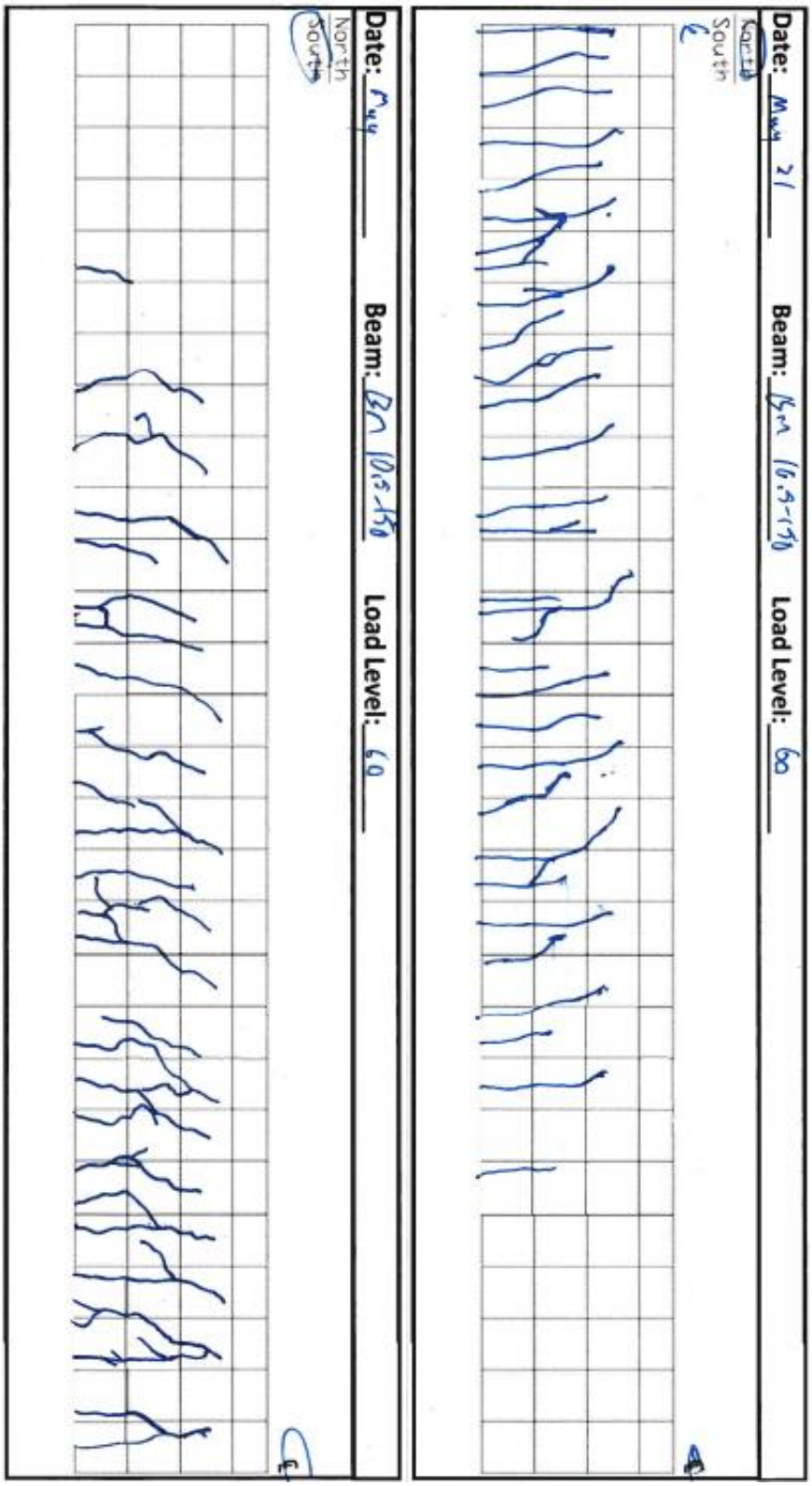

Figure A.63 - Crack tracking of BM 10.5-150 at 60 kN

APPENDIX B - CRACK PATTERNS AT FAILURE

B.1 Series BM 4.5

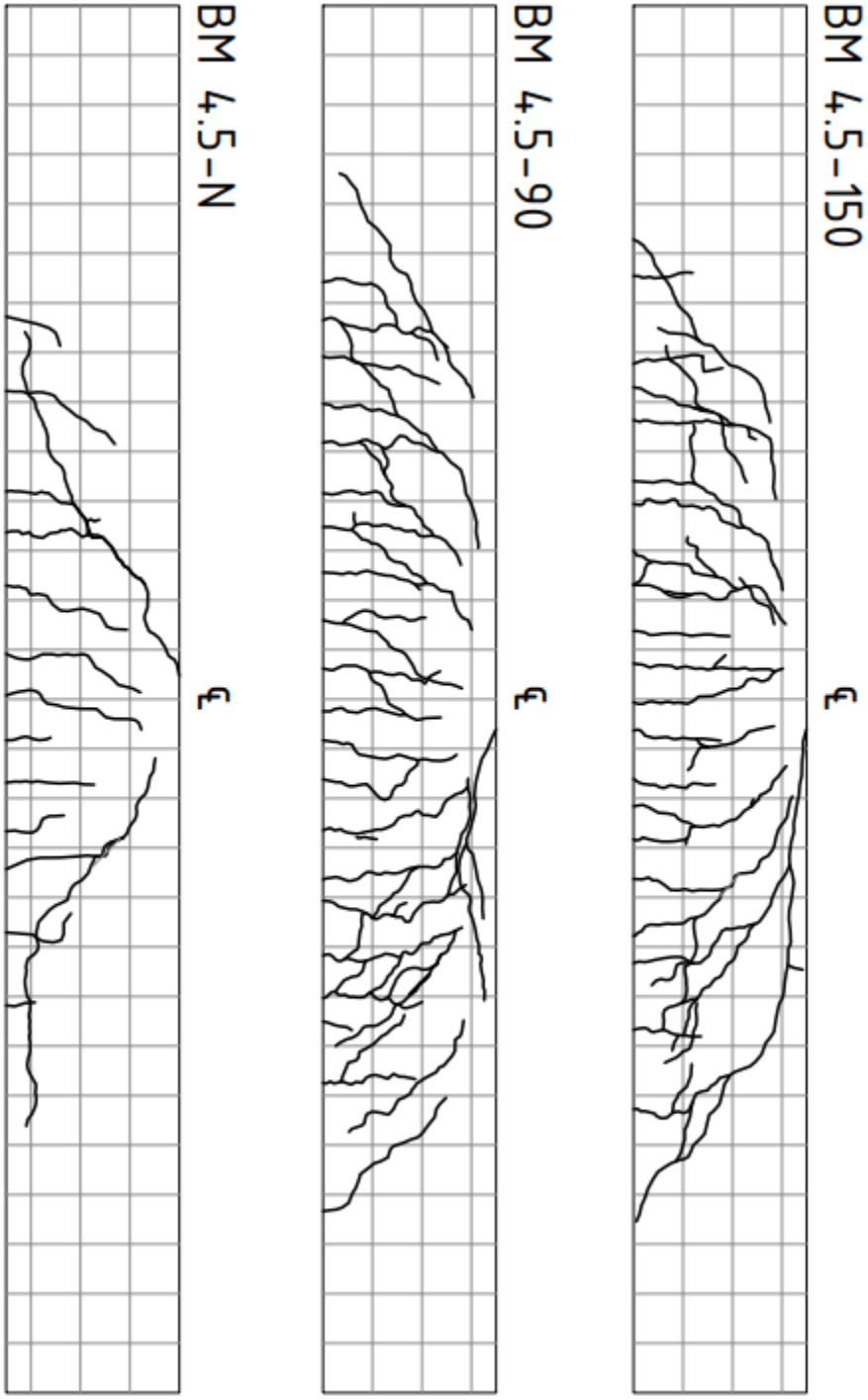

Figure B.1 - Series BM 4.5 crack patterns at failure

B.2 Series BM 6.5

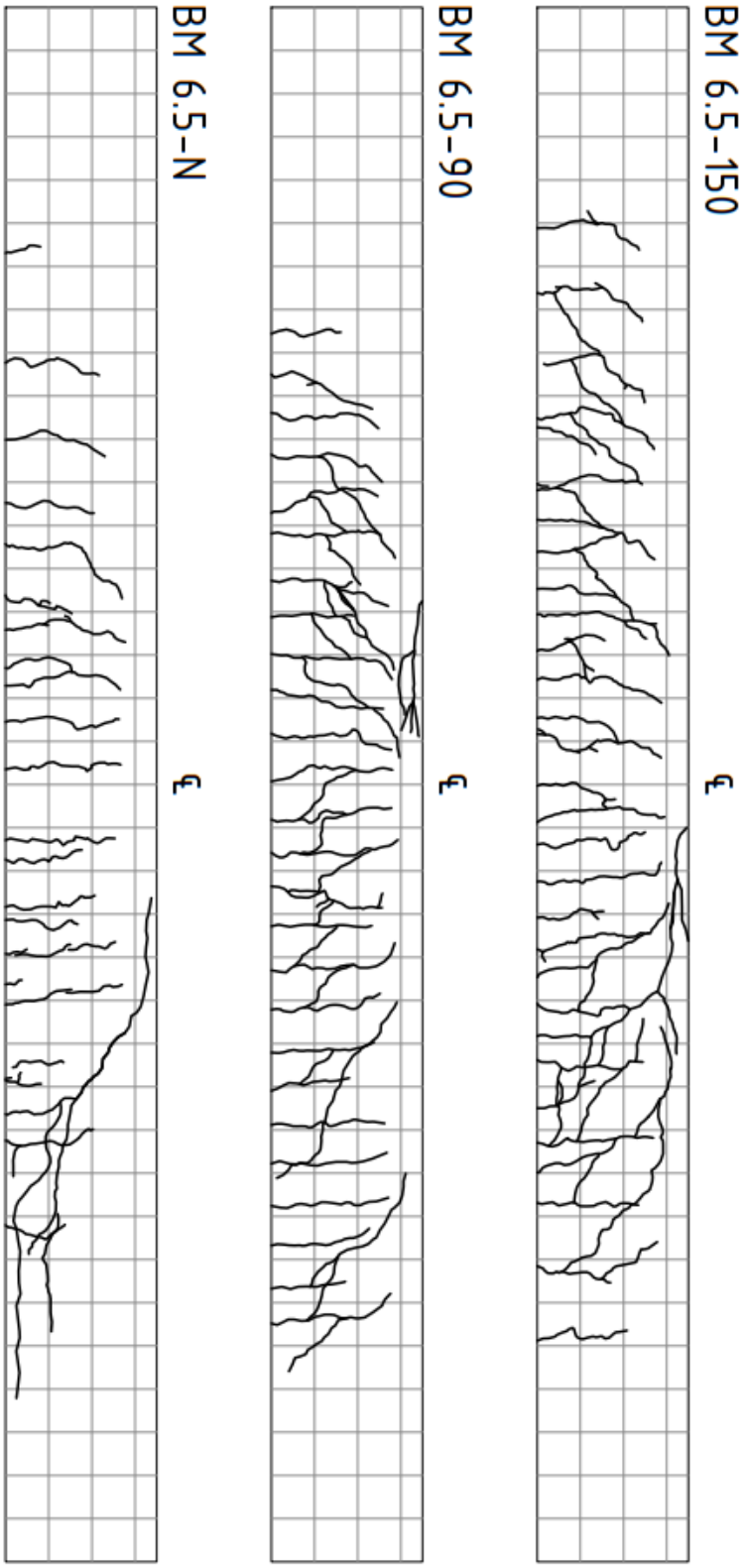

Figure B.2 - **Series BM 6.5 crack patterns at failure**

B.3 Series BM 8.5

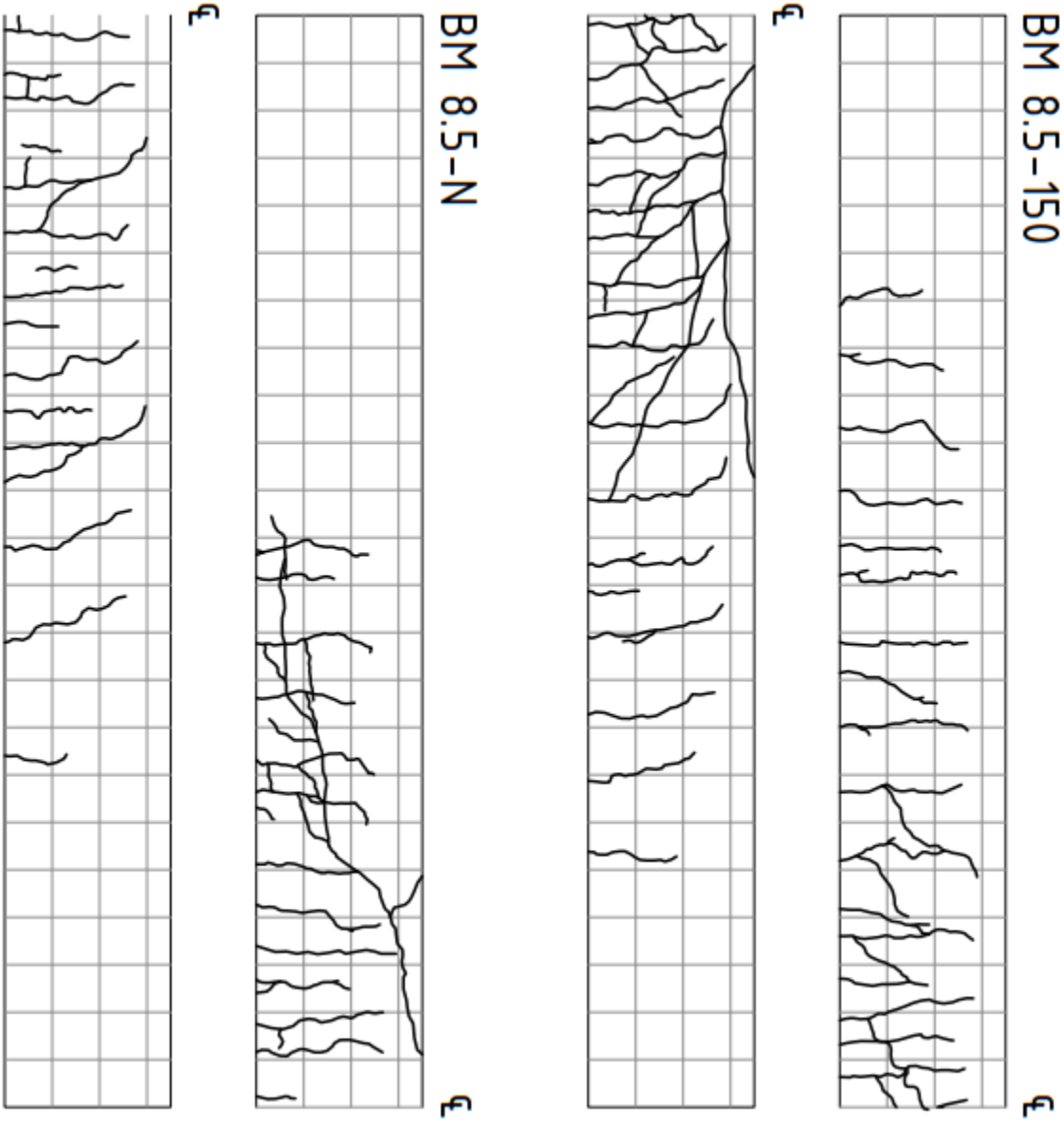

Figure B.3 - Series BM 8.5 crack patterns at failure

B.4 Series BM 10.5

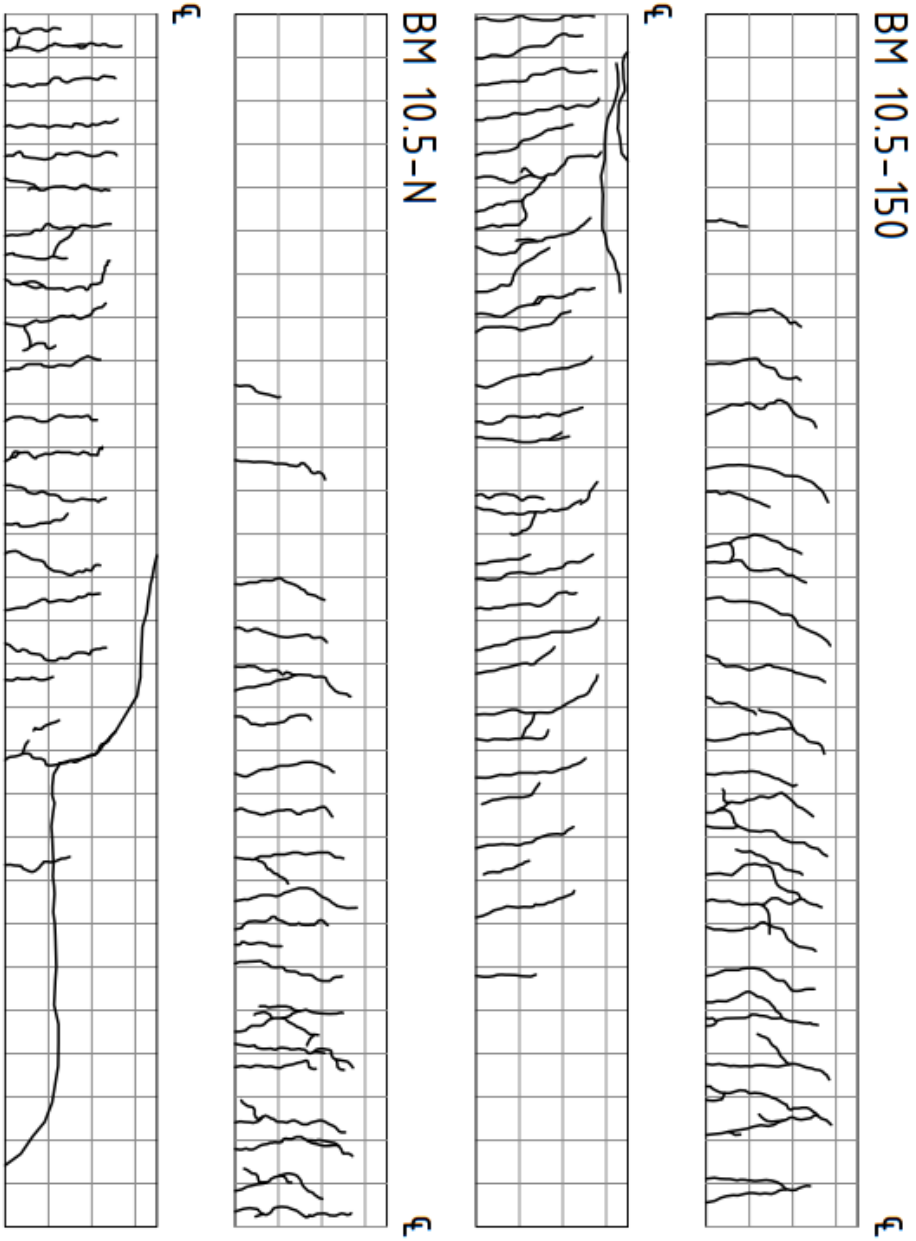

Figure B.4 - Series BM 10.5 crack patterns at failure

APPENDIX C - MEASURED SHEAR DISPLACEMENT

C.1 BM 4.5-N

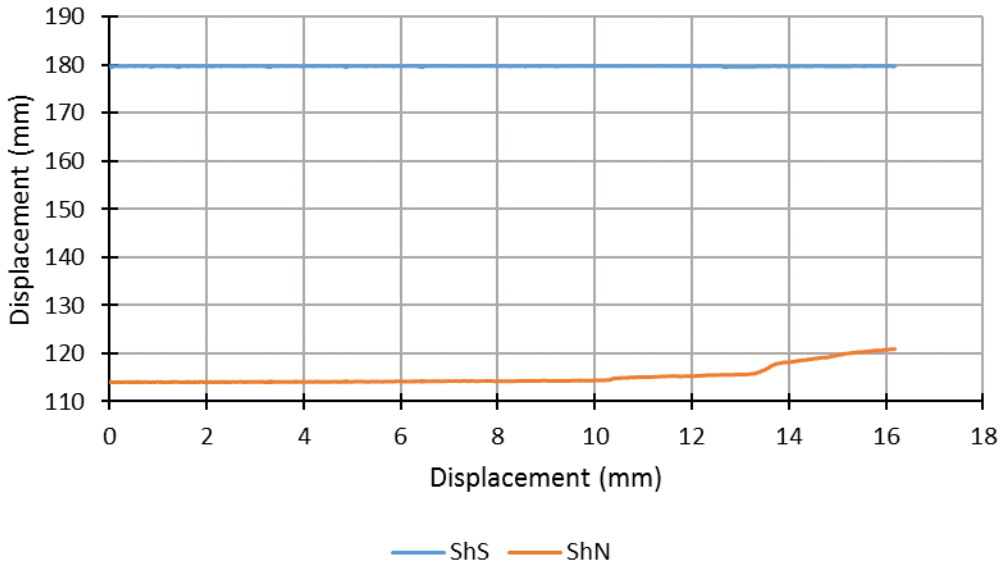

Figure C.1 - Shear vs midspan displacements for BM 4.5-N

C.2 BM 4.5-90

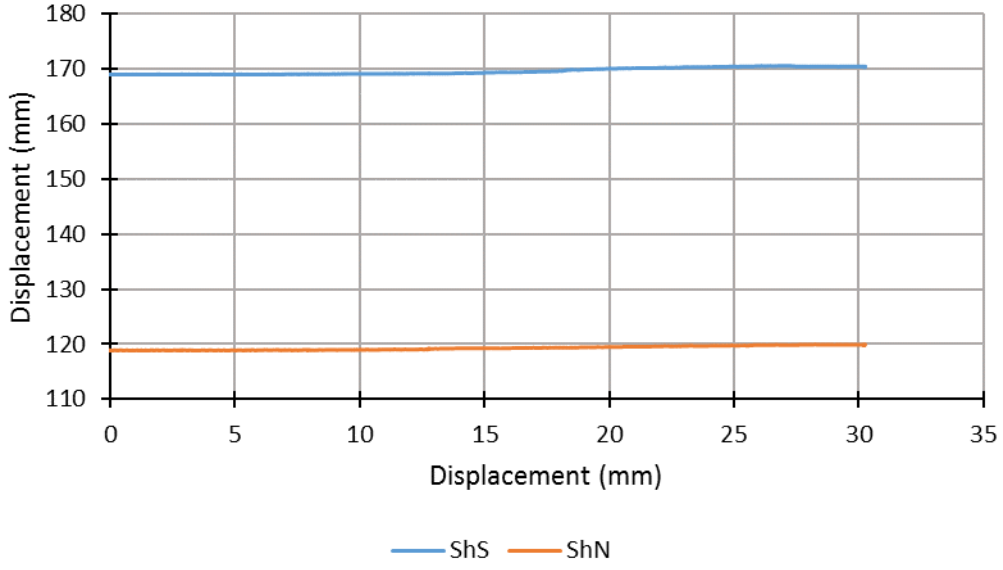

Figure C.2 - Shear vs midspan displacements for BM 4.5-90

C.3 BM 4.5-150

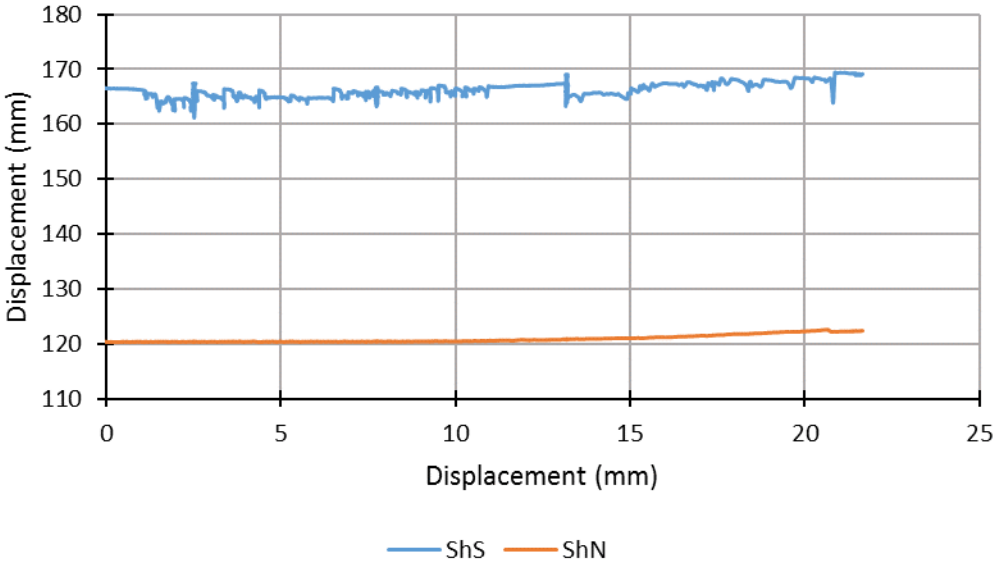

Figure C.3 - Shear vs midspan displacements for BM 4.5-150

C.4 BM 6.5-N

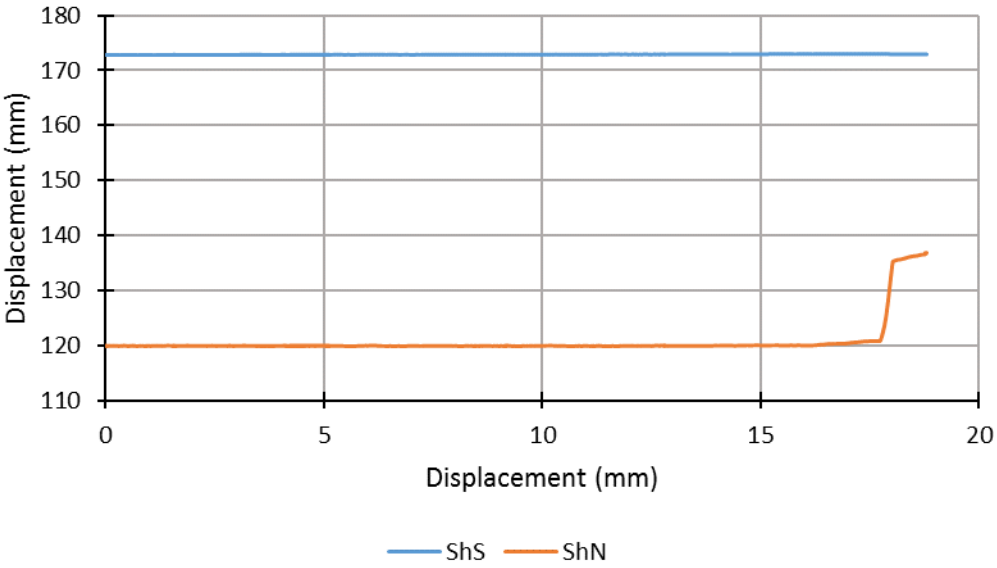

Figure C.4 - Shear vs midspan displacements for BM 6.5-N

C.5 BM 6.5-90

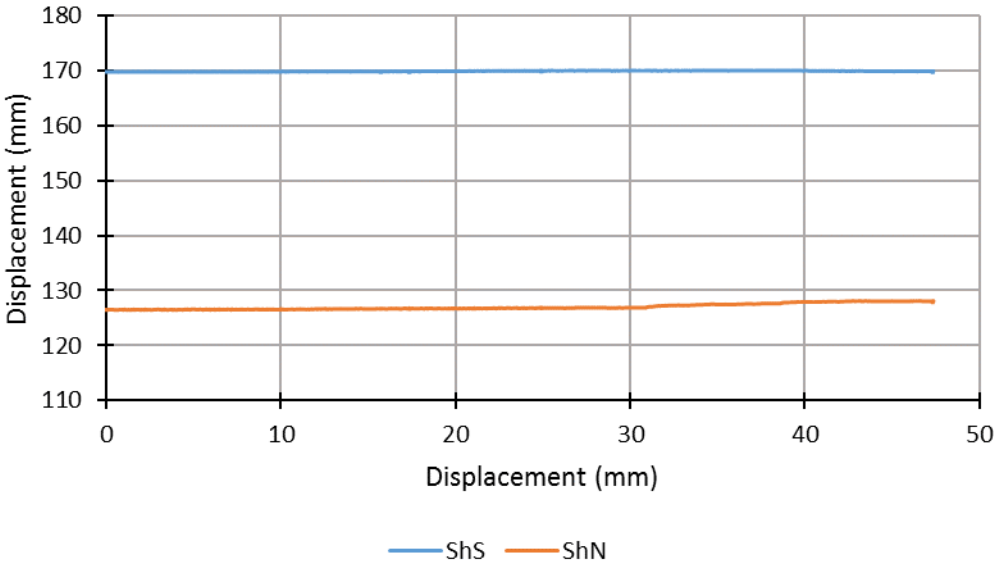

Figure C.5 - Shear vs midspan displacements for BM 6.5-90

C.6 BM 6.5-150

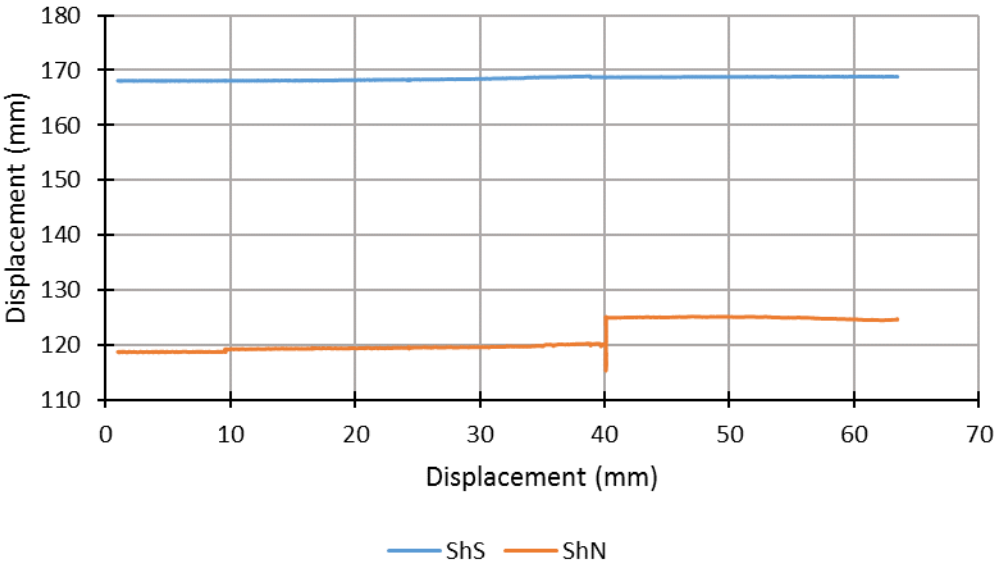

Figure C.6 - Shear vs midspan displacements for BM 6.5-150

C.7 BM 8.5-150

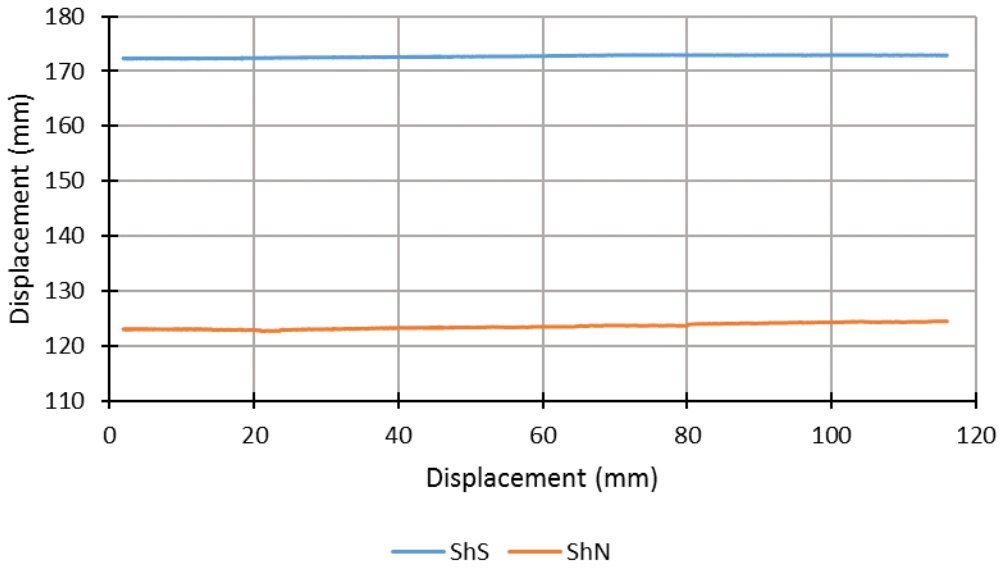

Figure C.7 - Shear vs midspan displacements for BM 8.5-150

C.8 BM 10.5-N

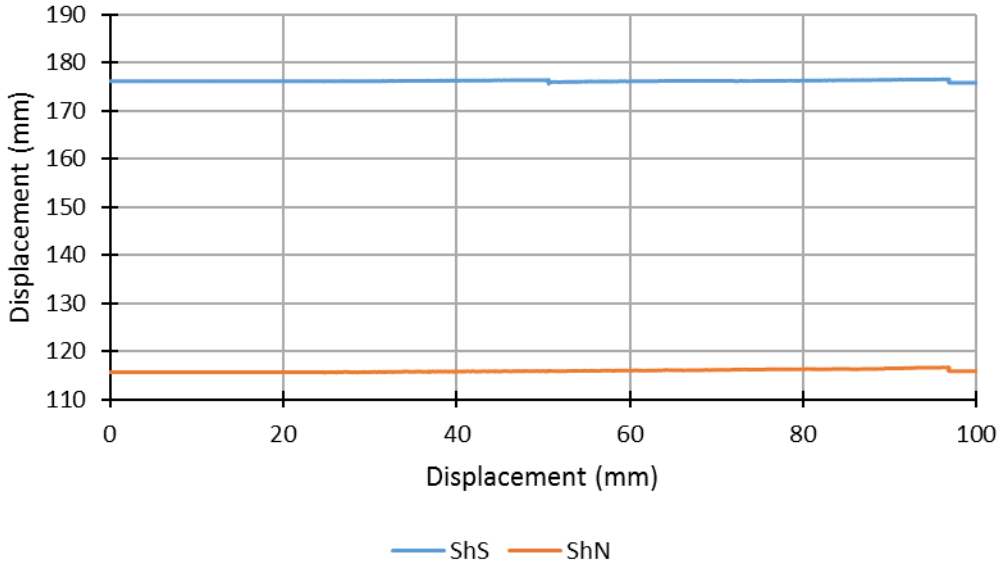

Figure C.8 - Shear vs midspan displacements for BM 10.5-N

C.9 BM 10.5-150

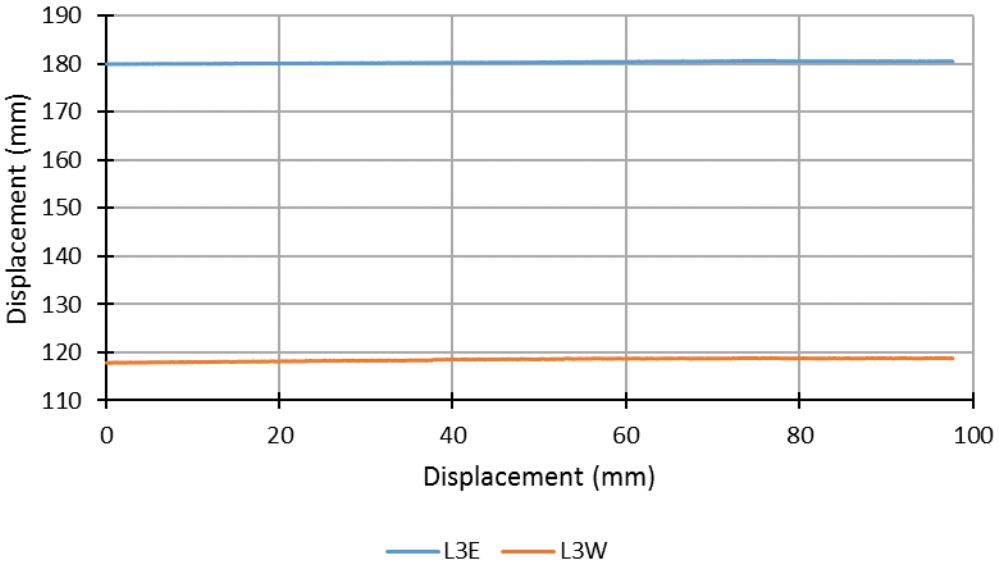

Figure C.9 - Shear vs midspan displacements for BM 10.5-150

APPENDIX D - COMPARISON OF FEA LOAD-DISPLACEMENT PREDICTIONS TO SPECIMEN BEHAVIOUR

D.1 BM 4.5-N

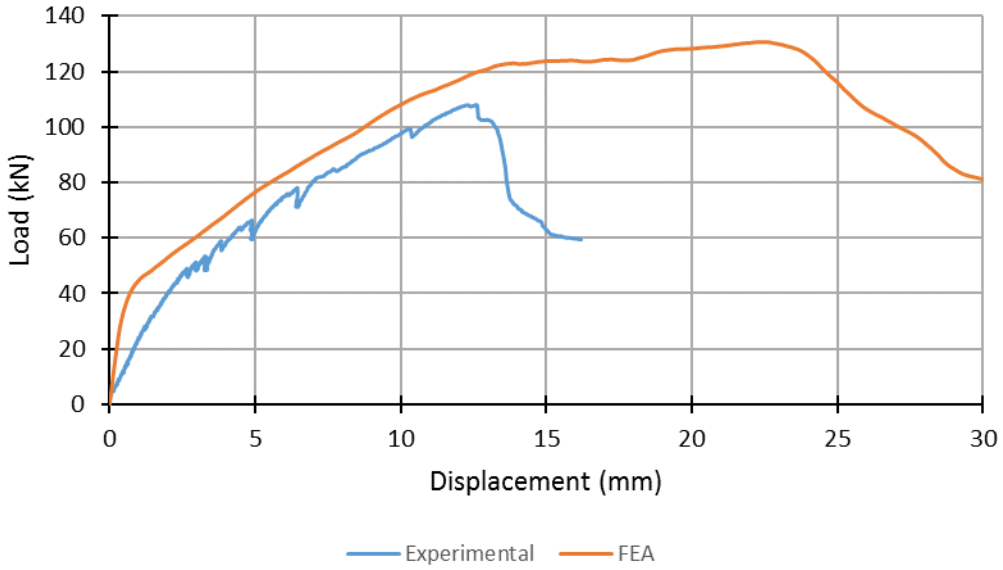

Figure D.1 - Comparison of FEA and experimental load-displacement behaviour for BM 4.5-N

D.2 BM 4.5-90

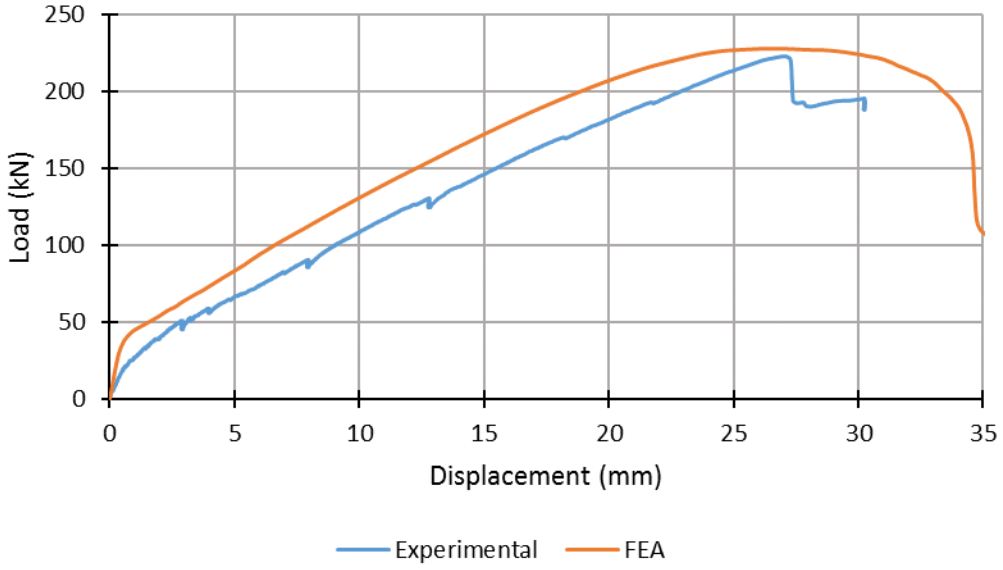

Figure D.2 - Comparison of FEA and experimental load-displacement behaviour for BM 4.5-90

D.3 BM 4.5-150

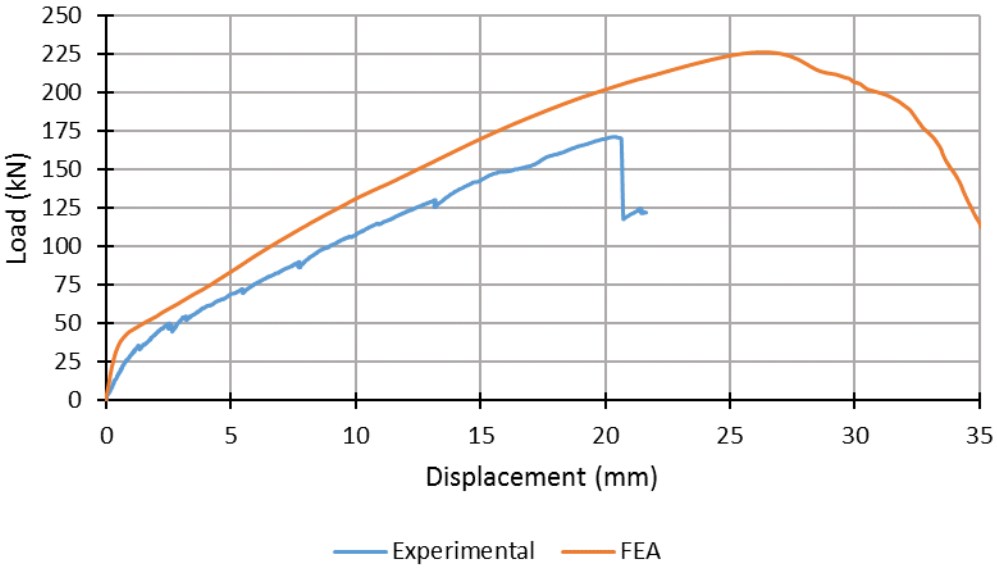

Figure D.3 - Comparison of FEA and experimental load-displacement behaviour for BM 4.5-150

D.4 BM 6.5-N

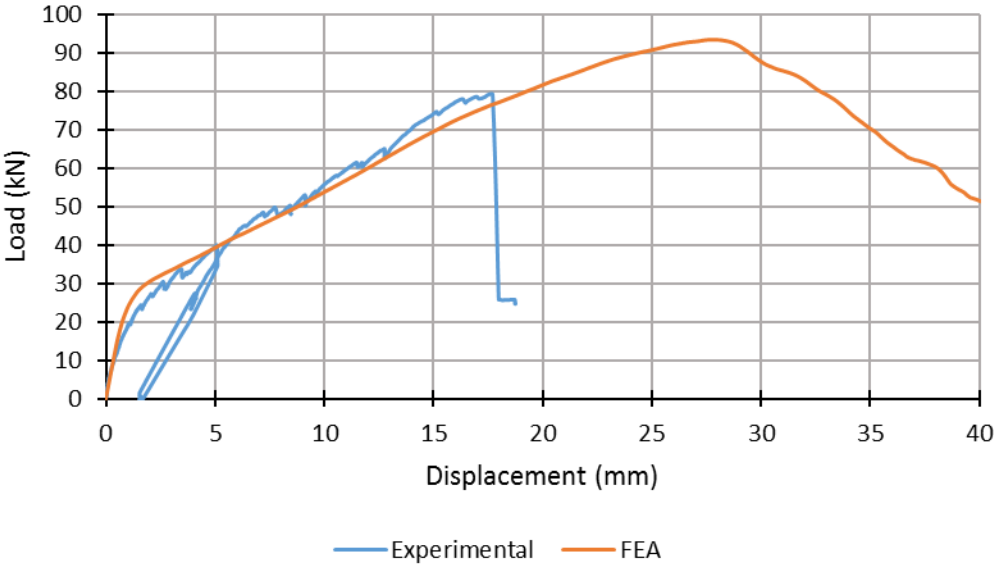

Figure D.4 - Comparison of FEA and experimental load-displacement behaviour for BM 6.5-N

D.5 BM 6.5-90

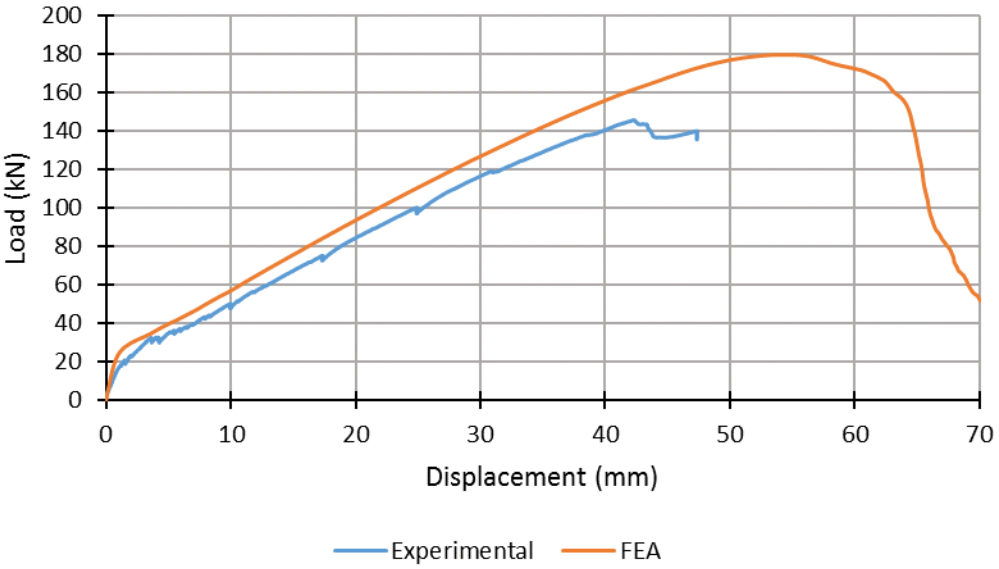

Figure D.5 - Comparison of FEA and experimental load-displacement behaviour for BM 6.5-90

D.6 BM 6.5-150

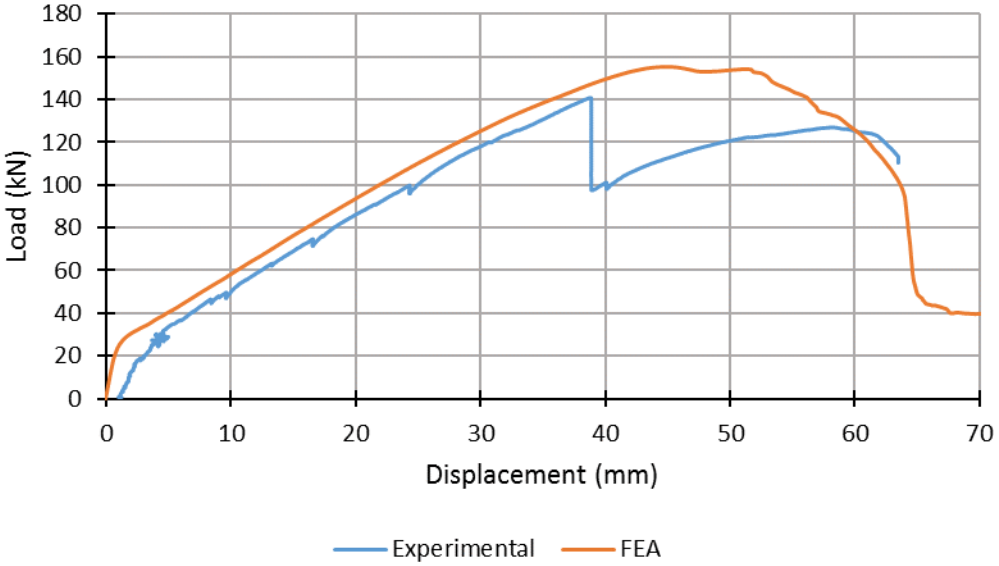

Figure D.6 - Comparison of FEA and experimental load-displacement behaviour for BM 6.5-150

D.7 BM 8.5-N

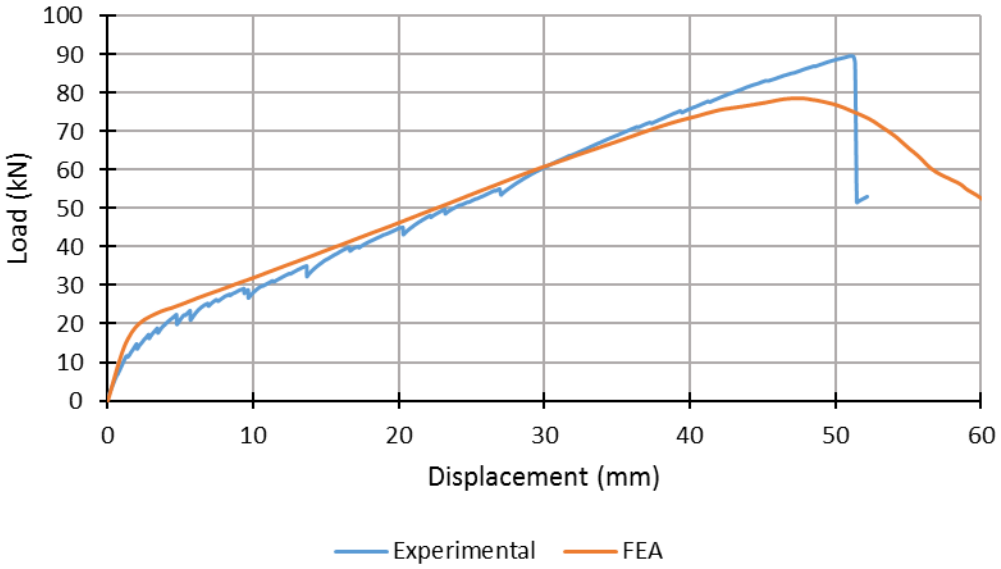

Figure D.7 - Comparison of FEA and experimental load-displacement behaviour for BM 8.5-N

D.8 BM 8.5-150

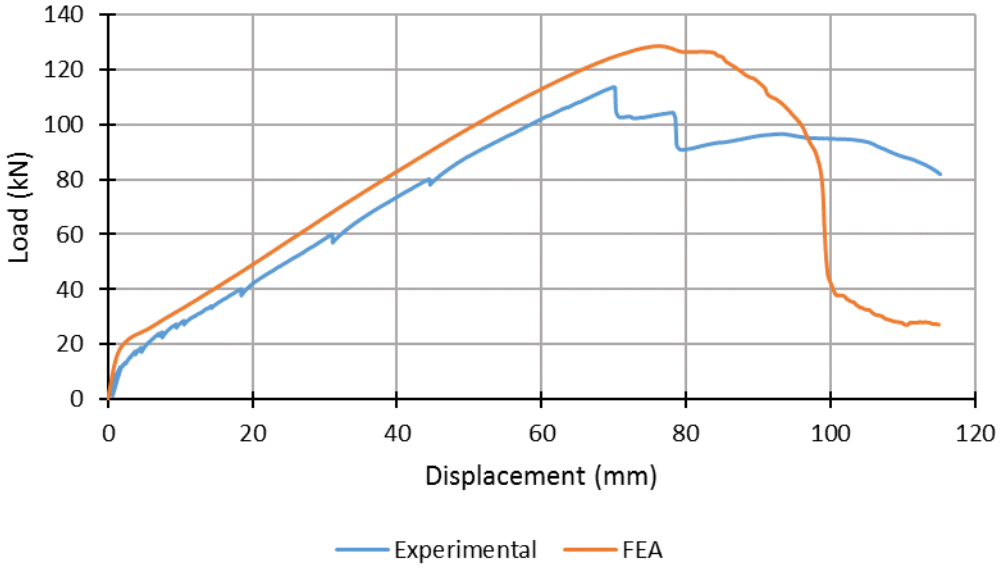

Figure D.8 - Comparison of FEA and experimental load-displacement behaviour for BM 8.5-150

D.9 BM 10.5-N

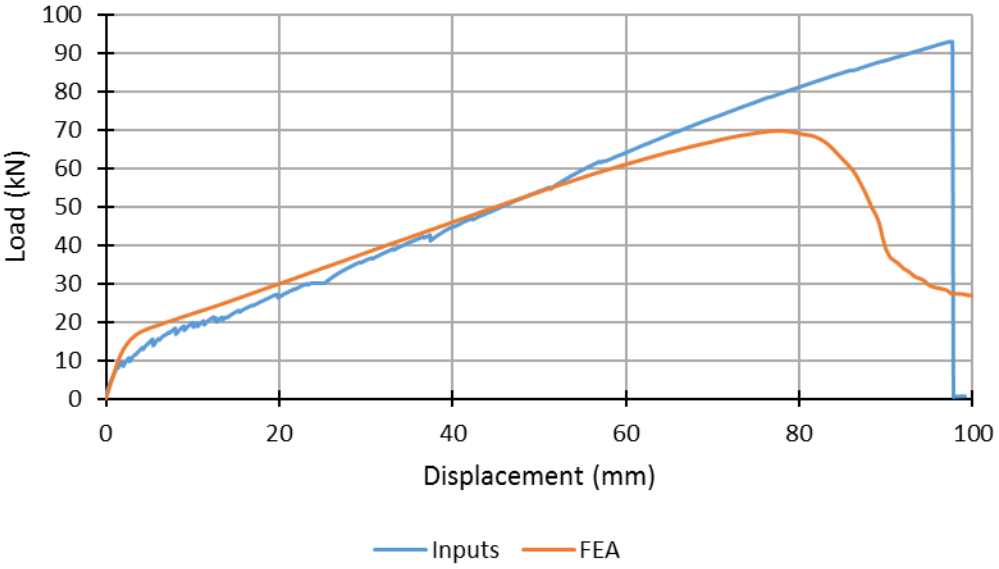

Figure D.9 - Comparison of FEA and experimental load-displacement behaviour for BM 10.5-N

D.10 BM 10.5-150

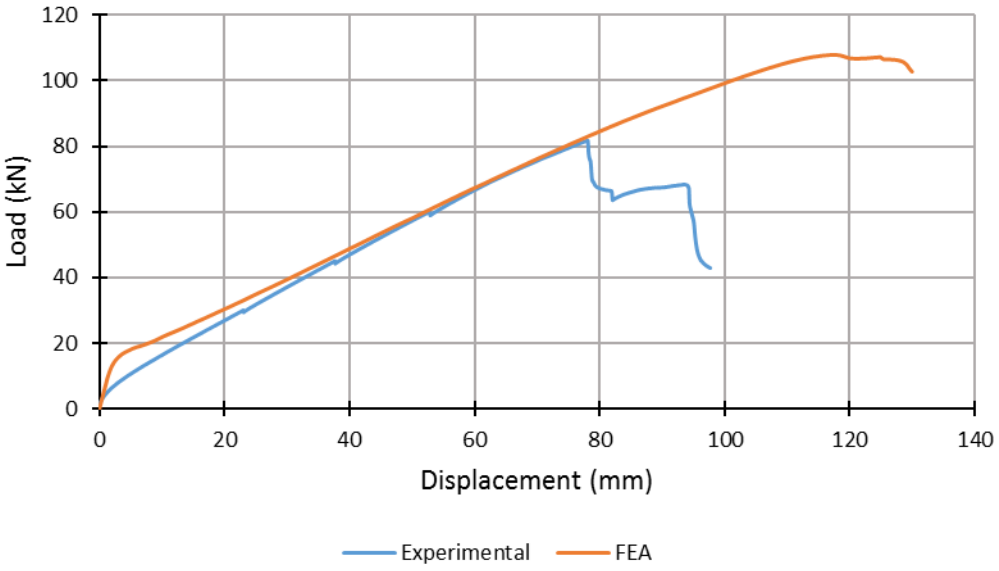

Figure D.10 - Comparison of FEA and experimental load-displacement behaviour for BM 10.5-150

APPENDIX E - COMPARSION OF FEA CRACK PATTERNS TO SPECIMEN BEHAVIOUR AND CRITICAL SHEAR ANGLES

E.1 BM 4.5-N

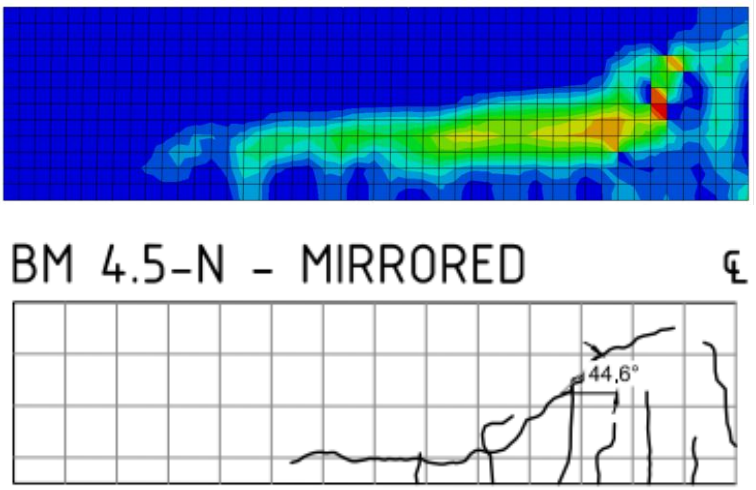

Figure E.1 - Comparison of FEA and experimental crack patterns at failure for BM 4.5-N

E.2 BM 4.5-90

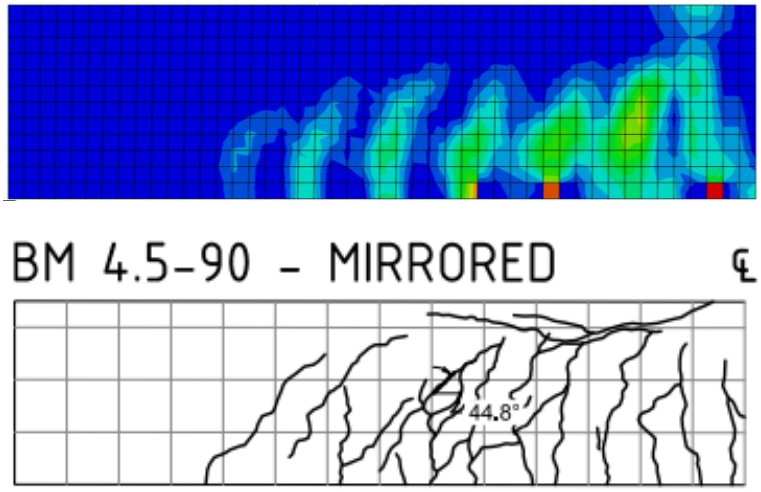

Figure E.2 - Comparison of FEA and experimental crack patterns at failure for BM 4.5-90

E.3 BM 4.5-150

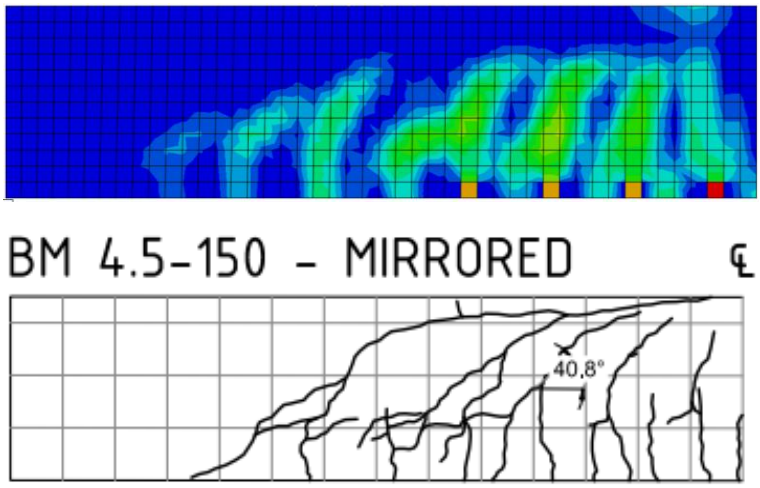

Figure E.3 - Comparison of FEA and experimental crack patterns at failure for BM 4.5-150

E.4 BM 6.5-N

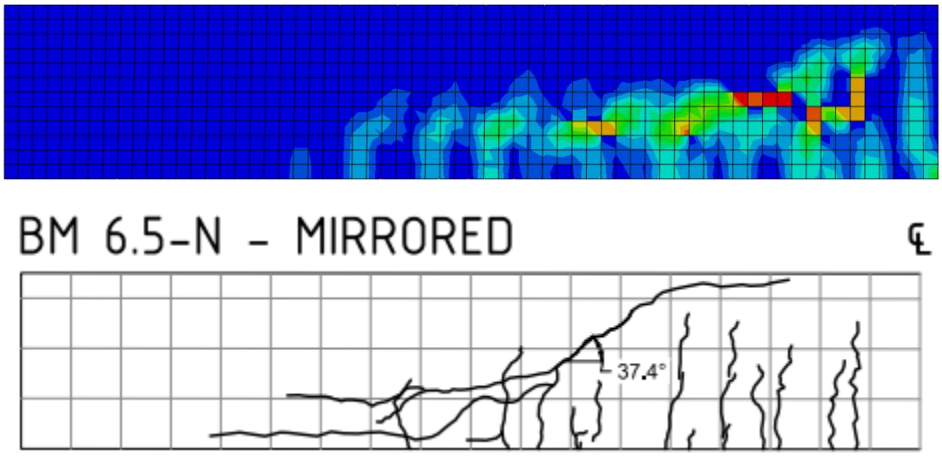

Figure E.4 - Comparison of FEA and experimental crack patterns at failure for BM 6.5-N

E.5 BM 6.5-90

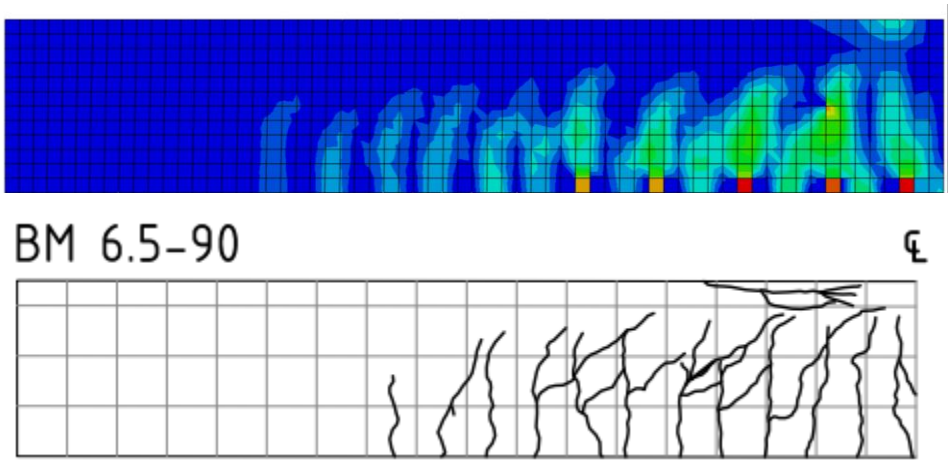

Figure E.5 - Comparison of FEA and experimental crack patterns at failure for BM 6.5-90

E.6 BM 6.5-150

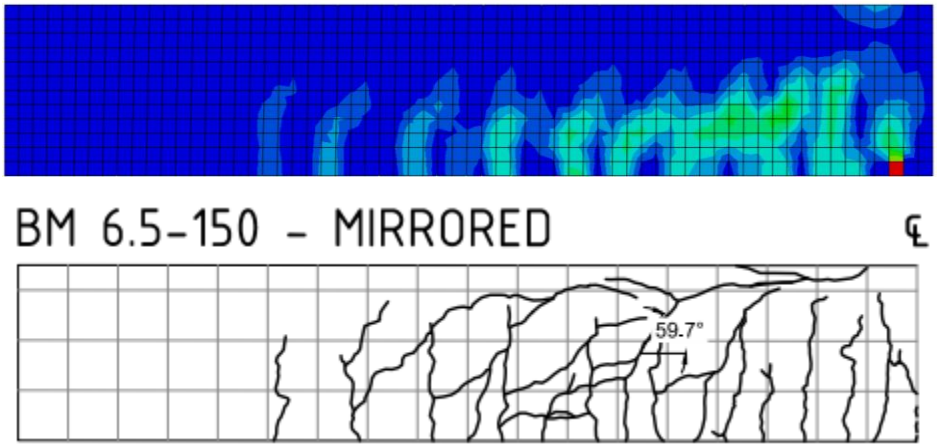

Figure E.6 - Comparison of FEA and experimental crack patterns at failure for BM 6.5-150

E.7 BM 8.5-N

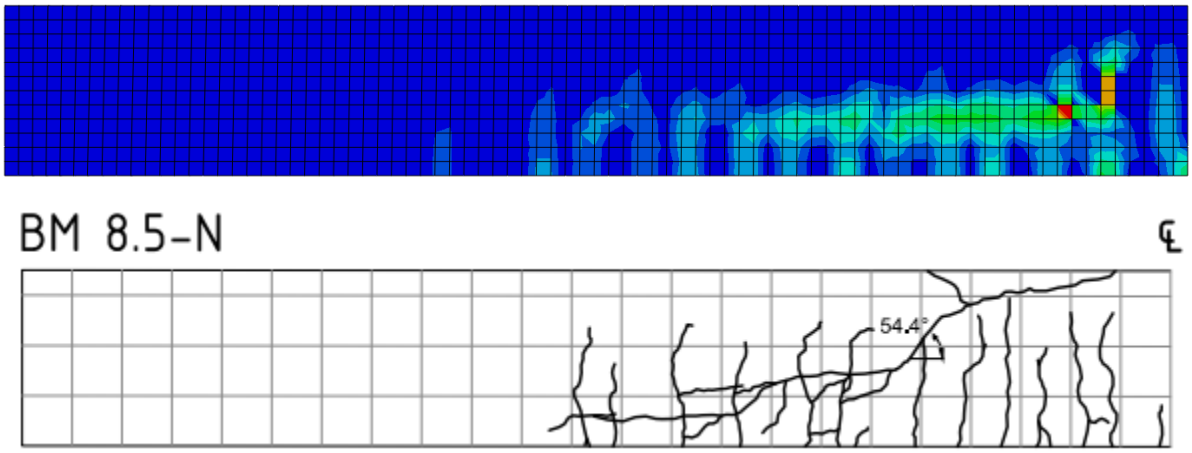

Figure E.7 - Comparison of FEA and experimental crack patterns at failure for BM 8.5-N

E.8 BM 8.5-150

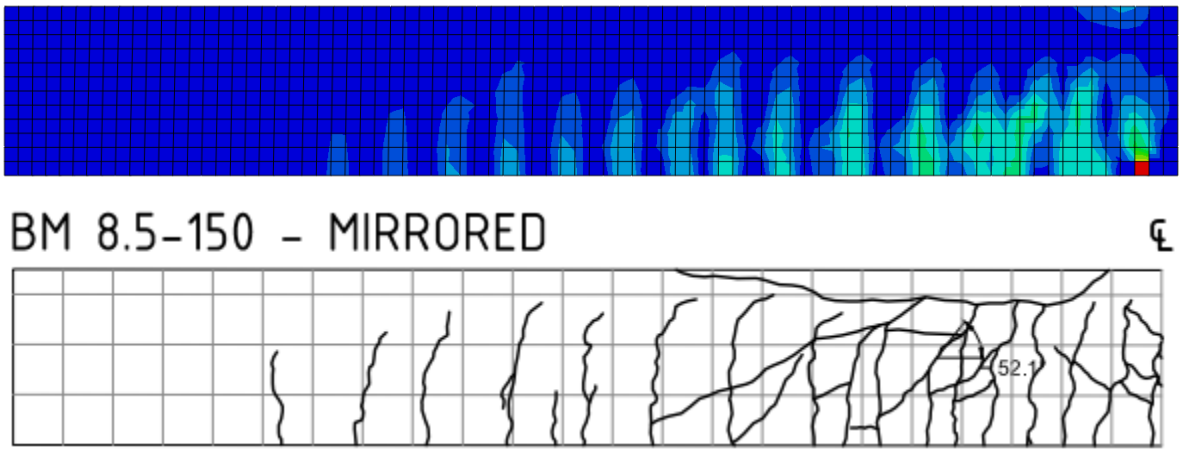

Figure E.8 - Comparison of FEA and experimental crack patterns at failure for BM 8.5-150

E.9 BM 10.5-N

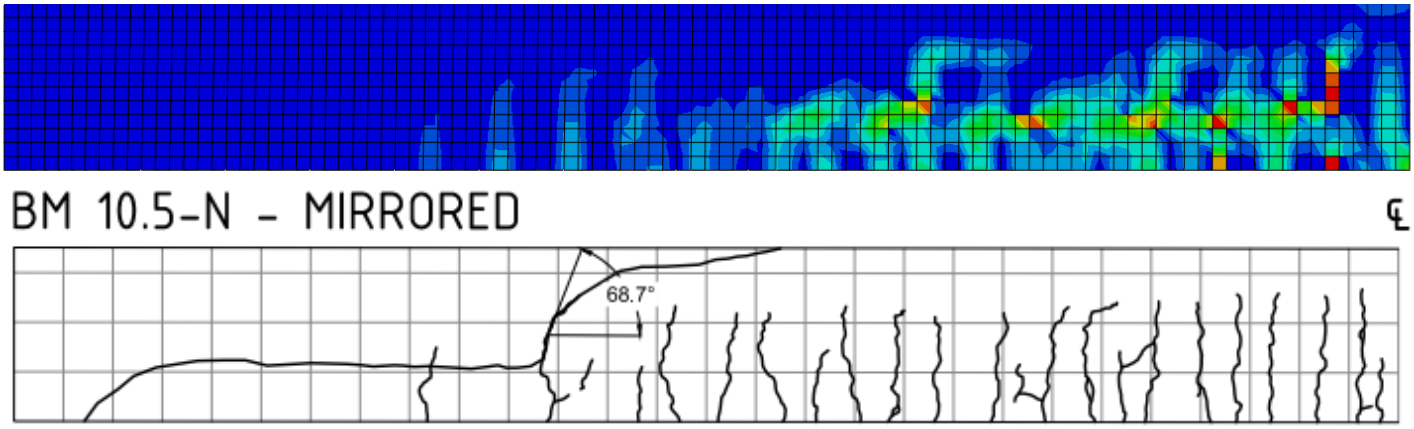

Figure E.9 - Comparison of FEA and experimental crack patterns at failure for BM 10.5-N

E.10 BM 10.5-150

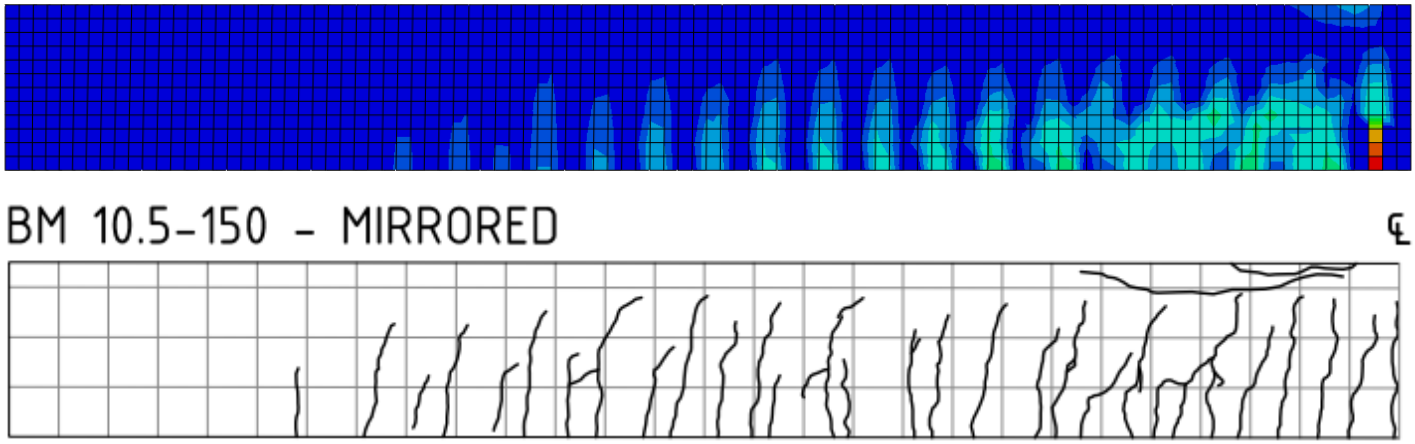

Figure E.10 - Comparison of FEA and experimental crack patterns at failure for BM 10.5-150

APPENDIX F - CSA S806 SPECIMEN CAPACITY SAMPLE CALCULATIONS

F.1 Specimen BM 6.5-90

Table F.1 – Specimen Material Properties

Concrete Material Properties			FRP Reinforcement Properties					
			General			Longitudinal		
f'_c =	51	MPa	f_u =	1000	MPa	d_b =	16	mm
E_c =	32.47511679	GPa	E_{FRP} =	64	GPa	b_c =	32	mm
ϕ_c =	1		ε_u =	0.015625		Spacing =	30	mm
a_{max} =	16	mm	ϕ_{FRP} =	1		# bars =	6	
α_1 =	0.7735		Shear			#bars/row =	3	
β_1 =	0.8425		d_b =	10	mm	# rows =	2	
ε_{cu} =	0.0035		Spacing =	90	mm	ρ_{FRPL} =	2.19%	
λ =	1		ρ_{FRPV} =	0.87%		A_{FRP} =	1206.372	mm^2
f_r =	4.28		A_v =	157.0796	mm^2	A_{fb} =	201.0619	mm^2
I_g =	745647916.67		E_v =	45	GPa			

Table F.2 – Specimen Geometry

Beam Properties		
b =	200	mm
h =	355	mm
d =	275	mm
a =	1.7875	m
a/d =	6.5	
L =	5.355443	m
L =	17.57035	ft
I_g =	7.46E+08	mm^4
k =	0.253962	

1. Flexural Capacity

a. Check mode of flexural failure:

$$\rho_b = \frac{\alpha_1 \beta_1 \phi_c}{\phi_{frp}} \left(\frac{\epsilon_c}{\epsilon_c + \epsilon_u} \right) \left(\frac{f_c}{f_u} \right)$$

$$\rho_b = 0.61\% < 0.87\% = \rho$$

Therefore, BM 6.5-90 flexural failure will be over-reinforced.

b. Calculate compression block height:

$$a = \frac{\left[\left(A_R E_R \epsilon_c + \sqrt{A_R E_R \epsilon_c}\right)^2 + 4[\alpha_1 \beta_1 f_c' b] A_R E_R d \epsilon_c\right]}{2\alpha_1 \beta_1 f_c' b}$$

$$a = 73.6\, mm$$

c. Calculate stress in longitudinal reinforcement:

$$f_{frp} = E_{frp}\epsilon_c \left(\frac{\beta_1 d}{a} - 1\right)$$
$$f_{frp} = 481.3\, MPa < 1000\, MPa = \boldsymbol{f_u}$$

d. Calculate moment capacity of section:

$$M_r = \phi_{frp} A_{frp} f_{frp} (d - \frac{a}{2})$$
$$M_r = 138.3\, kNm = 154.7\, kN\ @\ mid\boldsymbol{span}$$

Subtracting the self weight of the beam:

$$M_{SW} = bh * 24\frac{kN}{m^3} * \frac{\left(\frac{a}{2}\right)^2}{4}$$
$$M_{SW} = 5.4\, kNm$$

Therefore,

$$M_{r\,net} = 132.9\, kNm = 148.6\, kN\ @\ midspa\boldsymbol{n}$$

e. Check for concrete crushing (Cl 8.4.1.4)

$$\frac{c}{d} = 0.32 > 0.18 = \frac{7}{7 + 2000 * e_u}$$

Therefore, concrete is crushing at failure

f. Check minimum flexural reinforcement (Cl 8.4.2)

$$M_r = 138.3\, kNm = 27.0\, kNm = 1.5 M_{cr} = 1.5\left(\frac{f_r I_g}{\frac{h}{2}}\right)$$

g. Check flexural tension side reinforcement (Cl 8.4.6)

$$F_{lt} = 1206.4\, mm^2 > 603.8\, mm^2 = \frac{M_f}{d_v} + 1.3\left(V_f - 0.5 V_{sf}\right)$$

2. Shear capacity

a. Determine $\boldsymbol{V_c}$

$$V_C = 0.05\lambda\phi_c k_m k_r (f_c')^{\frac{1}{3}} b_w d_v$$
$$V_C = 0.05\lambda(1)(0.39)(12.20)(51)^{\frac{1}{3}}(200)(255.6)$$
$$V_C = 45.35\ kN$$

Note: Value of k_m determined based on iteration. k_m varies based on applied shear load and therefore guess and iteration is required to determine maximum resistance.

b. Check limits for V_c

$$V_{Cmin} = 0.11\phi_c\sqrt{f_c'}b_w d_v = 40.16\ kN < V_c = 45.35\ kN$$
$$V_{Cmax} = 0.22\phi_c\sqrt{f_c'}b_w d_v = 80.32\ kN > V_c = 45.35\ kN$$

c. Determine V_{sf} 0.4*phifrp*E13*N21*dv/(sv*TAN(N20*2*PI()/360))/1000

$$\boldsymbol{V_{sf} = 0.4\frac{\phi_{frp}A_v f_{fu} d_v}{s_v}\cot\theta}$$

where

$$\boldsymbol{f_{fu} = \min\begin{cases} f_u \\ 0.05E_v \end{cases} = 225\ MPa}$$

and

$$\boldsymbol{30° < \theta = 30 + 7000\epsilon_1 < 60°}$$

where

$$\boldsymbol{\varepsilon_1 = \frac{\frac{M_f}{d_v} + (V_f - V_p) + 0.5N_f - A_p f_{po}}{2(E_F A_F + E_p A_p)}}$$

as $\boldsymbol{\varepsilon_1}$ varies with applied load, $\boldsymbol{V_{sf}}$ also varies with iterization.

after iteration

$$\boldsymbol{V_{sf} = 26.90\ kN}$$

d. Calculate total shear resistance and check limit

$$\boldsymbol{V_r = V_c + V_s = 72.25\ kN < 573.57\ kN = 0.22\phi_c f_c' b_w d_v = V_{r_{max}}}$$

$$\boldsymbol{V_r = 72.25\ kN = 144.50\ kN\ @\ midspan}$$

e. Check minimum shear reinforcement area (Cl 8.4.5)

$$A_{vFmin} = \frac{0.07\sqrt{f_C'}b_w s_v}{0.4F_{fu}} = 100\ mm^2 < 157.1\ mm^2 = A_{VF}$$

f. Check maximum shear reinforcement spacing (Cl 8.4.6)

$$V_f = 72.25\ kN < 286.78\ kN = 0.11\lambda\phi_c f_c' b_w d_v$$

$$s_{vmax} = \min(0.6 d_v cot\theta, 400\ mm) = 102.7\ mm > 90\ mm = s_v$$

Therefore, the 90 mm stirrup spacing is OK.

3. Determine governing failure mode

$$\boldsymbol{V_{rP} = 144.50\ kN < 148.60\ kN = M_{rP}}$$

Therefore, the beam will fail at an applied load of 144.5 kN in shear.